

PLANT UPTAKE AND METABOLISM OF ANTIMICROBIALS AND ANTIBIOTICS

By

Khang Vinh Huynh

A DISSERTATION

Submitted to
Michigan State University
in partial fulfillment of the requirements
for the degree of

Biosystems Engineering—Doctor of Philosophy

2019

ABSTRACT

PLANT UPTAKE AND METABOLISM OF ANTIMICROBIALS AND ANTIBIOTICS

By

Khang Vinh Huynh

Targeted and untargeted metabolomics using high resolution mass spectrometry and multivariate statistical analysis, coupled with ^{14}C -labeled chemicals studies were used to identify novel phytometabolites and quantify the fate of common antimicrobials in plant tissues. Triclocarban (TCC), an antimicrobial that is commonly found in personal care products, was metabolized by jalapeno pepper plants during long-term exposure (12 weeks), leading to the formation of several phase I transformation products (e.g. 2'-OH-TCC and 6-OH-TCC) and phase II glycosylated OH-TCC. Importantly, the concentrations of TCC metabolites were more than 20 times greater than the concentrations of TCC in the above-ground tissues of the pepper plants after 12 weeks. Approximately 95.6% of the TCC was present as metabolites in the fruits. For sulfonamides, upon exposure to the model plant *Arabidopsis thaliana*, sulfamethazine (SMT) and sulfamethoxazole (SMX) were also prone to extensive metabolism in plant tissues. Untargeted screening of extractable metabolites revealed that glycosylated conjugates were the most abundant metabolites, which accounted for 80 – 90% of the total metabolites in plant tissues. Other conjugates, such as pterin- and methylsalicylate-, were present at lower concentrations. Phase I transformation products, such as hydroxyl-, acetyl-, desulfo, and desamino-, were identified as minor metabolites in plant tissues. For tetracyclines, abiotic transformation and plant metabolism played the key roles in their fate during exposure to *Arabidopsis thaliana*. Plant metabolism of chlortetracycline (CTC) also led to the formation of glycosylated conjugates and the corresponding 4-epi isomers. More importantly, although CTC was solely added into the experimental reactors, other tetracycline antimicrobials such as tetracycline, 4-epi-tetracycline, demeclocycline, and 4-

epi-demeclocycline were detected in the plant tissues. Preliminary studies using soil columns planted with *A. thaliana* plants showed that phytometabolism of sulfonamides was probably similar with that under hydroponic conditions, with glycosylated conjugates identified as the major phytometabolites. The majority of the uptaken parent sulfonamides and metabolites were found in the plant roots, with limited root-to-shoot translocation. In conclusion, this research indicates that untransformed antimicrobials only represent a small proportion of the total compounds taken up in plant tissues when transformed, conjugated, and sequestered phytometabolites are considered. Consequently, phytometabolism of antimicrobials in planted systems is a critical point for comprehensively addressing human exposure to contaminants of emerging concerns through food chains.

ACKNOWLEDGEMENTS

Firstly, a profound gratitude goes to the Vietnam Education Foundation for inspiring me to pursue a Ph.D., as well as providing partial financial support during my Ph.D. program in the United States. I am also grateful to other organizations that have funded my graduate work, including the National Science Foundation (NSF) and the U.S. Department of Agriculture (USDA).

I would like to express my sincere gratitude to my advisor, Dr. Dawn Reinhold, for the continuous support of my graduate studies and all related research over the past five years, for her patience, dedication, and understanding even during the toughest times in the Ph.D. pursuit. Dr. Reinhold's office was always open whenever I had a question about my research or writing. She consistently allowed this research project to be my own work, but steered me in the right direction whenever she thought I needed it.

Besides my advisor, I would also like to thank my committee members, Dr. Steven Safferman, Dr. Jade Mitchell, and Dr. Alison Cupples, for their insightful comments and encouragements, but also for the challenging questions that helped me widen my research from various perspective.

My sincere thanks also go to Dr. Dan Jones, Dr. Tony Schillmiller, and other staff at the Mass Spectrometry and Metabolomics Core Facility at Michigan State University, who provided me access to the UPLC-QTOF-MS, GC-MS, Progenesis QI, and EZInfo software, for their insightful discussions and technical assistance that have expanded my knowledge of the mass spectrometry and plant metabolomics. I am also thankful to Dr. Hui Li and Dr. Yingjie Zhang for

the use of their LC-MS/MS. Without their precious support, it would not be possible to conduct this research.

With a special mention to Emily Banach, Katerina Tsou, Niroj Aryal, Ronald Aguilar, Rebecca Bender, and other undergraduate students in Reinhold's lab. The group has been a source of friendships and good collaboration.

Special thanks to my Vietnamese friends at Michigan State University, Gerrit and Joette Laseur, the Cooper family, and the Swada family, who make me feel I have a family in the United States.

And finally, I would like to thank my family for all their love and encouragement. I am grateful to my Mom and late Dad, my brothers and sisters, and my in-laws who have supported me spiritually when I am half the globe away from home in the past five years. Most of all, words are powerless to express my gratitude to my wife Loan; thank you for your faithful and unconditional love and support during the most challenging moments in my life. My son Van and new-born daughter Ivy are, and always will be, my inner strength that drives me forward...

Khang Huynh
Michigan State University
February 2019

TABLE OF CONTENTS

LIST OF TABLES	x
LIST OF FIGURES	xii
KEY TO ABBREVIATIONS.....	xvi
CHAPTER 1.	1
INTRODUCTION AND SCOPE	1
CHAPTER 2.	4
LITERATURE REVIEW	4
2.1. The status quo of use and regulations of antibiotics	5
2.1.1. Antimicrobial use in livestock	9
2.1.2. Antimicrobial use in aquaculture	11
2.1.3. Curtailing antimicrobial use and resistance	13
2.2. Sources and occurrence of antimicrobials in the environment	17
2.2.1. Triclosan and triclocarban.....	17
2.2.1.1. Wastewater treatment plants.....	18
2.2.1.2. Biosolids-amended soils	20
2.2.2. Sulfonamides and tetracyclines.....	25
2.2.2.1. Wastewater treatment plants.....	26
2.2.2.2. Animal manure	31
2.2.2.3. Animal manure-amended soils	35
2.3. Environmental fate of antimicrobials following soil application.....	38
2.3.1. Triclosan and triclocarban.....	38
2.3.2. Sulfonamides and tetracyclines.....	45
2.3.2.1. Sulfonamides	45
2.3.2.2. Tetracyclines.....	48
2.4. Plant uptake, metabolism of antimicrobials, and the risk to humans exposed to contaminated food crops	55
2.4.1. Triclosan and triclocarban.....	55
2.4.2. Sulfonamides and tetracyclines.....	60
2.4.3. Human health risk from consumption of contaminated food crops.....	66
2.5. The hidden role of plant root exudates in transformation of organic xenobiotics	67
2.6. Metabolomics for identification of plant metabolites of organic xenobiotics	70
2.6.1. Target screening.....	72
2.6.2. Suspect screening.....	74
2.6.3. Non-target screening	76
APPENDIX.....	80
REFERENCES	82

CHAPTER 3.....	102
UPTAKE AND METABOLISM OF TRICLOCARBAN BY HYDROPONICALLY GROWN PEPPER.....	102
3.1. Introduction.....	103
3.2. Materials and Methods.....	106
3.2.1. Chemicals and plant material.....	106
3.2.2. Long-term exposure of pepper plants to TCC.....	106
3.2.3. Short-term exposure to TCC for metabolite screening.....	108
3.2.4. Sample preparation and chemical analysis.....	108
3.2.4.1. Quantification of TCC in plants and hydroponic media.....	108
3.2.4.2. Liquid Scintillation Analysis.....	110
3.2.4.3. Screening for potential metabolites of TCC using UPLC-QTOF-MS ^E and LC-MS/MS.....	110
3.2.4.4. Statistical analysis.....	113
3.3. Results and Discussion.....	114
3.3.1. Depletion of TCC in the hydroponic media.....	114
3.3.2. TCC exposure exerted no effect on growth of pepper plants.....	115
3.3.3. Accumulation and distribution of TCC and potential metabolites in plant tissues.....	116
3.3.4. Screening for TCC metabolites in plants and media.....	122
APPENDIX.....	133
REFERENCES.....	147

CHAPTER 4.....	153
UPTAKE AND METABOLISM OF SULFONAMIDES BY <i>ARABIDOPSIS THALIANA</i>	153
4.1. Introduction.....	154
4.2. Materials and Methods.....	156
4.2.1. Chemicals.....	156
4.2.2. Preparation of <i>Arabidopsis thaliana</i> seeds and culture media.....	156
4.2.3. Plant exposure to ¹⁴ C-SMX and unlabeled SMX.....	157
4.2.4. Plant exposure to ¹⁴ C-SMT and unlabeled SMT.....	158
4.2.5. Sample preparation.....	159
4.2.5.1. Hydroponic media.....	159
4.2.5.2. Plant tissues.....	160
4.2.6. Quantification of SMX and SMT by LC-MS/MS.....	160
4.2.7. Metabolite candidates screening by UPLC-QTOF-MS ^E and data processing.....	161
4.2.8. Radioactivity analysis.....	163
4.2.9. Statistical analysis.....	163
4.3. Results and Discussion.....	163
4.3.1. Sulfamethoxazole (SMX).....	163
4.3.1.1. Uptake of SMX by <i>A. thaliana</i>	163
4.3.1.2. Distribution of the ¹⁴ C-radioactivity in the <i>Arabidopsis</i> -planted treatments.....	164
4.3.1.3. Multivariate statistical analysis of the SMX dataset.....	166
4.3.1.4. Identification of the unlabeled metabolites using high-resolution MS.....	168
4.3.1.5. Identification of the ¹⁴ C-labeled metabolites on the LC-β-RAM-MS.....	171
4.3.1.6. Major transformation pathways of SMX in <i>A. thaliana</i> and implications to human health.....	174

4.3.2.	Sulfamethazine (SMT).....	183
4.3.2.1.	Root uptake and translocation of SMT.....	183
4.3.2.2.	Formation, distribution, and release of SMT metabolites	185
4.3.2.3.	Screening for SMT transformation products	188
4.3.2.4.	Abiotic transformations of SMT.....	189
4.3.2.5.	Transformation and conjugation pathways of SMT	191
4.3.2.6.	Implications to human and environmental health.....	195
	APPENDIX.....	200
	REFERENCES	239

CHAPTER 5.	247
UPTAKE AND METABOLISM OF TETRACYCLINES BY <i>ARABIDOPSIS THALIANA</i>		247
5.1.	Introduction.....	248
5.2.	Materials and Methods.....	250
5.2.1.	Chemicals.....	250
5.2.2.	Preparation of <i>Arabidopsis thaliana</i> seeds and culture media.....	250
5.2.3.	Plant material and exposure to CTC and OTC	251
5.2.4.	Sample preparation	252
5.2.5.	Quantification of CTC, 4-epi-CTC, 6-iso-CTC, and OTC by LC-MS/MS	253
5.2.6.	Metabolite candidates screening by UPLC-QTOF-MS ^E and data processing	254
5.2.7.	Statistical analysis.....	255
5.3.	Results and Discussion	256
5.3.1.	Chlortetracycline (CTC)	256
5.3.1.1.	The enol-keto forms of CTC, 4-epi-CTC, and 6-iso-CTC in the standard solutions	256
5.3.1.2.	CTC and its isomers in media and accumulation in plant tissues	257
5.3.1.3.	Screening of the CTC metabolites using multivariate statistical analysis.....	261
5.3.1.4.	Metabolism of CTC by <i>A. thaliana</i>	263
5.3.2.	Oxytetracycline (OTC)	272
5.3.2.1.	OTC dissipation in media and accumulation in plant tissues.....	272
5.3.2.2.	Screening of the OTC metabolites using multivariate statistical analysis.....	275
5.3.2.3.	Metabolism of OTC by <i>A. thaliana</i>	277
	APPENDIX.....	280
	REFERENCES	295

CHAPTER 6.	301
QUANTIFICATION OF PHYTOMETABOLITES OF SULFONAMIDES IN SOIL ECOSYSTEMS PLANTED WITH <i>ARABIDOPSIS THALIANA</i>		301
6.1.	Introduction.....	302
6.2.	Materials and Methods.....	303
6.2.1.	Chemicals.....	303
6.2.2.	Soil columns and experimental setups	304
6.2.3.	Sampling	307
6.2.4.	Sample preparation	307
6.2.5.	LC-MS-β-RAM and radioactivity analysis.....	308

6.2.6.	Statistical analysis	309
6.3.	Results and Discussion	310
6.3.1.	Dissipation of SMT and SMX in soils	310
6.3.2.	Accumulation and metabolism of SMT and SMX in plant tissues.....	313
6.3.3.	N ⁴ -glycosyl-SMT and N ⁴ -glycosyl-SMX in plant tissues	318
	REFERENCES	321
	CHAPTER 7.	325
	CONCLUSION REMARKS	325
7.1.	Research contribution to the field	326
7.2.	Research limitations.....	328

LIST OF TABLES

Table 2. 1. Current data on the antimicrobial classes recommend for use in human and veterinary medicine (as of December 2018).	7
Table 2. 2. Chemical structure and properties of TCS and TCC (Ying et al., 2007).....	18
Table 2. 3. Occurrence and concentrations of TCS and TCC in the influent, effluent, and biosolids produced in the WWTPs worldwide.....	22
Table 2. 4. Occurrence of TCS and TCC in agricultural soils receiving biosolids and/or reclaimed wastewater under “real-world” conditions.....	24
Table 2. 5. Chemical structure and properties of interested antibiotics (Peiris et al., 2017, USEPA, 2017)	26
Table 2. 6. Occurrence and concentrations of SMT and SMX in the influent, effluent, and biosolids produced in the WWTPs.....	29
Table 2. 7. Occurrence and concentrations of CTC and OTC in the influent, effluent, and biosolids produced in the WWTPs.....	30
Table 2. 8. Occurrence of SMT and SMX in animal manure	33
Table 2. 9. Occurrence of CTC and OTC in animal manure	34
Table 2. 10. Occurrence of SMT, SMX, CTC, and OTC in agricultural soils receiving animal manure under “real-world” conditions.....	37
Table 2. 11. Biotransformation products of SMT and SMX	50
Table 2. 12. Biotransformation products of CTC and OTC	53
Table 2. 13. Summary of reported TCS bioaccumulation in food crops	58
Table 2. 14. Summary of reported TCC bioaccumulation in food crops.....	59
Table 2. 15. Summary of reported SMT bioaccumulation in food crops	62
Table 2. 16. Summary of reported SMX bioaccumulation in food crops.....	63
Table 2. 17. Summary of reported CTC bioaccumulation in food crops.....	64
Table 2. 18. Summary of reported OTC bioaccumulation in food crops	65

Table 2. 19. General comparison of commercial mass analyzers in LC-MS instruments. Typical values for an m/z range of 300–400 are given. Specific instruments or configurations might achieve better figures of merits (Krauss et al., 2010).	71
Table 3. 1. Mass-Spectral Information and Proposed Structures of TCC Transformation Products Identified by Waters Progenesis QI 2.1 and MassLynx 4.1 Softwares.	130
Table 4. 1. Mass-Spectral Information and Proposed Structures of the SMX-Transformation Products Identified by Waters Progenesis QI 2.1 and MassLynx 4.1 Software.	180
Table 4. 2. Mass-Spectral Information and Proposed Structures of the SMT-Transformation Products Identified by Waters Progenesis QI 2.1 and MassLynx 4.1 Software.	197
Table 5. 1. Mass-Spectral Information and Proposed Structures of the CTC-Transformation Products Identified by Waters Progenesis QI 2.1 and MassLynx 4.1 Software.	268
Table 5. 2. Mass-Spectral Information and Proposed Structures of the OTC-Transformation Products Identified by Waters Progenesis QI 2.1 and MassLynx 4.1 Software.	279
Table 6. 1. Basic properties of the sandy loam topsoil used in this study.	304
Table 6. 2. The potential metabolites of SMT and SMX (as identified in Chapter 4), and their corresponding m/z monitored in this study.	309

LIST OF FIGURES

- Figure 2. 1. Sale and distribution of antimicrobial drugs approved for use in food-producing animals actively marketed in the U.S.: (A): During 2009-2016, (B): Data reported in 2016 by drug class and species-specific estimated sales, (C): Percentage of domestic sales and distribution in 2016 by drug class and species-specific (U.S. FDA, 2017)..... 11
- Figure 2. 2. A proposed biodegradation pathway for TCS by the *Sphingopyxis* strain KCY1 (Lee et al., 2012) 44
- Figure 2. 3. Proposed pathway for TCC biodegradation by *Sphingomonas* sp. strain YL-JM2C (Mulla et al., 2016a)..... 45
- Figure 2. 4. Proposed pathway of TCS metabolism in hair root cultures of horseradish (Macherius et al., 2014b) 57
- Figure 2. 5. Proposed metabolic pathways of TCC in jalapeno pepper plants (Huynh et al., 2018) 57
- Figure 2. 6. A proposed workflow for screening xenobiotic metabolites (Bletsou et al., 2015).. 72
- Figure 2. 7. A framework proposed by (Schymanski et al., 2014) for concisely and accurately communicating levels of confidence in high resolution mass spectrometric analysis. *Authors' note:* MS² is intended to also represent other forms of MS fragmentation (e.g. MS^e, MSⁿ). 78
- Figure 3. 1. Accumulation of TCC (¹⁴C-labeled and non-labeled) in different plant tissues: (A): roots, (B): stems, (C): leaves and (D): fruits during long-term exposure (12 weeks). Plant samples were extracted by acetone:methanol (1:1) mixture using an accelerated solvent extractor (ASE). For fruit samples, ¹⁴C was non-detectable in the ASE extracts; therefore, data of the NaClO extracts (Supplementary Table 3.1) were used. Error bars represent means ± SE (n = 5). In each panel, columns marked by different letters are significantly different from each other (*p* < 0.05)..... 116
- Figure 3. 2. Concentrations of TCC and metabolites (expressed as µg ¹⁴C-TCC equivalent/g dw) in (A): roots, (B): stems, (C): leaves and (D): fruits during long-term exposure (12 weeks). In this trial, the first fruit sampling event occurred at the 6th week. Root and stem data for week 6th and week 9th were not available since sacrificial sampling was only performed after 3 and 12 weeks. Error bars represent means ± SE (n = 5). Statistical analysis data are shown for the total ¹⁴C accumulation in plant tissues. In each panel, columns marked by different letters are significantly different from each other (*p* < 0.05)..... 119
- Figure 3. 3. Temporal variation of major phase I metabolites (2'-OH TCC, 6-OH TCC and M329) and phase II metabolites (M491a and M491b) in pepper plants during short-term metabolite screening trial. Initial exposure (0-7 days) and second exposure (7-28 days) were performed at TCC concentrations of 174.8 and 487.4 µg/L, respectively. M491a and M491b were only detected

in plant roots. Due to their trace concentrations, peak areas at $R_t = 8.39$ and 8.54 min (Figure S14) were combined and presented as M491a; likewise, peak areas at $R_t = 8.44$ and 8.59 min (Figure S15) were combined and presented as M491b. Error bars represent means \pm SE ($n = 3$). 124

Figure 3. 4. Proposed metabolic pathways of TCC in hydroponically grown jalapeno pepper plants. Accurate m/z of the metabolites were obtained using UPLC-QTOF-MS^E, and their structures were subsequently elucidated by characteristic fragmentations. The presence of DCC and 3'Cl-TCC in plant tissues was likely due to uptake of TCC impurities (dashed arrows). 125

Figure 4. 1. Distribution of the applied ¹⁴C-radioactivity in *Arabidopsis* treatments (A), and temporal variation in concentrations of ¹⁴C-SMX and its major metabolites detected in media and plant extracts using a radioactivity detector β -RAM (B and C). “M” represents media and “P” represents plant samples, respectively. Error bars represent standard error of duplicates. 164

Figure 4. 2. PCA score plots (A and B), OPLS-DA score plots (C and D) and S-plots (E and F) derived from the UPLC-QTOF-MS^E datasets of the control and SMX-exposed plants and media samples (1, 2, 4, 7, and 10 days). The ellipses represent Hotelling's T^2 with 95% confidence. The dashed rectangles on the S-plots include m/z variables that significantly contribute to the difference between the control and SMX-exposed extracts ($p(\text{corr}) \geq 0.5$). 166

Figure 4. 3. Proposed transformation pathways of SMX in *A. thaliana* plant. The occurrence of N⁴-OH SMX (TP270) was not unequivocally confirmed due to lack of adequate mass-spectral information (dashed arrow). The percentage represents the fractions of each metabolite observed over 10 days of exposure. 174

Figure 4. 4. Temporal variation of the major metabolites of SMX in plant tissues and culture media over 10 days of exposure. Error bars represent standard error of triplicates. For some points, the error bars were shorter than the height of the symbol and were not displayed on graphs. 174

Figure 4. 5. Extractable SMT concentrations in *A. thaliana* plant tissues (A), and mass balance of SMT in the culture media and plant tissues (B) over 21 days of exposure. Error bars represent standard error of triplicates; some error bars are obscured by data symbols. 183

Figure 4. 6. Formation and release of ¹⁴C-SMT metabolites by *A. thaliana* in whole-plant exposure. (A): distribution of ¹⁴C-SMT and its phytometabolites in various compartments, with radiolabel detection revealed two major extractable metabolites (M1 and M2) upon exposure of *A. thaliana* to ¹⁴C-SMT; (B) and (C): temporal variation in ¹⁴C-radioactivity of M1, M2 and ¹⁴C-SMT in plant tissues (B) and media (C) over 10 days of exposure. Error bars represent standard error of duplicates. 185

Figure 4. 7. Proposed transformation pathways of SMT in model plant *A. thaliana* and hydroponic media based on the metabolites identified in this study, and other transformation pathways of SMT in aqueous media previously described by (García-Galán et al., 2012), (Nassar et al., 2017), and (Fu et al., 2018). All of the metabolites detected in plant tissues were concurrently present in the culture media, suggesting that *A. thaliana* plants likely excreted a fraction of the metabolites following uptake and metabolism. The dashed arrows indicate that the corresponding metabolites

were also detected in the abiotic control media; consequently, their presence in plant tissues may also due to uptake of the abiotic transformation products from the media..... 191

Figure 5. 1. Temporal variations of CTC and its isomers in the *A. thaliana* plant tissues and culture media over 12 days of exposure. Data are presented as mean \pm SE of triplicates, with some error bars are obscured by data symbols..... 257

Figure 5. 2. PCA score plots (A), OPLS-DA score plots (B), and S-plots (C) derived from the UPLC-QTOF-MS^E datasets of the control and CTC-exposed plants (1, 4, 7, and 12 days). The ellipses represent Hotelling's T² with 95% confidence. The *m/z* variables on the S-plot that significantly contributed to the differences between control plants and CTC-exposed plants ($p(\text{corr}) \geq 0.5$) were selected for screening of CTC metabolites. 261

Figure 5. 3. XenoSite prediction of the glycosylation positions on the structures of CTC isomers. The scales from 0.0 to 1.0 indicate higher possibility of conjugation reactions (Dang et al., 2016). 264

Figure 5. 4. Temporal variations of the metabolites TP641 (glycosyl-CTC), TP445 (TC), and TP465 (DMC) in the *A. thaliana* plant tissues and culture media over 12 days of exposure. Data are presented as mean \pm SE of triplicates, with some error bars are obscured by data symbols. 267

Figure 5. 5. Temporal variations of OTC in the *A. thaliana* plant tissues and planted media (A), and in the control media (B) over 12 days of exposure. Data are presented as mean \pm SE of triplicates, with some error bars are obscured by data symbols. 272

Figure 5. 6. PCA score plots (A), OPLS-DA score plots (B), and S-plots (C) derived from the UPLC-QTOF-MS^E datasets of the control and OTC-exposed plants (1, 4, 7, and 12 days). The ellipses represent Hotelling's T² with 95% confidence. The *m/z* variables on the S-plot that significantly contributed to the differences between control plants and OTC-exposed plants ($p(\text{corr}) \geq 0.5$) were selected for screening of OTC metabolites. 275

Figure 6. 1 Soil column design for studying the fate of SMT and SMX in soil systems planted with *A. thaliana*..... 306

Figure 6. 2. Percentage of the extractable ¹⁴C (A) and parent SMT/SMX (B) in soils after 7 days of exposure compared to the initially added concentrations of approximately 3 nCi/g and 3 μ g/g, respectively. Error bars represent standard error of triplicates. 310

Figure 6. 3. Distribution of ¹⁴C-radioactivity into extractable and bound residues in plant tissues (A and B) and concentrations of parent SMT and SMX in *A. thaliana* plant tissues (C and D) after 7 days of exposure in the experimental soil columns. Error bars represent standard error of triplicates..... 313

Figure 6. 4. Distribution of ¹⁴C-radioactivity (in percentage) into extractable and bound residues in plant tissues after 7 days of exposure. (A): ¹⁴C-SMT treatments, (B): ¹⁴C-SMX treatments. Error bars represent standard error of triplicates..... 317

Figure 6. 5. Distribution of N⁴-glycosyl-SMT (A) and N⁴-glycosyl-SMX (B) in *A. thaliana* plant tissues after 7 days of separate exposure to SMT and SMX in the experimental soil columns. 319

KEY TO ABBREVIATIONS

3'Cl-TCC	3,3',4,4'-tetrachlorocarbanilide
ASE	Accelerated Solvent Extraction
CTC	Chlortetracycline
DCC	4,4'-dichlorocarbanilide
DPM	Disintegration Per Minute
HPLC	High Performance Liquid Chromatography
HR-MS	High Resolution-Mass Spectrometry
LC-MS	Liquid Chromatography-Mass Spectrometry
LC-MS/MS	Liquid Chromatography-Tandem Mass Spectrometry
LSC	Liquid Scintillation Counter
Me-TCS	Methyl-triclosan
MRM	Multiple Reaction Monitoring
OPLS-DA	Orthogonal Partial Least Squares-Discriminant Analysis
OTC	Oxytetracycline
PCA	Principal Component Analysis
PPCPs	Pharmaceuticals and Personal Care Products
RT	Retention time
TCC	Triclocarban
TCS	Triclosan
SMT	Sulfamethazine
SMX	Sulfamethoxazole

SPE	Solid Phase Extraction
UPLC-QTOF-MS	Ultra Performance Liquid Chromatography-Quadrupole Time of Flight- Mass Spectrometry
U.S. CDC	United States Center for Diseases Control
U.S. EPA	United States Environmental Protection Agency
U.S. FDA	United States Food and Drug Administration
VAs	Veterinary Antimicrobials
WHO	World Health Organization
WWTPs	Wastewater Treatment Plants

CHAPTER 1.
INTRODUCTION AND SCOPE

Ubiquitous occurrence of antimicrobials used in human and veterinary medicine have prompted growing concerns about antimicrobial contamination and resistance in the environment. When reaching the environment, antimicrobials undergo various degradation pathways, resulting in the formation of transformation products which are potentially bioactive or even more toxic than the parent compounds. However, the impacts of these transformation products on the ecosystems are still largely unknown.

Uptake and accumulation of antimicrobials by food crops grown in contaminated soils has been well-documented in the literature. Therefore, unintentional human exposure to antimicrobials through consuming contaminated food crops is obviously of great concern. While in the past, studies and risk assessments related to plant uptake and accumulation of these xenobiotics mainly addressed the unaltered parent compounds, recent research has shifted toward the formation, fate, and toxicity of their conjugated metabolites. It has been reported that these metabolites may account for more than 90% of all chemical species in the plant tissues. Nevertheless, their fate once ingested by humans and animals, with respect to back-transformation (from metabolites to parents) potential, is also largely unknown.

The *overall aim* of this research is to elucidate the metabolic pathways, including quantifying the production of metabolites of antimicrobials in plants. The proposed research will evaluate *the central hypothesis that plants will bioaccumulate antimicrobials upon exposure and subsequently metabolize these compounds through several transformation and conjugation reactions, forming metabolites that are readily reverted to the parent compound during human and animal digestion*. Accordingly, the obtained results will address the gaps of existing research on the fate of antimicrobials in planted systems, through use of state-of-the-art instrumentation (e.g. HPLC-high resolution mass spectrometer) in combination with targeted and untargeted

metabolomic approaches, which will facilitate the detection, confirmation and quantification of the antimicrobials and their transformation products at trace levels. In order to determine the role and relevance of phytometabolism in fate of antimicrobials, the following *specific aims* will be achieved:

1) *Elucidate the fate and metabolites of the antimicrobial triclocarban in crop plants, with a case study on hydroponically grown jalapeno pepper plants.* The *working hypothesis*, based on a current literature review and preliminary results, is that pepper plants will bioaccumulate considerable concentrations of triclocarban and subsequently transform the antimicrobial via the “green liver model” to produce phase I hydroxylated triclocarban followed by phase II conjugation with carbohydrates, or direct conjugation with glutathione.

2) *Elucidate the fate of antibiotics (sulfonamides and tetracyclines) in model plant Arabidopsis thaliana under hydroponic conditions.* The *working hypothesis*, based on a current literature review, is that *A. thaliana* will predominantly metabolize antibiotics through conjugation with glucopyranosides followed by further conjugation with malonyl and oligoglycoside molecules. Additionally, phase I transformations will be limited to hydroxylation prior to conjugation.

3) *Quantifying the production of phytometabolites of antimicrobials in soil ecosystems planted with Arabidopsis thaliana.* The *working hypothesis* is that plant uptake and phytometabolism will outcompete microbial and chemical degradation of antibiotics, thereby representing the largest mass loss of antibiotics from soils.

CHAPTER 2.
LITERATURE REVIEW

2.1. The status quo of use and regulations of antibiotics

“I did not invent penicillin. Nature did that. I only discovered it by accident”

– Alexander Fleming (1881 – 1955)

The discovery of penicillin by Sir Alexander Fleming in 1928 started the modern era of antibiotics, which has saved millions of lives and earned Dr. Fleming the 1945 Nobel Prize in Physiology/Medicine – together with Howard Florey and Ernst Chain, who devised methods for mass production of penicillin (Tan and Tatsumura, 2015).

According to the current definitions of the World Health Organization (WHO), ***antibiotics*** “are agents or substances that are produced from microorganisms that can act against another living microorganisms”, while ***antimicrobials*** “are derived from any sources (microorganisms, plants, animals, synthetic or semisynthetic) that act against any type of microorganism”. Accordingly, all antibiotics are antimicrobials, but not all antimicrobials are antibiotics (World Health Organization, 2017). Since 2005, WHO has published a list of important antimicrobials for human medicine, with regular revision, to be used as a basis for promoting their prudent use. The 5th revision list (published in April 2017) contains 32 drug classes (291 individual drugs) categorized as either “Critically important”, “Highly important”, or “Important”. Some antimicrobials are used only in humans, some in both humans and animals, and some only for animals (World Health Organization, 2017). Notably, most antimicrobials used in animals are medically important for humans. Quinolones, 3rd and higher generation cephalosporins, macrolides and ketolides, glycopeptides, and polymyxins (colistin) are considered highest priority amongst the important antimicrobials (World Health Organization, 2017). Of the 291 drugs on the WHO list of medically important antimicrobials, only 38 are currently recommended for use in food-producing animals (World Health Organization, 2017). In 2016, there were 42 antimicrobials being approved and

actively marketed for use in food-producing animals in the United States, of which 31 are categorized as important to humans medicine (U.S. FDA, 2017). These antimicrobial drug classes and their corresponding active ingredients are shown in the Supplementary Table 2.1.

Surveillance data on national and global trends of antimicrobial consumption over time is vitally important since the data will assist in forming policies that optimize the use of antimicrobials, as well as minimizing antimicrobial resistance. According to a recent study by Klein et al., between 2000 and 2015, global antimicrobial consumption in humans increased by 65%, from 21.1 to 34.8 defined daily doses (DDDs), while consumption rate increased 39%, from 11.3 to 15.7 DDDs per 1000 inhabitants per day, primarily driven by rising consumption in low- and middle-income countries. The massive increase in antimicrobial consumption in these countries correlates with the growing gross domestic product per capita and has been converging towards high-income country levels (Klein et al., 2018).

Table 2. 1. Current data on the antimicrobial classes recommend for use in human and veterinary medicine (as of December 2018).

Antimicrobial classes	Both humans and veterinary medicine (WHO)¹	Veterinary use only (WHO)¹	Approved for used in food animals (U.S.)²
Critically Important Antimicrobials			
Aminoglycosides	14	1	5
Ansamycins	5		
Carbapenems and other penems	7		
Cephalosporins (3rd, 4th, and 5th gen)	28	3	2
Glycopeptides and lipoglycopeptides	5	1	
Glycylcyclines	1		
Lipopeptides	1		
Macrolides and ketolides	18	7	7
Monobactams	2		
Oxazolidinones	4		
Penicillins (natural, aminopenicillins, and antipseudomonal)	29	1	
Phosphonic acid derivatives	1		
Polymyxins	2		1
Quinolones and fluoroquinolones	29	7	2
Drugs used solely to treat tuberculosis or other mycobacterial diseases	15		
Highly Important Antimicrobials			
Amidinopenicillins	2		
Amphenicols	2	1	1

Table 2.1 (cont'd). Current data on the antimicrobial classes recommend for use in human and veterinary medicine (as of December 2018).

Antimicrobial classes	Both humans and veterinary medicine (WHO)¹	Veterinary use only (WHO)¹	Approved for used in food animals (U.S.)²
Cephalosporins (1st and 2nd gen) and cephamycins	26	1	
Lincosamides	2	1	2
Penicillins (antistaphylococcal)	5		4
Pseudomonic acids	1		
Riminofenazines	1		
Steroid antibacterials	1		
Streptogramins	2	1	1
Sulfonamides, dihydrofolate reductase inhibitors and combinations	26	2	3*
Sulfones	2		
Tetracyclines	12		3
Important Antimicrobials			
Aminocyclitols	1		
Cyclic polypeptides	1		
Nitrofurantoin	4	1	
Nitroimidazoles	3		
Pleuromutilins	1	2	
Currently not used in humans (food animals only)		9	
Total	253	38	31

¹(World Health Organization, 2017); ²(U.S. FDA, 2017)

*Including ormetoprim, sulfadimethoxine, and sulfamethazine

2.1.1. Antimicrobial use in livestock

Agricultural sectors represent the largest shares of the global antimicrobial consumption, with veterinary antimicrobials (VAs) extensively used worldwide to protect or improve animal health, and to stimulate growth and maximize profits (Kuppusamy et al., 2018, O'Neill, 2015). Antimicrobials administered to healthy animals to enhance growth is potentially the most controversial use, which has been banned in many countries. However, implementing and monitoring of these bans are often insufficient, especially in the low- and middle-income countries (Schar et al., 2018). The actual amount of antimicrobials used in food-producing animals globally is difficult to estimate because of poor surveillance and data collection in many countries (Kuppusamy et al., 2018). It has been estimated that more than 50% of the medically important antimicrobials sold in most countries are used in animals (O'Neill, 2015), while that in the U.S. is approximately 80% (Ventola, 2015). A recent survey of the 28 European Union countries revealed that 3,821 tons of active antimicrobial substances were sold for human use, while 8,927 tons for food-producing animals in 2014 (ECDC/EFSA/EMA, 2017). The average consumption (expressed as mg/kg of estimated biomass) in food-producing animals was 152 mg/kg, compared to 124 mg/kg in humans. However, the antimicrobial consumption was lower in food-producing animals than in humans in 18 out of 28 countries included in the survey, with only eight countries had higher antimicrobial consumption in food-producing animals than in human (ECDC/EFSA/EMA, 2017).

China is one of the world's largest producers and consumers of antimicrobials for animals (Qiao et al., 2018). In 2013, the total antimicrobial consumption in China was approximately 162,000 tons, of which 84,240 tons were used in animals (Zhang et al., 2015). That was approximately six times larger than the total sale and distribution of antimicrobials approved for

used in food-producing animals in the U.S. in 2016 (approximately 14,000 tons) (Figure 1A) (U.S. FDA, 2017). Amoxicillin, florfenicol, lincomycin, penicillin, and enrofloxacin were the major VAs used in China, with the consumption rates >4,000 tons (Qiao et al., 2018, Van Boeckel et al., 2015, Zhang et al., 2015). In 2016, domestic sales of tetracyclines in the U.S. accounted for 70% of the medically important antimicrobials used in animals, followed by penicillins (10%), macrolides (7%), sulfonamides (sulfas) (4%), aminoglycosides (4%), and lincosamides (2%); each fluoroquinolones and cephalosporins accounted for less than 1% of the total sales (Figure 1B). Additionally, most of the domestic sales was intended for use in cattle (43%), followed by swine (37%), turkeys (9%), chickens (6%), and other species (4%) (Figure 1C). In European countries, the veterinary antimicrobial classes with highest consumption in 2014 were tetracyclines (33%), penicillins (25%), and sulfonamides (11%) (ECDC, 2015).

Using statistical models combining maps of livestock densities, economic projections of demands for meat products, and current estimates of antimicrobial consumption in high-income countries, Van Boeckel et al. projected a 67% increase in the global consumption of antimicrobials for food animals between 2010 and 2030, from approximately 63,000 tons to 105,000 tons, mainly due to shifting from “extensive farming” towards “large-scale intensive farming” operations in middle-income countries. The projected increase is set to double for the major emerging economies, including Brazil, Russia, India, China, and South Africa (BRICS countries). The authors also estimated that the global average annual consumption of antimicrobials per kilogram of animal produced was 45 mg/kg, 148 mg/kg, and 172 mg/kg for cattle, chicken, and pigs, respectively (Van Boeckel et al., 2015).

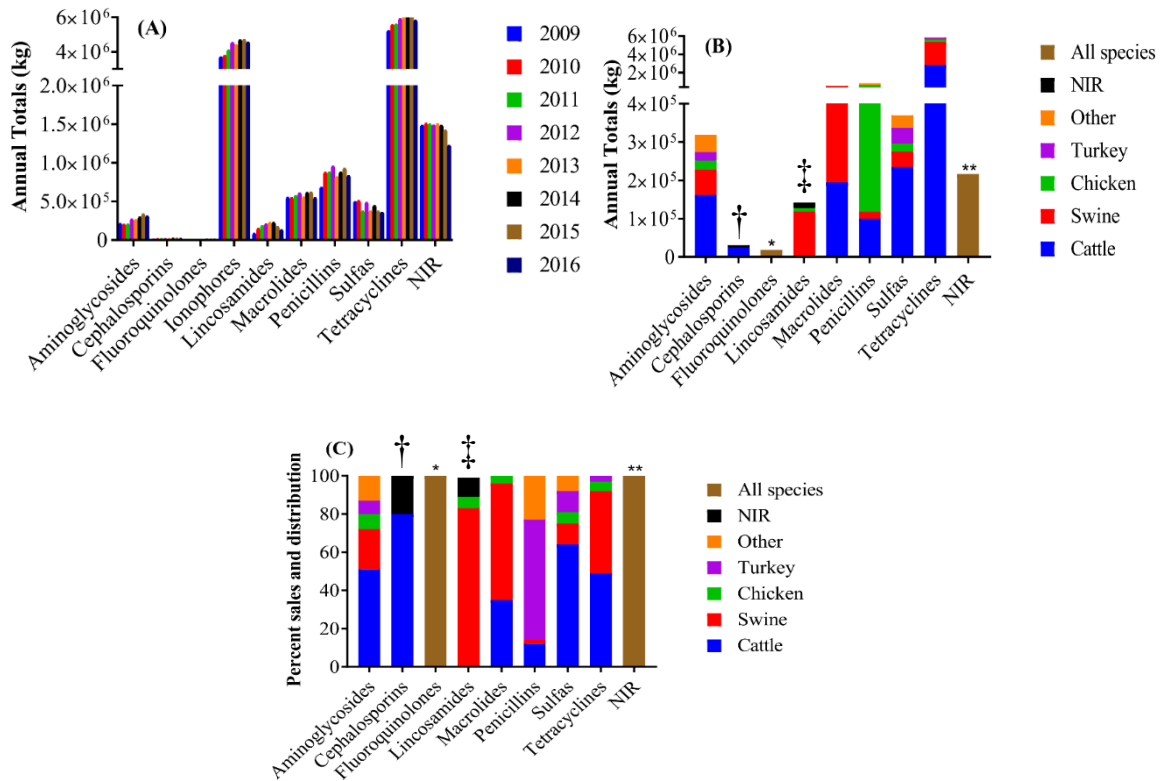


Figure 2. 1. Sale and distribution of antimicrobial drugs approved for use in food-producing animals actively marketed in the U.S.: (A): During 2009-2016, (B): Data reported in 2016 by drug class and species-specific estimated sales, (C): Percentage of domestic sales and distribution in 2016 by drug class and species-specific (U.S. FDA, 2017).

kg = kilogram of active ingredient.

* This category includes the following: Cattle, Swine, and Other.

** This category includes the following: Cattle, Swine, Chicken, Turkey, and Other.

† NIR = Not Independently Reported. Species-specific sales estimates for which there were fewer than three distinct sponsors actively marketing products domestically are not independently reported. This category includes the following: Swine, Chicken, and Other.

‡ NIR = Not Independently Reported. Species-specific sales estimates for which there were fewer than three distinct sponsors actively marketing products domestically are not independently reported. This category includes the following: Cattle and Other.

2.1.2. Antimicrobial use in aquaculture

Aquaculture is the fastest growing food-production industry that accounts for nearly half of the fish consumed by humans worldwide (Okocha et al., 2018). The rapid growth of aquaculture requires uses of intensive and semi-intensive practices, leading to higher densities of animals in

limited spaces of water, substantially promoting the conditions that favor the development of contagious diseases (Santos and Ramos, 2018). Therefore, antimicrobials have been widely used in aquaculture to prevent and treat bacterial diseases in fish and invertebrates (Cabello, 2006). Antimicrobials used in aquaculture are mainly administered in feed, occasionally by bath (immersion of the animals in closed containers with antimicrobials), and to groups with sick, healthy, and carrier individuals (Cabello et al., 2016). It has been reported that as much as 80% of the administered antimicrobials in aquaculture are dispersed into water and sediments close to the application sites (Santos and Ramos, 2018). Additionally, ingested antimicrobials are excreted largely intact, together with their metabolites. The residual antimicrobials and their metabolites persist in the aquatic sediments for months at sufficiently high concentrations to exert selection on the bacterial communities in the aquatic environments (Cabello et al., 2016).

Aquacultural use of antimicrobials has been restricted in developed countries in order to cope with the potential selection for antimicrobial resistance in humans (Cabello et al., 2013). In European countries, oxytetracycline, florfenicol, sarafloxacin, erythromycin, and sulfonamides are authorized for use in aquaculture, while oxytetracycline, florfenicol, and sulfadimethoxine/ormetoprim are authorized for used in aquaculture in the U.S. (Santos and Ramos, 2018). Except from these two regions, data on the amounts and classes of antimicrobials used in aquaculture are scarce, especially in countries where control is less stringent or lacking (Cabello et al., 2013). For example, China, accounting for 67% of the total worldwide aquaculture, does not require veterinary prescriptions for use of antimicrobials in animals. Despite its efforts to implement stricter regulations to the aquaculture industry in the last few years, several reports still indicate that the enforcement of these regulation is lax (Chen et al., 2012a). Likewise, antimicrobial sale and usage in India, the second largest aquaculture producer with 8% of the total worldwide

production, are not regulated (Done et al., 2015). Detection of nitrofurans in aquacultural products imported to the U.S. from China, as well as chloramphenicol and metronidazole imported from China, Indonesia, Taiwan, Thailand, and Vietnam, to European markets further demonstrated the lax for control of antimicrobial use in these top aquacultural producers (Cabello et al., 2013). Moreover, data regarding antimicrobial consumption in agricultural and aquaculture vary largely depending on the regions and differences between countries could be very pronounced. For example, the amount of antimicrobials used to produce 1 tons of salmon in Chile was approximately 279 g while in Norway, only 4.8 g of antimicrobials was used for the same amount of salmon (Santos and Ramos, 2018). Norway, the Netherlands, and Denmark can be considered the models in minimizing the use of antimicrobials in food-producing animals, without negative impacts on the quality and safety of the food, as well as without a damaging economic impact (Santos and Ramos, 2018).

2.1.3. Curtailing antimicrobial use and resistance

Recent studies and reports have revealed positive associations between antimicrobial consumption and resistance to different classes of antimicrobials in both humans and animals (ECDC/EFSA/EMA, 2017). According to WHO's definitions: "antimicrobial resistance (AMR) is the ability of a microorganism (like bacteria, viruses, and some parasites) to stop an antimicrobial (such as antibiotics, antivirals, and antimalarials) from working against it. As a result, standard treatments become ineffective, infections persist and may spread to others". This can occur naturally through adaptation to the environment or through exposure to synthetic antimicrobials that are inappropriately and excessively used in anthropogenic activities. The U.S. Center for Diseases Control estimates that 30% of all antimicrobials prescribed by outpatient clinics in the U.S. are unnecessary or incorrectly (CDC, 2017). Misuse of antimicrobials is even more

problematic in clinical centers in developing countries. In China, about 75% of patients with seasonal influenza are prescribed antibiotics, and the rate for inpatients is 80% (Qiao et al., 2018). In addition to inappropriate use of antimicrobials in human medicine, overuse of these drugs in food-producing animals and aquaculture has prompted serious concerns about antimicrobial contamination and resistance in the ecosystems. Due to their highly bioactive nature, the presence of antimicrobials, even at trace concentrations, has been linked to alteration of the composition of bacterial communities, causing or promoting antimicrobial resistance. More importantly, some last-resort antimicrobials for humans are also being extensively used in animals, such as colistin (polymyxins) (Santos and Ramos, 2018). In 2014, the consumption of polymyxins in food-producing animals greatly exceeded their use in human medicine (10 mg/kg versus 0.03 mg/kg of estimated biomass, respectively) (ECDC/EFSA/EMA, 2017). Recent outbreaks in hospitals with carbapenemase-producing *Enterobacteriaceae* and multidrug-resistant *Pseudomonas* and *Acinetobacter* species have led to the re-introduction of colistin as a last-resort antimicrobial (Santos and Ramos, 2018). In 2015, Liu et al. published the first evidence of a plasmid-mediated *mcr-1* gene that conferred colistin resistance in China (Liu et al., 2016). The authors reported the presence of this gene in 20% of the test animals and in 1% of the human population, clearly indicating that the use of colistin in animals has resulted in the selection of this resistance, and that the gene can be transferred to humans (Liu et al., 2016, Santos and Ramos, 2018).

Antimicrobial resistance is a global public health threat that requires aggressive actions from all stakeholders. In May 2015, the WHO endorsed a global action plan to tackle antimicrobial resistance. The global action plan sets out five strategic objectives: (i) to improve awareness and understanding of antimicrobial resistance; (ii) to strengthen knowledge through surveillance and research; (iii) to reduce the incidence of infection; (iv) to optimize the use of antimicrobial agents;

and (v) develop the economic case for sustainable investment that takes account of the needs of all countries and increase investment in new medicines, diagnostic tools, vaccines, and other interventions. On September 25th, 2018, the U.S. Centers for Disease Control and Prevention and U.S. Department of Health and Human Services launched the Antimicrobial Resistance Challenge at the United Nations General Assembly meeting. The challenge calls on governments, private industry, and civil society to commit to taking actionable steps that further progress in combating antibiotic resistance around the world. In 2014, the White House announced the National Strategy for Combating Antibiotic-Resistant Bacteria. The plan outlines five main goals for combating antibiotic resistance. Each goal has accompanying milestones to be achieved by 2020. The goals serve as a roadmap for the federal agencies working to preserve antibiotic efficacy. Many countries have already taken actions to reduce the use of antimicrobials in food-producing animals. In 2015, California was the first state in the U.S. to pass legislation that goes far beyond federal rules. California Senate Bill No. 27 (January 1st, 2018) requires a veterinarian's prescription for use of antimicrobials and ban non-therapeutic use of antimicrobials for disease prevention and growth promotion in livestock (State of California, 2015). In May 2017, the State of Maryland also adopted a law banning routine antimicrobial use for livestock on farms (State of Maryland, 2017). At the federal level, regulations by the U.S. FDA, that went into effect in January 1st, 2017, required retail establishments that sell medically important antimicrobials for use in feed or water for food-producing animals to change the marketing status from over-the-counter (OTC) to prescription (Rx) or to veterinary feed directive (VFD) (U.S. FDA, 2016a). In Europe, the European Union banned the use of antimicrobial growth promoters in animal feed in 2006. Several countries have also launched national programs and reporting systems for surveillance of

antimicrobial consumption and resistance in bacteria from animals, foods, and humans (e.g. DANMAP in Denmark, Nethmap in the Netherlands).

In order to effectively control the antimicrobial prescribing patterns, the Ministry of Health of China launch a National Action Plan in 2011 for antimicrobial stewardship targeting antimicrobial misuse in public hospitals (Bao et al., 2015). The Action Plan, which was a combination between managerial and professional strategies, effectively reduced the frequency and the intensity of antimicrobial consumption, patients' costs on antimicrobials, and duration of peri-operative antimicrobial treatment in clean surgeries (Bao et al., 2015). Antimicrobial prescription to hospitalized patients dropped from 68% in 2011 to 58% by the end of 2012. Additionally, the percentage of outpatients who were prescribed antimicrobial drugs also dropped from 25% to 15% in the same period (Qiao et al., 2018). Chinese government have also launched regulations on antimicrobial use in animals since the early 2000s (Xie et al., 2018). For example, use of chloramphenicol, metronidazole, and nitrofurantoin in animal production was banned in 2002 (Mo et al., 2017). The direct injections of oxytetracycline and chlortetracycline hydroxide were also banned in 2007. In 2014, prescription for veterinary antimicrobials was also required following implementation of the "Management of Prescription and Non-prescription Drugs for Animals" (Xie et al., 2018). Nevertheless, farmers can still purchase antimicrobial drugs directly from chemical companies, as well as via the internet (including the banned chloramphenicol and metronidazole), without a prescription (Mo et al., 2017). Additionally, limited legislation or regulations are currently available to control the misuse of antimicrobials in disease prevention and growth promotion (Xie et al., 2018).

2.2. Sources and occurrence of antimicrobials in the environment

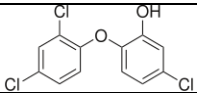
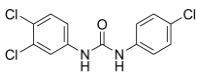
Overuse of antimicrobials in human medicine and food-producing animals has prompted concerns about occurrence of antimicrobial residues and metabolites in the environment, and the potential adverse impacts on ecological and human health. Antimicrobials enter the environment primarily through excreted wastes of animals and humans after medication, disposal of unused or expired drugs, manufacturing and hospital wastewater, field application of reclaimed wastewater, biosolids, and manure containing antimicrobial residues and metabolites (Pan and Chu, 2017a, Sarmah et al., 2006a). Antimicrobials prescribed for human use are eventually excreted into domestic sewage and are discharged to wastewater treatment plants (WWTPs) along with their metabolites. Elimination of antimicrobials in WWTPs was found to be relatively low; consequently, biosolids and sewage effluents are considered the main sources of these antimicrobials and metabolites (Pan and Chu, 2017a). Moreover, negative removal efficiencies for antibiotics are commonly reported (García-Galán et al., 2011a, Göbel et al., 2007, Gros et al., 2010). This observation can be attributed to the presence of transformation products (e.g. acetylated metabolites) that are totally or partially cleaved by bacteria and reverted back to the parent forms during wastewater treatment processes (García-Galán et al., 2012a). Likewise, the excretion of urine and feces from medicated animals and amendment of contaminated manures on agricultural soils as fertilizer serve as the major pathways by which antimicrobials and their metabolites enter the environment (Pan and Chu, 2017a).

2.2.1. Triclosan and triclocarban

Triclosan (5-chloro-2-[2,4-dichloro-phenoxy]-phenol; TCS) and triclocarban (3,4,4'-trichlorocarbanilide; TCC) are structurally similar antimicrobial agents (Table 2.2) commonly found in household and personal care products. The amount of TCS and TCC incorporated into

consumer products typically ranges from 0.1–0.3% (w/w), exhibiting a broad-spectrum activity against bacteria, molds, and yeasts (Clarke and Smith, 2011). It had been estimated that U.S. annual disposal of TCS and TCC into wastewater totals more than 300 and 330 tons/year, respectively (Halden and Paull, 2005). However, in 2016, the U.S. Food and Drug Administration (FDA) issued a final rule on elimination of over-the-counter consumer antiseptic wash products containing TCS and TCC due to lack of scientific evidence that they are more effective than plain soap and water in preventing human illness and reducing infection (U.S. FDA, 2016b). As a result, emission of both TCS and TCC into the municipal wastewater treatment systems in the U.S. is expected to decline in the coming years.

Table 2. 2. Chemical structure and properties of TCS and TCC (Ying et al., 2007).

Properties	TCS	TCC
Structure		
CAS No	3380-34-5	101-20-2
Formula	C ₁₂ H ₇ Cl ₃ O ₂	C ₁₃ H ₉ Cl ₃ N ₂ O
M.W	289.5	315.6
Boiling point (°C)	373.62	434.57
Melting point (°C)	136.79	182.04
pKa	7.9	12.7
Water solubility (mg/L)	4.621	0.6479
Vapor pressure (mm Hg at 25°C)	4.65 x 10 ⁻⁶	3.61 x 10 ⁻⁹
Log K _{ow}	4.7	4.9

2.2.1.1. Wastewater treatment plants

Given their wide use in personal care products, TCS and TCC are among the most frequently detected pollutants in both influents, effluents, and biosolids of WWTPs worldwide (Table 2.3). As such, municipal WWTPs are considered the main pollution source of TCS and TCC due to discharge of reclaimed wastewater and reuse of biosolids as fertilizer on agricultural soils. As shown in Table 2.3, the concentrations of TCS and TCC in the influents fluctuated and

greatly differed among countries, from below method limit of detection to several part-per-billion ($\mu\text{g/L}$). The highest concentrations were found in the U.S., with TCS and TCC concentrations in the effluents reached up to 86,161 ng/L and 36,221 ng/L, respectively (Kumar et al., 2010). These data were from studies conducted prior to the FDA's ban on the use of TCS and TCC in consumer wash products in the U.S (U.S. FDA, 2016b). Concentrations of both antimicrobials in WWTPs across the U.S. are expected to decrease when the ban came into effect in 2016; however, no published data with samples collected after 2016 to date could be found. The levels of TCS and TCC entering WWTPs also varied substantially among different sampling locations within the same country (e.g. China), most likely attributed to variations in sampling procedures, wastewater treatment technologies, and urbanization levels of the cities (Wang et al., 2018). In effluents, the levels of TCS and TCC were much lower than in the influents reported in most of the studies, mostly varying from below limit of detection to a few hundreds of ng/L. However, negative removal efficiencies were also reported in recent studies. For example, Wang et al. reported higher concentrations of both TCS and TCC in the effluents of WWTPs located in the southeast of China, likely due to conversion of their metabolites/conjugates to the parent compounds during wastewater treatment processes (Wang et al., 2018). Negative removal efficiencies were also observed for other pharmaceuticals in earlier studies (García-Galán et al., 2011a, Göbel et al., 2007, Gros et al., 2010, Hedgespeth et al., 2012, Jelic et al., 2015). Although the transformation products may not be as bioactive as the parent compounds, an estimation of the conjugated analytes in the influents is essential for subsequent mass balance calculation (Wang et al., 2018).

Due to their high octanol/water partitioning coefficients ($\log K_{ow}$ of 4.8 and 4.9 for TCS and TCC at neutral pH, respectively) the two antimicrobials are primarily removed from wastewater by adsorption to biosolids. TCS and TCC are the most frequently detected organic

pollutants in biosolids worldwide. The national sewage sludge survey by the U.S. EPA indicated that 92.4% and 100% of biosolids samples in the U.S contained TCS and TCC, respectively (U.S. EPA, 2009). Of the 72 pharmaceuticals and personal care products (PPCPs) in the U.S. EPA archived biosolids collected from 32 states and the District of Columbia, TCS and TCC were the most abundant contaminants with mean concentrations of 12,600 $\mu\text{g}/\text{kg dw}$ for TCS and 36,000 $\mu\text{g}/\text{kg dw}$ for TCC, respectively (McClellan and Halden, 2010). Therefore, the maximum projected annual land application of TCS and TCC is 52 tons/year and 150 tons/year, respectively (McClellan and Halden, 2010). However, emission of TCS and TCC through biosolids is also expected to decrease in the U.S. following the FDA's ban on use of TCS and TCC in personal care wash products (U.S. FDA, 2016b). The occurrence of TCS and TCC in biosolids have also been commonly reported in China (Sun et al., 2016, Wang et al., 2018), Singapore (Tran et al., 2016), South Korea (Ryu et al., 2014), India (Subedi et al., 2015), Canada (Kim et al., 2014) (Table 2.3).

2.2.1.2. Biosolids-amended soils

Land application of treated biosolids is a common practice in many countries. In the U.S., approximately 60%, or 3.4 - 4.2 million tons, of biosolids produced have annually been applied to land as soil amendment (McClellan and Halden, 2010). Fate of TCS and TCC in land applied biosolids has been reported in several studies (Al-Rajab et al., 2015, Chen et al., 2014, Fu et al., 2016, Higgins et al., 2011). However, most of these studies were conducted in laboratory settings or in small plots under well-controlled conditions, which are difficult for extrapolating to commercially applied fields (Lozano et al., 2018). Table 2.4 presents data from studies under "real-world" field conditions. Both TCS and TCC can be detected in soils several months after the last biosolids application, in which concentrations of TCC were found to be higher than those of TCS in most of the studies. Lozano et al. reported that TCC was highly persistent in biosolids-amended

soils several years after application (45.8 ± 6.09 and 72.4 ± 15.3 $\mu\text{g}/\text{kg}$ dw after 7 and 8 years, respectively) (Lozano et al., 2018).

Table 2. 3. Occurrence and concentrations of TCS and TCC in the influent, effluent, and biosolids produced in the WWTPs worldwide.

Country	Year of sampling	TCS			TCC			References
		Influent (ng/L)	Effluent (ng/L)	Biosolids ($\mu\text{g}/\text{kg dw}$)	Influent (ng/L)	Effluent (ng/L)	Biosolids ($\mu\text{g}/\text{kg dw}$)	
China	2016	<LOD – 62.9	<LOD – 88.8	43.9 – 659	<LOD – 129	4.78 – 500	365 – 3,760	(Wang et al., 2018)
China	2016 – 2017	59 – 2,900	13 – 180	na	100 – 1,900	1.5 – 86	na	(Li et al., 2018)
Ireland	2015	na	na	610	na	na	80	(Healy et al., 2017)
Singapore	2015	34.1 – 743.9	28.5 – 45.9 8.4 – 120.8	na	423.9 – 933.9	143.1 – 214.5 49.1 – 263.9	na	(Tran et al., 2016)
China	2014	1.3 – 211	25.9 – 111	354 – 608	4.7 – 76.2	27.6 – 109	1,130 – 2,180	(Sun et al., 2016)
Canada	2014*	2,230 – 3,380	<70.9	6,990 – 18,300	70.9 – 78.4	4.43 – 6.41	2,510 – 4,160	(Kim et al., 2014)
South Korea	2012 – 2013	86 – 190	62 – 63	na	76 – 198	33 – 45	na	(Ryu et al., 2014)
Australia	2012 – 2013	1,854 \pm 10.8 – 3,544 \pm 27.2	4.1 \pm 0.1 – 5.4 \pm 3.3	na	na	na	na	(Roberts et al., 2016)
India	2012	145 – 2,500	<10 – 2,500	645 – 1,470	515 – 8,880	22.4 – 5,860	5,570 – 8,460	(Subedi et al., 2015)
China	2012*	113 \pm 9	18.9 \pm 0.4	0.7 \pm 0.3	267 \pm 18	32.6 \pm 2.3	887 \pm 39	(Chen et al., 2012b)
Canada	2010 – 2012	340 – 2,900	64 – 490	2,000 – 11,000	14 – 270	3.1 – 33	1,200 – 8,900	(Guerra et al., 2014)
United States	2009 – 2010	1313 – 11,185	<50 – 409	na	1,030 – 11,600	43 – 1,260	na	(Hedgspeth et al., 2012)
United States	2009	8,050 \pm 210	230 \pm 60	16,200 \pm 2,600	4,920 \pm 450	120 \pm 10	12,600 \pm 2,100	(Lozano et al., 2013)
Spain	2009*	<LOQ – 936	<LOQ – 59.0	na	<LOQ – 4.7	<LOQ	na	(Gonzalez-Marino et al., 2009)
China	2008	711.5 – 2,301	80.7 – 111.8	na	1,217 – 2,354	129.5 – 202.4	na	(Yu et al., 2011)

Table 2.3 (cont'd). Occurrence and concentrations of TCS and TCC in the influent, effluent, and biosolids produced in the WWTPs worldwide.

United Kingdom	2008*	70	33	na	na	na	na	(Kasprzyk-Hordern et al., 2008)
United States	2007	13,703 – 86,161	261 – 4,760	515 – 1.611	3,505 – 36,221	157 – 1,372	466 – 1,425	(Kumar et al., 2010)
Hong Kong	2005 – 2006	142 ± 16.5 – 213.8 ± 20.6	22.5 ± 1.4 – 177.3 ± 21.5	na	na	na	na	(Wu et al., 2007)
United States	2002 – 2004	6,100 ± 1,600	35 ± 20	na	6,700 ± 100	110 ± 10	na	(Halden and Paull, 2005)
Canada	2004	870 – 1,830	50 – 360	na	na	na	na	(Lee et al., 2005)

Year of publication since sampling year was not clarified in the articles.

LOD: limit of detection; LOQ: limit of quantification

na: data not available

Table 2. 4. Occurrence of TCS and TCC in agricultural soils receiving biosolids and/or reclaimed wastewater under “real-world” conditions.

Country	Year of sampling	Sources	Number of sampling site	TCS (µg/kg dw)	TCC (µg/kg dw)	Reference
China	2012	Biosolids	3	0.7 ± 0.3	10.5 ± 2.4	(Chen et al., 2012b)
United States	2012	Biosolids	1	2.7 – 4.4*	14.8 – 27.3*	(Sherburne et al., 2016)
United States	2005-2007	Biosolids	26	na	45.8 ± 6.09 – 72.4 ± 15.3	(Lozano et al., 2018)
Canada	2012	Biosolids	1 (with 4 sub-plots)	1.3 – 5.5	11.3 – 21.8	(Macherius et al., 2014a)
Mexico	2010	Irrigation	4	nd – 35.3	na	(Gibson et al., 2010)
United States	2008	Biosolids	19	1.6 – 11	2.8 – 209	(Wu et al., 2010a)
United States	2009	Biosolids	19	nd	4.9 – 221	(Wu et al., 2010a)
United States	2007	Biosolids	10	0.39±0.26	3.6±2.1	(Cha and Cupples, 2009)
United States	2008	Biosolids	10	0.16±0.08	11.6±19.2	(Cha and Cupples, 2009)
United States	2005	Biosolids	3	nd – 833	na	(Kinney et al., 2008)

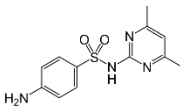
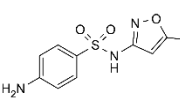
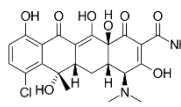
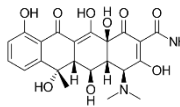
nd: not detected (< LOD values); na: data not available

*Concentrations reported on wet weight basis.

2.2.2. Sulfonamides and tetracyclines

Over the last few decades, antimicrobials have been recognized as emerging contaminants due to their negative impacts on the ecological and human health. Both sulfonamides and tetracyclines are broad-spectrum antimicrobials that are widely used in veterinary and human medicine. Sulfonamides inhibit growth of bacteria by interrupting their utilization of *p*-aminobenzoic acid in the synthesis of folic acid and ultimately of purine and DNA (García-Galán et al., 2008). Sulfonamide molecules consist of a benzene ring, an amine moiety (-NH₂), and a sulfonamide group (-SO₂NH₂). The amine and sulfonamide groups must be at the *para* position to each other for the sulfonamide to have antibacterial properties (Sarmah et al., 2006b). Most sulfonamides have at least two active nitrogen atoms in their molecules: the -NH₂ attached to the -SO₂ referred to as N¹ and deprotonated at pH >5.5–7. The -NH₂ attached to the aromatic ring referred to as N⁴ and deprotonated at pH 2.5. Therefore, most sulfonamides are positively charged under acidic conditions, neutral between 2.5–6, and negatively charged at alkaline conditions (Sarmah et al., 2006b). Tetracyclines inhibit synthesis of bacterial protein by preventing the association of aminoacyl-tRNA with the bacterial ribosome (Chopra and Roberts, 2001). Tetracyclines are characterized by a partially conjugated four-ring structure with several ionizable functional groups, and the charge of tetracycline molecules depends on the solution pH (Sarmah et al., 2006b). At environmental pH, tetracyclines may exist as cation, zwitterion, or net negatively charge ion (Sarmah et al., 2006b).

Table 2. 5. Chemical structure and properties of interested antibiotics (Peiris et al., 2017, USEPA, 2017).

Properties	SMT	SMX	CTC	OTC
Structure				
CAS No	57-68-1	723-46-6	57-62-5	79-57-2
Formula	C ₁₂ H ₁₄ N ₄ O ₂ S	C ₁₀ H ₁₁ N ₃ O ₃ S	C ₂₂ H ₂₃ ClN ₂ O ₈	C ₂₂ H ₂₄ N ₂ O ₉
M.W	278.3	253.3	478.9	460.4
Boiling point (°C)	451.2	414.0	764.0	781.7
Melting point (°C)	189.8	172.4	335.9	344.2
pKa (at 25°C)	2.65; 7.65	1.6; 5.7	3.33; 7.55; 9.33	3.22; 7.46; 8.94
Water solubility (mg/L)	1,500	610	4,200	17,000
Vapor pressure (mm Hg at 25°C)	6.82 x 10 ⁻⁹	1.3 x 10 ⁻⁷	5.84 x 10 ⁻²²	9.05 x 10 ⁻²³
Log Kow	0.14	0.89	-0.62	-0.9

SMT: sulfamethazine, SMX: sulfamethoxazole, CTC: chlortetracycline, OTC: oxytetracycline.

2.2.2.1. Wastewater treatment plants

Tetracyclines and sulfonamides administered to humans and animals are poorly absorbed in the digestive tract, with approximately 50 – 90% of the doses are excreted via urine and feces as parent and metabolized forms (e.g. acetyl and glucuronides) (Tran et al., 2016, Tran et al., 2018, Yuan et al., 2019). Due to intensive use in humans, the mixture of antimicrobials and their metabolites has been continuously released into the municipal WWTPs (Ezzariai et al., 2018). However, incomplete elimination of antimicrobials and their metabolites during wastewater treatment processes leads to their ubiquitous presence in the effluents and treated sludge (biosolids). The occurrence of SMT, SMX, CTC, and OTC in WWTPs is summarized in Table 2.6 and Table 2.7.

Sulfonamides were frequently detected in both WWTPs influents and effluents worldwide. As showed in Table 2.6, SMT and SMX have been detected in WWTPs of Asia, Europe, North and South America, and Australia, in which concentrations of SMX were generally higher than

those of SMT. The highest concentrations of SMX in the effluents were 3,100 ng/L in Canada (Guerra et al., 2014) and 2,260 ng/L in India (Subedi et al., 2015), while the highest concentrations of SMT were detected in Singapore (1,814 ng/L) and China (176.4 ng/L). A study by Yuan et al. reported SMT concentrations in the effluent (88.9 ng/L) were approximately 5-fold higher than in the influent (16 ng/L) (Yuan et al., 2019). It has been reported that N⁴-acetyl-SMX can be back-transformed to the parent SMX during wastewater treatment processes (Göbel et al., 2007, Gobel et al., 2005), suggesting a possible explanation to the negative removal efficiencies of SMT in Yuan et al.'s study. N⁴-acetyl- and N¹-glucuronide-sulfonamides are the dominant metabolites of sulfonamides in humans (Vree et al., 1991) and their occurrence in municipal WWTPs has been reported in literature (García-Galán et al., 2008). Because these metabolites can undergo back-transformation to release the bioactive parent compounds during treatment processes, their occurrence in WWTPs should also be monitored. Tetracyclines present a high range of concentrations in wastewater, particularly OTC. As shown in Table 2.7, OTC had higher detection frequency than CTC in WWTPs influent and effluent worldwide. The concentrations of OTC in the influent and effluent ranged from below detection limit to thousands of ng/L. Tran et al. reported the highest concentration of OTC (approximately 30,049 ng/L) in the influent of a WWTP in Singapore (Tran et al., 2016). Highest concentration of CTC was also detected at the same WWTP, at 15,911 ng/L (Tran et al., 2016). OTC were also found in several WWTPs located in China, and substantially varied among different sampling locations (Table 2.7). The lowest concentrations of tetracyclines were founds in WWTPs in North American countries (e.g. U.S. and Canada).

Conventional WWTPs are not designed for effective elimination of antimicrobials; consequently, fractions of antimicrobials in the influents can go through wastewater treatment

processes unchanged and be sorbed to biosolids. Concentrations of SMT, SMX, CTC, and OTC in treated biosolids produced by WWTPs are presented in Table 2.6 and Table 2.7. Many studies have reported occurrence of tetracyclines (CTC and OTC) in biosolids at relatively high concentrations, mostly in Asian countries (e.g. China). Recently, Ashfaq et al. reported concentrations of CTC and OTC up to 2,150 $\mu\text{g}/\text{kg dw}$ and 5,116 $\mu\text{g}/\text{kg dw}$, respectively, in biosolids sampled from WWTPs in China (Ashfaq et al., 2017, Ben et al., 2018). Under environmental pH, tetracyclines mainly exist as cations and zwitterion forms and sorb strongly onto suspended particles via electrostatic interactions. Tetracyclines also form complexes with divalent cations (e.g. Ca^{2+} , Cu^{2+} , and Mg^{2+}) present in biosolids, resulting in their high concentrations in the particulate phase (Tran et al., 2016). It has been found that the concentrations of antimicrobials in WWTPs in each country depend largely on several factors, such as usage patterns, population size/density, weather conditions, treatment systems etc. (Tran et al., 2018). Data from recent studies suggest that consumption of these antimicrobials in humans is still high in many developing countries. Compared to tetracyclines, sulfonamides were detected at lower concentrations in biosolids, from below limit of detection to hundreds of $\mu\text{g}/\text{kg dw}$ (Table 2.6).

Table 2. 6. Occurrence and concentrations of SMT and SMX in the influent, effluent, and biosolids produced in the WWTPs.

Country	Year of sampling	SMT			SMX			Reference
		Influent (ng/L)	Effluent (ng/L)	Biosolids ($\mu\text{g}/\text{kg dw}$)	Influent (ng/L)	Effluent (ng/L)	Biosolids ($\mu\text{g}/\text{kg dw}$)	
China	2017	16	88.9	na	124.1	50.4	na	(Yuan et al., 2019)
Colombia	2016	na	na	na	439 – 827 123 – 558	446 – 831 279 – 434	na	(Botero-Coy et al., 2018)
China	2016	<LOD – 33.4	<LOD – 49.7	na	4.3 – 850	3.2 – 780.9	na	(Zhang et al., 2017)
China	2016	<LOD – 6.08	<LOD – 3.16	<LOD – 9.4	30 – 62.2	7.5 – 37.5	<LOD – 7.33	(Ashfaq et al., 2017)
China	2016	176.39 \pm 22.67	64.23 \pm 14.37	12.36 \pm 5.75	na	na	na	(Hu et al., 2018)
Singapore	2015	449.9 – 1,814	73 – 260.8 41.1 – 105.2	na	893.4 – 1,389	301.5 – 463.4 290.2 – 562	na	(Tran et al., 2016)
China	2015	0.1 – 39.9	0.1 – 10.5	0.1 – 122.7	102.3 – 3,931	1.8 – 465.6	0.8 – 16.4	(Ben et al., 2018)
China	2014	na	na	na	<LOD – 95.2	<LOD – 22.4	<LOD – 2.9	(Sun et al., 2016)
Canada	2014*	<3.84 – 10.9	<1.53 – 2.56	<4.18 – 6.2	603 – 1,630	361 – 468	32.3 – 164	(Kim et al., 2014)
Greece	2013 – 2014	na	na	na	<LOD – 507	<LOD – 80	na	(Papageorgiou et al., 2016)
South Korea	2012 – 2013	na	na	na	74 – 400	50 – 117	na	(Ryu et al., 2014)
India	2012	na	na	na	195 – 2,260	<5 – 318	<5 – 31	(Subedi et al., 2015)
Canada	2010 – 2012	17 – 45	< LOD	<LOD	59 – 3,100	33 – 1,800	1.5 – 51	(Guerra et al., 2014)
China	2010	12.8 \pm 0.84 – 131 \pm 0.42	7.3 \pm 0.16 – 23.3 \pm 1.32	<LOD – 3.83 \pm 0.73	216 \pm 9.8 – 543 \pm 47	65.2 \pm 1.17 – 106 \pm 8.24	<LOD – 10 \pm 0.4	(Zhou et al., 2013)
United States	2010	25.6 \pm 1.9	<LOD	3.5 \pm 0.1	1,474 \pm 628	191.6 \pm 172	26.7 \pm 15.3	(Gao et al., 2012)
South Korea	2010	<LOD – 343	<LOD – 408	na	79 – 216	20 – 162	na	(Behera et al., 2011)
Spain	2009	3.36 – 145	0.46 – 36.4	0.4 – 23.0	17.4 – 665	10.8 – 284	<LOD – 0.108	(García-Galán et al., 2012b)
United Kingdom	2008	na	na	na	<LOQ	12	na	(Kasprzyk-Hordern et al., 2008)
Australia	2006	na	na	na	360 – 500	270 – 320	na	(Watkinson et al., 2007)

*Year of publication since sampling year was not clarified in the articles.

LOD: limit of detection; LOQ: limit of quantification

na: data not available

Table 2. 7. Occurrence and concentrations of CTC and OTC in the influent, effluent, and biosolids produced in the WWTPs.

Country	Year of sampling	CTC			OTC			Reference
		Influent (ng/L)	Effluent (ng/L)	Biosolids ($\mu\text{g}/\text{kg dw}$)	Influent (ng/L)	Effluent (ng/L)	Biosolids ($\mu\text{g}/\text{kg dw}$)	
China	2016	na	na	na	<LOD – 1,164	<LOD – 578.7	na	(Zhang et al., 2017)
China	2016	<LOD – 55.2	<LOD – 31.0	289 – 2,150	78.2 – 394	14.4 – 35.0	1,300 – 2,970	(Ashfaq et al., 2017)
China	2016	na	na	na	196.32 ± 31.64	24.12 ± 4.68	80.27 ± 16.28	(Hu et al., 2018)
China	2016	na	na	na	39.6-398	<LOD-89.2	287-2,180	(Wang et al., 2018)
Singapore	2015	2,333 – 15,911	1,472 – 1,986 505.3 – 1,732	na	1,629 – 30,049	839.8 – 2,014 335.4 – 1,069	na	(Tran et al., 2016)
China	2015	0.8 – 39.4	2.1 – 3.8	0.3 – 276.6	3.7 – 626.6	0.4 – 64.5	4.1 – 5,116	(Ben et al., 2018)
China	2014	na	na	na	8.6 – 230	<LOD – 51.5	208 – 3,790	(Sun et al., 2016)
Canada	2014*	<23 – 35.5	<6.57 – 7.09	<41.8 – 61.3	<22 – 24.2	<6.57 – 7.09	<41.8 – 61.3	(Kim et al., 2014)
Canada	2010 – 2012	<LOD	<LOD	11 – 12	<LOD	<LOD	8.3 – 21	(Guerra et al., 2014)
United States	2010	51.0 ± 33.6	<LOD	<LOD	22.6 ± 13.2	21.0 ± 5.7	16.5 ± 9.6	(Gao et al., 2012)
China	2010	7.46 ± 0.2 – 35.7 ± 2.77	<LOD	34.6 ± 1.05 – 455 ± 47.5	79.1 ± 3.72 – 560 ± 41.1	10.8 ± 0.98 – 17.6 ± 1.19	417 ± 18.1 – $1,680 \pm 16.7$	(Zhou et al., 2013)
Australia	2006	<LOD	<LOD – 5	na	<LOD	<LOD – 20	na	(Watkinson et al., 2007)

*Year of publication since sampling year was not clarified in the articles.

LOD: limit of detection; LOQ: limit of quantification; na: data not available

2.2.2.2. Animal manure

Ubiquitous use of veterinary antimicrobials is another hotspot of antimicrobial dissemination into the environment (Ezzariai et al., 2018). Similar to their pharmacokinetics in human, large proportions of antimicrobials in medicated animals are excreted via urine and feces as parent (50–90%) and metabolized forms (Tran et al., 2016, Tran et al., 2018, Yuan et al., 2019). In animals, sulfonamides are mainly metabolized in the liver, inducing formation of several metabolites. Oxidation, acetylation, and hydroxylation at the N⁴-nitrogen atom or glucuronidation of the N¹- or N⁴-nitrogen atoms are the most common mammalian metabolites documented in literature (García-Galán et al., 2008). Acetic acid conjugates comprise 5-60% of the excreted dose of sulfonamides in mammals (García-Galán et al., 2008). N⁴-acetylation and N¹-glucuronidation have also been reported as a major metabolism pathways for sulfonamides in animals, accounting for 50-70% and 15-20% of the administered dose excreted in urine, respectively (Baran et al., 2011, García-Galán et al., 2008). Even though these transformation products are not as highly bioactive as their parent molecules, the activity can be easily restored in *in vitro* conditions (Baran et al., 2011).

Annually, there are approximately 130 million tons and 177.5 million tons of farm-animal manure are produced in the U.S. and Canada, respectively. In France, over 274 million tons of livestock wastes were produced and applied to soil in 2012 (Ezzariai et al., 2018). In South Korea, 46.5 million tons of animal manure were produced in 2011 (Tasho and Cho, 2016). Considering high excretion rate of antimicrobials by animals, animal manures serve as a major reservoir of antimicrobials. Antimicrobial concentrations in animal manures ranged from several µg/kg to mg/kg, depending on sampling locations and animal species (Table 2.8 and Table 2.9). The concentrations of antimicrobials in manures in China were generally higher than those found in

European countries (e.g. Spain, Germany, and Austria). Tetracyclines are among the most highly used antimicrobial classes in animals thanks to their low cost and broad-spectrum application (Pollard and Morra, 2018, U.S. FDA, 2017). Therefore, tetracyclines are expected to be detected in animal manure at high frequencies and concentrations, although their residues largely depend on variations in the doses prescribed for different animal species and the metabolic characteristic of the animals (Conde-Cid et al., 2018a). Hou et al. reported that 81.3–90.6% of swine, chicken, and cattle manure collected at several concentrated animal farming operations (CAFOs) in Northern China contained tetracycline residues (Hou et al., 2015). CTC and OTC were the two most predominant antimicrobials in manure, which detection frequencies of 90.6% and 87.5%, respectively, and peak concentrations of 124,579 $\mu\text{g}/\text{kg}$ dry weight (dw) and 21,332 $\mu\text{g}/\text{kg}$ dw, respectively (Hou et al., 2015). Similarly, CTC and OTC were also detected with highest detection frequencies (96.8% and 90.5%, respectively) in swine manure sampled from CAFOs in Shandong Province (China), with the maximum concentrations were approximately 764,400 $\mu\text{g}/\text{kg}$ dw and 150,000 $\mu\text{g}/\text{kg}$ dw (Pan et al., 2011). Hu et al. reported concentrations of 26,800 $\mu\text{g}/\text{kg}$ dw and 183,500 $\mu\text{g}/\text{kg}$ dw for CTC and OTC in livestock manure used as fertilizers in organic vegetable farms in Tianjin (China) (Hu et al., 2010a). These results suggest that tetracyclines may have been overused in the animal feeding industry in China (Hou et al., 2015). Sulfonamides are often present at lower concentrations than those found for tetracyclines in manure samples. For example, the peak concentrations of SMT and SMX in swine manure in Hou et al.'s study were approximately 9,356 $\mu\text{g}/\text{kg}$ dw and 100.8 $\mu\text{g}/\text{kg}$ dw, respectively (Hou et al., 2015). The highest concentration of SMX in Pan et al.'s study was approximately 700 $\mu\text{g}/\text{kg}$ dw (Pan et al., 2011).

Table 2. 8. Occurrence of SMT and SMX in animal manure.

Country	Year of sampling	SMT		SMX		Reference
		Concentrations (µg/kg dw)	Animals	Concentrations (µg/kg dw)	Animals	
China	2016 – 2017	93.2 ± 3.96	Mixture of swine/poultry manure (4:2) for commercial compost	na	na	(Zhang et al., 2019)
Spain	2016	<25 <25 <25	Cow Pig Chicken	na	na	(Conde-Cid et al., 2018a)
China	2013	1.2 - 61	Chicken, duck, pig, cow, and commercial organic fertilizers	<LOD – 102	Chicken, duck, pig, cow, and commercial organic fertilizers	(Li et al., 2015)
China	2013	<LOD – 9,356 ± 1,029 <LOD - 47.8 ± 3.4 <LOD – 51.1 ± 2.9	Swine Chicken Cattle	2.2 ± 0.2 – 100.8 ± 8.0 5.3 ± 0.4 – 8.7 ± 0.6 3.2 ± 0.2 – 53.7 ± 2.9	Swine Chicken Cattle	(Hou et al., 2015)
China	2013*	na	na	220 – 1,020 250 – 7,110 210 – 2,160	Cow Chicken Pig	(Li et al., 2013b)
China	2009-2010	na	na	110 - 700	Swine	(Pan et al., 2011)
China	2007 – 2008	na	na	230 – 5,700	Livestock	(Hu et al., 2010a)
China	2007	90 – 6,040 60 – 1,730 100 – 180	Chicken Pig Cow	na	na	(Zhao et al., 2010)
Germany	2000 - 2002	<LOD – 7,200	Pig	na	na	(Hamscher et al., 2005)

*Year of publication since sampling year was not clarified in the articles.

LOD: limit of detection; LOQ: limit of quantification

na: data not available.

Table 2. 9. Occurrence of CTC and OTC in animal manure.

Country	Year of sampling	CTC		OTC		Reference
		Concentrations ($\mu\text{g}/\text{kg dw}$)	Animals	Concentrations ($\mu\text{g}/\text{kg dw}$)	Animals	
China	2016 - 2017	$26,500 \pm 1,130$	Mixture of swine/poultry manure (4:2) for commercial compost	$22,000 \pm 2,080$	Mixture of swine/poultry manure (4:2) for commercial compost	(Zhang et al., 2019)
Spain	2016	<25 <25 – 4,000 <25	Cow Pig Chicken	<25 – 2,900 4,600 – 35,000 <25 – 4,100	Cow Pig Chicken	(Conde-Cid et al., 2018a)
China	2013	107 – 26,218	Chicken, duck, pig, cow, and commercial organic fertilizers	187 – 23,271	Chicken, duck, pig, cow, and commercial organic fertilizers	(Li et al., 2015)
China	2013	<LOD – 124,579 \pm 9,468 5.6 \pm 0.3 – 8,492 \pm 654 <LOD – 1,144 \pm 30	Swine Chicken Cattle	<LOD – 21,332 \pm 1,706 <LOD – 4,427 \pm 390 <LOD – 101.7 \pm 2.0	Swine Chicken Cattle	(Hou et al., 2015)
China	2013*	610 – 1,940 570 – 3,110 680 – 22,340	Cow Chicken Pig	210 – 10,370 960 – 13,390 730 – 56,810	Cow Chicken Pig	(Li et al., 2013b)
China	2009-2010	70 – 764,400	Swine	50 – 150,000	Swine	(Pan et al., 2011)
China	2007 – 2008	140 – 26,800	Livestock	80 – 183,500	Livestock	(Hu et al., 2010a)
China	2007	160 – 17,680 160 – 21,060 240 – 27,590	Chicken Pig Cow	270 – 10,560 150 – 59,060 320 – 59,590	Chicken Pig Cow	(Zhao et al., 2010)
Austria	2003 - 2004	100 – 46,000	Swine	210 – 29,000	Swine	(Martinez-Carballo et al., 2007)
Germany	2000 – 2002	<LOD – 1,000	Pig	na	na	(Hamscher et al., 2005)

*Year of publication since sampling year was not clarified in the articles.

LOD: limit of detection; LOQ: limit of quantification

na: data not available.

2.2.2.3. Animal manure-amended soils

Application of antibiotic-laden manure in agricultural soils as fertilizer can be a significant point source for antimicrobials release into the environment (Mullen et al., 2019). As the veterinary antimicrobial classes with highest detection frequency in animal manure, sulfonamides and tetracyclines have been intensively studied with respect to their occurrence in manured soils and subsequent accumulation in crop plants. Recently, the demand for organic food and other products has been growing rapidly, reaching \$63 billion worldwide in 2012 and accounted for approximately 0.9% of total world farmland (37 million ha) in 2011 (Tasho and Cho, 2016). In this context, livestock and poultry manure, as a source of organic fertilizer, is becoming an excellent alternative to chemical fertilizers. Nevertheless, these organic agricultural practices are potentially spreading manure-associated antibiotic residues and antibiotic resistance into farming settings. Many recent studies have found residuals of sulfonamide and tetracycline antibiotics in manured soils from organic farms in China and agricultural soils in South Korea, Kenya, Turkey (Table 2.10). For example, Xiang et al. detected residues of 4 tetracycline compounds (oxytetracycline, tetracycline, chlortetracycline and doxycycline) in soils from different organic vegetable farms in Guangzhou (China), with the concentrations ranging from 0.04 to 184.8 $\mu\text{g}/\text{kg}$ dw (Xiang et al., 2016). In another study on agricultural soils of the Yangtze River Delta, Sun et al. reported that antibiotics were detected in 100% ($n = 241$) soil samples, with the total concentrations ranging from 4.55 to 2,010 $\mu\text{g}/\text{kg}$ dw (Sun et al., 2017). The concentrations of tetracyclines (mean 34.9 $\mu\text{g}/\text{kg}$ dw) was higher than those of sulfonamides (mean 2.35 $\mu\text{g}/\text{kg}$ dw) (Sun et al., 2017). Hu et al. reported concentrations of 1,079 $\mu\text{g}/\text{kg}$ dw and 2,683 $\mu\text{g}/\text{kg}$ dw for CTC and OTC in soils receiving organic livestock manure (Hu et al., 2010a). Residues of SMX were also detected in soils amended with cattle or chicken manure in Turkey (Karcı and Balcıoğlu,

2009). In general, higher occurrence of tetracyclines with respect to sulfonamides in several studies likely due to higher adsorption of tetracyclines in soils, resulting in their persistence in the environment (Conde-Cid et al., 2018a).

Table 2. 10. Occurrence of SMT, SMX, CTC, and OTC in agricultural soils receiving animal manure under “real-world” conditions.

Country	Year of sampling	SMT (µg/kg dw)	SMZ (µg/kg dw)	CTC (µg/kg dw)	OTC (µg/kg dw)	Reference
Brazil	2018*	<LOD – 20.9 ± 11.9	<LOD – 2.4 ± 1.2	na	<LOD – 9.8 ± 7.9	(Bastos et al., 2018)
China	2017	na	na	23.33 – 71.19	23.56 – 224.71	(Li et al., 2017)
China	2017	<LOD – 0.63	<LOD – 2.44	na	<LOD - 530	(Sun et al., 2017)
S. Korea	2017	na	na	na	<LOD – 0.87	(Yeom et al., 2017)
Spain	2016	<50 – 100	na	na	<50 - 200	(Conde-Cid et al., 2018a)
China	2016	na	na	0.29 – 161.5	0.04 – 31.85	(Xiang et al., 2016)
Kenya	2016	<LOD – 24.23	<LOD – 14.47	<LOD – 38.79	<LOD– 29.38	(Yang et al., 2016)
China	2015	<LOD – 0.37	<LOD – 0.06	17	80	(Li et al., 2015)
China	2014	nd - 110	na	nd - 111	< 20	(Ostermann et al., 2014)
China	2013	<LOD – 59.2 ± 1.8	<LOQ – 46.6 ± 9.8	4.9 ± 0.1 – 6,192 ± 124	<LOQ – 325.6 ± 20.2	(Hou et al., 2015)
China	2011	<LOD– 74.0	<LOD – 54.5	<LOD – 104.6	<LOD – 79.7	(Li et al., 2011)
China	2007 – 2008	na	0.03 – 0.9	<LOD – 1,079	<LOD – 2,683	(Hu et al., 2010a)
Turkey	2009	na	<LOD - 100	<LOD - 100	20 - 500	(Karcı and Balcıoğlu, 2009)
Germany	2001 – 2003	<LOQ – 2 ± 1	na	<LOD – 39	na	(Hamscher et al., 2005)

*Year of publication since sampling year was not clarified in the articles.

LOD: limit of detection; LOQ: limit of quantification

na: data not available.

2.3. Environmental fate of antimicrobials following soil application

2.3.1. Triclosan and triclocarban

Given the large amount of TCS and TCC introduced to land annually, a thorough understanding of their environmental fate in soils and biosolids-amended soils is necessary to address public concerns about potential bioaccumulation, translocation, and toxicity of these organic pollutants to plants, soil organisms, as well as leaching potential. Cha and Cupples showed a very low leaching potential for both TCS and TCC in amended agricultural soils (K_d and K_{oc} values were 33–55 L/kg and 3,968–6,310 L/kg for TCS and 193–296 L/kg and 18,175–33,991 L/kg for TCC), indicating that TCS and TCC are unlikely to contaminate groundwater (Cha and Cupples, 2010). However, TCS leaching to deeper soil layers (up to 30 cm) has been documented during periods of high soil hydraulic conductivity from heavy snow fall and rainfall events, and bioturbation (e.g. by earthworms) (Butler et al., 2012).

Once land applied, TCS and TCC can undergo various transformation processes in soils, in which biodegradation is an important transformation mechanism (Cha and Cupples, 2010, Lozano et al., 2010). Half-lives of TCS and TCC in aerobic conditions have been reported in multiple studies. The observed values considerably vary, on the order of hours to years, depending on soil composition and environmental conditions (Waria et al., 2011). In general, TCC is more recalcitrant than TCS, indicating longer persistence in soils. Under aerobic conditions in laboratory, TCS and TCC spiked directly to soil were primarily degraded by microbial processes, with estimated half-lives of 18 days and 108 days, respectively (Ying et al., 2007). In addition, both compounds were persistent in anaerobic soil and sterilized soil, further demonstrating that aerobic microbial degradation was a key mechanism of soil TCS and TCC removal. In other studies, Kwon et al. also reported that soil sterilization considerably slowed the TCS

transformation rates, evidenced by longer half-lives of TCS in autoclaved soils (51-60 days) than in nonsterilized soils (2-13 days), and that addition of biosolids slowed degradation of TCS (Kwon et al., 2010). On the other hand, effects of soil sterilization on TCC dissipation were subjected to change with different type of soils and that abiotic processes, rather than biotic ones, are more of a controlling factor governing TCC transformation in soils (Kwon et al., 2010). Transformation of TCS and TCC also greatly differs in soils with different physico-chemical properties. For example, Waria et al. reported degradation half-lives of TCS was 78 days in a silty clay loam and up to 421 days in a fine sand soil under laboratory study (Waria et al., 2011). Wu et al. observed faster degradation rates of TCS and TCC in sandy loam soil compared to that in silt clay soil, attributed to differences in soil texture, microbial activity and water content (Wu et al., 2009). Similarly, Kwon et al. observed that TCS transformation in fine loam and coarse loam was much faster than transformation of TCC in the same media, as well as a more favorable transformation of both compounds in fine loam than in coarse loam (Kwon et al., 2010). As both compounds are weak acids ($pK_a = 7.9$ for TCS and 12.7 for TCC, respectively) and are hydrophobic ($\log K_{ow} = 4.8$ for TCS and 4.9 for TCC, respectively), their environmental fate in soils can be affected by changes in soil pH and organic content. Within the environmentally relevant pH range, TCS predominantly exists in deprotonated form which is readily biodegradable, whereas TCC mainly presents neutral form due to a high pK_a value. Wu et al. suggested that hydrophobic interaction of un-ionized species is more important to overall sorption (Wu et al., 2009). Therefore, a larger proportion of TCC is expected to be attached to soil particles. As soil microorganisms have only limited access to sorbed material, the microbial processes occur primarily in the unsorbed phase. As a result, TCC becomes less available for biodegradation than TCS and is more likely to persist in the soil environment (Cha and Cupples, 2010).

Biosolids land applied can alter soil properties, particularly increasing soil pH, organic matter content, organic carbon content and cation exchange capacity (Wu et al., 2009), which ultimately affecting the transformation and sorption characteristics of biosolids-associated TCS and TCC in treated soils. Besides, dissipation of both compounds also depends on the physico-chemical characteristics of the application matrix and substantially differ between laboratory studies and field practices. In a study using radiolabeled ^{14}C -TCS and ^{14}C -TCC, which were directly added to loam soil or were applied via either liquid biosolids or dewater biosolids under laboratory conditions, Al-Rajab et al. observed that liquid biosolids accelerated mineralization of TCS and TCC while dewatered biosolids suppressed the process as compared to soil that received the two chemicals directly in water (Al-Rajab et al., 2009). For TCS, mineralization rate constants were $0.17 \pm 0.02/\text{day}$, $0.40 \pm 0.04/\text{day}$, and $0.06 \pm 0.00/\text{day}$ in water-added soil, liquid biosolids-amended soil and dewatered biosolids-amended soil, respectively. For TCC, these values were: $-1.03 \pm 0.04/\text{day}$, $-2.13 \pm 0.07/\text{day}$, and $-0.73 \pm 0.07/\text{day}$, respectively (Al-Rajab et al., 2009). In addition, the methods by which biosolids are treated prior to land applied have also been found to affect transformation rates of TCS under controlled laboratory conditions (Langdon et al., 2011). The authors reported that half-life of TCS in soil amended with centrifuge dried biosolids was considerably longer than that of TCS in soil treated with solar dried biosolids (301 days vs. 73 days). The variations observed in controlled laboratory studies further emphasize the complexity of the behavior of TCS and TCC under “real world” conditions when a mixture of biosolids are applied to agricultural soils. Most of the current studies on environmental fate of TCS and TCC following biosolids land applied have been conducted under laboratory and greenhouse conditions; therefore, there is a need for studies that address their fate in fields receiving sewage sludge. Lozano et al. reported TCS concentrations in top soils (10 cm) collected from 26 commercial farms

in Virginia (U.S.) varied between 23.6 and 66.6 $\mu\text{g}/\text{kg dw}$ when sampling time after a single application was less than 365 days. Mean TCS concentration decreased over time to background levels, ranging from 4.1 to 4.5 $\mu\text{g}/\text{kg dw}$ 480 days after application. For multiple biosolids application farms, there was a slight residual build-up of TCS, even though the concentrations for these farms were low (ca. 10 $\mu\text{g}/\text{kg dw}$) (Lozano et al., 2010). In another field trial with initial TCS concentrations of 39-106 $\mu\text{g}/\text{kg dw}$, no significant decrease in the soil concentrations of TCS was observed over the course of 336 days (Langdon et al., 2012). This observation is not in agreement with their previous laboratory study using the same soil and biosolids treatments with initial soil TCS concentrations of 184-361 $\mu\text{g}/\text{kg dw}$, that resulted in significant degradation of TCS (Langdon et al., 2011). In contrast to Langdon et al. (2012), Al-Rajab revealed that degradation of TCS under field conditions did occur to some extent as evident by mineralization of ^{14}C -TCS, although the dissipation was much slower in the field than in the laboratory experiments (Al-Rajab et al., 2009). A large fluctuation in soil temperature and moisture in “real world” conditions may substantially lower the degradation rate of TCS than in optimal laboratory conditions, indicating that TCS is more persistent in field soils. As a result, the extrapolation of laboratory data for assessing the persistence of pollutants and the potential risks following land application of biosolids should be used with caution (Langdon et al., 2012).

Along with microbial degradation, formation of non-extractable (or bound) fraction of either TCS or TCC in soils receiving sewage sludge have been reported in a number of studies. The mechanism of non-extractable residues formation may include covalent binding, polymerization of the chemicals in soil organic matter or physical entrapment of the compounds in the soil organic or mineral matrix (Butler et al., 2012). Notably, the non-extractable fractions of TCS and TCC considerably vary depending on the physico-chemical properties of soils and

biosolids applied, ranging from 6-51% and 14-16% of the initial concentrations for TCS and TCC, respectively (Al-Rajab et al., 2009, Langdon et al., 2011). Bound residues are often assumed to be stable and biologically unavailable (Butler et al., 2012). Therefore, the presence of recalcitrant fractions of TCS and TCC in soils is of great concern due to potential accumulation in soils where biosolids have repeatedly been applied to land.

Hundt et al. reported that microbial degradation of TCS forms Me-TCS, dichlorophenols, and conjugates that have carbonhydrates connected to the hydroxyl group (Hundt et al., 2000). According to Waria et al., Me-TCS is the most significant metabolite resulting from the biodegradation of TCS in agricultural soils receiving biosolids, suggesting an in situ biomethylation reaction occurring under aerobic condition (Waria et al., 2011). So far, little is known about the fate of Me-TCS after field applications of biosolids. TCS biodegradation occurs right after biosolids application to form Me-TCS, and the process may have been taking place both within the biosolids and in the treated soils thanks to indigenous TCS-degrading bacteria that readily exist in activated sludge (Lozano et al., 2012). Lozano et al. estimated half-lives of the two compounds that were 104 days for TCS and 443 days for Me-TCS, indicating a low dissipation of Me-TCS in treated soils and that Me-TCS is much more persistent in the environment than its parents TCS (Lozano et al., 2012). Over the course of that study, Me-TCS concentrations increased from $0.6 \pm 0.1 \mu\text{g/kg dw}$ on the application day to $34 \pm 6.7 \mu\text{g/kg dw}$ one year after biosolids application, and it would take 7.2 years for soil Me-TCS to reach soil background levels (Lozano et al., 2012). In another field trial using three different soils (loamy sand, sandy clay loam and clay) amended with sewage sludge in the top layer of 10 cm, Butler et al. detected both TCS and Me-TCS in three depth ranges (0-10 cm, 10-20 cm and 20-30 cm) of all treatments, although most of these two compounds recovered at the end of the experiments was still in the top 10 cm layer

(Butler et al., 2012). In this study, despite the fact that most Me-TCS in each layer was formed in situ, the authors also supposed that there may have been some translocation of Me-TCS from above layers via leaching or bioturbation (Butler et al., 2012).

Biodegradation of TCS and TCC generally results in formation of lesser or non-chlorinated end products. Lee et al. isolated the *Sphingopyxis* strain KCY1 which is capable of degrading TCS via *meta*-cleavage. The maximum-specific TCS degradation rate (q_m) and the half-velocity constant (K_m) was 0.13 mg TCS/mg protein/day and 2.8 mg TCS/L, respectively (Lee et al., 2012). As the biodegradation progressed, five transformation products were identified and these metabolites continue to transform into non-chlorinated products, leading to a sharp drop in androgenic potential (Lee et al., 2012). The degradation pathway of TCS by strain KCY1 is proposed in Figure 2.2. An initial attack at the 2,3- position of TCS resulted in the formation of 6-chloro-3-(2,4-dichlorophenoxy)-4-hydroxycyclohexa-3,5-diene-1,2-dione and monohydroxy-triclosan and dihydroxy-triclosan (reactions a and a_1). The monohydroxy- and dihydroxy-triclosan were further attacked by 2,3-dioxygenase and then subjected to an ether cleavage to produce 2,4-dichlorophenol (reaction a_2 or a_3 or a_4). At the end of the degradation experiment, 107% of the theoretical amount of chloride release was observed, suggesting that TCS was completely dechlorinated by strain KCY1 (reaction a_6). Recently, a similar degradation pathway for TCS by *Sphingomonas* sp. strain YL-JM2C isolated from activated sludge has also been reported by Mulla et al. (Mulla et al., 2016b). In addition to the abovementioned metabolites, TCS-O-sulfate and TCS-O-CH₃ have also been detected in activated sludge under aerobic conditions (Chen et al., 2015, Chen et al., 2011). Ying et al. reported no biodegradation of TCS under anaerobic conditions (Ying et al., 2003). However, TCS microbial degradation under anoxic/reduced oxygen has been reported in recent studies, although at a comparatively slower than aerobic

degradation (Carr et al., 2011, Gangadharan Puthiya Veetil et al., 2012). The products of TCS degradation under both the conditions were phenol, catechol, and dichlorophenol metabolites (Gangadharan Puthiya Veetil et al., 2012, Kim et al., 2011).

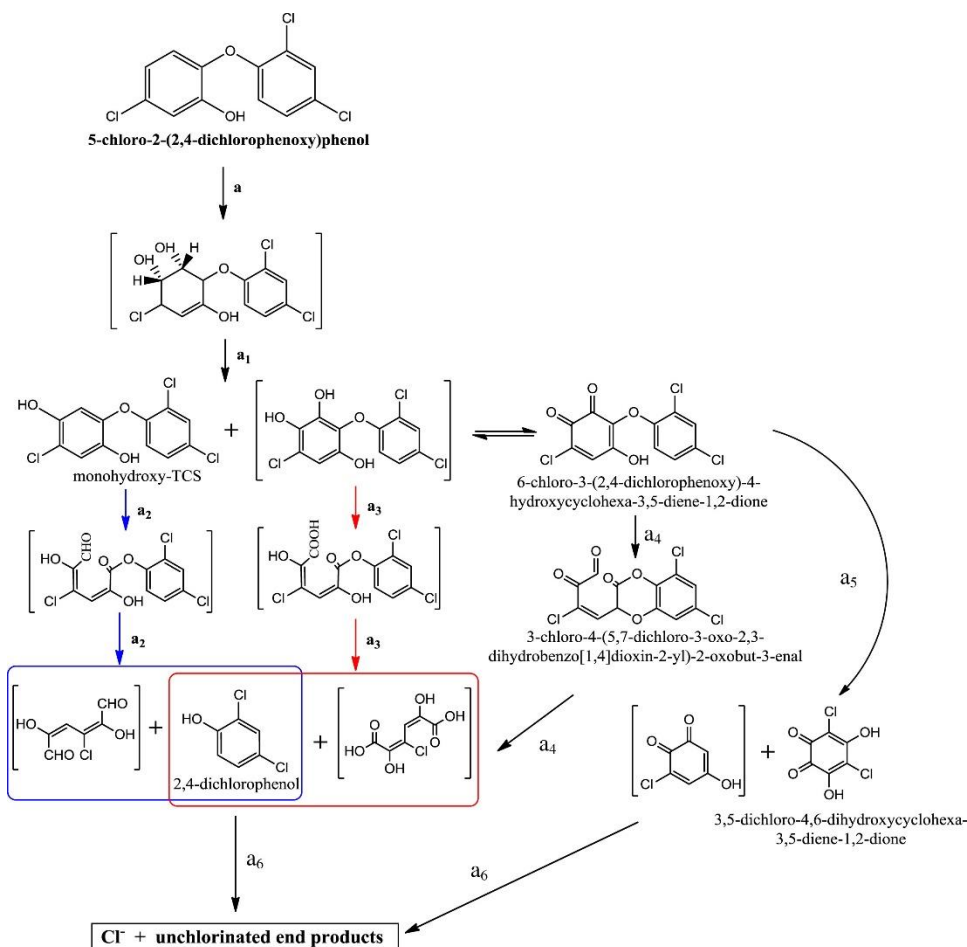


Figure 2. 2. A proposed biodegradation pathway for TCS by the *Sphingopyxis* strain KCY1 (Lee et al., 2012).

The abovementioned TCS-degrading bacteria *Sphingomonas* sp. strain YL-JM2C is also capable of degrading TCC under aerobic conditions. Mulla et al. reported that, in strain YL-JM2C, TCC was transformed into 3,4-dichloroaniline and 4-chloroaniline; subsequently, 3,4-dichloroaniline was further transformed into 4-chloroaniline with the release of chlorine ions. In the third step, 4-chloroaniline was converted into 4-chlorocatechol (Figure 2.3) (Mulla et al.,

2016a). Reductive dechlorination of TCC into 4,4'-dichlorocarbanilide (4,4'-DCC) was found to be predominated in anoxic sediment (Souchier et al., 2015, Souchier et al., 2016) and into 3,4'-dichlorocarbanilide (3,4'-DCC) under aerobic conditions (Souchier et al., 2016), suggesting that strict anaerobic conditions might not be required for TCC reductive dechlorination in the environment.

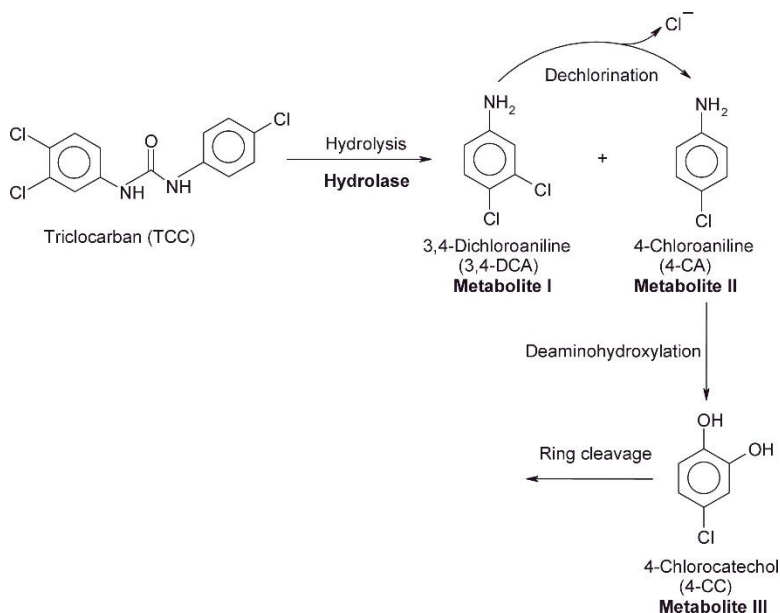


Figure 2. 3. Proposed pathway for TCC biodegradation by *Sphingomonas* sp. strain YL-JM2C (Mulla et al., 2016a).

2.3.2. Sulfonamides and tetracyclines

2.3.2.1. Sulfonamides

Animal manure and farm runoff are reported as major sources of sulfonamides (Baran et al., 2011). SMX and sulfadiazine are most commonly used in human therapies (although sulfadiazine is used in both human and veterinary medicine) and therefore are ubiquitous in urban wastewaters due to ineffective removal during activated sludge wastewater treatment (García-Galán et al., 2011a). However, SMT is predominantly used in veterinary medicine, so its occurrence can only be explained by diffuse contamination from confined animal feeding

operations or the presence of agricultural fields where either contaminated manure or biosolids were applied (García-Galán et al., 2012b). Interestingly, in wastewater treatment, negative removal efficiencies for antibiotics are commonly reported (García-Galán et al., 2011a, Göbel et al., 2007, Gros et al., 2010). This observation can be attributed to the presence of transformation products (e.g. acetylated metabolites) that are totally or partially cleaved by bacteria and reverted back to the parent antibiotics during wastewater treatment (García-Galán et al., 2012a).

Sulfonamides prescribed for human use are eventually excreted into domestic sewage and are discharged to WWTPs along with their metabolites. Likewise, the excretion of urine and feces from medicated animals and amendment of contaminated manure on agricultural soils as fertilizer serve as the major pathways by which sulfonamide antibiotics and their metabolites enter the environment. Once land applied, sulfonamides may persist in the soil for months; for instance, sulfamethazine was still detected at 10.4 µg/kg in manured soil one year since the last application (Aust et al., 2008, Stoob et al., 2006). While tetracyclines exhibit high affinity to soil particles, sulfonamides have greater potential for leaching as evident in several recent studies (Pan and Chu, 2017b, Spielmeyer et al., 2017, Wei et al., 2016). For instance, the residual concentrations of SMX, SMT, and sulfadoxine in manure-amended soils (40-60 cm layers) have been reported up to 1692, 1688 and 1163 µg/kg, respectively, which exceeded the minimum inhibitory concentrations of sulfonamides for *Escherichia coli* (Wei et al., 2016). The presence of sulfonamides (e.g. SMT at 105 ng/L) was also observed in groundwater sampled below an agriculture field within an area of intensive livestock farming (Spielmeyer et al., 2017). These results clearly indicate a high risk of subsoil and groundwater contamination of sulfonamide antibiotics.

N⁴-acetylated and 4-hydroxylated conjugates have been documented as the most common forms of sulfonamide antibiotics in wastewater and manure applied to agricultural soils (García-

Galán et al., 2012b, Lamshöft et al., 2007). Once land applied, parent antibiotics and metabolites are prone to microbial transformation (Jechalke et al., 2014), likely resulting in the reversion of metabolites into parent antibiotics (Förster et al., 2009, Zarfl et al., 2009). Photodegradation in soils is expected to be negligible due to poor light penetration (photolysis occurs in the 0.5 mm depth layer) (Durán-Álvarez et al., 2015). Additionally, mineralization of many antibiotics is frequently insignificant, accounting for less than 2% of the added amounts (Förster et al., 2009, Junge et al., 2011). In soil, antibiotics primarily interact with the soil solid phase through sorption and desorption reactions, which govern their mobility and uptake by plants and biotransformation and biological effects. These primary reactions are followed by a subsequent kinetic sorption/desorption with slow release rates, reducing the bioavailability of the antibiotic in soil. As the contact time increases, a fraction of antibiotics may form non-extractable complexes with soil organic matter, metal oxides, and clays (Jechalke et al., 2014). While the primary and secondary sorption/desorption reactions are reversible, non-extractable fractions are assumed to be based on covalent bonds and to be irreversible (Zarfl et al., 2009).

The NH_2 - group, which is part of SMT and SMX molecules, is an active site for biotransformation of sulfonamides. Hydroxylation, nitration, and acetylation, where the parent molecules are not decomposed, are among the most common reactions mediated by bacteria or fungus (Table 2.11). Breakdown products, resulting from cleavage of parent compounds, were also observed (Jia et al., 2017). It is worth noting that, contrary to transformation products, breakdown products have been shown to lose their antibacterial activity and therewith also their potential to cause antibiotic resistance of microbes (Majewsky et al., 2015). Transformation products are also prone to microbial transformation, likely resulting in the reversion into parent compounds (Förster

et al., 2009, Zarfl et al., 2009). For these reasons, focus should be on the identification and quantification of transformation products as well as their back-conversion rate.

2.3.2.2. Tetracyclines

Tetracyclines have several orders-of-magnitude higher adsorption affinity than sulfonamides in the same soil type (Rabolle and Spliid, 2000); therefore, they are often regarded as very stable and environmentally persistent (Conde-Cid et al., 2018a). For example, the adsorption coefficient (K_d) of tetracycline in a clay-loam agricultural soil was 1,093 L/kg while that of SMT was only 1.365 L/kg (Pan and Chu, 2016). Under the environmental pH, sulfonamides exist mainly in neutral form in the test soil solution, leading to lower sorption ability (Figueroa-Diva et al., 2010). On the contrary, under environmental pH, tetracyclines mainly exist as cations and zwitterion forms and sorb strongly onto suspended particles via electrostatic interactions. Tetracyclines also form complexes with divalent cations (e.g. Ca^{2+} , Cu^{2+} , and Mg^{2+}) ubiquitously present in soil, resulting in their higher affinity to soil matrices (Tran et al., 2016). Their highest adsorption coefficients than other classes of antimicrobials suggest that tetracyclines are preferentially retained in soil rather than highly mobile like sulfonamides (Pan and Chu, 2016).

Tetracyclines in soil are also subjected to transformation through biotic and abiotic reactions, in which biodegradation plays a key role in their dissipation from the environment (Pan and Chu, 2016). For CTC, loss of chlorine atom during biotransformation reactions results in the formation of tetracycline (Liao et al., 2017), which still exhibit antibacterial activity. Besides, 4-epi-chlortetracycline, anhydrochlortetracycline and 4-epi-anhydrotetracycline have also been reported as bacterial transformation products of CTC (Aydin et al., 2016). For OTC, 4-epi-oxytetracycline and 2-acetyl-2-decarboxamido-oxytetracycline are the two major biotransformation products in *Anaerolineae*, *Flavobacteriaceae* and *Pleurotus ostreatus* mycelium

(Cao et al., 2018, Migliore et al., 2012) (Table 2.12). Hu et al. reported that biodegradation of tetracyclines was accelerated in the summer compared to that in the winter, likely due to higher temperatures and microbial activity in the summer time (Hu et al., 2010a). Additionally, other degradation processes also affect the fate of tetracyclines in soils such as photodegradation (Conde-Cid et al., 2018b), laccase-mediated oxidation coupled with soil adsorption (Ding et al., 2016), and adsorption to soil humic acids (Conde-Cid et al., 2018b).

Table 2. 11. Biotransformation products of SMT and SMX.

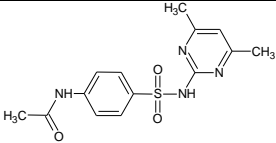
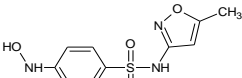
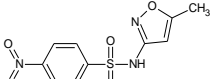
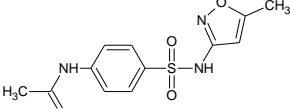
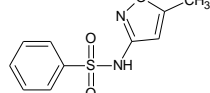
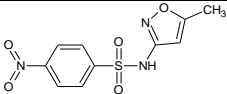
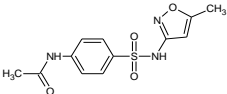
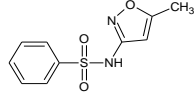
Bacteria/fungus species	Antibiotic concentrations in water/soil	Transformation products		Reference
		SMT	SMX	
Water and cobble biofilms collected on-site	1 and 5 µg/L (SMT, SMX)	 <p>Acetyl SMT</p>	 <p>Hydroxyl SMX</p>  <p>Nitro SMX</p>  <p>Acetyl SMX</p>  <p>Desamino SMX</p>	(Vila-Costa et al., 2017)
Ammonia oxidizing bacteria	11.2 ± 0.8 and 101.7 ± 12.2 µg/L (SMX)		 <p>Nitro SMX</p>  <p>Acetyl SMX</p>  <p>Desamino SMX</p>	(Kassotaki et al., 2016)

Table 2.11 (cont'd). Biotransformation products of SMT and SMX.

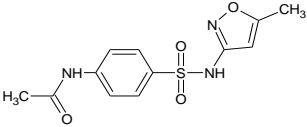
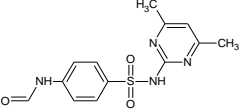
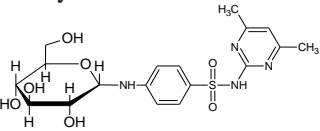
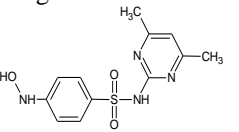
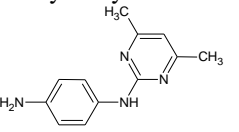
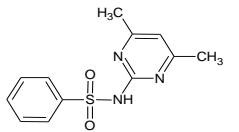
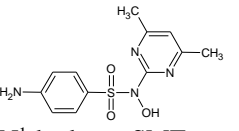
<p><i>Bacillus firmus</i> and <i>Bacillus cereus</i></p>	<p>0.61 – 59.75 mg/L (SMX) 1.46 – 119.83 mg/kg (SMX)</p>		 <p>Acetyl SMX</p>	<p>(Xu et al., 2011)</p>
<p>White-rot fungus <i>Trametes versicolor</i></p>	<p>9 mg/L (SMT)</p>	 <p>Formyl SMT</p>  <p>N⁴-glucose SMT</p>  <p>N⁴-hydroxyl SMT</p>  <p>Desulfo SMT</p>  <p>Desamino SMT</p>  <p>N¹-hydroxy SMT</p>		<p>(García-Galán et al., 2011b)</p>

Table 2.11 (cont'd). Biotransformation products of SMT and SMX

<p>Anaerobic sulfate-reducing bacteria sludge system</p>	<p>25-200 µg/L (SMX)</p>	<p>.</p>		<p>(Jia et al., 2017)</p>
--	--------------------------	----------	--	---------------------------

Table 2. 12. Biotransformation products of CTC and OTC.

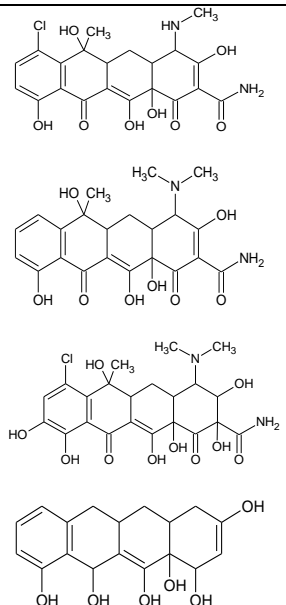
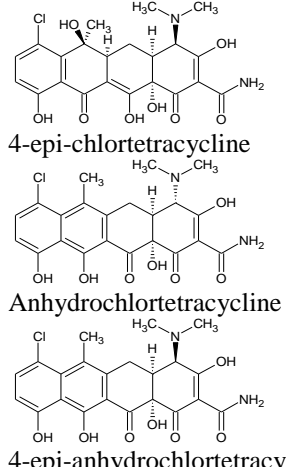
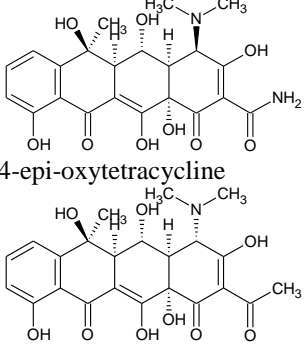
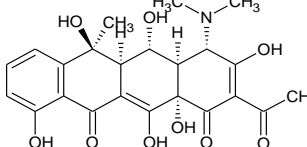
Bacteria/fungus species	Antibiotic concentrations in water/soil	Transformation products		Reference
		CTC	OTC	
<i>Firmicutes, Proteobacteria and Bacteroidetes</i>	100 µg/L (CTC)			(Liao et al., 2017)
<i>Betaproteobacteria</i>	0.5 mg/L	 <p>4-epi-chlortetracycline</p> <p>Anhydrochlortetracycline</p> <p>4-epi-anhydrochlortetracycline</p>		(Aydin et al., 2016)

Table 2.12 (cont'd). Biotransformation products of CTC and OTC.

<p>Class Anaerolineae and family Flavobacteriaceae stimulated by arbuscular mycorrhizal fungus hyphae and earthworm</p>	<p>99.3 mg/kg (OTC)</p>		 <p>4-epi-oxytetracycline</p> <p>2-acetyl-2-decarboxamido-oxytetracycline</p>	<p>(Cao et al., 2018)</p>
<p><i>Pleurotus ostreatus</i> mycelium</p>	<p>50 and 100 mg/L (OTC)</p>		 <p>2-acetyl-2-decarboxamido-oxytetracycline</p>	<p>(Migliore et al., 2012)</p>

2.4. Plant uptake, metabolism of antimicrobials, and the risk to humans exposed to contaminated food crops

2.4.1. Triclosan and triclocarban

Several studies on uptake and bioaccumulation of TCS and TCC by crop plants have been reported. Wu et al. found that TCS and TCC are taken up by soybean (*Glycine max* L. Merr.) from a biosolids amended soil under greenhouse conditions. These two compounds were translocated into above ground parts and were even detectable in the beans. The bioaccumulation factors (BAF), which is defined as the ratio of a compound's concentration in plant tissues to its concentration in soil, were 2.2–5.8 for TCS and 1.8–2.0 for TCC, respectively (Wu et al., 2010b). Besides, substantially higher BAF values were reported by Aryal and Reinhold; for TCS, BAF values ranged from 972 in pumpkin (*Cucurbita pepo* cultivar Howden) to 1822 in zucchini (*Cucurbita pepo* cultivar Gold Rush); for TCC, the corresponding values were 11 and 40, respectively (Aryal and Reinhold, 2011). Additionally, uptake and bioaccumulation of TCS and TCC has also been observed in root and leafy vegetables. Carrots grown in soil contained an average TCS concentration of 3 mg/kg dw accumulated about 20 µg of this antimicrobial in the edible root parts after the plants maturation (Macherius et al., 2012c). Pannu et al. also reported the uptake and translocation of biosolids-associated TCS into lettuce and radish leaves, ranging from 0.01–0.90 µg/g dw (Pannu et al., 2012). The bioaccumulation factor of TCC was from 0.31–0.73 for five common vegetables (Wu et al., 2012). Generally, documented TCS and TCC contamination in different edible parts of vegetables clearly presents an introduction of these antimicrobials into food chain via biosolids application. Accumulation of antimicrobials in plants may impose toxic effects on these species themselves and also pose potential risks to animals and human through

consumption of contaminated foods (Wu et al., 2010b). Recent studies on bioaccumulation of TCS and TCC by food crops are presented in Table 2.13 and Table 2.14.

TCS and TCC may undergo various biotransformation processes after plant uptake. Macherius et al. observed a fast metabolism of TCS in carrot cell cultures and identified eight unknown phase II metabolites conjugated with saccharides, disaccharides, malonic acid and sulfate in both the cell cultures and extracts of carrot plants cultivated in TCS contaminated soil (Macherius et al., 2012b). Importantly, the amount of TCS in the form of conjugates in the carrot roots (peel and core) was about 100 μg , obviously exceeds the 20 μg of the unaltered TCS detected in a previous study (Macherius et al., 2012b, Macherius et al., 2012c). More diverse groups of phase II metabolites of TCS were detected in horseradish hairy root culture using high resolution mass spectrometry and multivariate analysis approaches (Figure 2.4) (Macherius et al., 2014b). Structure proposals were elaborated for 23 TCS metabolites based on their MS data. The conjugation of the phenolic OH- group of TCS with glucose plays a central role, forming an intermediate for a number of further metabolites, such as malonylhexoside, acetylhexoside, sulfohexoside, disaccharides, malonylsulfohexoside, malonyldisulfohexoside). Phase I reactions apparently play a minor role in the phytometabolic pathways of TCS in the hairy root culture of horseradish (Macherius et al., 2014b).

Although plant uptake of TCC have been reported for several plant species, phytometabolism of TCC has not been clearly elucidated. Recently, Macherius et al. and Wu et al. observed that TCC was recalcitrant to metabolism, whereas TCS was largely metabolized by carrot cell cultures within 120 h and 90 h, respectively (Macherius et al., 2012b, Wu et al., 2016). Compared to TCS, TCC lacks functional groups that are suitable for direct phase II conjugation reactions (e.g hydroxyl group); therefore, metabolism of TCC potentially requires an activation by

phase I transformation reactions to allow conjugation in phase II (Macherius et al., 2012b). Accordingly, a longer exposure time may be required for plant metabolism of TCC to be detectable. In a recent study by Huynh et al., jalapeno pepper plants were hydroponically exposed to TCC at a concentration of 500 $\mu\text{g/L}$ for up to 12 weeks. The data suggested that hydroxylated TCC were the primary phase I transformation products, including 2'-OH TCC and 6-OH TCC, both bearing the hydroxyl group in the *ortho* position; and 3'-OH TCC with the hydroxyl group in the *meta* position relative to the urea group. In phase II, the OH-TCC metabolites were subsequently conjugated with glucose to form TCC-O-glucose, followed by sequestration to cell wall compartments (Huynh et al., 2018) (Figure 2.5).

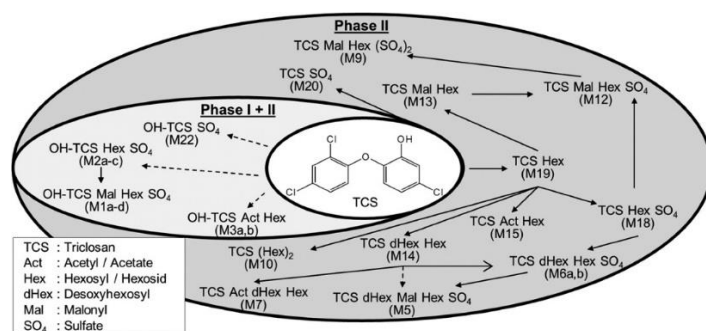


Figure 2. 4. Proposed pathway of TCS metabolism in hair root cultures of horseradish (Macherius et al., 2014b).

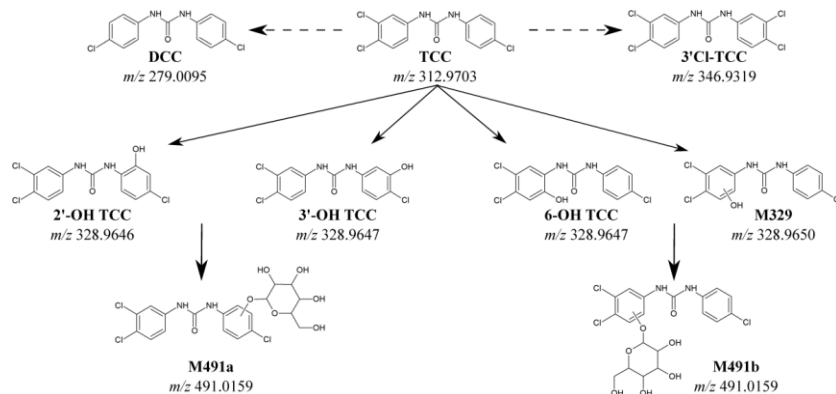


Figure 2. 5. Proposed metabolic pathways of TCC in jalapeno pepper plants (Huynh et al., 2018).

Table 2. 13. Summary of reported TCS bioaccumulation in food crops.

Concentrations in soil (ng/g dw)	Vegetables species	Plant tissues	Concentrations (ng/g dw)	Reference
13.2	Soybean	Root	76.8	(Wu et al., 2010b)
		Stem	136	
		Leaf	120	
		Bean	12.6	
433.7	Cabbage	Root	2,456.3	(Holling et al., 2012)
		Shoot	62	
180 (in applied biosolids)	Pumpkin	Root	20,000	(Aryal and Reinhold, 2011)
		Stem	8,000	
		Leaf	1,000	
	Zucchini	Root	40,000	
		Stem	5,000	
		Leaf	6,000	
1,000	Lettuce	Shoot	10	(Pannu et al., 2012)
4,600	Lettuce	Shoot	120	
10,000	Lettuce	Shoot	900	
990	Radish	Root	100	
		Shoot	<1	
4,500	Radish	Root	1,200	
		Shoot	17	
9,900	Radish	Root	9,200	
		Shoot	63	
4.9 – 29.2	Green pepper	Edible tissues	<2.8	(Prosser et al., 2014)
	Carrot		<2.8	
	Cucumber		<2.8 – 4.0	
	Radish		<2.8 – 5.2	
	Lettuce		< 2.8	

Table 2. 14. Summary of reported TCC bioaccumulation in food crops.

Concentrations in soil (ng/g dw)	Vegetables species	Plant tissues	Concentrations (ng/g)	Reference	
82.5	Soybean	Root	168	(Wu et al., 2010b)	
		Stem	16.5		
		Leaf	37.6		
		Bean	2.6		
8180 (in applied biosolids)	Pumpkin	Root	2,000	(Aryal and Reinhold, 2011)	
		Stem	2,000		
		Leaf	750		
	Zucchini	Root	15,000		
		Stem	2,000		
		Leaf	3,000		
957	Pepper	Root	400	(Wu et al., 2012)	
		Shoot	400		
		Fruit	150		
901	Collard	Root	450		
		Shoot	250		
935	Lettuce	Root	200		
		Shoot	250		
887	Radish	Root	225		
		Shoot	280		
942	Tomato	Root	550		
		Shoot	400		
		Fruit	250		
7.5 – 47.3	Green pepper	Edible tissues	<2.5 – 5.1		(Prosser et al., 2014)
	Carrot		<2.5 – 4.6		
	Cucumber		<2.5 – 5.7		
	Radish		<2.5		
	Lettuce		<2.5		

2.4.2. Sulfonamides and tetracyclines

Uptake and accumulation of tetracyclines and sulfonamides, especially in edible organs, have been confirmed for a broad spectrum of crop plants, including carrot, radish, potato, lettuce, cabbage, cucumber, tomato, rape, pea, celery, coriander, wheat, and corn (Ahmed et al., 2015, Boxall et al., 2006, Dolliver et al., 2007, Franklin et al., 2016, Hu et al., 2010b, Li et al., 2013a, Tanoue et al., 2012). In most cases, accumulation of sulfonamides was markedly higher than that of tetracyclines. Sulfonamides are low molecular weight molecules that are water soluble and weakly adsorbed to soil particles—properties which facilitate diffusion through root membranes. Once uptaken by roots, translocation of antibiotics via the xylem depends on their chemical properties. Due to low octanol-water partition coefficient ($\log K_{ow} < 2$) and a neutral charge in the xylem vessels, sulfonamides are expected to be easily translocated to above ground biomass, including edible organs. Recent studies on bioaccumulation of SMT, SMX, CTC, and OTC by food crops are presented in Tables 2.15 – 2.18.

Farkas et al. exposed pinto beans (*Phaseolus vulgaris*) and maize (*Zea mays*) to CTC and reported the formation of CTC-glutathione conjugate only in maize, suggesting that maize is able to detoxify CTC via the glutathione pathway, whereas pinto bean cannot (Farkas et al., 2007). However, other unknown pathways may also involve in the detoxification of CTC in plants, which merit further research to better understand the phytometabolic pathways of tetracyclines. Although bioaccumulation of sulfonamides has been well documented in literature, details on phytometabolism of sulfonamides is still not well understood. Transformation of organic xenobiotics in plants largely depends on their chemical structures and physiochemical properties, in which conjugation with amino acids and glycosides represent the most common pathways (Fu et al., 2017a, Macherius et al., 2012b, Riemenschneider et al., 2017b). Recently, Dudley et al.

observed that SMX was extensively metabolized by *A. thaliana* cells and cucumber seedlings via oxidation and conjugation with glutathione and leucine, or direct conjugation via acetylation and glucuronidation (Dudley et al., 2018). Additionally, more than 50% of the radiolabeled SMX was present in plant tissues as bound residues, suggesting extensive phase III metabolism and detoxification (Dudley et al., 2018). Although accumulation of the parent SMX was universal, conclusions as to its metabolic fate in plant tissues drastically differ. For instance, no metabolites of SMX were detected in Chinese cabbage and water spinach exposed to 100 µg/mL SMX after 5 days (Chen et al., 2017). Conversely, several phase I and phase II metabolites of SMX were observed in *A. thaliana* cells during a 4-day exposure, of which N⁴-acetyl-SMX was the major metabolite (Dudley et al., 2018). Similar metabolites were also detected in the intact cucumber seedlings, although at lower concentrations compared to those in the cell culture trials (Dudley et al., 2018).

Table 2. 15. Summary of reported SMT bioaccumulation in food crops.

Concentrations in soil (ng/g dw)	Vegetables species	Plant tissues	Concentrations (ng/g)	Concentrations (ng/g fw)	Reference
50 mg/L (in applied manure)	Corn		950		(Dolliver et al., 2007)
	Lettuce		1,000		
	Potato		100		
100 mg/L (in applied manure)	Corn		1,200		
	Lettuce		1,100		
	Potato		200		
56.2 – 72.6	Radish	Leaf	<0.8 – 0.8		(Kang et al., 2013)
		Peel	<0.8		
		Pith	<0.8		
	Lettuce	Leaf	1.8		
	Carrot	Peel	<0.8		
		Pith	<0.8		
	Garlic	Bulb	<0.8		
		Scape	<0.8		
	Onion	Bulb	<0.8		
		Pith	<0.8		
	Potato	Peel	<0.8 – 1.2		
		Tomato	Fruit	<0.8	
	Spinach	Leaf	1.2 – 5		
Cabbage	Leaf	<0.8			
Pepper	Fruit	<0.8			
Corn	Fruit	<0.8			
5,000	Cucumber	Root		5,000	(Ahmed et al., 2015)
		Leaf		200	
		Fruit		24	
	Tomato	Root		7,500	
		Leaf		190	
		Fruit		25	
Lettuce	Root		6,000		
	Leaf		1,000		
10,000	Cucumber	Root		7,500	
		Leaf		800	
		Fruit		20	
	Tomato	Root		10,000	
		Leaf		2,200	
		Fruit		37	
Lettuce	Root		14,000		
	Leaf		2,250		
20,000	Cucumber	Root		12,000	
		Leaf		4,000	
		Fruit		37	
	Tomato	Root		27,000	
		Leaf		14,000	
		Fruit		41	
Lettuce	Root		23,000		
	Leaf		2,300		

Table 2. 16. Summary of reported SMX bioaccumulation in food crops.

Concentrations in soil (ng/g dw)	Vegetables species	Plant tissues	Concentrations (ng/g)	Concentrations (ng/g fw)	Reference
5,000	Cucumber	Root		5,700	(Ahmed et al., 2015)
		Leaf		200	
		Fruit		27	
	Tomato	Root		16,000	
		Leaf		400	
		Fruit		10	
	Lettuce	Root		7,500	
		Leaf		600	
	10,000	Cucumber	Root		
Leaf				500	
Fruit				15	
Tomato		Root		20,000	
		Leaf		1,000	
		Fruit		22	
Lettuce		Root		12,000	
		Leaf		600	
20,000		Cucumber	Root		
	Leaf			1,700	
	Fruit			20	
	Tomato	Root		34,000	
		Leaf		3,800	
		Fruit		40	
	Lettuce	Root		27,000	
		Leaf		3,200	
	0.1 – 0.9	Radish	Root	ND	
Stalk			ND		
Leaf			0.9 – 2.7		
Rape		Root	ND		
		Leaf	0.2		
Celery		Stalk	ND		
		Leaf	ND		
Coriander		Root	ND		
		Leaf	ND		

ND: not detected

Table 2. 17. Summary of reported CTC bioaccumulation in food crops.

Concentrations in soil (ng/g dw)	Vegetables species	Plant tissues	Concentrations (ng/g dw)	Concentrations (ng/g fw)	Reference
n.a.	Green onion	Shoot	12.8 – 14.4		(Kumar et al., 2005)
	Cabbage	Shoot	10.0 – 11.4		
240	Wheat	Root	111 – 1,104		(Grote et al., 2007)
		Stem/Leaf	822		
		Grain	43		
0.7 – 0.9	Radish	Leaf	<0.4		(Kang et al., 2013)
		Peel	<0.4		
		Pith	<0.4		
	Lettuce	Leaf	<0.4		
	Carrot	Peel	<0.4		
		Pith	<0.4		
	Garlic	Bulb	<0.4		
		Scape	<0.4		
	Onion	Bulb	<0.4		
	Potato	Pith	<0.4		
		Peel	<0.4		
	Tomato	Fruit	<0.4		
	Spinach	Leaf	0.5		
Cabbage	Leaf	<0.4			
Pepper	Fruit	<0.4			
Corn	Fruit	<0.4			
5,000	Cucumber	Root		200	(Ahmed et al., 2015)
		Leaf		100	
		Fruit		7	
	Tomato	Root		200	
		Leaf		100	
		Fruit		18	
Lettuce	Root		220		
	Leaf		90		
10,000	Cucumber	Root		480	(Ahmed et al., 2015)
		Leaf		180	
		Fruit		12	
	Tomato	Root		250	
		Leaf		200	
		Fruit		25	
Lettuce	Root		600		
	Leaf		150		
20,000	Cucumber	Root		1,000	(Ahmed et al., 2015)
		Leaf		280	
		Fruit		17.5	
	Tomato	Root		400	
		Leaf		400	
		Fruit		22	
Lettuce	Root		1180		
	Leaf		200		
33.1 – 1,079	Radish	Root	ND		(Hu et al., 2010b)
		Stalk	9.4		
		Leaf	6 – 18		
	Rape	Root	ND		
		Leaf	3.3		

Table 2. 18. Summary of reported OTC bioaccumulation in food crops.

Concentrations in soil (ng/g dw)	Vegetables species	Plant tissues	Concentrations (ng/g dw)	Concentrations (ng/g fw)	Reference
5,000	Cucumber	Root		180	(Ahmed et al., 2015)
		Leaf		20	
		Fruit		2	
	Tomato	Root		350	
		Leaf		200	
		Fruit		18	
	Lettuce	Root		40	
		Leaf		5	
10,000	Cucumber	Root		380	
		Leaf		100	
		Fruit		7	
	Tomato	Root		500	
		Leaf		600	
		Fruit		70	
	Lettuce	Root		100	
		Leaf		10	
20,000	Cucumber	Root		800	
		Leaf		700	
		Fruit		7.5	
	Tomato	Root		1,400	
		Leaf		1,650	
		Fruit		110	
	Lettuce	Root		220	
		Leaf		70	
124 – 2,683	Radish	Root	8.3		(Hu et al., 2010b)
		Stalk	14.7		
		Leaf	17 – 57		
	Rape	Root	ND		
		Leaf	56 – 187		
	Celery	Stalk	ND		
		Leaf	ND		
	Coriander	Root	35 – 205		
Leaf		78 – 330			

ND: not detected

2.4.3. Human health risk from consumption of contaminated food crops

Antimicrobials have been intensively studied with respect to their occurrence in agricultural soils and subsequent accumulation in crop plants. However, human health risk assessment regarding unintentional exposure to antimicrobials via consuming contaminated food crops is still limited and merits further research. Most recent studies have concluded that antimicrobial residues in the edible tissues of vegetables represent a *de minimis* risk to human health (Prosser and Sibley, 2015). It is worth noting that the estimated exposure values for human vary widely because the data regarding plant accumulation of antimicrobials were obtained under different experimental condition (e.g. hydroponic, greenhouse or field). Mathews et al. estimated that TCS and TCC exposure from hydroponically grown vegetables (cucumber, tomato, cabbage, pepper, celery, beet, and onion) is 10^3 times greater than exposure from drinking water and $10^{0.5}$ times less than exposure from product use. The total estimated exposure is $10^{2.9}$ to $10^{3.3}$ times less than the acute no observed adverse effect level (NOAEL) for TCS and TCC, indicating that current exposure does not present a regulated human health risk (Mathews et al., 2014). Likewise, human exposure to other antimicrobials is likely to be low through annual consumption of edible crops grown in manure-amended or wastewater-irrigated soil (Pan and Chu, 2017a). Typically, the estimated values of annual potential human exposure of antimicrobials in edible plants were much lower than the minimum therapeutic doses (typically between 20 and 200 mg/day) or below the recommended acceptable daily intake (ADI) values. The estimated annual sulfonamides exposure for spinach leaf were 1.32 μg per capita (Wu et al., 2013). Human exposure to tetracyclines and sulfonamides in Chinese white cabbage, spinach, radish, corn, and rice under long-term irrigation with wastewater or fishpond water ranged from 0.003 to 21.8 μg (Pan et al., 2014). Matamoros et al. predicted that human consumption of vegetable crops irrigated with

antibiotic-contaminated water would cause an exposure of 500 ng sulfonamides/day, a level well below the therapeutic dose for sulfonamides (Matamoros et al., 2012).

However, these risk assessment studies on human consumption of contaminated crops often overlook the metabolism of antimicrobials in plants, which has been addressed in recent plant uptake studies (Malchi et al., 2015). The uptaken xenobiotics have been reported to undergo extensive metabolism in plant tissues, in which the parent compounds often account for only negligible proportions (e.g. <10%) of all products detected in plant tissues (LeFevre et al., 2015, LeFevre et al., 2016, Riemenschneider et al., 2017b). A large proportion of the metabolites have been found to be conjugated with glucose. In human systems, after ingestion, materials encounter salivary, gastric, and intestinal secretions, which are a mixture of salts, acids/bases, and enzymes. Gastrointestinal secretions include both α -amylase and amyloglucosidase, both of which specifically act on glycosidic linkages within ingested materials. α -amylase hydrolyze α -1,4 glycosidic bonds at random locations, while amyloglucosidase hydrolyzes both α -1,4- and α -1,6-glycosidic bonds. Consequently, phytometabolites are likely hydrolyzed during digestion (Kemper, 2008), releasing the parent aglycone. As a result, human exposure to antibiotics during digestion is expected to be exaggerated. In addition, metabolites such as methyl-triclosan derived from TCS is potentially more toxic than the parent compound and have been found at significantly higher concentrations than the parent compounds (Malchi et al., 2015). Accordingly, antimicrobial metabolism warrants discussion in assessing human health risk of consuming contaminated vegetables.

2.5. The hidden role of plant root exudates in transformation of organic xenobiotics

In addition to uptake of biologically active chemicals, plant roots continuously produce and release a wide array of compounds into the rhizosphere. The excreted compounds are often

categorized into two classes: low-molecular weight compounds (e.g. amino acids, organic acids, sugars, phenolics, secondary metabolites) accounting for much of the diversity of root exudates; while high-molecular weight exudates (e.g. polysaccharides and protein) are less diverse but often compose a larger proportions of root exudates by mass (Bais et al., 2006). A plant may secrete 10-20% of its photosynthate in root exudates (Azaizeh et al., 2011), which exhibit a multitude of functions in ecological interactions with the microbial soil community, acting not only as signaling molecules, attractants, stimulants but also as inhibitors or repellants (Baetz and Martinoia, 2014). Consequently, the nature and relative abundance of root exudates play a key role in shaping the soil microbial community in both positive and negative ways. Bacteria thrive on abundant carbohydrates and amino acids in the root exudates and some of these rhizobacteria provide benefits to plants through synthesis of plant growth hormones or controlling plant diseases caused by soil fungi and bacteria (Bais et al., 2006). On the other hand, root exudates also comprise of a variety of compounds with antimicrobial activity to cope with relentless attacks of pathogens inhabiting the soil surrounding the root system (e.g. pathogenic microbes, fungi or nematodes) (Baetz and Martinoia, 2014)—indicating that root exudates may exert selective pressure for antibiotic resistance, especially through generic drug efflux genes, even in the absence of antibiotics.

Root exudates can potentially enhance biodegradation of organic xenobiotics in different ways: (i) facilitate the co-metabolic transformation of pollutants with similar structures, (ii) induce genes coding enzymes involved in the degradation process, (iii) increase contaminant bioavailability, and (iv) selectively increase the number and activity of pollutant degraders in the rhizosphere (Azaizeh et al., 2011). However, the critical role of root exudates in degradation of contaminants surrounding the rhizosphere is often overlooked. Exudate-enhanced biodegradation

has been observed for a wide range of organic pollutants, such as polycyclic aromatic hydrocarbons (PAHs) and polychlorinated biphenyls (PCBs). An *in vitro* study by Techer et al. demonstrated that secondary plant metabolites in root exudates of *Miscanthus x giganteus* selectively promoted growth of PAH-degrading bacterial consortia, biostimulating degradation of polycyclic compounds including PAH (Técher et al., 2011). The ability of plants to extract and metabolize PCBs is limited due to the recalcitrance and low bioavailability of these pollutants in soils. In fact, microbes are key players of PCB degradation, in both aerobic and anaerobic conditions (Vergani et al., 2017). In this specific niche, root exudates play a pivotal role by promoting the biphenyl catabolic pathway responsible for microbial oxidative PCB metabolism and by improving the overall PCB degradation performance (Vergani et al., 2017). Along with specialized carbon compounds, plants also exude several antimicrobial compounds (e.g. phytoalexins, salicylic acid and flavonoids) that create a strongly selective environment in the rhizosphere, resulting in increased expression of ARG. The presence of contaminants in the soils imposes further selection pressure on microorganisms. Under this double-selection pressure, only microorganisms that can use specialized carbon sources can cope with the presence of contaminants and are highly competitive will be significantly activated (Bais et al., 2006, Yergeau et al., 2014). Yergeau et al. observed significant increases in the expression of antimicrobial resistance genes in the rhizosphere of willows, with stronger increases in contaminated soils (Yergeau et al., 2014). Moreover, potential induction or selection of ARG in bacteria that proliferate in the presence of veterinary antibiotics may also occur in the rhizosphere. For example, the resistance of sulfadiazine resistant bacteria was studied in the presence of artificial root exudates with an organic carbon amendment rate of $134 \mu\text{g C g}^{-1} \text{d}^{-1}$. Bacterial tolerance to antibiotic sulfadiazine significantly increased with pulse additions of artificial root exudates and

was coupled with a rapid dissipation of sulfadiazine in the presence of the root exudates due to an increase in microbial activity in the presence of added carbon (Brandt et al., 2009, Mathews and Reinhold, 2013).

2.6. Metabolomics for identification of plant metabolites of organic xenobiotics

Organic xenobiotic contaminants are prone to extensive phytometabolism following plant uptake, leading to formation of a diverse metabolite pool that often accounts for more than 90% of the uptaken chemicals in plant tissues (Dudley et al., 2018, Huynh et al., 2018). However, structural elucidation of these xenobiotic metabolites is inherently challenging due to metabolites' reactivity, structural diversity—mostly unknown, and often low concentrations (Lu et al., 2017). Additionally, the complexity of plant matrices frequently results the interferences between compounds of similar molecular weight (Lu et al., 2017). Little et al. classified the metabolites to be identified into three categories: (i) “known knowns”, (ii) “known unknowns”, and (iii) “unknown unknowns” (Little et al., 2011). In general, a “known known” refers to a compound whose structure is known to the investigator and its presence need to be confirmed. For example, Riemenschneider et al. studied metabolism of carbamazepine by intact tomato plants and was able to quantified a total of 11 transformation products of carbamazepine in plant tissues by liquid chromatography–tandem mass spectrometry using reference standards. However, their total amount corresponded to only 33% of the carbamazepine taken up by plants (Riemenschneider et al., 2017b). The results imply that a larger proportion of the metabolites was overlooked by this targeted approach. A “known unknown” is a compound that is unknown to the investigator but is available in the chemical literature or mass spectral database. Lastly, a “unknown unknown” is a compound that is not cited elsewhere (Little et al., 2011). Identification of “known unknowns” and “unknown unknowns” in studies of plant metabolism of xenobiotics requires access to more

advanced instruments, versatile mass-spectral database, and an in-depth interpretation of the acquired mass spectra (Ma and Yates, 2018). Since plant metabolites of organic xenobiotics are polar, thermo-labile compounds, liquid chromatography coupled with mass spectrometry (LC-MS), using different types of mass analyzers, is the technique of choice (Bletsou et al., 2015). Mass analyzers commonly used are triple quadrupole (tandem MS/MS), tight-of-flight (TOF), Fourier transform ion cyclotron resonance (FT-ICR), ion trap (IT), Orbitrap and hybrid (e.g. quadrupole time-of-flight (QTOF), quadrupole-linear ion trap (Q-LIT), linear ion trap-orbitrap, and quadrupole-Orbitrap) (Bletsou et al., 2015). A brief overview of commercially available mass spectrometers coupled with LC and their figures of merits are showed in Table 2.19. Now, high resolution mass analyzers (e.g. TOF, Orbitrap, FT-ICR) are the driving force in establishing robust and reliable analytical methodologies for studying plant metabolism of organic xenobiotic, thanks to its sensitivity in full-scan mode with high mass accuracy.

Table 2. 19. General comparison of commercial mass analyzers in LC-MS instruments. Typical values for an m/z range of 300–400 are given. Specific instruments or configurations might achieve better figures of merits (Krauss et al., 2010).

Mass spectrometer	Resolving power ^a	Mass accuracy	Linear dynamic range	Sensitivity ^b
Triple quadrupole (tandem MS/MS, QqQ)	unit resolution ^c	50	10^4	Femto- to picogram (MRM)
Quadrupole ion trap (QIT)	10,000	50	10^3	Femto- to picogram (MRM, full scan)
Time-of-flight (TOF)	20,000	3	$10^2 - 10^3$	Picogram (full scan)
Orbitrap	100,000	2	$10^3 - 10^4$	Femto- to picogram (full scan)
Fourier transform ion cyclotron resonance (FT-ICR)	1,000,000	≤ 1	10^4	Picogram (full scan)

^aResolving power depends on m/z range and scan speed on most instruments

^bSensitivity depends strongly on the ionization efficiency of the compound in the ion source

^cUnit mass resolution is the resolution for standard quadrupole instruments; with special hyperbolic quadrupole instruments a resolving power of 5,000 and a mass accuracy of 5 ppm can be achieved without a major loss of signal intensity.

The workflows for identification of xenobiotic metabolites in any matrices largely depend on the instrumentation and available software (Bletsou et al., 2015). Based on Little et al.'s classification of the metabolite candidates discussed above, an outline for the screening procedure is presented in Figure 2.6.

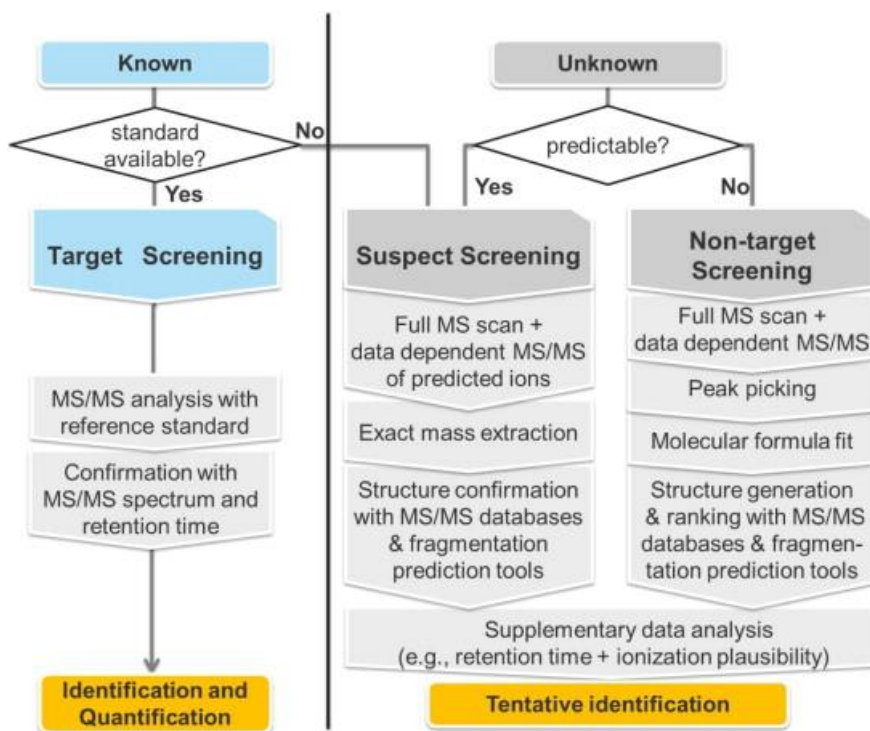


Figure 2. 6. A proposed workflow for screening xenobiotic metabolites (Bletsou et al., 2015).

2.6.1. Target screening

In target screening, the metabolites of certain xenobiotics have been routinely reported in literature and authentic reference standards are available for qualitative and quantitative analyses. Modern LC-MS/MS instruments with multiple reaction monitoring (MRM) of precursor-product ions transitions (QqQ or QIT instruments) have been considered a workhorse in target quantitative analysis of the parent xenobiotics and their metabolites in plant and/or tissue culture matrices. The MRM mode provides many advantages for target analysis, such as increased selectivity, high sensitivity, reduced interferences of complex plant matrices, which allows robust quantification

(Bletsou et al., 2015). Several studies have suggested that monitoring of at least two transitions are required to eliminate potential false positive identifications for individual compounds, which might occur when only one transition is monitored (Krauss et al., 2010, Pozo et al., 2006). So far, LC-MS/MS has been widely used for simultaneous quantification of multiple emerging contaminants (e.g. pharmaceuticals and personal care products) and metabolites in plant and/or tissue culture matrices with detection limit of part-per-billion (Riemenschneider et al., 2016, Riemenschneider et al., 2017a, Riemenschneider et al., 2017b). However, LC-MS/MS in MRM mode only allows for quantification of a limited number of metabolites, which often account for a smaller proportion of all possible metabolites in plant tissues (Malchi et al., 2014, Riemenschneider et al., 2017b).

While adequate results have been obtained for the analysis of organic xenobiotics and their metabolites using LC-MS/MS, this approach also exhibits some limitations as indicated by (Krauss et al., 2010):

- (i) MRM methods are typically limited to 100–150 target analytes under the constraints of at least two transitions; otherwise accuracy or sensitivity deteriorate due to insufficient peak resolution or too short acquisition times for the individual MS/MS transition, respectively.
- (ii) For some analytes, only non-specific transitions (e.g. neutral loss of H₂O or CO₂) might occur, which are also common for matrix interferences.
- (iii) For some analytes, particularly low-molecular-weight compounds, only one MRM transition can be obtained.

High resolution mass spectrometers (HR-MS) offer promising solutions to the limitations of MRM analysis. Technically, all compounds present in a sample can be determined

simultaneously with HRMS instruments operating in full-scan mode, making pre-determination of compounds and associated MRM transitions unnecessary. Additionally, hybrid instruments (e.g. QTOF-MS) also offer the possibility of data-dependent MS/MS acquisition; in other words, the MS/MS analysis is only triggered if the compounds of interest can be detected in full-scan mode. However, the sensitivity and dynamic range of the QTOF-MS instruments are typically 1–2 orders-of-magnitude lower than those of the tandem MS/MS in MRM mode. Alternatively, a better dynamic range and sensitivity that are comparable to MS/MS can be achieved with the Orbitrap MS instruments (Table 2.19) (Krauss et al., 2010).

2.6.2. Suspect screening

Suspect screening is the method of choice when authentic standards for confirmation of the metabolites are not available. However, the formula and molecular structure of the suspects can be predicted using computational (*in-silico*) prediction tools (Bletsou et al., 2015) or have been reported in literature. Plants are capable of metabolizing uptaken xenobiotics to hundreds of different products in plant cells; most of them are “unknowns” (Macherius et al., 2012a, Macherius et al., 2014c, Marsik et al., 2017). Consequently, confirmation of these analytes with reference standards is impossible. However, metabolic pathways of organic xenobiotic in plant tissues are predictable to some extent. In general, metabolic pathways of xenobiotic chemicals in plants consist of three phases that are analogous to mammalian liver metabolism (Sandermann, 1992). Phase I reactions render parent molecules more polar and biologically active through multiple reactions, such as hydroxylation, hydrolysis, or oxidation due to cytochrome P450 enzymes (Fu et al., 2017b, Macherius et al., 2012b, Marsik et al., 2017, Sandermann, 1992). Phase II, which consists of conjugation reactions, forms compounds of higher molecular weight by adding amino acids, glutathione, or carbohydrates to phase I transformation products or the parent molecule to

reduce their biological activities and to increase their solubility in water (Fu et al., 2017b, Macherius et al., 2012b, Marsik et al., 2017, Sandermann, 1992). In phase III, plants sequester the phase II conjugates in the vacuoles for storage or incorporate the conjugates into the cell wall (Fu et al., 2017b, Macherius et al., 2012b, Sandermann, 1992). The extractable fractions of accumulated xenobiotics in plant tissues contain unaltered parent molecules, phase I and phase II soluble metabolites, and some smaller phase III vacuolar-stored metabolites. Conversely, fractions of metabolites that are incorporated into cell walls form non-extractable (or bound) residues.

To date, a plethora of computational methods and integrated approaches have been developed for the prediction of drug metabolism (Kirchmair et al., 2015, Kirchmair et al., 2012). Although there have been no *in-silico* tools specifically designed for predicting xenobiotic metabolism in plants, the available tools can be utilized to predict the sites of metabolism or structures of the potential metabolites of the uptaken xenobiotics in plant tissues. It has been reported that common reactions in phase I (transformation) and phase II (conjugation) are shared between plants and animals, especially those catalyzed by the CYP450s super family enzymes (Pascal-Lorber et al., 2008, Sandermann, 1992). Overview of the available computational methods for drug metabolism prediction can be found in a recent review by (Kirchmair et al., 2015). The molecular formula obtained from the prediction tools or literature search will allow for the calculation of the accurate mass-to-charge (m/z) ratio of the suspected metabolite, which is then extracted from the high-resolution full-scan mass spectra. In order to prevent false positive findings, the suspected peaks in the extracted chromatograms must exclusively present in the treatments and absent from the blank controls with the mass error $<5\text{ppm}$ (between the observed and calculated accurate mass) (Kern et al., 2009). The number of candidate peaks are filtered further using an intensity-threshold cut off value (e.g. 10^5), the plausibility of the chromatographic

retention time, isotopic pattern, and ionization efficiency (Bletsou et al., 2015, Kern et al., 2009). In the next step, structures of the suspected metabolites are suggested using their MS/MS fragmentation patterns.

2.6.3. Non-target screening

In contrast to suspect screening, non-target screening starts without a priori information available on the compound to be identified and is usually conducted after target and suspect screening (Bletsou et al., 2015). For plant metabolism of xenobiotics, the parent compounds usually remain intact throughout the transformation and/or conjugation reactions. Therefore, the structural information of the parent molecules (e.g. molecular formula, accurate mass, MS/MS fragmentation patterns, retention time, and other physicochemical properties) can be used for identification of the metabolite candidates by eliminating those that do not show any close relationship with the parent compounds. A tentative identification of non-target metabolites is challenging, which involves multiple work-intensive data acquisition and data processing steps. Typical non-targeted MS-based metabolomics workflows includes the following steps.

- (i) Full scan of xenobiotic-exposed samples and the corresponding blank controls to identify signals of potential metabolites and their molecular ions ($[M+H]^+$ and $[M-H]^-$).
- (ii) Acquisition of fragmentation patterns based on collision-induced dissociation (CID).
- (iii) Assignment of molecular structure based on the acquired molecular ions and product ions.
- (iv) Structural elucidation using reference standards. However, if the reference standards are not available, the levels of confidence for each structural assignment

need to be clarified. Currently, the framework proposed by (Schymanski et al., 2014) is commonly used for communicating the levels of confidence in several studies of untargeted xenobiotic metabolism (Figure 2.7).

Quadrupole TOF (QTOF) and Orbitrap mass spectrometers are strongly preferred in order to obtain sufficient mass accuracy required for confirmation of the molecular formula and subsequent interpretation of the fragmentation patterns (Bletsou et al., 2015). Generally, Orbitrap mass analyzers often outperform QTOFs in term of mass resolving power, but at the expense of longer accumulation times; therefore, they may be less applicable for accurate quantification of compounds eluting as narrow LC peaks. On the contrary, QTOFs are often characterized by enhanced duty cycles with the ability to acquire up to 100 MS/MS spectra per second, independently of the resolving power (Fenaille et al., 2017). The ability of modern high-resolution MS instruments to operate in full-scan and MS/MS modes simultaneously generate massive quantities of data in a single run, which require *in silico* data-processing tools for post-acquisition data mining. Currently, there are several open-source and commercial software that can be used for high-resolution spectral processing, such as MZmine 2 (<http://mzmine.github.io/>), XCMS (<https://xcmsonline.scripps.edu>), and vendors' software (e.g. Waters Progenesis QI, Agilent MassHunter).

As shown in Figure 2.6, the first major step in data-processing procedure is “peak picking”, in which chromatograms of treated samples are compared with those of blank controls to exclude the irrelevant signals, remove noise signals, mass recalibration, and componentization of isotopes and adducts (Bletsou et al., 2015). It has been estimated that approximately 100–1000 suspected peaks can be recorded in a usual non-target screening data acquisition (Matsuda, 2016), clearly indicating that structural elucidation of all those peaks is challenging. Nevertheless, in studies of

plant metabolism of xenobiotics, the number of chemically meaningful structures assigned to an “unknown” peak can be limited to those that show a close relationship with the parent compound (Krauss et al., 2010) since the structure of the parent xenobiotic is usually unaltered throughout phase I and phase II reactions in plant cells.

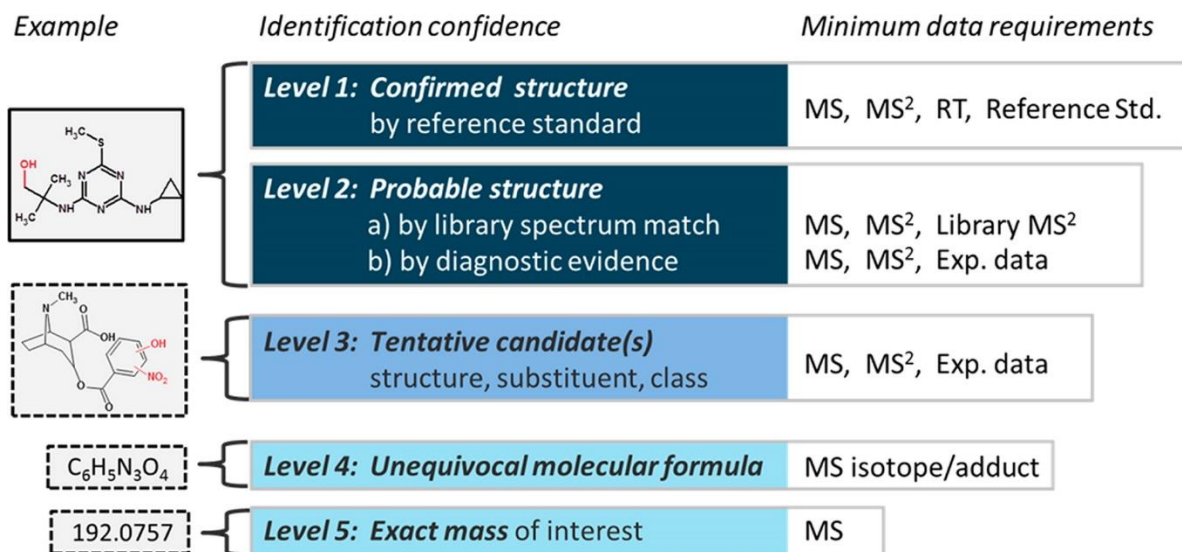


Figure 2. 7. A framework proposed by (Schymanski et al., 2014) for concisely and accurately communicating levels of confidence in high resolution mass spectrometric analysis. *Authors' note*: MS² is intended to also represent other forms of MS fragmentation (e.g. MS^e, MSⁿ).

Following “peak picking”, molecular formula will be assigned to each “unknown” peak based upon its accurate mass, using heuristic filters (e.g. the Seven Golden Rules of Kind and Fiehn (Kind and Fiehn, 2007)). For ranking the candidate structures, the high-resolution MS/MS spectra can be compared with *in silico* mass spectral fragmentation, such as METLIN (<https://metlin.scripps.edu>), MassBank (<http://massbank.eu/MassBank/>), MetFrag (<http://c-ruttikies.github.io/MetFrag/>), MassFrontier (Thermo Scientific). It is worth noting that predictions tools of MS/MS spectra often yield a large number of possible fragments depending on the default collision energy, of which a rather small number are actually observed (Krauss et al., 2010). In

any case, selection criteria must be established for the success of the identification of the metabolite by mass accuracy of the molecular ion (e.g. mass error <5 ppm) and the characteristic fragmentation patterns in MS/MS mode (purity score ≥ 65 recommended) (Aguera et al., 2013, Bletsou et al., 2015).

APPENDIX

Supplementary Table 2.1. Medically important antimicrobial drug classes and active ingredients approved for use in food-producing animals actively marketed in the U.S in 2016 (U.S. FDA, 2017).

Antimicrobial drug classes	Active ingredients
Medically Important	
Aminoglycosides	Dihydrostreptomycin Gentamicin Hygromycin B Neomycin Spectinomycin
Amphenicols	Florfenicol
Cephalosporins	Ceftiofur Cephapirin
Diaminopyrimidines	Ormetoprim
Fluoroquinolones	Danofloxacin Enrofloxacin
Lincosamides	Lincomycin Pirlimycin
Macrolides	Erythromycin Gamithromycin Tildipirosin Tilmicosin Tulathromycin Tylosin Tylvalosin
Penicillins	Amoxicillin Ampicillin Cloxacillin Penicillin
Polymyxins	Polymyxin B
Streptogramins	Virginiamycin
Sulfonamides	Sulfadimethoxine Sulfamethazine
Tetracyclines	Chlortetracycline Oxytetracycline Tetracycline
Not Medically Important	
Aminocoumarins	Novobiocin
Glycolipids	Bambermycins
Ionophores	Laidlomycin Lasalocid Monesin Narasin Salinomycin
Orthosomycins	Avilamycin
Pleuromutilins	Tiamulin
Polypeptides	Bacitracin
Quinoxalines	Carbadox

REFERENCES

REFERENCES

- Aguera, A., Martinez Bueno, M.J. and Fernandez-Alba, A.R., 2013. New trends in the analytical determination of emerging contaminants and their transformation products in environmental waters. *Environ. Sci. Pollut. Res. Int.* 20, 3496-3515.
- Ahmed, M.B.M., Rajapaksha, A.U., Lim, J.E., Vu, N.T., Kim, I.S., King, H.M., Lee, S.S. and Ok, Y.S., 2015. Distribution and Accumulative Pattern of Tetracyclines and Sulfonamides in Edible Vegetables of Cucumber, Tomato, and Lettuce. *J. Agric. Food Chem.* 63, 398-405.
- Al-Rajab, A.J., Sabourin, L., Lapen, D.R. and Topp, E., 2015. Dissipation of triclosan, triclocarban, carbamazepine and naproxen in agricultural soil following surface or sub-surface application of dewatered municipal biosolids. *Sci. Total Environ.* 512–513, 480–488.
- Al-Rajab, A.J., Sabourin, L., Scott, A., Lapen, D.R. and Topp, E., 2009. Impact of biosolids on the persistence and dissipation pathways of triclosan and triclocarban in an agricultural soil. *Sci. Total Environ.* 407, 5978–5985.
- Aryal, N. and Reinhold, D.M., 2011. Phytoaccumulation of antimicrobials from biosolids: Impacts on environmental fate and relevance to human exposure. *Water Res.* 45, 5545-5552.
- Ashfaq, M., Li, Y., Wang, Y., Chen, W., Wang, H., Chen, X., Wu, W., Huang, Z., Yu, C.P. and Sun, Q., 2017. Occurrence, fate, and mass balance of different classes of pharmaceuticals and personal care products in an anaerobic-anoxic-oxic wastewater treatment plant in Xiamen, China. *Water Res.* 123, 655-667.
- Aust, M.-O., Godlinski, F., Travis, G.R., Hao, X., McAllister, T.A., Leinweber, P. and Thiele-Bruhn, S., 2008. Distribution of sulfamethazine, chlortetracycline and tylosin in manure and soil of Canadian feedlots after subtherapeutic use in cattle. *Environ. Pollut.* 156, 1243-1251.
- Aydin, E., Sahin, M., Taskan, E., Hasar, H. and Erdem, M., 2016. Chlortetracycline removal by using hydrogen based membrane biofilm reactor. *J. Hazard. Mater.* 320, 88-95.
- Azaizeh, H., Castro, P.M.L. and Kidd, P., 2011. Schroder, P. and Collins, C.D. (eds), pp. 191-215. Baetz, U. and Martinoia, E., 2014. Root exudates: the hidden part of plant defense. *Trends Plant Sci.* 19, 90-98.
- Bais, H.P., Weir, T.L., Perry, L.G., Gilroy, S. and Vivanco, J.M., 2006. The role of root exudates in rhizosphere interactions with plants and other organisms. *Annu. Rev. Plant Biol.* 57, 233-266.
- Bao, L., Peng, R., Wang, Y., Ma, R., Ren, X., Meng, W., Sun, F., Fang, J., Chen, P., Chen, Q., Cai, J., Jin, J., Guo, J., Yang, S., Mo, X., Zhang, E., Zhang, Y., Lu, Z., Chen, B., Yue, X., Zhu, M., Li, X., Bian, Y., Kong, S., Pan, W., Ding, Q., Cao, J., Liu, R., Chen, N., Huang, X., B, A. and Lyu, H., 2015. Significant reduction of antibiotic consumption and patients' costs after an action plan in China, 2010-2014. *PLoS One* 10, e0118868.

- Baran, W., Adamek, E., Ziemiańska, J. and Sobczak, A., 2011. Effects of the presence of sulfonamides in the environment and their influence on human health. *J. Hazard. Mater.* 196, 1-15.
- Bastos, M.C., dos Santos, D.R., Aubertheau, E., Lima, J., Le Guet, T., Caner, L., Mondamert, L. and Labanowski, J., 2018. Antibiotics and microbial resistance in Brazilian soils under manure application. *Land Degradation & Development* 29, 2472-2484.
- Behera, S.K., Kim, H.W., Oh, J.E. and Park, H.S., 2011. Occurrence and removal of antibiotics, hormones and several other pharmaceuticals in wastewater treatment plants of the largest industrial city of Korea. *Sci. Total Environ.* 409, 4351-4360.
- Ben, W., Zhu, B., Yuan, X., Zhang, Y., Yang, M. and Qiang, Z., 2018. Occurrence, removal and risk of organic micropollutants in wastewater treatment plants across China: Comparison of wastewater treatment processes. *Water Res.* 130, 38-46.
- Bletsou, A.A., Jeon, J., Hollender, J., Archontaki, E. and Thomaidis, N.S., 2015. Targeted and non-targeted liquid chromatography-mass spectrometric workflows for identification of transformation products of emerging pollutants in the aquatic environment. *TrAC, Trends Anal. Chem.* 66, 32-44.
- Botero-Coy, A.M., Martinez-Pachon, D., Boix, C., Rincon, R.J., Castillo, N., Arias-Marin, L.P., Manrique-Losada, L., Torres-Palma, R., Moncayo-Lasso, A. and Hernandez, F., 2018. 'An investigation into the occurrence and removal of pharmaceuticals in Colombian wastewater'. *Sci. Total Environ.* 642, 842-853.
- Boxall, A.B.A., Johnson, P., Smith, E.J., Sinclair, C.J., Stutt, E. and Levy, L.S., 2006. Uptake of Veterinary Medicines from Soils into Plants. *J. Agric. Food Chem.* 54, 2288-2297.
- Brandt, K.K., Sjøholm, O.R., Krogh, K.A., Halling-Sørensen, B. and Nybroe, O., 2009. Increased Pollution-Induced Bacterial Community Tolerance to Sulfadiazine in Soil Hotspots Amended with Artificial Root Exudates. *Environ. Sci. Technol.* 43, 2963-2968.
- Butler, E., Whelan, M.J., Sakrabani, R. and van Egmond, R., 2012. Fate of triclosan in field soils receiving sewage sludge. *Environ. Pollut.* 167, 101-109.
- Cabello, F.C., 2006. Heavy use of prophylactic antibiotics in aquaculture: a growing problem for human and animal health and for the environment. *Environ. Microbiol.* 8, 1137-1144.
- Cabello, F.C., Godfrey, H.P., Buschmann, A.H. and Dolz, H.J., 2016. Aquaculture as yet another environmental gateway to the development and globalisation of antimicrobial resistance. *Lancet Infect. Dis.* 16, e127-e133.
- Cabello, F.C., Godfrey, H.P., Tomova, A., Ivanova, L., Dolz, H., Millanao, A. and Buschmann, A.H., 2013. Antimicrobial use in aquaculture re-examined: its relevance to antimicrobial resistance and to animal and human health. *Environ. Microbiol.* 15, 1917-1942.

Cao, J., Wang, C., Dou, Z., Liu, M. and Ji, D., 2018. Hyphospheric impacts of earthworms and arbuscular mycorrhizal fungus on soil bacterial community to promote oxytetracycline degradation. *J. Hazard. Mater.* 341, 346-354.

Carr, D.L., Morse, A.N., Zak, J.C. and Anderson, T.A., 2011. Microbially Mediated Degradation of Common Pharmaceuticals and Personal Care Products in Soil Under Aerobic and Reduced Oxygen Conditions. *Water, Air, Soil Pollut.* 216, 633-642.

CDC (2017) Antibiotic Use in the United States, 2017: Progress and Opportunities, US Department of Health and Human Services, Atlanta, GA.

Cha, J. and Cupples, A.M., 2009. Detection of the antimicrobials triclocarban and triclosan in agricultural soils following land application of municipal biosolids. *Water Res.* 43, 2522-2530.

Cha, J. and Cupples, A.M., 2010. Triclocarban and triclosan biodegradation at field concentrations and the resulting leaching potentials in three agricultural soils. *Chemosphere* 81, 494-499.

Chen, F., Ying, G.-G., Ma, Y.-B., Chen, Z.-F., Lai, H.-J. and Peng, F.-J., 2014. Field dissipation and risk assessment of typical personal care products TCC, TCS, AHTN and HHCB in biosolid-amended soils. *Sci. Total Environ.* 470-471, 1078-1086.

Chen, H.R., Rairat, T., Loh, S.H., Wu, Y.C., Vickroy, T.W. and Chou, C.C., 2017. Assessment of veterinary drugs in plants using pharmacokinetic approaches: The absorption, distribution and elimination of tetracycline and sulfamethoxazole in ephemeral vegetables. *PLoS One* 12, e0183087.

Chen, X., Casas, M.E., Nielsen, J.L., Wimmer, R. and Bester, K., 2015. Identification of Triclosan-O-Sulfate and other transformation products of Triclosan formed by activated sludge. *Sci. Total Environ.* 505, 39-46.

Chen, X., Nielsen, J.L., Furgal, K., Liu, Y., Lolas, I.B. and Bester, K., 2011. Biodegradation of triclosan and formation of methyl-triclosan in activated sludge under aerobic conditions. *Chemosphere* 84, 452-456.

Chen, Y., Zhang, H., Luo, Y. and Song, J., 2012a. Occurrence and dissipation of veterinary antibiotics in two typical swine wastewater treatment systems in east China. *Environ. Monit. Assess.* 184, 2205-2217.

Chen, Z.F., Ying, G.G., Lai, H.J., Chen, F., Su, H.C., Liu, Y.S., Peng, F.Q. and Zhao, J.L., 2012b. Determination of biocides in different environmental matrices by use of ultra-high-performance liquid chromatography-tandem mass spectrometry. *Anal. Bioanal. Chem.* 404, 3175-3188.

Chopra, I. and Roberts, M., 2001. *Microbiol. Mol. Biol. Rev.*, pp. 232-260.

Clarke, B.O. and Smith, S.R., 2011. Review of 'emerging' organic contaminants in biosolids and assessment of international research priorities for the agricultural use of biosolids. *Environ. Int.* 37, 226-247.

Conde-Cid, M., Álvarez-Esmorís, C., Paradelo-Núñez, R., Nóvoa-Muñoz, J.C., Arias-Estévez, M., Álvarez-Rodríguez, E., Fernández-Sanjurjo, M.J. and Núñez-Delgado, A., 2018a. Occurrence of tetracyclines and sulfonamides in manures, agricultural soils and crops from different areas in Galicia (NW Spain). *Journal of Cleaner Production* 197, 491-500.

Conde-Cid, M., Fernandez-Calvino, D., Novoa-Munoz, J.C., Arias-Estevéz, M., Diaz-Ravina, M., Fernandez-Sanjurjo, M.J., Nunez-Delgado, A. and Alvarez-Rodriguez, E., 2018b. Biotic and abiotic dissipation of tetracyclines using simulated sunlight and in the dark. *Sci. Total Environ.* 635, 1520-1529.

Ding, H., Wu, Y., Zou, B., Lou, Q., Zhang, W., Zhong, J., Lu, L. and Dai, G., 2016. Simultaneous removal and degradation characteristics of sulfonamide, tetracycline, and quinolone antibiotics by laccase-mediated oxidation coupled with soil adsorption. *J. Hazard. Mater.* 307, 350-358.

Dolliver, H., Kumar, K. and Gupta, S., 2007. Sulfamethazine Uptake by Plants from Manure-Amended Soil. *J Environ. Qual.* 36, 1224-1224.

Done, H.Y., Venkatesan, A.K. and Halden, R.U., 2015. Does the Recent Growth of Aquaculture Create Antibiotic Resistance Threats Different from those Associated with Land Animal Production in Agriculture? *Aaps j* 17, 513-524.

Dudley, S., Sun, C., Jiang, J. and Gan, J., 2018. Metabolism of sulfamethoxazole in *Arabidopsis thaliana* cells and cucumber seedlings. *Environ. Pollut.* 242, 1748-1757.

Durán-Álvarez, J.C., Prado, B., González, D., Sánchez, Y. and Jiménez-Cisneros, B., 2015. Environmental fate of naproxen, carbamazepine and triclosan in wastewater, surface water and wastewater irrigated soil — Results of laboratory scale experiments. *Sci. Total Environ.* 538, 350-362.

ECDC, E.A.E., 2015. ECDC/EFSA/EMA first joint report on the integrated analysis of the consumption of antimicrobial agents and occurrence of antimicrobial resistance in bacteria from humans and food-producing animals. *EFSA Journal* 13, 4006.

ECDC/EFSA/EMA, 2017. ECDC/EFSA/EMA second joint report on the integrated analysis of the consumption of antimicrobial agents and occurrence of antimicrobial resistance in bacteria from humans and food-producing animals. *EFSA Journal* 15.

Ezzariai, A., Hafidi, M., Khadra, A., Aemig, Q., El Fels, L., Barret, M., Merlina, G., Patureau, D. and Pinelli, E., 2018. Human and veterinary antibiotics during composting of sludge or manure: Global perspectives on persistence, degradation, and resistance genes. *J. Hazard. Mater.* 359, 465-481.

Farkas, M.H., Berry, J.O. and Aga, D.S., 2007. Chlortetracycline detoxification in maize via induction of glutathione S-transferases after antibiotic exposure. *Environ. Sci. Technol.* 41, 1450-1456.

Fenaille, F., Barbier Saint-Hilaire, P., Rousseau, K. and Junot, C., 2017. Data acquisition workflows in liquid chromatography coupled to high resolution mass spectrometry-based metabolomics: Where do we stand? *J. Chromatogr. A* 1526, 1-12.

Figuerola-Diva, R.A., Vasudevan, D. and MacKay, A.A., 2010. Trends in soil sorption coefficients within common antimicrobial families. *Chemosphere* 79, 786-793.

Förster, M., Laabs, V., Lamshöft, M., Groeneweg, J., Zühlke, S., Spiteller, M., Krauss, M., Kaupenjohann, M. and Amelung, W., 2009. Sequestration of Manure-Applied Sulfadiazine Residues in Soils. *Environ. Sci. Technol.* 43, 1824-1830.

Franklin, A.M., Williams, C.F., Andrews, D.M., Woodward, E.E. and Watson, J.E., 2016. Uptake of Three Antibiotics and an Antiepileptic Drug by Wheat Crops Spray Irrigated with Wastewater Treatment Plant Effluent. *J Environ. Qual.* 45, 546-546.

Fu, Q., Sanganyado, E., Ye, Q. and Gan, J., 2016. Meta-analysis of biosolid effects on persistence of triclosan and triclocarban in soil. *Environ. Pollut.* 210, 137-144.

Fu, Q., Ye, Q., Zhang, J., Richards, J., Borchardt, D. and Gan, J., 2017a. Diclofenac in Arabidopsis cells: Rapid formation of conjugates. *Environ. Pollut.* 222, 383-392.

Fu, Q., Zhang, J., Borchardt, D., Schlenk, D. and Gan, J., 2017b. Direct Conjugation of Emerging Contaminants in Arabidopsis : Indication for an Overlooked Risk in Plants? *Environ. Sci. Technol.* 51, 6071-6081.

Gangadharan Puthiya Veetil, P., Vijaya Nadaraja, A., Bhasi, A., Khan, S. and Bhaskaran, K., 2012. Degradation of triclosan under aerobic, anoxic, and anaerobic conditions. *Appl. Biochem. Biotechnol.* 167, 1603-1612.

Gao, P., Munir, M. and Xagorarakis, I., 2012. Correlation of tetracycline and sulfonamide antibiotics with corresponding resistance genes and resistant bacteria in a conventional municipal wastewater treatment plant. *Sci. Total Environ.* 421, 173-183.

García-Galán, M.J., Díaz-Cruz, M.S. and Barceló, D., 2011a. Occurrence of sulfonamide residues along the Ebro river basin: Removal in wastewater treatment plants and environmental impact assessment. *Environ. Int.* 37, 462-473.

García-Galán, M.J., Frömel, T., Müller, J., Peschka, M., Knepper, T., Díaz-Cruz, S. and Barceló, D., 2012a. Biodegradation studies of N 4-acetylsulfapyridine and N 4-acetylsulfamethazine in environmental water by applying mass spectrometry techniques. *Anal. Bioanal. Chem.* 402, 2885-2896.

García-Galán, M.J., González Blanco, S., López Roldán, R., Díaz-Cruz, S. and Barceló, D., 2012b. Ecotoxicity evaluation and removal of sulfonamides and their acetylated metabolites during conventional wastewater treatment. *Sci. Total Environ.* 437, 403-412.

García-Galán, M.J., Rodríguez-Rodríguez, C.E., Vicent, T., Caminal, G., Díaz-Cruz, M.S. and Barceló, D., 2011b. Biodegradation of sulfamethazine by *Trametes versicolor*: Removal from sewage sludge and identification of intermediate products by UPLC–QqTOF-MS. *Sci. Total Environ.* 409, 5505-5512.

García-Galán, M.J., Silvia Díaz-Cruz, M. and Barceló, D., 2008. Identification and determination of metabolites and degradation products of sulfonamide antibiotics. *TrAC, Trends Anal. Chem.* 27, 1008-1022.

Gibson, R., Duran-Alvarez, J.C., Estrada, K.L., Chavez, A. and Jimenez Cisneros, B., 2010. Accumulation and leaching potential of some pharmaceuticals and potential endocrine disruptors in soils irrigated with wastewater in the Tula Valley, Mexico. *Chemosphere* 81, 1437-1445.

Göbel, A., McArdell, C.S., Joss, A., Siegrist, H. and Giger, W., 2007. Fate of sulfonamides, macrolides, and trimethoprim in different wastewater treatment technologies. *Sci. Total Environ.* 372, 361-371.

Gobel, A., Thomsen, A., McArdell, C.S., Joss, A. and Giger, W., 2005. Occurrence and sorption behavior of sulfonamides, macrolides, and trimethoprim in activated sludge treatment. *Environ. Sci. Technol.* 39, 3981-3989.

Gonzalez-Marino, I., Quintana, J.B., Rodriguez, I. and Cela, R., 2009. Simultaneous determination of parabens, triclosan and triclocarban in water by liquid chromatography/electrospray ionisation tandem mass spectrometry. *Rapid Commun. Mass Spectrom.* 23, 1756-1766.

Gros, M., Petrović, M., Ginebreda, A. and Barceló, D., 2010. Removal of pharmaceuticals during wastewater treatment and environmental risk assessment using hazard indexes. *Environ. Int.* 36, 15-26.

Grote, M., Schwake-Anduschus, C., Michel, R., Stevens, H., Heyser, W., langenkamper, G., Betsche, T. and Freitag, M., 2007. Incorporation of veterinary antibiotics into crops from manured soil. *Landbauforschung Volkenrode* 57, 25-32.

Guerra, P., Kim, M., Shah, A., Alae, M. and Smyth, S.A., 2014. Occurrence and fate of antibiotic, analgesic/anti-inflammatory, and antifungal compounds in five wastewater treatment processes. *Sci. Total Environ.* 473-474, 235-243.

Halden, R.U. and Paull, D.H., 2005. Co-occurrence of triclocarban and triclosan in U.S. water resources. *Environ. Sci. Technol.* 39, 1420-1426.

- Hamscher, G., Pawelzick, H.T., Hoper, H. and Nau, H., 2005. Different behavior of tetracyclines and sulfonamides in sandy soils after repeated fertilization with liquid manure. *Environ. Toxicol. Chem.* 24, 861-868.
- Healy, M.G., Fenton, O., Cormican, M., Peyton, D.P., Ordsmith, N., Kimber, K. and Morrison, L., 2017. Antimicrobial compounds (triclosan and triclocarban) in sewage sludges, and their presence in runoff following land application. *Ecotoxicol. Environ. Saf.* 142, 448-453.
- Hedgespeth, M.L., Sapozhnikova, Y., Pennington, P., Clum, A., Fairey, A. and Wirth, E., 2012. Pharmaceuticals and personal care products (PPCPs) in treated wastewater discharges into Charleston Harbor, South Carolina. *Sci. Total Environ.* 437, 1-9.
- Higgins, C.P., Paesani, Z.J., Abbott Chalew, T.E., Halden, R.U. and Hundal, L.S., 2011. Persistence of triclocarban and triclosan in soils after land application of biosolids and bioaccumulation in *Eisenia foetida*. *Environ. Toxicol. Chem.* 30, 556-563.
- Holling, C.S., Bailey, J.L., Heuvel, B.V. and Kinney, C.A., 2012. Uptake of human pharmaceuticals and personal care products by cabbage (*Brassica campestris*) from fortified and biosolids-amended soils. *J. Environ. Monit.* 14, 3029-3036.
- Hou, J., Wan, W., Mao, D., Wang, C., Mu, Q., Qin, S. and Luo, Y., 2015. Occurrence and distribution of sulfonamides, tetracyclines, quinolones, macrolides, and nitrofurans in livestock manure and amended soils of Northern China. *Environ. Sci. Pollut. Res. Int.* 22, 4545-4554.
- Hu, J., Zhou, J., Zhou, S., Wu, P. and Tsang, Y.F., 2018. Occurrence and fate of antibiotics in a wastewater treatment plant and their biological effects on receiving waters in Guizhou. *Process Saf. Environ. Prot.* 113, 483-490.
- Hu, X., Zhou, Q. and Luo, Y., 2010a. Occurrence and source analysis of typical veterinary antibiotics in manure, soil, vegetables and groundwater from organic vegetable bases, northern China. *Environ. Pollut.* 158, 2992-2998.
- Hu, X., Zhou, Q. and Luo, Y., 2010b. Occurrence and source analysis of typical veterinary antibiotics in manure, soil, vegetables and groundwater from organic vegetable bases, northern China. *Environ. Pollut.* 158, 2992-2998.
- Hundt, K., Martin, D., Hammer, E., Jonas, U., Kindermann, M.K. and Schauer, F., 2000. Transformation of triclosan by *Trametes versicolor* and *Pycnoporus cinnabarinus*. *Appl. Environ. Microbiol.* 66, 4157-4160.
- Huynh, K., Banach, E. and Reinhold, D., 2018. Transformation, Conjugation, and Sequestration Following the Uptake of Triclocarban by Jalapeno Pepper Plants. *J. Agric. Food Chem.* 66, 4032-4043.
- Jechalke, S., Heuer, H., Siemens, J., Amelung, W. and Smalla, K., 2014. Fate and effects of veterinary antibiotics in soil. *Trends Microbiol.* 22, 536-545.

Jelic, A., Rodriguez-Mozaz, S., Barcelo, D. and Gutierrez, O., 2015. Impact of in-sewer transformation on 43 pharmaceuticals in a pressurized sewer under anaerobic conditions. *Water Res.* 68, 98-108.

Jia, Y., Khanal, S.K., Zhang, H., Chen, G.-H. and Lu, H., 2017. Sulfamethoxazole degradation in anaerobic sulfate-reducing bacteria sludge system. *Water Res.* 119, 12-20.

Junge, T., Meyer, K.C., Ciecieski, K., Adams, A., Schaffer, A. and Schmidt, B., 2011. Characterization of non-extractable ¹⁴C- and ¹³C-sulfadiazine residues in soil including simultaneous amendment of pig manure. *Journal of Environmental Science and Health, Part B* 46, 137-149.

Kang, D.H., Gupta, S., Rosen, C., Fritz, V., Singh, A., Chander, Y., Murray, H. and Rohwer, C., 2013. Antibiotic uptake by vegetable crops from manure-applied soils. *J. Agric. Food Chem.* 61, 9992-10001.

Karacı, A. and Balcıoğlu, I.A., 2009. Investigation of the tetracycline, sulfonamide, and fluoroquinolone antimicrobial compounds in animal manure and agricultural soils in Turkey. *Sci. Total Environ.* 407, 4652-4664.

Kasprzyk-Hordern, B., Dinsdale, R.M. and Guwy, A.J., 2008. Multiresidue methods for the analysis of pharmaceuticals, personal care products and illicit drugs in surface water and wastewater by solid-phase extraction and ultra performance liquid chromatography-electrospray tandem mass spectrometry. *Anal. Bioanal. Chem.* 391, 1293-1308.

Kassotaki, E., Buttiglieri, G., Ferrando-Climent, L., Rodriguez-Roda, I. and Pijuan, M., 2016. Enhanced sulfamethoxazole degradation through ammonia oxidizing bacteria co-metabolism and fate of transformation products. *Water Res.* 94, 111-119.

Kemper, N., 2008. Veterinary antibiotics in the aquatic and terrestrial environment. *Ecol. Indic.* 8, 1-13.

Kern, S., Fenner, K., Singer, H.P., Schwarzenbach, R.P. and Hollender, J., 2009. Identification of transformation products of organic contaminants in natural waters by computer-aided prediction and high-resolution mass spectrometry. *Environ. Sci. Technol.* 43, 7039-7046.

Kim, M., Guerra, P., Shah, A., Parsa, M., Alaei, M. and Smyth, S.A., 2014. Removal of pharmaceuticals and personal care products in a membrane bioreactor wastewater treatment plant. *Water Sci. Technol.* 69, 2221-2229.

Kim, Y.M., Murugesan, K., Schmidt, S., Bokare, V., Jeon, J.R., Kim, E.J. and Chang, Y.S., 2011. Triclosan susceptibility and co-metabolism--a comparison for three aerobic pollutant-degrading bacteria. *Bioresour. Technol.* 102, 2206-2212.

Kind, T. and Fiehn, O., 2007. Seven Golden Rules for heuristic filtering of molecular formulas obtained by accurate mass spectrometry. *BMC Bioinformatics* 8, 105.

Kinney, C.A., Furlong, E.T., Kolpin, D.W., Burkhardt, M.R., Zaugg, S.D., Werner, S.L., Bossio, J.P. and Benotti, M.J., 2008. Bioaccumulation of pharmaceuticals and other anthropogenic waste indicators in earthworms from agricultural soil amended with biosolid or swine manure. *Environ. Sci. Technol.* 42, 1863-1870.

Kirchmair, J., Goller, A.H., Lang, D., Kunze, J., Testa, B., Wilson, I.D., Glen, R.C. and Schneider, G., 2015. Predicting drug metabolism: experiment and/or computation? *Nat. Rev. Drug Discov.* 14, 387-404.

Kirchmair, J., Williamson, M.J., Tyzack, J.D., Tan, L., Bond, P.J., Bender, A. and Glen, R.C., 2012. Computational prediction of metabolism: sites, products, SAR, P450 enzyme dynamics, and mechanisms. *J. Chem. Inf. Model.* 52, 617-648.

Klein, E.Y., Van Boeckel, T.P., Martinez, E.M., Pant, S., Gandra, S., Levin, S.A., Goossens, H. and Laxminarayan, R., 2018. Global increase and geographic convergence in antibiotic consumption between 2000 and 2015. *Proc. Natl. Acad. Sci. U. S. A.* 115, E3463-e3470.

Krauss, M., Singer, H. and Hollender, J., 2010. LC-high resolution MS in environmental analysis: from target screening to the identification of unknowns. *Anal. Bioanal. Chem.* 397, 943-951.

Kumar, K., Gupta, S.C., Baidoo, S.K., Chander, Y. and Rosen, C.J., 2005. Antibiotic uptake by plants from soil fertilized with animal manure. *J. Environ. Qual.* 34, 2082-2085.

Kumar, K.S., Priya, S.M., Peck, A.M. and Sajwan, K.S., 2010. Mass Loadings of Triclosan and Triclocarbon from Four Wastewater Treatment Plants to Three Rivers and Landfill in Savannah, Georgia, USA. *Arch. Environ. Contam. Toxicol.* 58, 275-285.

Kuppusamy, S., Kakarla, D., Venkateswarlu, K., Megharaj, M., Yoon, Y.-E. and Lee, Y.B., 2018. Veterinary antibiotics (VAs) contamination as a global agro-ecological issue: A critical view. *Agric. Ecosyst. Environ.* 257, 47-59.

Kwon, J.W., Armbrust, K.L. and Xia, K., 2010. Transformation of triclosan and triclocarban in soils and biosolids-applied soils. *J. Environ. Qual.* 39, 1139-1144.

Lamshöft, M., Sukul, P., Zühlke, S. and Spitteller, M., 2007. Metabolism of ¹⁴C-labelled and non-labelled sulfadiazine after administration to pigs. *Anal. Bioanal. Chem.* 388, 1733-1745.

Langdon, K.A., Warne, M.S., Smernik, R.J., Shareef, A. and Kookana, R.S., 2011. Degradation of 4-nonylphenol, 4-t-octylphenol, bisphenol A and triclosan following biosolids addition to soil under laboratory conditions. *Chemosphere* 84, 1556-1562.

- Langdon, K.A., Warne, M.S., Smernik, R.J., Shareef, A. and Kookana, R.S., 2012. Field dissipation of 4-nonylphenol, 4-t-octylphenol, triclosan and bisphenol A following land application of biosolids. *Chemosphere* 86, 1050-1058.
- Lee, D.G., Zhao, F., Rezenom, Y.H., Russell, D.H. and Chu, K.H., 2012. Biodegradation of triclosan by a wastewater microorganism. *Water Res.* 46, 4226-4234.
- Lee, H.B., Peart, T.E. and Svoboda, M.L., 2005. Determination of endocrine-disrupting phenols, acidic pharmaceuticals, and personal-care products in sewage by solid-phase extraction and gas chromatography-mass spectrometry. *J. Chromatogr. A* 1094, 122-129.
- LeFevre, G.H., Müller, C.E., Li, R.J., Luthy, R.G. and Sattely, E.S., 2015. Rapid Phytotransformation of Benzotriazole Generates Synthetic Tryptophan and Auxin Analogs in Arabidopsis. *Environ. Sci. Technol.* 49, 10959-10968.
- LeFevre, G.H., Portmann, A.C., Muller, C.E., Sattely, E.S. and Luthy, R.G., 2016. Plant Assimilation Kinetics and Metabolism of 2-Mercaptobenzothiazole Tire Rubber Vulcanizers by Arabidopsis. *Environ. Sci. Technol.* 50, 6762-6771.
- Li, C., Chen, J., Wang, J., Ma, Z., Han, P., Luan, Y. and Lu, A., 2015. Occurrence of antibiotics in soils and manures from greenhouse vegetable production bases of Beijing, China and an associated risk assessment. *Sci. Total Environ.* 521-522, 101-107.
- Li, J., Xin, Z., Zhang, Y., Chen, J., Yan, J., Li, H. and Hu, H., 2017. Long-term manure application increased the levels of antibiotics and antibiotic resistance genes in a greenhouse soil. *Applied Soil Ecology* 121, 193-200.
- Li, W.L., Zhang, Z.F., Ma, W.L., Liu, L.Y., Song, W.W. and Li, Y.F., 2018. An evaluation on the intra-day dynamics, seasonal variations and removal of selected pharmaceuticals and personal care products from urban wastewater treatment plants. *Sci. Total Environ.* 640-641, 1139-1147.
- Li, X., Yu, H., Xu, S. and Hua, R., 2013a. Uptake of three sulfonamides from contaminated soil by pakchoi cabbage. *Ecotoxicol. Environ. Saf.* 92, 297-302.
- Li, Y.W., Wu, X.L., Mo, C.H., Tai, Y.P., Huang, X.P. and Xiang, L., 2011. Investigation of sulfonamide, tetracycline, and quinolone antibiotics in vegetable farmland soil in the Pearl River Delta area, southern China. *J. Agric. Food Chem.* 59, 7268-7276.
- Li, Y.X., Zhang, X.L., Li, W., Lu, X.F., Liu, B. and Wang, J., 2013b. The residues and environmental risks of multiple veterinary antibiotics in animal faeces. *Environ. Monit. Assess.* 185, 2211-2220.
- Liao, X., Zou, R., Li, B., Tong, T., Xie, S. and Yuan, B., 2017. Biodegradation of chlortetracycline by acclimated microbiota. *Process Saf. Environ. Prot.* 109, 11-17.

- Little, J.L., Cleven, C.D. and Brown, S.D., 2011. Identification of "known unknowns" utilizing accurate mass data and chemical abstracts service databases. *J. Am. Soc. Mass Spectrom.* 22, 348-359.
- Liu, Y.Y., Wang, Y., Walsh, T.R., Yi, L.X., Zhang, R., Spencer, J., Doi, Y., Tian, G., Dong, B., Huang, X., Yu, L.F., Gu, D., Ren, H., Chen, X., Lv, L., He, D., Zhou, H., Liang, Z., Liu, J.H. and Shen, J., 2016. Emergence of plasmid-mediated colistin resistance mechanism MCR-1 in animals and human beings in China: a microbiological and molecular biological study. *Lancet Infect. Dis.* 16, 161-168.
- Lozano, N., Rice, C.P., Ramirez, M. and Torrents, A., 2010. Fate of triclosan in agricultural soils after biosolid applications. *Chemosphere* 78, 760–766.
- Lozano, N., Rice, C.P., Ramirez, M. and Torrents, A., 2012. Fate of Triclosan and Methyltriclosan in soil from biosolids application. *Environ. Pollut.* 160, 103–108.
- Lozano, N., Rice, C.P., Ramirez, M. and Torrents, A., 2013. Fate of Triclocarban, Triclosan and Methyltriclosan during wastewater and biosolids treatment processes. *Water Res.* 47, 4519–4527.
- Lozano, N., Rice, C.P., Ramirez, M. and Torrents, A., 2018. Fate of triclocarban in agricultural soils after biosolid applications. *Environ. Sci. Pollut. Res. Int.* 25, 222-232.
- Lu, W., Su, X., Klein, M.S., Lewis, I.A., Fiehn, O. and Rabinowitz, J.D., 2017. Metabolite Measurement: Pitfalls to Avoid and Practices to Follow. *Annu. Rev. Biochem.* 86, 277-304.
- Ma, L. and Yates, S.R., 2018. A review on structural elucidation of metabolites of environmental steroid hormones via liquid chromatography–mass spectrometry. *TrAC, Trends Anal. Chem.* 109, 142-153.
- Macherius, A., Eggen, T., Lorenz, W., Moeder, M., Ondruschka, J. and Reemtsma, T., 2012a. Metabolization of the Bacteriostatic Agent Triclosan in Edible Plants and its Consequences for Plant Uptake Assessment. *Environ. Sci. Technol.* 46, 10797-10804.
- Macherius, A., Eggen, T., Lorenz, W., Moeder, M., Ondruschka, J. and Reemtsma, T., 2012b. Metabolization of the Bacteriostatic Agent Triclosan in Edible Plants and its Consequences for Plant Uptake Assessment. *Environ. Sci. Technol.* 46, 10797-10804.
- Macherius, A., Eggen, T., Lorenz, W.G., Reemtsma, T., Winkler, U. and Moeder, M., 2012c. Uptake of Galaxolide, Tonalide, and Triclosan by Carrot, Barley, and Meadow Fescue Plants. *J. Agric. Food Chem.* 60, 7785-7791.
- Macherius, A., Lapen, D.R., Reemtsma, T., Römbke, J., Topp, E. and Coors, A., 2014a. Triclocarban, triclosan and its transformation product methyl triclosan in native earthworm species four years after a commercial-scale biosolids application. *Sci. Total Environ.* 472, 235-238.

- Macherius, A., Seiwert, B., Schroder, P., Huber, C., Lorenz, W. and Reemtsma, T., 2014b. Identification of Plant Metabolites of Environmental Contaminants by UPLC-QToF-MS: The in Vitro Metabolism of Triclosan in Horseradish. *J. Agric. Food Chem.* 62, 1001-1009.
- Macherius, A., Seiwert, B., Schröder, P., Huber, C., Lorenz, W. and Reemtsma, T., 2014c. Identification of Plant Metabolites of Environmental Contaminants by UPLC-QToF-MS: The in Vitro Metabolism of Triclosan in Horseradish. *J. Agric. Food Chem.* 62, 1001-1009.
- Majewsky, M., Glauner, T. and Horn, H., 2015. Systematic suspect screening and identification of sulfonamide antibiotic transformation products in the aquatic environment. *Anal. Bioanal. Chem.* 407, 5707-5717.
- Malchi, T., Maor, Y. and Chefetz, B., 2015. Comments on “Human health risk assessment of pharmaceuticals and personal care products in plant tissue due to biosolids and manure amendments, and wastewater irrigation”. *Environ. Int.* 82, 110-112.
- Malchi, T., Maor, Y., Tadmor, G., Shenker, M. and Chefetz, B., 2014. Irrigation of Root Vegetables with Treated Wastewater: Evaluating Uptake of Pharmaceuticals and the Associated Human Health Risks. *Environ. Sci. Technol.* 48, 9325–9333.
- Marsik, P., Sisa, M., Lacina, O., Motkova, K., Langhansova, L., Rezek, J. and Vanek, T., 2017. Metabolism of ibuprofen in higher plants: A model *Arabidopsis thaliana* cell suspension culture system. *Environ. Pollut.* 220, 383-392.
- Martinez-Carballo, E., Gonzalez-Barreiro, C., Scharf, S. and Gans, O., 2007. Environmental monitoring study of selected veterinary antibiotics in animal manure and soils in Austria. *Environ. Pollut.* 148, 570-579.
- Matamoros, V., Calderón-Preciado, D., Domínguez, C. and Bayona, J.M., 2012. Analytical procedures for the determination of emerging organic contaminants in plant material: A review. *Anal. Chim. Acta* 722, 8-20.
- Mathews, S., Henderson, S. and Reinhold, D., 2014. Uptake and accumulation of antimicrobials, triclocarban and triclosan, by food crops in a hydroponic system. *Environ. Sci. Pollut. Res.* 21, 6025-6033.
- Mathews, S. and Reinhold, D., 2013. Biosolid-borne tetracyclines and sulfonamides in plants. *Environmental Science and Pollution Research* 20, 4327-4338.
- Matsuda, F., 2016. Technical Challenges in Mass Spectrometry-Based Metabolomics. *Mass Spectrom (Tokyo)* 5, S0052.
- McClellan, K. and Halden, R.U., 2010. Pharmaceuticals and personal care products in archived U.S. biosolids from the 2001 EPA national sewage sludge survey. *Water Res.* 44, 658–668.

- Migliore, L., Fiori, M., Spadoni, A. and Galli, E., 2012. Biodegradation of oxytetracycline by *Pleurotus ostreatus* mycelium: a mycoremediation technique. *J. Hazard. Mater.* 215-216, 227-232.
- Mo, W.Y., Chen, Z., Leung, H.M. and Leung, A.O., 2017. Application of veterinary antibiotics in China's aquaculture industry and their potential human health risks. *Environ. Sci. Pollut. Res. Int.* 24, 8978-8989.
- Mulla, S.I., Hu, A., Wang, Y., Sun, Q., Huang, S.-L., Wang, H. and Yu, C.-P., 2016a. Degradation of triclocarban by a triclosan-degrading *Sphingomonas* sp strain YL-JM2C. *Chemosphere* 144, 292-296.
- Mulla, S.I., Wang, H., Sun, Q., Hu, A. and Yu, C.-P., 2016b. Characterization of triclosan metabolism in *Sphingomonas* sp. strain YL-JM2C. *Sci. Rep.* 6, 1-11.
- Mullen, R.A., Hurst, J.J., Naas, K.M., Sassoubre, L.M. and Aga, D.S., 2019. Assessing uptake of antimicrobials by *Zea mays* L. and prevalence of antimicrobial resistance genes in manure-fertilized soil. *Sci. Total Environ.* 646, 409-415.
- O'Neill, J. (2015) *Antimicrobials in Agriculture and the Environment: Reducing Unnecessary Use and Waste. Review on Antimicrobial Resistance*, UK.
- Okocha, R.C., Olatoye, I.O. and Adedeji, O.B., 2018. Food safety impacts of antimicrobial use and their residues in aquaculture. *Public Health Rev.* 39, 21.
- Ostermann, A., Gao, J., Welp, G., Siemens, J., Roelcke, M., Heimann, L., Nieder, R., Xue, Q., Lin, X., Sandhage-Hofmann, A. and Amelung, W., 2014. Identification of soil contamination hotspots with veterinary antibiotics using heavy metal concentrations and leaching data--a field study in China. *Environ. Monit. Assess.* 186, 7693-7707.
- Pan, M. and Chu, L.M., 2016. Adsorption and degradation of five selected antibiotics in agricultural soil. *Sci. Total Environ.* 545-546, 48-56.
- Pan, M. and Chu, L.M., 2017a. Fate of antibiotics in soil and their uptake by edible crops. *Sci. Total Environ.* 599-600, 500-512.
- Pan, M. and Chu, L.M., 2017b. Leaching behavior of veterinary antibiotics in animal manure-applied soils. *Sci. Total Environ.* 579, 466-473.
- Pan, M., Wong, C.K. and Chu, L.M., 2014. Distribution of antibiotics in wastewater-irrigated soils and their accumulation in vegetable crops in the Pearl River Delta, southern China. *J. Agric. Food Chem.* 62, 11062-11069.
- Pan, X., Qiang, Z., Ben, W. and Chen, M., 2011. Residual veterinary antibiotics in swine manure from concentrated animal feeding operations in Shandong Province, China. *Chemosphere* 84, 695-700.

Pannu, M.W., Toor, G.S., O'Connor, G.A. and Wilson, P.C., 2012. Toxicity and bioaccumulation of biosolids-borne triclosan in food crops. *Environ. Toxicol. Chem.* 31, 2130-2137.

Papageorgiou, M., Kosma, C. and Lambropoulou, D., 2016. Seasonal occurrence, removal, mass loading and environmental risk assessment of 55 pharmaceuticals and personal care products in a municipal wastewater treatment plant in Central Greece. *Sci. Total Environ.* 543, 547-569.

Pascal-Lorber, S., Despoux, S., Rathahao, E., Canlet, C., Debrauwer, L. and Laurent, F., 2008. Metabolic Fate of [¹⁴C] Chlorophenols in Radish (*Raphanus sativus*), Lettuce (*Lactuca sativa*), and Spinach (*Spinacia oleracea*). *J. Agric. Food Chem.* 56, 8461–8469.

Peiris, C., Gunatilake, S.R., Mlsna, T.E., Mohan, D. and Vithanage, M., 2017. Biochar based removal of antibiotic sulfonamides and tetracyclines in aquatic environments: A critical review. *Bioresour. Technol.* 246, 150-159.

Pollard, A.T. and Morra, M.J., 2018. Fate of tetracycline antibiotics in dairy manure-amended soils. *Environ. Rev.* 26, 102-112.

Pozo, Ó.J., Sancho, J.V., Ibáñez, M., Hernández, F. and Niessen, W.M.A., 2006. Confirmation of organic micropollutants detected in environmental samples by liquid chromatography tandem mass spectrometry: Achievements and pitfalls. *TrAC, Trends Anal. Chem.* 25, 1030-1042.

Prosser, R.S., Lissemore, L., Topp, E. and Sibley, P.K., 2014. Bioaccumulation of triclosan and triclocarban in plants grown in soils amended with municipal dewatered biosolids. *Environ. Toxicol. Chem.* 33, 975-984.

Prosser, R.S. and Sibley, P.K., 2015. Human health risk assessment of pharmaceuticals and personal care products in plant tissue due to biosolids and manure amendments, and wastewater irrigation. *Environ. Int.* 75, 223-233.

Qiao, M., Ying, G.G., Singer, A.C. and Zhu, Y.G., 2018. Review of antibiotic resistance in China and its environment. *Environ. Int.* 110, 160-172.

Rabolle, M. and Spliid, N.H., 2000. Sorption and mobility of metronidazole, olaquinox, oxytetracycline and tylosin in soil. *Chemosphere* 40, 715-722.

Riemenschneider, C., Al-Raggad, M., Moeder, M., Seiwert, B., Salameh, E. and Reemtsma, T., 2016. Pharmaceuticals, Their Metabolites, and Other Polar Pollutants in Field-Grown Vegetables Irrigated with Treated Municipal Wastewater. *J. Agric. Food Chem.* 64, 5784-5792.

Riemenschneider, C., Seiwert, B., Goldstein, M., Al-Raggad, M., Salameh, E., Chefetz, B. and Reemtsma, T., 2017a. An LC-MS/MS method for the determination of 28 polar environmental contaminants and metabolites in vegetables irrigated with treated municipal wastewater. *Anal. Methods* 9, 1273-1281.

Riemenschneider, C., Seiwert, B., Moeder, M., Schwarz, D. and Reemtsma, T., 2017b. Extensive Transformation of the Pharmaceutical Carbamazepine Following Uptake into Intact Tomato Plants. *Environ. Sci. Technol.* 51, 6100-6109.

Roberts, J., Kumar, A., Du, J., Hepplewhite, C., Ellis, D.J., Christy, A.G. and Beavis, S.G., 2016. Pharmaceuticals and personal care products (PPCPs) in Australia's largest inland sewage treatment plant, and its contribution to a major Australian river during high and low flow. *Sci. Total Environ.* 541, 1625-1637.

Ryu, J., Oh, J., Snyder, S.A. and Yoon, Y., 2014. Determination of micropollutants in combined sewer overflows and their removal in a wastewater treatment plant (Seoul, South Korea). *Environ. Monit. Assess.* 186, 3239-3251.

Sandermann, H., 1992. Plant metabolism of xenobiotics. *Trends Biochem. Sci.* 17, 82-84.

Santos, L. and Ramos, F., 2018. Antimicrobial resistance in aquaculture: Current knowledge and alternatives to tackle the problem. *Int. J. Antimicrob. Agents* 52, 135-143.

Sarmah, A.K., Meyer, M.T. and Boxall, A.B., 2006a. A global perspective on the use, sales, exposure pathways, occurrence, fate and effects of veterinary antibiotics (VAs) in the environment. *Chemosphere* 65, 725-759.

Sarmah, A.K., Meyer, M.T. and Boxall, A.B.A., 2006b. A global perspective on the use, sales, exposure pathways, occurrence, fate and effects of veterinary antibiotics (VAs) in the environment. *Chemosphere* 65, 725-759.

Schar, D., Sommanustweechai, A., Laxminarayan, R. and Tangcharoensathien, V., 2018. Surveillance of antimicrobial consumption in animal production sectors of low- and middle-income countries: Optimizing use and addressing antimicrobial resistance. *PLoS Med.* 15, e1002521.

Schymanski, E.L., Jeon, J., Gulde, R., Fenner, K., Ruff, M., Singer, H.P. and Hollender, J., 2014. Identifying Small Molecules via High Resolution Mass Spectrometry: Communicating Confidence. *Environ. Sci. Technol.* 48, 2097-2098.

Sherburne, J.J., Anaya, A.M., Fernie, K.J., Forbey, J.S., Furlong, E.T., Kolpin, D.W., Dufty, A.M. and Kinney, C.A., 2016. Occurrence of Triclocarban and Triclosan in an Agro-ecosystem Following Application of Biosolids. *Environ. Sci. Technol.* 50, 13206-13214.

Souchier, M., Benali-Raclot, D., Benanou, D., Boireau, V., Gomez, E., Casellas, C. and Chiron, S., 2015. Screening triclocarban and its transformation products in river sediment using liquid chromatography and high resolution mass spectrometry. *Sci. Total Environ.* 502, 199-205.

Souchier, M., Casellas, C., Ingrand, V. and Chiron, S., 2016. Insights into reductive dechlorination of triclocarban in river sediments: Field measurements and in vitro mechanism investigations. *Chemosphere* 144, 425-432.

Spielmeier, A., Höper, H. and Hamscher, G., 2017. Long-term monitoring of sulfonamide leaching from manure amended soil into groundwater. *Chemosphere* 177, 232-238.

State of California (2015) Senate Bill No. 27. Bureau, L.C. (ed).

State of Maryland (2017) Keep Antibiotics Effective Act of 2017.

Stoob, K., Singer, H.P., Stettler, S., Hartmann, N., Mueller, S.R. and Stamm, C.H., 2006. Exhaustive extraction of sulfonamide antibiotics from aged agricultural soils using pressurized liquid extraction. *J. Chromatogr.* 1128, 1-9.

Subedi, B., Balakrishna, K., Sinha, R.K., Yamashita, N., Balasubramanian, V.G. and Kannan, K., 2015. Mass loading and removal of pharmaceuticals and personal care products, including psychoactive and illicit drugs and artificial sweeteners, in five sewage treatment plants in India. *Journal of Environmental Chemical Engineering* 3, 2882-2891.

Sun, J., Zeng, Q., Tsang, D.C.W., Zhu, L.Z. and Li, X.D., 2017. Antibiotics in the agricultural soils from the Yangtze River Delta, China. *Chemosphere* 189, 301-308.

Sun, Q., Li, M., Ma, C., Chen, X., Xie, X. and Yu, C.P., 2016. Seasonal and spatial variations of PPCP occurrence, removal and mass loading in three wastewater treatment plants located in different urbanization areas in Xiamen, China. *Environ. Pollut.* 208, 371-381.

Tan, S.Y. and Tatsumura, Y., 2015. Alexander Fleming (1881-1955): Discoverer of penicillin. *Singapore Med. J.* 56, 366-367.

Tanoue, R., Sato, Y., Motoyama, M., Nakagawa, S., Shinohara, R. and Nomiyama, K., 2012. Plant Uptake of Pharmaceutical Chemicals Detected in Recycled Organic Manure and Reclaimed Wastewater. *J. Agric. Food Chem.* 60, 10203-10211.

Tasho, R.P. and Cho, J.Y., 2016. Veterinary antibiotics in animal waste, its distribution in soil and uptake by plants: A review. *Sci. Total Environ.* 563-564, 366-376.

Técher, D., Laval-Gilly, P., Henry, S., Bennisroune, A., Formanek, P., Martinez-Chois, C., D'Innocenzo, M., Muanda, F., Dicko, A., Rejšek, K. and Falla, J. (2011) Contribution of *Miscanthus x giganteus* root exudates to the biostimulation of PAH degradation: An in vitro study, pp. 4489-4495.

Tran, N.H., Chen, H., Reinhard, M., Mao, F. and Gin, K.Y., 2016. Occurrence and removal of multiple classes of antibiotics and antimicrobial agents in biological wastewater treatment processes. *Water Res.* 104, 461-472.

Tran, N.H., Reinhard, M. and Gin, K.Y., 2018. Occurrence and fate of emerging contaminants in municipal wastewater treatment plants from different geographical regions-a review. *Water Res.* 133, 182-207.

U.S. EPA (2009) Targeted National Sewage Sludge Survey Statistical Report, U.S. Environmental Protection Agency, Washington DC.

U.S. FDA (2016a) Over-the-Counter (OTC) Animal Drugs Becoming Veterinary Feed Directive (VFD) or Prescription (Rx). Seviles, D.o.H.a.H. (ed).

U.S. FDA (2016b) Safety and Effectiveness of Consumer Antiseptics; Topical Antimicrobial Drug Products for Over-the-Counter Human Use. Department of Health and Human Services (ed), pp. 61106-61130.

U.S. FDA (2017) 2016 Summary Report on Antimicrobials Sold or Distributed for Use in Food-Producing Animals.

USEPA (2017) Estimation Programs Interface Suite™ for Microsoft® Windows, v 4.11, United States Environmental Protection Agency, Washington, DC, USA.

Van Boeckel, T.P., Brower, C., Gilbert, M., Grenfell, B.T., Levin, S.A., Robinson, T.P., Teillant, A. and Laxminarayan, R., 2015. Global trends in antimicrobial use in food animals. *Proc. Natl. Acad. Sci. U. S. A.* 112, 5649-5654.

Ventola, C.L., 2015. The antibiotic resistance crisis: part 1: causes and threats. *Pharmacy and Therapeutics* 40, 277-283.

Vergani, L., Mapelli, F., Zanardini, E., Terzaghi, E., Di Guardo, A., Morosini, C., Raspa, G. and Borin, S., 2017. Phyto-rhizoremediation of polychlorinated biphenyl contaminated soils: An outlook on plant-microbe beneficial interactions. *Sci. Total Environ.* 575, 1395-1406.

Vila-Costa, M., Gioia, R., Aceña, J., Pérez, S., Casamayor, E.O. and Dachs, J., 2017. Degradation of sulfonamides as a microbial resistance mechanism. *Water Res.* 115, 309-317.

Vree, T.B., Beneken Kolmer, E.W. and Hekster, Y.A., 1991. Pharmacokinetics, N1-glucuronidation and N4-acetylation of sulfamethomidine in humans. *Pharm. Weekbl. Sci.* 13, 198-206.

Wang, Y., Li, Y., Hu, A., Rashid, A., Ashfaq, M., Wang, H., Luo, H., Yu, C.P. and Sun, Q., 2018. Monitoring, mass balance and fate of pharmaceuticals and personal care products in seven wastewater treatment plants in Xiamen City, China. *J. Hazard. Mater.* 354, 81-90.

Waria, M., O'Connor, G.A. and Toor, G.S., 2011. Biodegradation of triclosan in biosolids-amended soils. *Environ. Toxicol. Chem.* 30, 2488-2496.

Watkinson, A.J., Murby, E.J. and Costanzo, S.D., 2007. Removal of antibiotics in conventional and advanced wastewater treatment: implications for environmental discharge and wastewater recycling. *Water Res.* 41, 4164-4176.

Wei, R., Ge, F., Zhang, L., Hou, X., Cao, Y., Gong, L., Chen, M., Wang, R. and Bao, E., 2016. Occurrence of 13 veterinary drugs in animal manure-amended soils in Eastern China. *Chemosphere* 144, 2377-2383.

World Health Organization (2017) Critically Important Antimicrobials for Human Medicine, 5th Revision 2016.

Wu, C., Spongberg, A.L. and Witter, J.D., 2009. Adsorption and Degradation of Triclosan and Triclocarban in Soils and Biosolids-Amended Soils. *J. Agric. Food Chem.* 57, 4900–4905.

Wu, C., Spongberg, A.L., Witter, J.D., Fang, M., Ames, A. and Czajkowski, K.P., 2010a. Detection of Pharmaceuticals and Personal Care Products in Agricultural Soils Receiving Biosolids Application. *CLEAN – Soil, Air, Water* 38, 230-237.

Wu, C., Spongberg, A.L., Witter, J.D. and Sridhar, B.B.M., 2012. Transfer of wastewater associated pharmaceuticals and personal care products to crop plants from biosolids treated soil. *Ecotoxicol. Environ. Saf.* 85, 104-109.

Wu, C.X., Spongberg, A.L., Witter, J.D., Fang, M. and Czajkowski, K.P., 2010b. Uptake of Pharmaceutical and Personal Care Products by Soybean Plants from Soils Applied with Biosolids and Irrigated with Contaminated Water. *Environ. Sci. Technol.* 44, 6157-6161.

Wu, J.L., Lam, N.P., Martens, D., Kettrup, A. and Cai, Z., 2007. Triclosan determination in water related to wastewater treatment. *Talanta* 72, 1650-1654.

Wu, X., Ernst, F., Conkle, J.L. and Gan, J., 2013. Comparative uptake and translocation of pharmaceutical and personal care products (PPCPs) by common vegetables. *Environ. Int.* 60, 15-22.

Wu, X., Fu, Q. and Gan, J., 2016. Metabolism of pharmaceutical and personal care products by carrot cell cultures. *Environ. Pollut.* 211, 141–147.

Xiang, L., Wu, X.L., Jiang, Y.N., Yan, Q.Y., Li, Y.W., Huang, X.P., Cai, Q.Y. and Mo, C.H., 2016. Occurrence and risk assessment of tetracycline antibiotics in soil from organic vegetable farms in a subtropical city, south China. *Environ. Sci. Pollut. Res. Int.* 23, 13984-13995.

Xie, W.Y., Shen, Q. and Zhao, F.J., 2018. Antibiotics and antibiotic resistance from animal manure to soil: a review. *Eur. J. Soil Sci.* 69, 181–195.

Xu, B., Mao, D., Luo, Y. and Xu, L., 2011. Sulfamethoxazole biodegradation and biotransformation in the water–sediment system of a natural river. *Bioresour. Technol.* 102, 7069-7076.

Yang, Y., Owino, A.A., Gao, Y., Yan, X., Xu, C. and Wang, J., 2016. Occurrence, composition and risk assessment of antibiotics in soils from Kenya, Africa. *Ecotoxicology* 25, 1194-1201.

- Yeom, J.-R., Yoon, S.-U. and Kim, C.-G., 2017. Quantification of residual antibiotics in cow manure being spread over agricultural land and assessment of their behavioral effects on antibiotic resistant bacteria. *Chemosphere* 182, 771-780.
- Yergeau, E., Sanschagrín, S., Maynard, C., St-Arnaud, M. and Greer, C.W., 2014. Microbial expression profiles in the rhizosphere of willows depend on soil contamination. *The ISME Journal* 8, 344-358.
- Ying, G.-G., Yu, X.-Y. and Kookana, R.S., 2007. Biological degradation of triclocarban and triclosan in a soil under aerobic and anaerobic conditions and comparison with environmental fate modelling. *Environ. Pollut.* 150, 300–305.
- Ying, G.G., Kookana, R.S. and Dillon, P., 2003. Sorption and degradation of selected five endocrine disrupting chemicals in aquifer material. *Water Res.* 37, 3785-3791.
- Yu, Y., Huang, Q., Wang, Z., Zhang, K., Tang, C., Cui, J., Feng, J. and Peng, X., 2011. Occurrence and behavior of pharmaceuticals, steroid hormones, and endocrine-disrupting personal care products in wastewater and the recipient river water of the Pearl River Delta, South China. *J. Environ. Monit.* 13, 871-878.
- Yuan, S.-f., Liu, Z.-h., Yin, H., Dang, Z., Wu, P.-x., Zhu, N.-w. and Lin, Z., 2019. Trace determination of sulfonamide antibiotics and their acetylated metabolites via SPE-LC-MS/MS in wastewater and insights from their occurrence in a municipal wastewater treatment plant. *Sci. Total Environ.* 653, 815-821.
- Zarfl, C., Klasmeier, J. and Matthies, M., 2009. A conceptual model describing the fate of sulfadiazine and its metabolites observed in manure-amended soils. *Chemosphere* 77, 720-726.
- Zhang, M., He, L.Y., Liu, Y.S., Zhao, J.L., Liu, W.R., Zhang, J.N., Chen, J., He, L.K., Zhang, Q.Q. and Ying, G.G., 2019. Fate of veterinary antibiotics during animal manure composting. *Sci. Total Environ.* 650, 1363-1370.
- Zhang, Q.Q., Ying, G.G., Pan, C.G., Liu, Y.S. and Zhao, J.L., 2015. Comprehensive evaluation of antibiotics emission and fate in the river basins of China: source analysis, multimedia modeling, and linkage to bacterial resistance. *Environ. Sci. Technol.* 49, 6772-6782.
- Zhang, X., Zhao, H., Du, J., Qu, Y., Shen, C., Tan, F., Chen, J. and Quan, X., 2017. Occurrence, removal, and risk assessment of antibiotics in 12 wastewater treatment plants from Dalian, China. *Environ. Sci. Pollut. Res. Int.* 24, 16478-16487.
- Zhao, L., Dong, Y.H. and Wang, H., 2010. Residues of veterinary antibiotics in manures from feedlot livestock in eight provinces of China. *Sci. Total Environ.* 408, 1069-1075.
- Zhou, L.J., Ying, G.G., Liu, S., Zhao, J.L., Yang, B., Chen, Z.F. and Lai, H.J., 2013. Occurrence and fate of eleven classes of antibiotics in two typical wastewater treatment plants in South China. *Sci. Total Environ.* 452-453, 365-376.

CHAPTER 3.
UPTAKE AND METABOLISM OF TRICLOCARBAN BY HYDROPONICALLY
GROWN PEPPER

3.1. Introduction

Triclocarban (3,4,4'-trichlorocarbanilide, TCC) is an antimicrobial agent commonly added to a variety of household and personal care products at concentrations of 0.5 – 5% on a mass basis (Halden and Paull, 2005). Studies on the fate of TCC in wastewater treatment plants indicate that only 21% of TCC mass in the influent is degraded or transformed during conventional treatment processes, with approximately 3% remaining in the effluent and 76% partitioning into the biosolids (Heidler et al., 2006). As a result, TCC is among the most frequently detected emerging contaminants in biosolids samples, with concentrations ranging from 2.17-51 mg/kg dry weight (Lozano et al., 2013). Land application of biosolids and reclaimed wastewater in agriculture can therefore lead to accumulation of TCC in soils and crop plants. For example, Wu et al. found that soybean accumulated and translocated TCC from soil into various plant tissues, with TCC concentrations in roots, stems, leaves and mature bean were 168 ± 34 , 16.5 ± 14.0 , 37.6 ± 9.9 , and 2.6 ± 0.3 $\mu\text{g}/\text{kg}$ dw, respectively, in biosolids application treatments (Wu et al., 2010). In irrigation water treatments, TCC concentrations in plant tissues were 7.1 ± 2.6 , 4.8 ± 1.7 , 14.9 ± 1.6 and 4.0 ± 1.5 $\mu\text{g}/\text{kg}$ dw, respectively (Wu et al., 2010). Substantially higher TCC concentrations accumulated in pumpkin and zucchini plants grown in biosolids amended soils were reported by Aryal and Reinhold, ranging from approximately 750 $\mu\text{g}/\text{kg}$ dw in leaves and approximately 14,000 $\mu\text{g}/\text{kg}$ dw in roots, respectively (Aryal and Reinhold, 2011). In addition, Wu et al. (2012) reported TCC accumulation in five common vegetables, with TCC concentrations ranging from 190–580 $\mu\text{g}/\text{kg}$ dw in the roots and 90 – 400 $\mu\text{g}/\text{kg}$ dw in the shoots (Wu et al., 2012a). After 4 weeks of hydroponic exposure to TCC at concentration of 500 $\mu\text{g}/\text{L}$, Mathews et al. observed that TCC was mainly sorbed to roots of eleven common food crops, with less than 1.9% of the antimicrobial translocated from roots to shoots (Mathews et al., 2014). Interestingly, in both

studies by Wu et al. and Mathews et al., pepper plants exhibited the greatest root-to-shoot translocation among the treated vegetables, which was evident by relatively high concentrations of TCC detected in shoots (approximately 400–3,000 $\mu\text{g}/\text{kg dw}$) (Mathews et al., 2014, Wu et al., 2012a) and edible fruits (approximately 130 $\mu\text{g}/\text{kg dw}$) (Wu et al., 2012a).

Several studies on fate of organic xenobiotic chemicals in food crops have recently revealed great potential for plants to metabolize xenobiotic chemicals following uptake (Goldstein et al., 2014, Macherius et al., 2012, Malchi et al., 2014, Pascal-Lorber et al., 2010, Pascal-Lorber et al., 2008, Sun et al., 2015, Wu et al., 2016). In general, metabolic pathways of xenobiotic chemicals in plants consist of three phases that are analogous to mammalian liver metabolism (Sandermann, 1992). Phase I reactions render parent molecules more polar and biologically active through multiple reactions such as hydroxylation, hydrolysis, or oxidation due to cytochrome P450 enzymes (Fu et al., 2017, Macherius et al., 2012, Marsik et al., 2017, Sandermann, 1992). Phase II, which consists of conjugation reactions, forms compounds of higher molecular weight by adding amino acids, glutathione, or carbohydrates to phase I transformation products or the parent molecule to reduce their biological activities and to increase their solubility in water (Fu et al., 2017, Macherius et al., 2012, Marsik et al., 2017, Sandermann, 1992). In phase III, plants sequester the phase II conjugates in the vacuoles for storage or incorporate the conjugates into the cell wall (Fu et al., 2017, Macherius et al., 2012, Sandermann, 1992). The extractable fractions of accumulated xenobiotics in plant tissues contain unaltered parent molecules, phase I and phase II soluble metabolites, and some smaller phase III vacuolar-stored metabolites. Conversely, fractions of metabolites that are incorporated into cell walls form non-extractable (or bound) residues. Studies have indicated that extractable metabolites of xenobiotic compounds in edible plants are

absorbed in the human digestive system (Paltiel et al., 2016), emphasizing the importance of identifying and quantifying the phytometabolism of xenobiotic compounds to human health.

Although uptake and accumulation of TCC by crop plants has been extensively studied, distribution and fate of TCC in plant tissues following uptake is still unclear, especially with regards to phytometabolism. Recently, Macherius et al. and Wu et al. observed that TCC was recalcitrant to metabolism, whereas its chemical analogue, triclosan, was largely metabolized by carrot cell cultures within 120 h and 90 h, respectively (Macherius et al., 2012, Wu et al., 2016). Compared to triclosan, TCC lacks functional groups that are suitable for direct phase II conjugation reactions (e.g hydroxyl group); therefore, metabolism of TCC potentially requires an activation by phase I transformation reactions to allow conjugation in phase II (Macherius et al., 2012). Accordingly, a longer exposure time may be required for plant metabolism of TCC to be detectable. In studies with hydroponically grown vegetables by Mathews et al., a mass balance after four weeks of TCC exposure revealed that the mass of TCC present in plant tissues and media was less than the initial mass added to the systems (Mathews et al., 2014), suggesting additional processes, such as metabolism, may affect the fate of TCC in planted systems .

In this context, the present study aimed to investigate the uptake, distribution, and metabolism of the antimicrobial TCC and its metabolites in whole plants of jalapeno pepper (*Capsicum annuum*) under hydroponic conditions. Specifically, the objectives of this study were to (1) quantify the fractions of parent TCC, extractable and bound metabolites in plant tissues following uptake and (2) identify extractable metabolites of TCC.

3.2. Materials and Methods

3.2.1. Chemicals and plant material

Unlabeled TCC (>98% purity) was purchased from Tokyo Chemical Industry (Portland, OR). ¹⁴C-TCC uniformly labeled on the chlorophenyl ring was obtained from Moravek Biochemicals (Brea, CA) with a specific activity of 25.4 mCi/mmol and radiochemical purity of ≥98%. Hydroxylated metabolites of TCC (2'-OH, 3'-OH and 6-OH TCC; reported purity >99%) were provided by Dr. Bruce Hammock (University of California, Davis). Stock solutions of ¹⁴C-TCC (2.22×10^{10} dpm/L), TCC (1,000 mg/L), 2'-OH TCC (260 mg/L), 3'-OH TCC (600 mg/L) and 6-OH TCC (700 mg/L) were individually dissolved in methanol and stored in amber glass vials at -20°C before use. Organic mobile phases (methanol, acetonitrile) for LC-MS analysis were of MS grade from Sigma-Aldrich (St Louis, MO). All other organic solvents (HPLC grade) and chemicals (ACS grade) were purchased from VWR, Inc. (Chicago, IL).

Jalapeno pepper seeds (Burpee, USA) were germinated in a potting mix (Miracle-Gro, USA). To acclimatize plant seedlings, four to five leaf-stage seedlings were transferred to hydroponic media containing Hoagland solution (Hoagland and Arnon, 1950) and cultured for one week with constant aeration and a light intensity of approximately 325 $\mu\text{mol}/\text{m}^2/\text{s}$ for a 16 h photoperiod. During this study, laboratory temperature and humidity varied in the range of $26 \pm 3^\circ\text{C}$ and $52 \pm 7\%$, respectively.

3.2.2. Long-term exposure of pepper plants to TCC

Acclimatized plants were exposed to both unlabeled and ¹⁴C-labeled TCC and grown in full-strength Hoagland solution in 1 L amber glass bottles under the aforementioned conditions for three weeks. The Hoagland solution was spiked with 0.5 mL of TCC stocks, yielding initial concentrations of 7.8×10^5 dpm/L (approximately 5 μg ¹⁴C-TCC/L) and 500 $\mu\text{g}/\text{L}$ of unlabeled

TCC. Methanol from the stock constituted less than 0.05% by volume of the nutrient solution, was allowed to volatilize in a fume hood overnight prior to addition of plants to the nutrient solution. One treatment, in which plants were grown in Hoagland solution without TCC, served as a control for plant health; additionally, one treatment, in which Hoagland solution with TCC but no plants, served as a control for TCC loss in the absence of plants. Pepper plants were suspended in the nutrient solution by means of a cotton ball around the stem in the neck of the bottle (Supplementary Figure 3.1). Each treatment included five replicates, with each replicate consisting of one plant. High concentrations of unlabeled TCC used in this study allowed for observation of transformation and/or uptake processes that would otherwise be hidden by an aqueous depletion due to sorption. Accordingly, concentrations of TCC in the hydroponic media exceeded its solubility, which is approximately 315 $\mu\text{g/L}$ as experimentally observed by (Aryal and Reinhold, 2013).

During the experiment, fresh nutrient solution was added to the bottles every three days to replace water lost from evapotranspiration and to provide nutrients. In addition, medium was continuously aerated using 2.4 W aquarium pumps and stainless-steel needles (1 mm diameter). After three weeks, five plants were sacrificed for ^{14}C and unlabeled TCC analysis. Remaining plants were transferred to fresh nutrient solution containing the same initial concentrations of TCC (7.8×10^5 dpm/L and 500 $\mu\text{g/L}$, respectively) in 2 L flasks covered with aluminum foil to minimize photodegradation of the chemicals. Following plant transfer, plants were grown for another 9 weeks without sacrificial sampling. Instead, only leaf and fruit samples were collected at 6 and 9 weeks. Remaining plants were sacrificed after 12 weeks for analysis of ^{14}C and unlabeled TCC accumulation and distribution. The total exposure time of 12 weeks approximates commercial growth time of peppers. Each whole plant was washed with deionized water, blotted dry gently to

remove excess water, separated into roots, stems, leaves and fruits (if available). Plant fresh biomass was weighed, oven-dried at 55°C to constant weight, and stored at -20°C until analysis.

3.2.3. Short-term exposure to TCC for metabolite screening

Acclimatized pepper plants were grown in half-strength Hoagland solution containing 174.8 µg unlabeled TCC/L for 1 week in a growth chamber set to the aforementioned conditions. At each sampling point (0.5, 1, 2, and 5 days after TCC exposure), triplicates of containers, including the plants and nutrient media, were sacrificed and analyzed.

One week after initial TCC exposure, the remaining plants were transferred to fresh half-strength Hoagland solution containing 487.4 µg unlabeled TCC/L in amber glass bottles and grown for an additional 21 days. During the initial, week-long exposure of plants to TCC in this short-term trial, quick depletion of aqueous TCC was observed, likely attributed to sorption of TCC to root surfaces (Macherius et al., 2012, Wu et al., 2016). Therefore, during the second exposure, a higher concentration of TCC was used to facilitate detection of potential metabolites in plant tissues. Nutrient media and plants were subsequently sampled in triplicate at 7-days intervals. Each whole plant was separated into roots, stems, and leaves, and fresh biomass of each plant tissue was weighed. For metabolite screening, stem and leaf samples were combined as shoots. Plant materials were ground to fine powder in liquid nitrogen and stored at -20°C until analysis.

3.2.4. Sample preparation and chemical analysis

3.2.4.1. Quantification of TCC in plants and hydroponic media

Plant samples were extracted as described by (Mathews et al., 2014). Briefly, dried plant samples were extracted using a Dionex ASE 200 accelerated solvent extractor (Sunnyvale, CA) with equal parts of methanol and acetone at 100°C and 1500 psi. To decrease signal suppression or isobaric interference from the plant matrices during mass spectrometry (MS) analysis (Wu et al.,

2012b), plant extracts were cleaned with solid phase extraction (SPE) (Oasis HLB 6 cc cartridge, 150 mg, Waters) as described by (Wu et al., 2012b). Briefly, plant extracts were dried under nitrogen gas and reconstituted in 2 mL of methanol. An aliquot of 1 mL was dissolved in 20 mL of Milli-Q water prior to SPE. SPE cartridges were sequentially conditioned and rinsed with methanol and Milli-Q water. Analytes were dried under nitrogen gas, reconstituted in 1 mL of methanol and filtered through 0.2 μm PTFE membranes (13 mm, VWR) into 2 mL amber vials. Media samples (1 mL) were diluted in 1 mL of methanol and filtered through 0.2 μm PTFE membranes into 2 mL amber vials.

Analysis of TCC concentrations was performed on a Shimadzu LC-MS 2010 EV with negative electrospray ionization (ESI) in selected ion monitoring (SIM) mode using an Allure biphenyl column (5 μm , 150 x 2.1 mm, Restek) at 40°C. Mobile phases were 5 mM ammonium acetate in Milli-Q water (A) and methanol (B) following the gradient: 0-1 min, 75% B; 3 min, 85% B; 8 min, 100% B; 13 min, 100% B; 14 min, 75% B and 20 min, 75% B. The flow rate was 0.2 mL/min. TCC was identified by retention time ($t_{\text{R}} \pm 0.1$ min), detection of characteristic molecular ions (m/z 313), and detection of reference ions (m/z 315 and 317) (Halden and Paull, 2005). Matrix-matched standard curves with ten concentrations of TCC (0.2 – 500 $\mu\text{g/L}$) were developed. Control plant extracts, cleaned by SPE as described above, were used as the dilution solvent for preparation of standards. The detection limits and quantification limits for TCC were 0.01 and 0.1 $\mu\text{g/L}$ for media samples and 0.1 and 1.0 $\mu\text{g/kg}$ dry weight for plant samples, respectively (Aryal and Reinhold, 2011, Mathews et al., 2014). Recovery samples were prepared by adding 20 ng of TCC standard to blank controls and were subjected to the same extraction procedures. In this study, method recoveries were $81.4 \pm 4.5\%$ and $95.5 \pm 2.6\%$ for plant and media samples, respectively.

3.2.4.2. Liquid Scintillation Analysis

Aliquots of 3 mL of media samples were mixed with 15 mL of Ultima Gold scintillation cocktail (PerkinElmer, MA) in 20 mL glass scintillation vials. All vials were kept at room temperature for 1 hour prior to ^{14}C quantification.

Oven-dried plant samples were digested using a mixture of perchloric acid:nitric acid (1:1) or sodium hypochlorite (NaClO) as described by (Thomson, 2012). NaClO was used as a separate solubilizer capable of dissolving only the portion of radiolabel that is not assimilated within the cellulose structure (Thomson, 2012). As a result, fractions of ^{14}C as bound residues (versus NaClO -extractable residues) in plant tissues can be evaluated using acid digestion. Acid digestion of ^{14}C -labeled plant materials potentially results in loss of ^{14}C - CO_2 during solubilization (Thomson, 2012). However, the loss of ^{14}C - CO_2 was not quantified in this study and ^{14}C concentrations determined by the acid digestion method were calculated as the total accumulated ^{14}C in plant tissues. In addition, fractions of solvent extractable ^{14}C were also determined to quantify the sum of parent TCC and its extractable metabolites. Aliquots of 0.3 mL of reconstituted plant extracts for LC-MS analysis were transferred to 20 mL glass scintillation vials containing 15 mL of Ultima Gold and subsequently analyzed by LSC.

^{14}C -radioactivity in samples was measured on a Beckman LS 6500 Liquid Scintillation Counter (LSC) (Fullerton, CA) with a background of approximately 30 dpm. LSC data were corrected for the background by subtracting the dpm value of a blank from that of the samples.

3.2.4.3. Screening for potential metabolites of TCC using UPLC-QTOF-MS^E and LC-MS/MS

Room-temperature extractions of plant tissues were conducted to screen for potential metabolites of TCC, as elevated temperatures during ASE might decay metabolites. Freshly

ground plant tissues (approximately 0.5 g) were weighed into 50 mL centrifuge tubes. Five mL of methanol was then added to each tube, followed by vortexing for 2 min and sonication for 15 min. Subsequently, samples were centrifuged at 3000 rpm for 15 min. Supernatant was removed and the extraction was repeated two additional times. Extracts were combined, dried under nitrogen, reconstituted in 1.0 mL of methanol and filtered through 0.2 μ m PTFE syringe filter (13 mm, VWR) into a 2.0 mL amber vial. Dodgen et al. (2013) observed that a fraction of polar metabolites of pharmaceutical compounds in plant tissues was likely not retained by HLB cartridges and eluted into the aqueous filtrate during sample loading (Dodgen et al., 2013). Therefore, SPE cleaning procedures were omitted in this trial to minimize the loss of minor metabolites in plant extracts.

Additionally, to facilitate detection of potential transformation products in hydroponic media, triplicates of nutrient samples at each sampling point were combined and aliquot of 100 mL was concentrated to 1 mL using SPE following the methods described previously.

Extracts were analyzed on an Acquity Ultra Performance Liquid Chromatography system coupled with a Xevo G2-XS QTOF mass spectrometer (UPLC-QTOF-MS^E, Waters, Milford, MA). Chromatographic separation was achieved using an Acquity BEH C18 column (50 x 2.1 mm, 1.7 μ m) at a flow rate of 0.3 mL/min and temperature of 40°C. The mobile phases consisted of (A) 10 mM ammonium acetate in Milli-Q water and (B) acetonitrile. The elution gradient was: 0-1 min, 1% B; 16 min, 98% B; 18 min, 98% B; 18.1 min, 1% B; and 20 min, 1% B. The mass spectral analyses utilized ESI in negative mode with a mass range of 50-1500 m/z . The MS source and desolvation temperatures were 100°C and 450°C, respectively. Desolvation gas flow was 450 L/h. The lock mass spray for accurate m/z measurement used a solution containing 0.1 mg/L of leucine enkephalin (m/z 554.2615 in negative ion mode). Data was collected in centroid mode

with two scan functions using MS^E acquisition: function 1 with low collision energy (0 eV) and function 2 with dynamic ramp of collision energy of 20–80 eV.

Centroided MS raw data obtained under low collision energy were processed using Progenesis QI 2.1 software (Waters) for alignment, normalization, and peak picking and then introduced to EZinfo 3.0 software (Umetrics, Sweden) for orthogonal projection to latent structures-discriminant analysis (OPLS-DA). The obtained S-plot (Supplementary Figure 3.2), which is a covariance-correlation-based analysis, was subsequently used to determine the variables that significantly contribute to the observed differences between control and TCC-treated groups. Metabolite candidates were primarily selected from variables scattered on the top right corner of the S-plot with $p(\text{corr}) \geq 0.7$, indicating an increase in intensity of these m/z variables in TCC-treated groups compared to control groups. Candidates from the S-plot were imported back to Progenesis QI as the first tag set. In addition, the ANOVA p -values calculated by Progenesis QI that were < 0.05 (reflecting significant differences between variables of control and TCC-treated groups), were used as a second tag set. Data was then filtered using both tag sets. An output table of paired m/z retention times and raw and normalized peak intensities for group and individual samples. Proposed metabolite candidates were based on the presence in the treatments and absence in the controls. MassLynx 4.1 software (Waters) was used to generate possible chemical formulas for the suspected metabolites with a mass accuracy error ≤ 5 ppm and the following element limits: C (0-100), H (0-100), O (0-30), N (0-6), S (0-4) and Cl (1-6). Assuming the metabolites contain at least one chlorine atom from the three-chlorine parent TCC, the metabolite candidates were further processed via a chlorine-isotopic filter (Macherius et al., 2014). Briefly, this filter method uses the isotopic pattern of chlorinated compounds: signals with $\Delta m/z$ of 1.9970 u (± 0.0030 u) and a relative intensity of $m+2/m$ of $> 32\%$. Following primary identification of metabolite candidates, the

proposed structures were further confirmed by characteristic fragmentations and chlorine isotopic distribution.

Fragmentation of TCC metabolite candidates (Table 3.1), reported by (Warren et al., 1978) and (Schebb et al., 2012b), was performed on a Shimadzu Prominence high performance liquid chromatography (Columbia, MD, USA) coupled with an Applied Biosystems Sciex 3200 triple quadrupole mass spectrometer (Foster City, CA, USA), applying ESI negative in multiple reaction monitoring (MRM) mode. Chromatographic separation was performed at room temperature on an Ultra biphenyl column (5 μ m, 150 x 2.1 mm, Restek). Milli-Q water containing (A) 10 mM ammonium acetate and 0.1% acetic acid and (B) acetonitrile were used as the mobile phases. The elution gradient was: 0.0 min, 30% B; 1.0 – 7.5 min, 85% B; 8.5 min, 100% B; 9.5 min, 100% B; 10.5 min, 30% B and 15.0 min, 30% B with a flow rate of 0.2 mL/min. Additional settings were: IonSpray voltage -3500 V at 350⁰C, curtain gas pressure 20 psi, collision gas pressure 6 psi, and ion source gas pressure 60 psi. The MS/MS parameters for semi-quantification of TCC metabolites can be found in the Supplementary Table 3.2.

3.2.4.4. Statistical analysis

One-way ANOVA and post-hoc comparisons of means using the Tukey's HSD test were performed using SPSS 22 statistical package (IBM Corp.) to determine significant differences ($p < 0.05$). Values are presented as mean \pm standard error. Data representing ¹⁴C-TCC concentrations were adjusted for the ratio of ¹⁴C-TCC:¹²C-TCC added to the system (¹⁴C:¹²C=1:100). Concentrations in plant tissues were calculated based on dry weight (dw).

3.3. Results and Discussion

3.3.1. Depletion of TCC in the hydroponic media

The presence of plants significantly increased removal of TCC from the media ($p < 0.001$). During the initial short-term exposure to 174.8 $\mu\text{g/L}$, TCC concentrations decreased quickly to $18.1 \pm 7.3 \mu\text{g/L}$ after only 12 h, indicating that plants removed approximately 89.7% of the initially added TCC in hours following exposure (Supplementary Figure 3.3). After that, TCC concentrations in media remained constant at $7.2 \pm 2.2 \mu\text{g/L}$ after 5 days. Despite quick depletion in the media, approximately 88.5% of the initially spiked TCC was present in plant tissues as unaltered TCC after 5 days. Upon second exposure at 487.4 $\mu\text{g/L}$, TCC concentrations in the nutrient solution with plants were 160.0 ± 17.9 , 45.1 ± 5.0 and $25.8 \pm 11.0 \mu\text{g/L}$ after 14, 21 and 28 days, respectively. Dissipation of TCC in the planted media was substantially slower than that of the initial exposure, with approximately 31.4% of the TCC mass added to the systems still remaining in the media at 7 days following plant transfer (Supplementary Figure 3.3). The data indicated that the loss of TCC was primarily due to surface sorption by plant roots. These results are in agreement with previous studies reporting that carrot cells removed TCC from solutions mostly due to sorption of the unaltered parent molecules during 120 and 90 hours of incubation, respectively (Macherius et al., 2012, Wu et al., 2016). In this study, precipitates were observed in all treatments as the exposure time increased, which potentially accounted for a proportion of TCC loss in the nutrient media.

Increasing exposure time also resulted in significant decreases in TCC concentrations in no-plant control media (Supplementary Figure 3.3, Supplementary Figure 3.4). Henry's law constant for TCC ($4.52 \times 10^{-11} \text{ atm}\cdot\text{m}^3/\text{mole}$) (Aryal and Reinhold, 2011) indicates a negligible loss by volatilization. In addition, TCC is subject to very slow hydrolysis in neutral solution (pH

= 6.5) (Audu and Heyn, 1988, Ding et al., 2015). According to Ding et al. the degradation rate constant is in range of 0.0660-0.0504/h for 500 µg TCC/L under simulated sunlight irradiation (Ding et al., 2015). Besides, phototransformation was not expected to contribute to depletion of aqueous TCC in this study, as amber glass reactors or aluminum foil were used to prevent the exposure of the nutrient solution to light. At the end of the long-term exposure, precipitates formed in the media were allowed to deposit at the bottoms of the containers and then collected for ¹⁴C-TCC/TCC analysis. ¹⁴C-TCC and TCC concentrations in the precipitate residues of the no-plant controls (754.1 ± 38.0 µg/g and 1262.0 ± 43.3 µg/g, respectively) were substantially higher than those found in the treatments with plants (40.3 ± 8.7 µg/g and 10.7 ± 3.0 µg/g, respectively). Consequently, co-precipitation of TCC also accounted for the proportion of TCC loss in the nutrient media, which was consistent with previous studies by Mathews et al. where inorganic salt precipitates acted as the major sink of TCC under hydroponic conditions using basal nutrient media (Mathews et al., 2014).

3.3.2. TCC exposure exerted no effect on growth of pepper plants

Root, stem, leaf, and total biomass production after 12 weeks was not affected by TCC exposure (Supplementary Figure 3.5), as there was no significant difference in root, stem, leaf, and total biomass production between control plants and those exposed to TCC ($p = 0.859, 0.255, 0.270,$ and $0.292,$ respectively). Moreover, data revealed that plants cultured in nutrient solution containing TCC produced higher fruit biomass than that of the control plants ($p = 0.037$). Recent studies indicated an absence of phytotoxicity upon exposure of crop plants to a number of emerging contaminants via irrigation water or biosolids amendment (Herklotz et al., 2010, Shenker et al., 2011, Wu et al., 2012a). Moreover, the variation in plant growth was found to be species-specific and might be attributed to experimental variables rather than exposure to

pharmaceutical and personal care products (Herklotz et al., 2010, Shenker et al., 2011). In this study, our current data does not allow for clarification of the factor(s) leading to higher fruit yield in TCC-exposed pepper plants.

3.3.3. Accumulation and distribution of TCC and potential metabolites in plant tissues

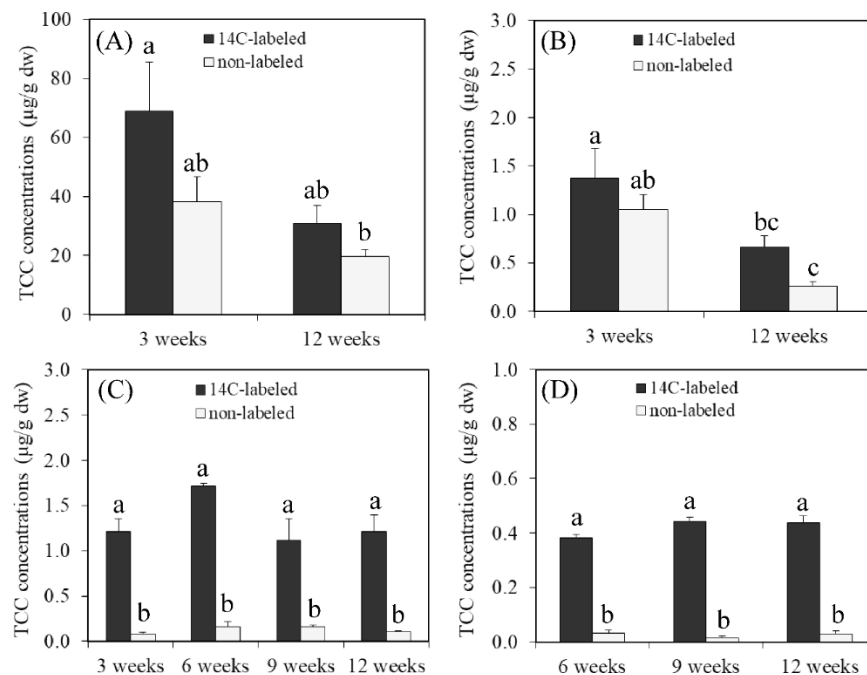


Figure 3. 1. Accumulation of TCC (^{14}C -labeled and non-labeled) in different plant tissues: (A): roots, (B): stems, (C): leaves and (D): fruits during long-term exposure (12 weeks). Plant samples were extracted by acetone:methanol (1:1) mixture using an accelerated solvent extractor (ASE). For fruit samples, ^{14}C was non-detectable in the ASE extracts; therefore, data of the NaClO extracts (Supplementary Table 3.1) were used. Error bars represent means \pm SE (n = 5). In each panel, columns marked by different letters are significantly different from each other ($p < 0.05$).

Concentrations of unlabeled TCC were 19.74 ± 2.26 , 0.26 ± 0.04 , 0.11 ± 0.01 and, 0.03 ± 0.01 µg/g in roots, stems, leaves, and fruits of pepper plants during the long-term exposure, respectively. In this study, root concentrations of TCC was found to be higher than those reported for soybean (Wu et al., 2010) and other common vegetables (e.i. pepper, collard, lettuce, radish and tomato) (Wu et al., 2012a) grown on biosolids-amended soils, mostly attributed to higher bioavailability of TCC under hydroponic conditions. However, TCC concentrations in the above

ground biomass were consistent with previous studies (Wu et al., 2012a, Wu et al., 2010). Mathews et al. reported substantially higher concentrations of TCC in roots and shoots of hydroponically grown pepper plants (approximately 700 and 3 $\mu\text{g/g}$, respectively) after four weeks of TCC exposure at the concentration of 500 $\mu\text{g/L}$ (Mathews et al., 2014). The observed differences can be explained by a robust plant biomass production, leading to dilution of the accumulated TCC in plant tissues. For example, dried root biomass obtained in this study was approximately 20 times higher than that of Mathews et al.'s study. Plant uptake and translocation of organic xenobiotics is highly dependent on the physiochemical properties of the chemicals, growing conditions, and plant composition (Briggs et al., 1982, Collins et al., 2006). Weak acids and bases may undergo partial dissociation and be present in both ionized and neutral forms under environmental and biological pHs (Wu et al., 2013). TCC can dissociate to form a cationic acid and its corresponding anionic conjugate base. Modeling plant uptake of organic chemicals suggested that the passive uptake of neutral molecule into plant roots occurs at a higher rate than its corresponding anionic species (Trapp, 2000), due to the fact that biological membranes are negatively charged, leading to repulsion of anions. In this study, pH of the nutrient solution was approximately 6.50; therefore, TCC exists predominantly in its neutral form ($\text{pK}_a=12.70; f_n=1.00$) (Wu et al., 2013) and can easily cross the biomembranes of the plant roots. In addition, substantial accumulation of TCC in the roots of jalapeno pepper plants compared to other above ground tissues observed in this study might be attributed to its strong lipophilic sorption ($\log K_{ow}=4.90$) to the cell membrane, which is rich in lipids. Previously, (Wild and Jones, 1992) categorized non-ionized organic chemicals with $\log K_{ow}>4$ as having greater tendency to partition into plant root lipids from the surrounding aqueous environment, which is a passive uptake mechanism governed by the non-specific interaction between the root and the dissolved solutes (Hyland et al., 2015). TCC molecules were

favorably adsorbed to the epidermis of the outer root (Hyland et al., 2015, Wu et al., 2013), followed by partitioning into cell biomembranes. Once taken up by the roots, xenobiotics are translocated upward to other plant tissues through the xylem. This flux is driven by the transpiration stream which reflects the root-to-shoot movement of water and other solutes in plants (Collins et al., 2006). At the conclusion of this study, TCC concentrations in stems, leaf, and fruits indicated that TCC was distributed through the entire plant but at much lower concentrations in the leaves and fruits than in the stems. Partitioning of non-ionized chemicals to plant shoots has been demonstrated to be linearly related to their log K_{ow} values (Briggs et al., 1983). Therefore, TCC (log K_{ow} = 4.9 at neutral pH) (Halden and Paull, 2005) transported in the xylem may diffuse laterally into adjacent tissues and partition to the lipophilic stem solids (Collins et al., 2006), leading to reduced accumulation in leaves and fruits. Figure 3.1 depicts the concentrations of unlabeled TCC and extractable ^{14}C concentrations in pepper plants during the long-term exposure trial; ^{14}C concentrations were adjusted for the ratio of ^{14}C -TCC: ^{12}C -TCC added to the system (^{14}C : ^{12}C =1:100). In general, concentrations of unlabeled TCC were less than the extractable ^{14}C concentrations in all plant tissues; however, the difference was only significant for leaves and fruits. Unaltered TCC only accounted for approximately 63.9, 39.2, 7.2, and 7.0% of the extractable ^{14}C in roots, stems, leaves, and fruits after 12 weeks, respectively. In addition, ^{14}C concentrations in all plant tissues extracted with NaClO or organic solvents (acetone:methanol = 1:1) were lower than the corresponding fractions in the acid digestants (Supplementary Table 3.1), indicating that a portion of ^{14}C was sequestered into cell walls. Our data also indicated no significant variation in the extraction efficiencies between NaClO and the organic solvent mixture, except for the fruits. However, at multiple sampling time intervals, liquid scintillation counting of

fruit samples extracted with solvents showed undetectable ^{14}C residues, while NaClO extracts still contained a detectable fraction of ^{14}C (Supplementary Table 3.1).

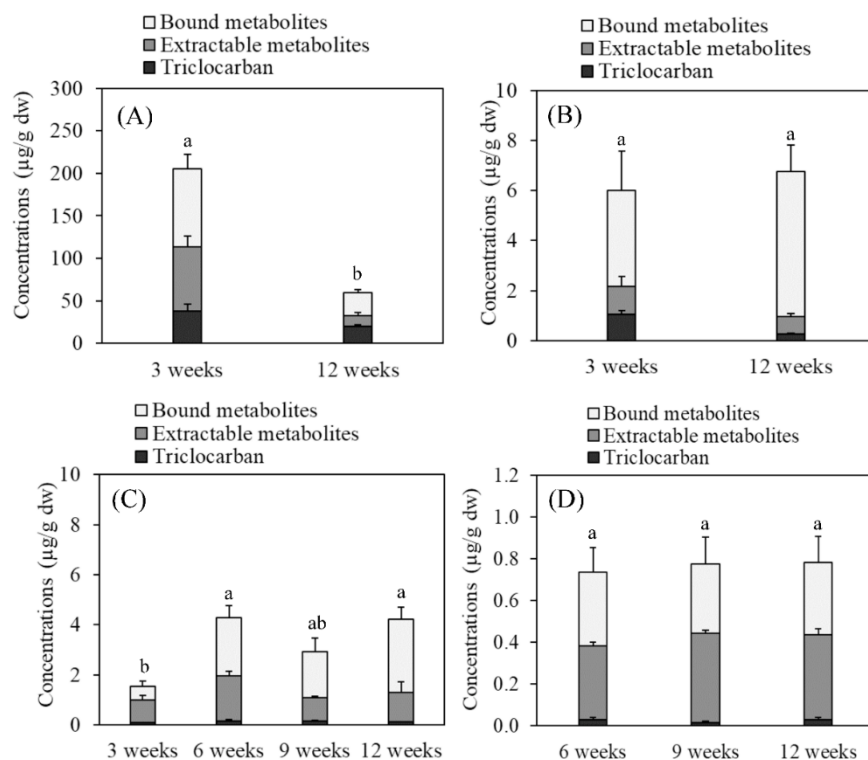


Figure 3. 2. Concentrations of TCC and metabolites (expressed as $\mu\text{g }^{14}\text{C-TCC equivalent/g dw}$) in (A): roots, (B): stems, (C): leaves and (D): fruits during long-term exposure (12 weeks). In this trial, the first fruit sampling event occurred at the 6th week. Root and stem data for week 6th and week 9th were not available since sacrificial sampling was only performed after 3 and 12 weeks. Error bars represent means \pm SE ($n = 5$). Statistical analysis data are shown for the total ^{14}C accumulation in plant tissues. In each panel, columns marked by different letters are significantly different from each other ($p < 0.05$).

Sandermann proposed a “green liver” model for the fate of organic xenobiotics following plant uptake, in which the pollutants undergo several potential transformation processes prior to being conjugated and sequestered into the cell wall compartments (Sandermann, 1992). After sequestration, the pollutant residues became non-extractable using conventional organic solvent extraction methods (Dodgen et al., 2013, Sandermann, 1992). As a result, only the fractions of unaltered parent molecules and soluble metabolites can be extracted. Accordingly, the extractable

^{14}C in this study included both TCC parent molecule and its extractable metabolites. Observed discrepancies between ^{14}C and unlabeled TCC concentrations in different plant tissues clearly indicated metabolism of TCC by pepper plants.

Figure 3.2 presents the distribution of TCC and its potential metabolites into extractable and bound residues (expressed as $\mu\text{g } ^{14}\text{C-TCC equivalent/g dw}$) in different plant tissues. This illustration allows for a rapid visualization of how TCC and its metabolites are partitioned within plant tissues with time. Accumulation of $^{14}\text{C-TCC}$ in roots was substantially higher than in other plant compartments ($p < 0.001$), with accumulation following the order of roots > stems > leaves > fruits. In roots, total ^{14}C concentrations after 3 weeks and 12 weeks were 205.40 ± 34.22 and $59.60 \pm 8.79 \mu\text{g/g dw}$, respectively. The observed decrease can be attributed to robust root biomass production throughout the experiments, resulting in dilution of the accumulated chemicals within plant tissues (Collins et al., 2011), as has been previously observed for carbamazepine (Dordio et al., 2011). In addition, absorption of TCC by plant roots, defined as the passive equilibrium partitioning of TCC into root tissues that precedes active uptake, decreases as the concentrations of TCC in the aqueous phase decreases. The data revealed that metabolism and sequestration of parent TCC occurred within the root tissues. Concentrations of extractable and bound metabolites were 75.57 ± 12.28 and $91.65 \pm 16.47 \mu\text{g/g}$, respectively, while unaltered TCC was only $38.18 \pm 8.51 \mu\text{g/g}$ in the root extracts 3 weeks following exposure. Root uptake of TCC biotransformation products may also occur due to bacterial-mediated transformation of TCC in nutrient solution. For example, bacterial cleavage of urea bridge in TCC to form 3,4-dichloroaniline (3,4-DCA), 4-chloroaniline (4-CA), and 4-chlorocatechol (4-CC) intermediates has been reported previously (Kwon and Xia, 2012, Mulla et al., 2016). Therefore, TCC was incubated with plant root exudates to elucidate the role of enzymatic and rhizobacterial

transformation of TCC in the nutrient solution without presence of pepper plants. Data revealed that only 3,4-DCA and 4-CA were detected in the media, accounting for 0.7% and 1.4% of the initially applied TCC, respectively. The results indicated a trivial role of biodegradation in the dissipation of TCC in the aqueous phase and that plant roots predominantly accumulated TCC as the parent molecule and that the metabolism occurred within the root tissues. Relatively high concentrations of extractable TCC in the roots of pepper plants, even after 12 weeks of exposure, might be a possible explanation for previous studies reporting that peppers had the highest concentrations of TCC in aerial tissues when compared to other leaf and fruit-producing plants (Mathews et al., 2014, Wu et al., 2012a). It has been generally supposed that a rapid metabolism and sequestration of xenobiotics in roots will lower their translocation to the above ground biomass.

In leaves, ^{14}C concentrations after 6 weeks were significantly higher than those in the leaves after 3 weeks of TCC exposure ($p = 0.017$), most likely due to plant transfer to fresh media containing the same concentrations of TCC after 3 weeks. After that, there was no significant variation in leaf ^{14}C concentrations at 6, 9, or 12 weeks following exposure. As shown in Figure 3.2, unaltered TCC fractions were less than 10% of the total TCC species in most of the aerial parts of the jalapeno pepper plants. For example, highest concentrations of unaltered TCC in pepper leaves were only $0.16 \pm 0.02 \mu\text{g/g}$; while that of the soluble and bound metabolites were 1.78 ± 0.18 and $2.91 \pm 0.48 \mu\text{g/g}$, respectively, suggesting vigorous metabolism of TCC in leaves.

In Figure 3.2, accumulation of ^{14}C in stems and fruits showed no considerable variation at different sampling times ($p = 0.795$ and 0.871 , respectively). Concentrations of ^{14}C in the stems was 5.91 ± 1.96 and $6.76 \pm 1.13 \mu\text{g/g}$ after 3 weeks and 12 weeks, respectively. The concentrations of extractable and bound metabolites in stems were 0.71 ± 0.11 and $5.78 \pm 1.05 \mu\text{g/g}$, respectively,

whereas the corresponding parent TCC was only $0.26 \pm 0.04 \mu\text{g/g}$ at the conclusion of the experiment. In fruits, ^{14}C concentrations varied in range of 0.65 to $0.78 \pm 0.12 \mu\text{g/g}$, with no significant differences between extractable and bound residues during the study ($p = 0.504\text{-}0.909$). The highest concentrations of unaltered TCC, extractable, and bound metabolites accumulated in fruit tissues after 12 weeks were 0.03 ± 0.01 , 0.41 ± 0.03 , and $0.37 \pm 0.10 \mu\text{g/g}$, respectively.

3.3.4. Screening for TCC metabolites in plants and media

The fractions of extractable metabolites in plant roots was substantially larger than in shoot tissues (Figure 3.2); therefore, the initial step in TCC metabolite identification was on root extracts using UPLC-QTOF-MS^E. All peaks of interest found in the root extracts were further subjected to MS/MS fragmentation to obtain more information on the structure of the metabolites. The latter information was then employed for designing a MS/MS method (in MRM mode) allowing semi-quantification of these compounds, even at much lower concentrations in the shoot extracts.

To identify the m/z variables which significantly contributed to differentiation between control and TCC-exposed root extracts, an S-plot from the OPLS-DA model was constructed. In the S-plot, points represent all variables in the dataset, with the x-axis ($p1$) representing magnitude of the variables while the y-axis ($p(\text{corr})[1]$) represents the reliability for classification (Yang et al., 2016). Accordingly, in this study, metabolite candidates were selected from the variables scattered in the upper right quadrant of the S-plot with $p(\text{corr}) \geq 0.7$ (Supplementary Figure 3.2). Table 3.1 summarizes the TCC transformation and conjugation products detected in this study. Under the elution gradient applied in UPLC-QTOF-MS^E, TCC eluted at 10.86 min with the molecular ions of $[\text{M-H}]^-$ (m/z 312.9703) and the most abundant fragment ions of $[\text{C}_6\text{H}_4\text{NCl}_2]^-$ (m/z 159.9721) and $[\text{C}_6\text{H}_5\text{NCl}]^-$ (m/z 126.0107). Following TCC ($p(\text{corr}) = 0.97$), the variable that contributed most to the differentiation between the extracts of TCC-exposed and control groups was eluted at a

retention time of 10.52 min ($p(\text{corr}) = 0.82$), which coincided with that of 2'-OH TCC and 6-OH TCC standards. The low energy collision mass spectrum showed a signal at m/z 328.9647, with a mass 15.9944 Da heavier than the parent TCC. The high collision energy mass spectrum gave rise to intense fragment ions at m/z 167.9857 and 201.9464, corresponding with 2'-OH TCC and 6-OH TCC. Another signal at m/z 328.9650 ($p(\text{corr}) = 0.75$) eluted at a retention time of 9.86 min, exhibiting the similar characteristic fragmentation patterns observed for 6-OH TCC standard (m/z 175.9671 and m/z 201.9472). Accordingly, this metabolite was expected to be the monohydroxylated TCC, with the OH- group added at the dichloroaniline ring (M329). 3'-OH TCC ($R_t=9.30$ min) was also detected in root extracts at various sampling times. Additionally, an ion at m/z 491.0159 ($R_t=8.61$ min, $p(\text{corr}) = 0.70$) differing by 162.05 Da from that of the hydroxylated TCC metabolites was observed, suggesting the formation of TCC-*O*-glucosides (Levsen et al., 2005). Nevertheless, the characteristic fragments of these metabolites could not be identified in the high collision energy mass spectrum, likely attributed to low intensity of the corresponding precursor ions. An alternative approach was subsequently used to confirm the presence of TCC-*O*-glucosides. According to Majewsky et al., mass shifts of a given transformation product compared to its parent compound can also be observable in the characteristic m/z of the product ions during MS/MS fragmentation (Majewsky et al., 2015). For example, Schebb et al. observed that TCC, its hydroxylated and glucuronidated metabolites exhibited identical fragmentation patterns on the urea bridge bonds, forming product ions differing by 16 Da (-OH) and 192 Da (-*O*-glucuronic acid) from the product ions of parent TCC, respectively (Schebb et al., 2012b). Therefore, the same approach was employed for identification of the TCC-*O*-glucoside metabolites, with their predicted product ions shifting by 178 Da (-*O*-glucose) from the product ions of parent TCC during MS/MS fragmentation in MRM mode (Table 3.1,

Supplementary Figure 3.7). As expected, the predicted characteristic fragment ions were exclusively observed for TCC-exposed roots (Supplementary Figure 3.14 and Supplementary Figure 3.15), suggesting the presence of glycosylated TCC metabolites in plant tissues. Based on the fragmentations of the m/z 491, we concluded that glycosylation of the hydroxylated TCC metabolites occurred on both monochloroaniline and dichloroaniline rings; however, our current data does not allow for an explicit confirmation of the exact glycosylation positions.

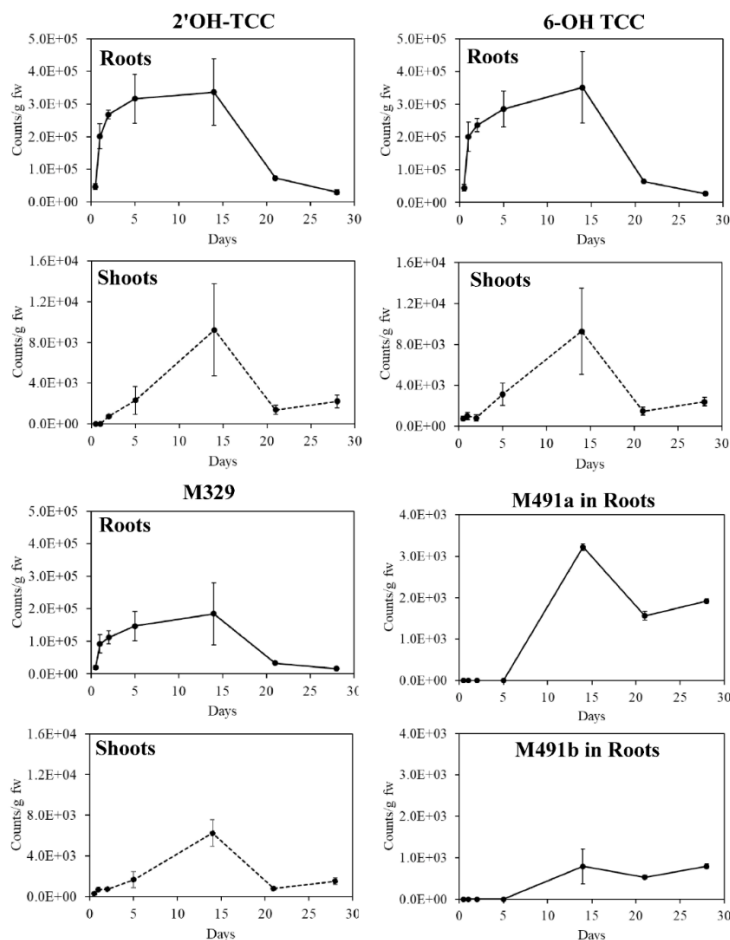


Figure 3. 3. Temporal variation of major phase I metabolites (2'-OH TCC, 6-OH TCC and M329) and phase II metabolites (M491a and M491b) in pepper plants during short-term metabolite screening trial. Initial exposure (0-7 days) and second exposure (7-28 days) were performed at TCC concentrations of 174.8 and 487.4 $\mu\text{g/L}$, respectively. M491a and M491b were only detected in plant roots. Due to their trace concentrations, peak areas at $R_t = 8.39$ and 8.54 min (Figure S14) were combined and presented as M491a; likewise, peak areas at $R_t = 8.44$ and 8.59 min (Figure S15) were combined and presented as M491b. Error bars represent means \pm SE ($n = 3$).

In addition to TCC, its hydroxylated and glycosylated metabolites, two other halogenated diaryl urea compounds were also detected in the TCC-exposed roots and were identified by retention time, accurate mass, and fragmentation patterns as 4,4'-dichlorocarbanilide (m/z 279.0095, eluted at 9.91 min, DCC) with $p(\text{corr}) = 0.77$ and 3,3',4,4'-tetrachlorocarbanilide (m/z 346.9319, eluted at 11.77 min, 3'Cl-TCC) with $p(\text{corr}) = 0.76$. The high energy mass spectra of these two transformation products revealed intense fragment ions at m/z 126.0115 and m/z 159.9730, respectively. The presence of these suspected metabolites in root and shoot samples were further confirmed by characteristic fragment ions on the LC-MS/MS system using the MRM mode (Supplementary Figure 3.9–3.15). The precursor ion mass and fragment ion mass are presented in Table 3.1. These fragment ions were subsequently used for semi-quantifying the concentrations of major transformation products of TCC in plant and media samples (Figure 3.3 and Supplementary Figure 3.16).

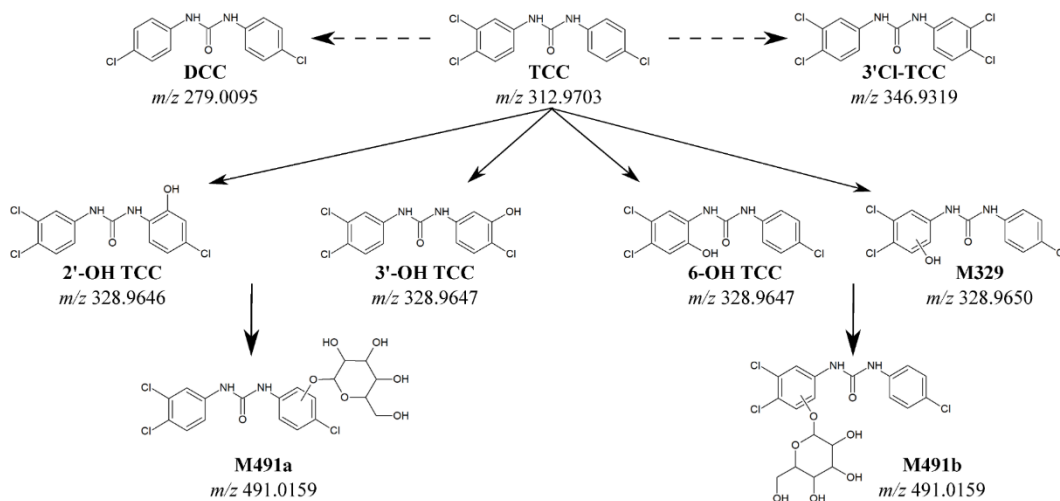


Figure 3. 4. Proposed metabolic pathways of TCC in hydroponically grown jalapeno pepper plants. Accurate m/z of the metabolites were obtained using UPLC-QTOF-MS^E, and their structures were subsequently elucidated by characteristic fragmentations. The presence of DCC and 3'Cl-TCC in plant tissues was likely due to uptake of TCC impurities (dashed arrows).

Based on the metabolites identified during the course of exposure, metabolic pathways of TCC in pepper plant tissues are proposed in Figure 3.4. To the best of our knowledge, plant metabolism of TCC has been reported for the first time in this study. Previous studies have demonstrated that TCC is metabolized in rodents, monkeys, fish, and humans (Birch et al., 1978, Schebb et al., 2011a, Schebb et al., 2011b), catalyzed by cytochrome P450 enzymes (Schebb et al., 2014). In all species, monohydroxylated TCC appeared to be the primary phase I transformation products, including 2'-OH TCC and 6-OH TCC (both bearing the hydroxyl group in the *ortho* position) and 3'-OH TCC (with the hydroxyl group in the *meta* position) (Baumann et al., 2010). These reactive metabolites undergo extensive phase II metabolism to form sulfate and glucuronic acid conjugates in fish and mammals (Birch et al., 1978, Schebb et al., 2011a), in which the glucuronide of 2'-OH TCC has been reported as the most abundant metabolite in fish tissues (Schebb et al., 2011a). Phase I transformation products of TCC also form glutathione adducts (Schebb et al., 2014) and covalently bound to small protein (Schebb et al., 2012a). In addition, Schebb et al. reported that direct *N*-glucuronidation of TCC is an important metabolic pathway in humans following showering with TCC-containing soap (Schebb et al., 2011b). Our study demonstrated that hydroxylated metabolites are also the main phase I transformation products of TCC in plants. Temporal variation of major hydroxylated and glycosylated metabolites of TCC is shown in Figure 3.3. Due to plant transfer to fresh media, data for plant roots and shoots at 7 days were not available. In this trial, phase I transformation products were detected in plant roots after only 12 hours of exposure, increased up to 14 days, and then substantially decreased until the end of exposure. After 28 days, the concentrations of the hydroxylated metabolites in plant roots were identical to those measured at 12 hours of exposure. Shoot concentrations of the hydroxylated metabolites followed the same trend; however, shoot concentrations were

approximately 1-2 orders of magnitude lower than root concentrations. Reduction of the hydroxylated metabolites in plant tissues after 14 days may be explained by phase II conjugation reactions and subsequent phase III sequestration. In this study, glycosylated OH-TCC were the only phase II metabolites detected in plant tissues, and they were only present at trace levels. While unlikely, it is also possible that the methods used in this study were insufficient for capturing other potential phase II metabolites. Since soluble conjugates of parent xenobiotic chemicals are frequently transient intermediates in plants, they may be present at very low concentrations (Reinhold et al., 2011), as the rate of sequestration may be faster than the rate of transformation or conjugation. Furthermore, direct conjugation of transformation products with low-molecular-mass peptides, lignin, hemicellulose and pectin via hydroxyl group (Burken, 2003, Kvesitadze et al., 2006, Schebb et al., 2012a) can also occur, hindering the identification of TCC phase II metabolites. In this study, ¹⁴C-radioactivity, as bound residues, was detected and quantified (Figure 3.2), clearly demonstrating the partitioning of ¹⁴C-TCC into the cell wall compartments. While the glycosylated OH-TCC metabolites were only detected at trace levels, they probably play an important role in phytometabolism of TCC, serving as intermediates required for incorporation of TCC into the cell wall and/or vacuoles. Previous studies with duckweeds indicated that glycosylation is the first step in sequestration of halogenated phenols, as the glycosylated halogenated phenols were subsequently conjugated with malonyl (a glycoside affiliated with vacuolar sequestration) and apiose (a glycosidic component of cell walls in duckweeds) (Day and Saunders, 2004, Reinhold et al., 2011).

DCC and 3'Cl-TCC are known to be present as impurities (~0.2%, w/w) in technical grade TCC (Souchier et al., 2015) (Supplementary Figure 3.12 and Supplementary Figure 3.13). Consequently, the estimated concentrations of DCC and 3'Cl-TCC spiked into the hydroponic

media during the initial exposure (0-7 days) and second exposure (7-28 days) were 0.35 µg/L and 0.97 µg/L, respectively. Therefore, these two products were present in the media throughout the experiments primarily as by-products of TCC. Root uptake and subsequent translocation of DCC and 3'Cl-TCC to aerial tissues were also observed in this study, as evident by detection of both DCC and 3'Cl-TCC in both roots and shoots at different sampling times (Supplementary Figure 3.16). It is possible that DCC detected in hydroponic media and plant tissues could also be a transformation product of TCC. Reductive dehalogenation is a common transformation pathway for halogenated pollutants in the environment. For example, dechlorination of PCBs stimulated by plant exudates in the rhizospheres of switchgrass and poplar was observed by (Meggo et al., 2013). On the other hand, *in vivo* metabolism of PCBs in maize (Wang et al., 2011) and 1,2,5,5,6,9,10-heptachlorodecane in pumpkin (Li et al., 2017) also resulted in the formation of lesser chlorinated phytometabolites.

In general, long-term exposure resulted in significant metabolism of TCC in various tissues of pepper plants: 66.2, 95.5, 97.1, and 95.6% of uptaken TCC in roots, stems, leaves, and fruits after 12 weeks was metabolized, respectively. Hydroxylated TCC metabolites (e.g. 2'-OH TCC and 6-OH TCC) were identified as major phase I transformation product of TCC in plants, followed by *O*-glycosylation in phase II. In addition, approximately 44.6 – 85.6% of uptaken TCC was sequestered into the cell walls. Since pepper fruits are commonly eaten fresh, human exposure to both TCC and its metabolites through consumption of contaminated products is expected. Organic xenobiotics and their soluble metabolites present in crop plants, especially edible parts, have been found to be absorbed in digestive tract of human and subsequently excreted in urine (Paltiel et al., 2016). Therefore, the soluble metabolites of TCC in pepper fruits likely contribute to overall exposure. TCC is considered an endocrine disruptor and can enter into the binding pocket

of human serum albumin (Zhang et al., 2017); however, the potential adverse effects of its hydroxylated metabolites on human health are still largely unknown. In human systems, after ingestion, materials encounter salivary, gastric, and intestinal secretions, which are capable of hydrolyzing glycosidic linkages. Consequently, the TCC-*O*-glucosides are likely prone to hydrolysis during digestion, releasing the hydroxylated TCC aglycones. Although the TCC-*O*-glucosides are present only at trace levels, their contribution to the overall toxicity of TCC and soluble metabolites merits discussion in assessing human health risk of consuming contaminated food crops. On the contrary, sequestration of TCC into cell wall compartments may alleviate the adverse effects since dietary cellulose is thought not to be digested in the stomach and small intestine, and ultimately excreted from human body (Cummings, 1984).

Table 3. 1. Mass-Spectral Information and Proposed Structures of TCC Transformation Products Identified by Waters Progenesis QI 2.1 and MassLynx 4.1 Software.

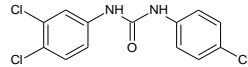
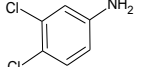
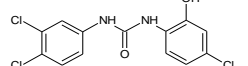
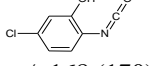
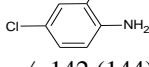
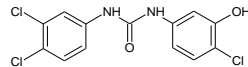
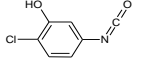
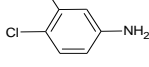
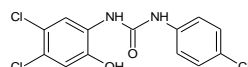
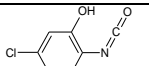
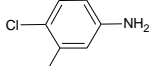
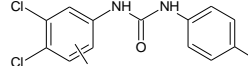
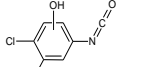
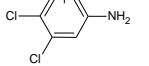
denotation	RT (min) ^a	calc. m/z^b (obs. m/z^c)	error (ppm)	predicted formula	proposed structure	characteristic fragments (M+2 isotopic ions) ^d	confidence level ^e
Triclocarban (TCC)	10.86 (11.33)	312.9708 (312.9703)	1.6	C ₁₃ H ₉ Cl ₃ N ₂ O		 m/z 160 (162, 164)	Level 1
2'-OH TCC	10.52 (10.96)	328.9657 (328.9646)	3.3	C ₁₃ H ₉ Cl ₃ N ₂ O ₂		 m/z 168 (170)  m/z 142 (144)	Level 1
3'-OH TCC	9.30 (9.63)	328.9657 (328.9647)	3.0	C ₁₃ H ₉ Cl ₃ N ₂ O ₂		 m/z 168 (170)  m/z 142 (144)	Level 1
6-OH TCC	10.52 (10.94)	328.9657 (328.9647)	3.0	C ₁₃ H ₉ Cl ₃ N ₂ O ₂		 m/z 202 (204, 206)  m/z 176 (178, 180)	Level 1
M329	9.86 (10.76)	328.9657 (328.9650)	2.1	C ₁₃ H ₉ Cl ₃ N ₂ O ₂		 m/z 202 (204, 206)  m/z 176 (178, 180)	Level 2b

Table 3.1 (cont'd). Mass-Spectral Information and Proposed Structures of TCC Transformation Products Identified by Waters Progenesis QI 2.1 and MassLynx 4.1 Software.

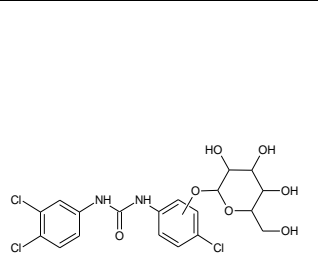
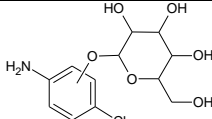
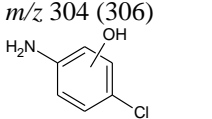
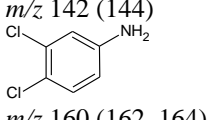
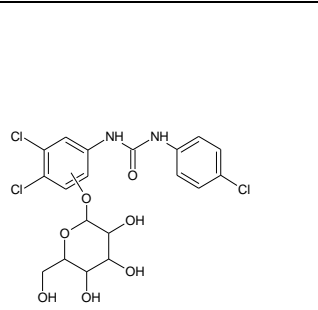
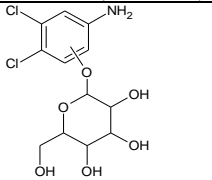
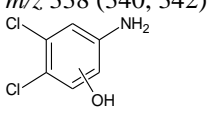
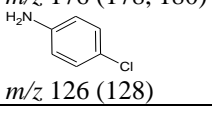
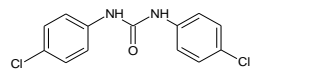
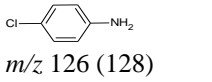
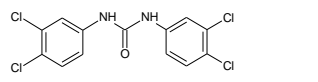
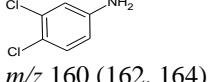
TCC- <i>O</i> -Glucose (M491a)	8.61 (8.39 and 8.54)	491.0185 (491.0159)	5.3	$C_{19}H_{19}Cl_3N_2O_7$		 m/z 304 (306)  m/z 142 (144)  m/z 160 (162, 164)	Level 2b
TCC- <i>O</i> -Glucose (M491b)	8.61 (8.44 and 8.59)	491.0185 (491.0159)	5.3	$C_{19}H_{19}Cl_3N_2O_7$		 m/z 338 (340, 342)  m/z 176 (178, 180)  m/z 126 (128)	Level 2b
4,4'-dichlorocarbanilide (DCC)	9.91 (10.46)	279.0092 (279.0095)	1.1	$C_{13}H_{10}Cl_2N_2O$		 m/z 126 (128)	Level 2b
3,3',4,4'-tetrachlorocarbanilide (3'Cl-TCC)	11.77 (12.07)	346.9312 (346.9319)	2.0	$C_{13}H_8Cl_4N_2O$		 m/z 160 (162, 164)	Level 2b

Table 3.1 (cont'd). Mass-Spectral Information and Proposed Structures of TCC Transformation Products Identified by Waters Progenesis QI 2.1 and MassLynx 4.1 Software.

^aRetention time of TCC and its metabolites when analyzed on the UPLC-QTOF-MS^E and LC-MS/MS systems. The Rt on the LC-MS/MS are presented in parentheses. For TCC glycosylated conjugates, only one signal (m/z 491.0159) was observed on the UPLC-QTOF-MS^E system (Rt = 8.61 min).

^{b, c}Accurate calculated mass (calc. m/z) and observed mass (obs. m/z) were obtained from Chemskech software ver. 2016.2.2 (ACD/Labs) and high-resolution mass analyzer (QTOF-MS^E, Waters Xevo G2-XS), respectively.

^dAccording to (Warren et al., 1978) and (Schebb et al., 2012b) or reference standards, if available. Fragment ions were acquired using a tandem mass analyzer (MS/MS, Applied Biosystems Sciex 3200). Full MS/MS fragmentation of TCC and its transformation products are presented in the Supplementary Figure 3.8–3.13.

^eAccording to (Schymanski et al., 2014): Level 1: reference standard, HR-MS, MS/MS, RT confirmed; Level 2b: fragmentation pattern reported, HR-MS, MS/MS.

APPENDIX

Supplementary Table 3.1. ¹⁴C-radioactivity extracted by different extraction methods: acid digestion (HNO₃:HClO₄), sodium hypochlorite digestion (NaClO) and accelerated solvent extraction (ASE, acetone:methanol = 1:1) in various plant tissues during the long-term exposure (12 weeks). In this trial, the first fruit sampling event occurred at the 6th week. Root and stem data for week 6th and week 9th were not available since sacrificial sampling was only performed after 3 and 12 weeks. Data are presented as μg ¹⁴C-TCC equivalent/g, mean ± SE (n = 5).

	3 weeks			6 weeks			9 weeks			12 weeks		
	HNO ₃ :HClO ₄	NaClO	ASE	HNO ₃ :HClO ₄	NaClO	ASE	HNO ₃ :HClO ₄	NaClO	ASE	HNO ₃ :HClO ₄	NaClO	ASE
Roots	205.40±34.22	113.75±17.91	68.99±16.51	NA	NA	NA	NA	NA	NA	59.60±8.79	33.01±5.30	30.92±6.09
Stems	5.91±1.96	2.07±0.56	1.37±0.31	NA	NA	NA	NA	NA	NA	6.76±1.13	0.97±0.09	0.67±0.11
Leaves	1.52±0.24	1.00±0.16	1.21±0.14	4.28±0.58	1.95±0.14	1.71±0.04	2.93±0.57	1.08±0.08	1.11±0.24	4.21±0.77	1.31±0.40	1.52±0.36
Fruits	NA	NA	NA	0.65±0.18	0.38±0.01	ND	0.78±0.12	0.44±0.02	ND	0.78±0.11	0.44±0.03	ND

NA: not analyzed, ND: not detected.

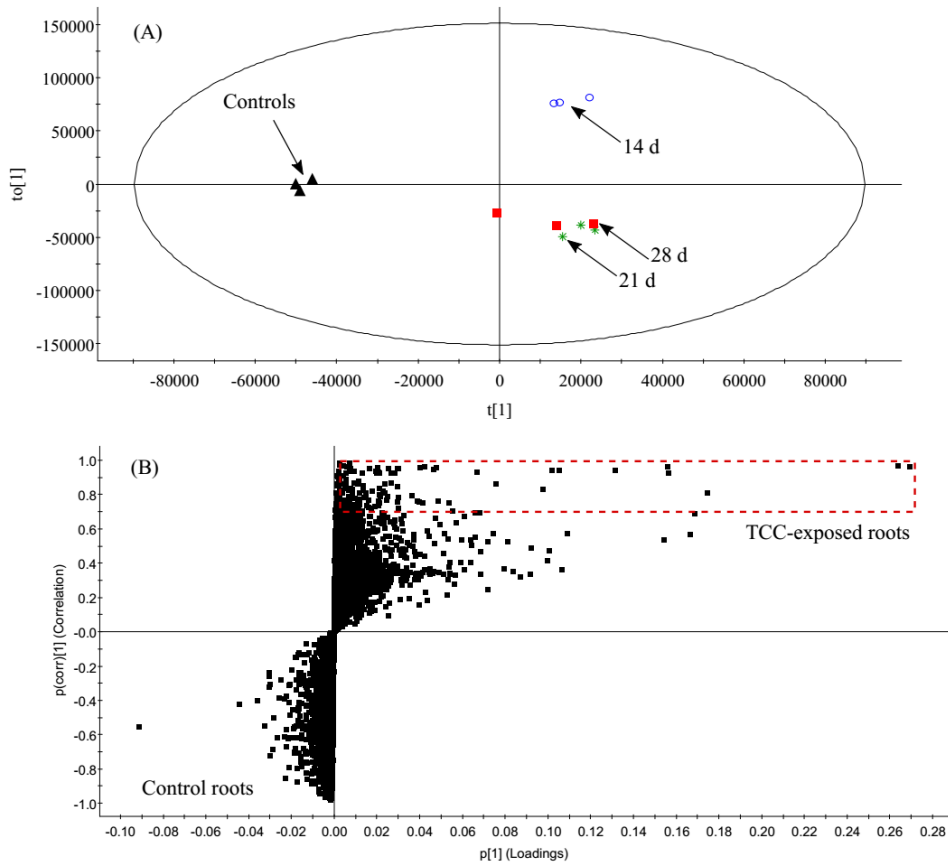
Supplementary Table 3.2. MS/MS (in MRM mode) parameters for semi-quantification of TCC metabolites.

Compounds	Precursor ion <i>m/z</i>	Product ion <i>m/z</i>	Dwell time (msec)	DP (eV)	EP (eV)	CEP (eV)	CXP (eV)	CE (eV)
2'-OH TCC	329	168	100	-40	-5	-22	-6	-30
6-OH TCC	329	176	100	-40	-5	-22	-2	-30
M329	329	176	100	-40	-5	-22	-2	-30
M491a	491	304	100	-40	-5	-31	-2	-20
M491b	491	338	100	-40	-5	-31	-2	-20
DCC	279	126	100	-40	-5	-20	-2	-30
3'-Cl-TCC	347	160	100	-40	-5	-23	-2	-30

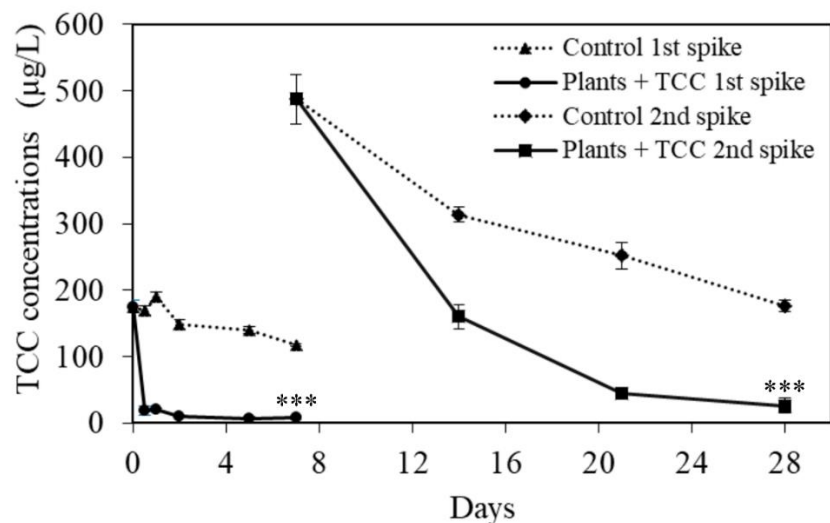
DP: Declustering Potential; EP: Entrance Potential; CEP: Collision Cell Entrance Potential;
CXP: Collision Cell Exit Potential; CE: Collision Energy.



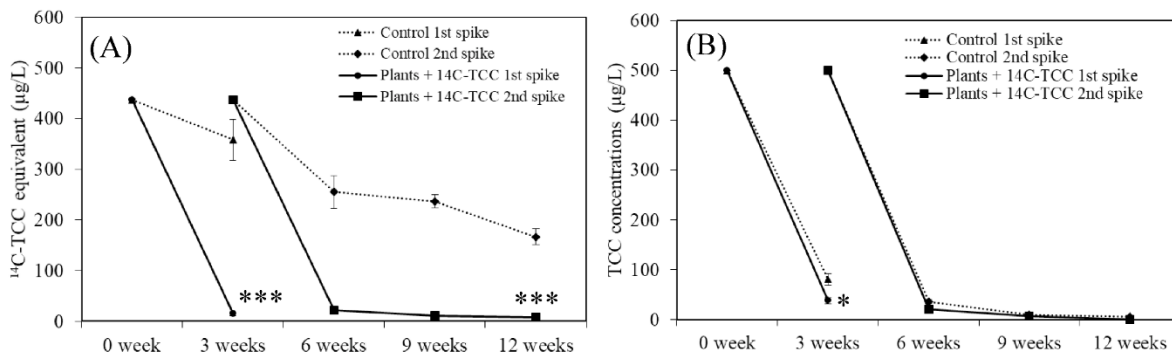
Supplementary Figure 3.1. Jalapeno pepper plants exposed to TCC in long-term study. (A): Plants after 3 weeks of exposure and (B): Plants bearing fruits after 12 weeks of exposure.



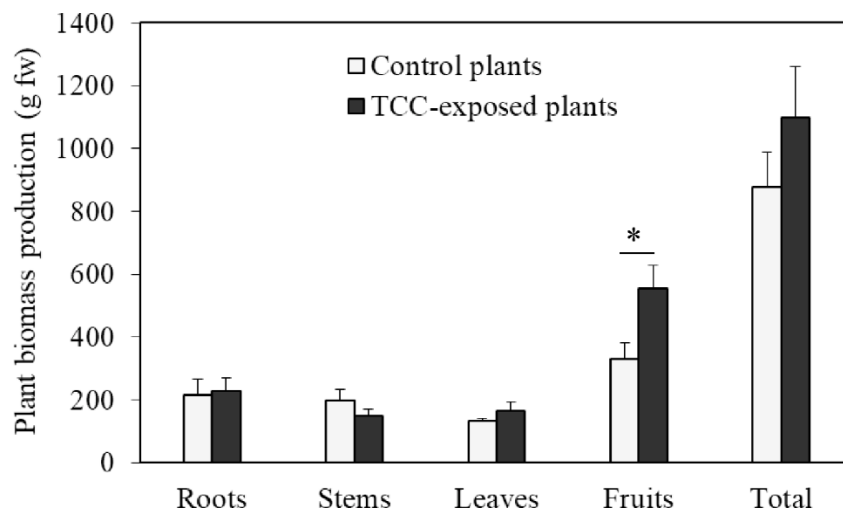
Supplementary Figure 3.2. Processing Progenesis QI data (root extracts) using EZinfo software. (A): Orthogonal projection to latent structures-discriminant analysis (OPLS-DA), Controls: control roots; 14 d, 21 d and 28 d: roots exposed to TCC for 14, 21 and 28 days, respectively, (B): The S-plot obtained from OPLS-DA model. The dashed rectangle on the S-plot includes m/z variables that significantly contribute to the difference between the control and TCC-exposed root extracts ($p(\text{corr}) \geq 0.7$).



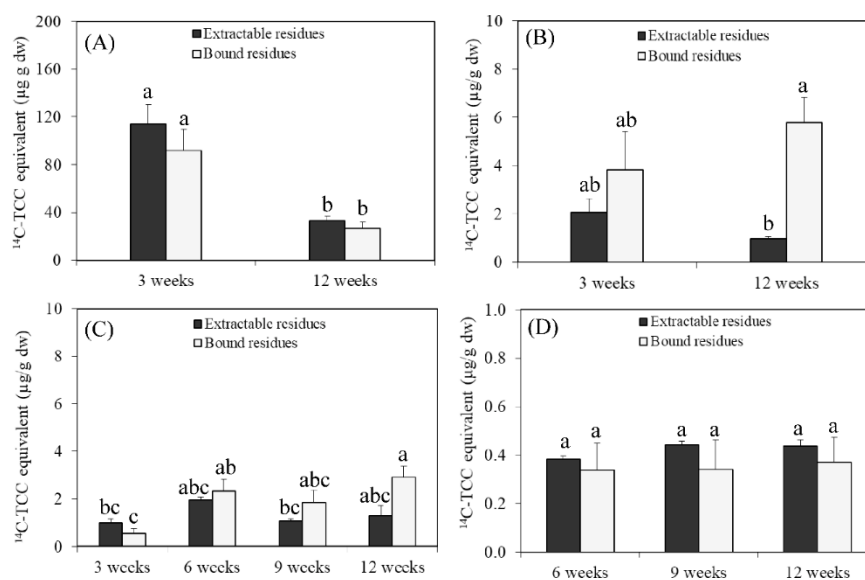
Supplementary Figure 3.3. Dissipation of TCC in the hydroponic media during the short-term metabolite screening study. Error bars represent means \pm SE ($n = 3$). Some error bars are obscured by data symbols. *** indicates significant difference between no-plant control and planted media at the end of each exposure at $p < 0.001$.



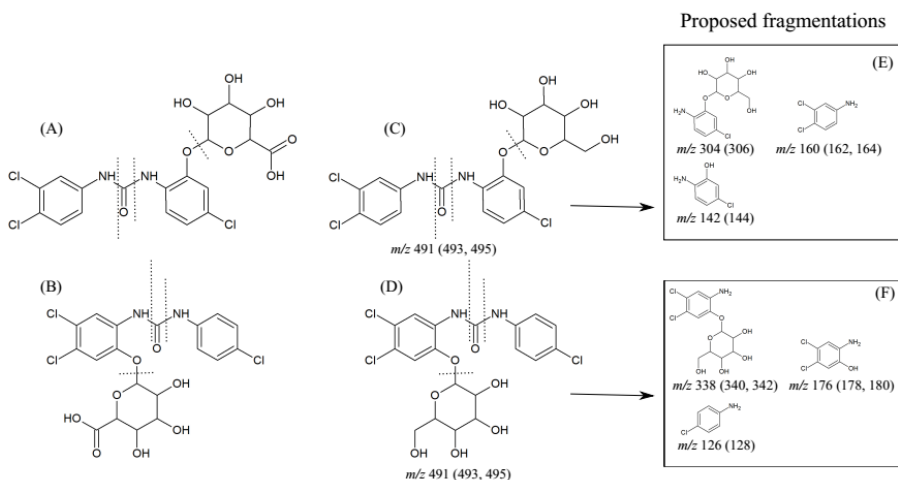
Supplementary Figure 3.4. Concentrations of ^{14}C -TCC (A) and non-labeled TCC (B) in the nutrient solutions during long-term exposure study. ^{14}C -labeled concentrations were adjusted for the ratio of $^{14}\text{C}:^{12}\text{C}$ -TCC added to the system ($^{14}\text{C}:^{12}\text{C} = 1:100$). Error bars represent means \pm SE ($n = 5$). Some error bars are obscured by data symbols. * and *** indicate significant differences between no-plant control and planted media at the end of each exposure at $p < 0.05$ and $p < 0.001$, respectively.



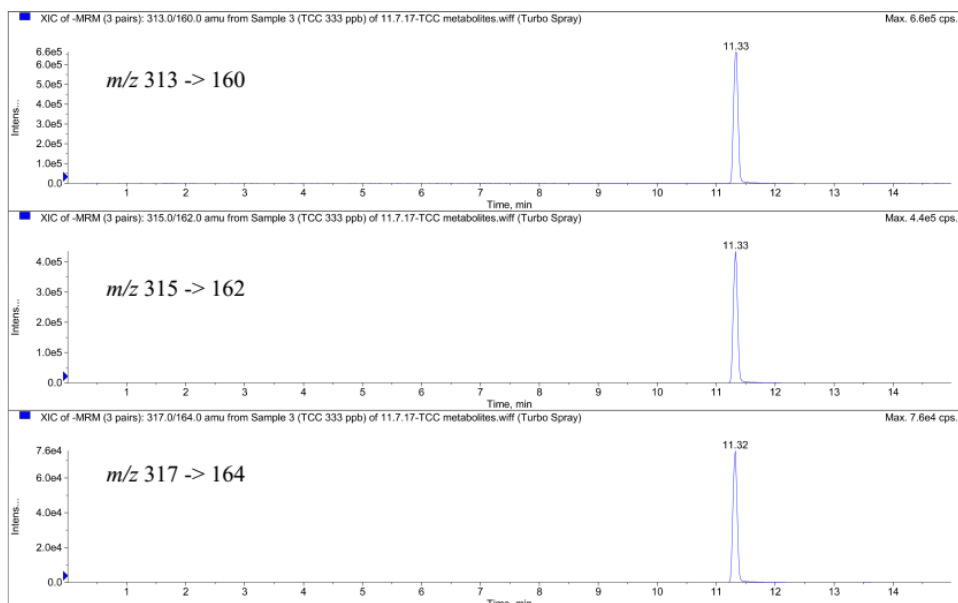
Supplementary Figure 3.5. Plant biomass production (in gram fresh weight) of Jalapeno pepper plants exposed to TCC for 12 weeks. Error bars represent means \pm SE ($n = 5$). * indicates significant difference between control plants and TCC-exposed plants at $p < 0.05$.



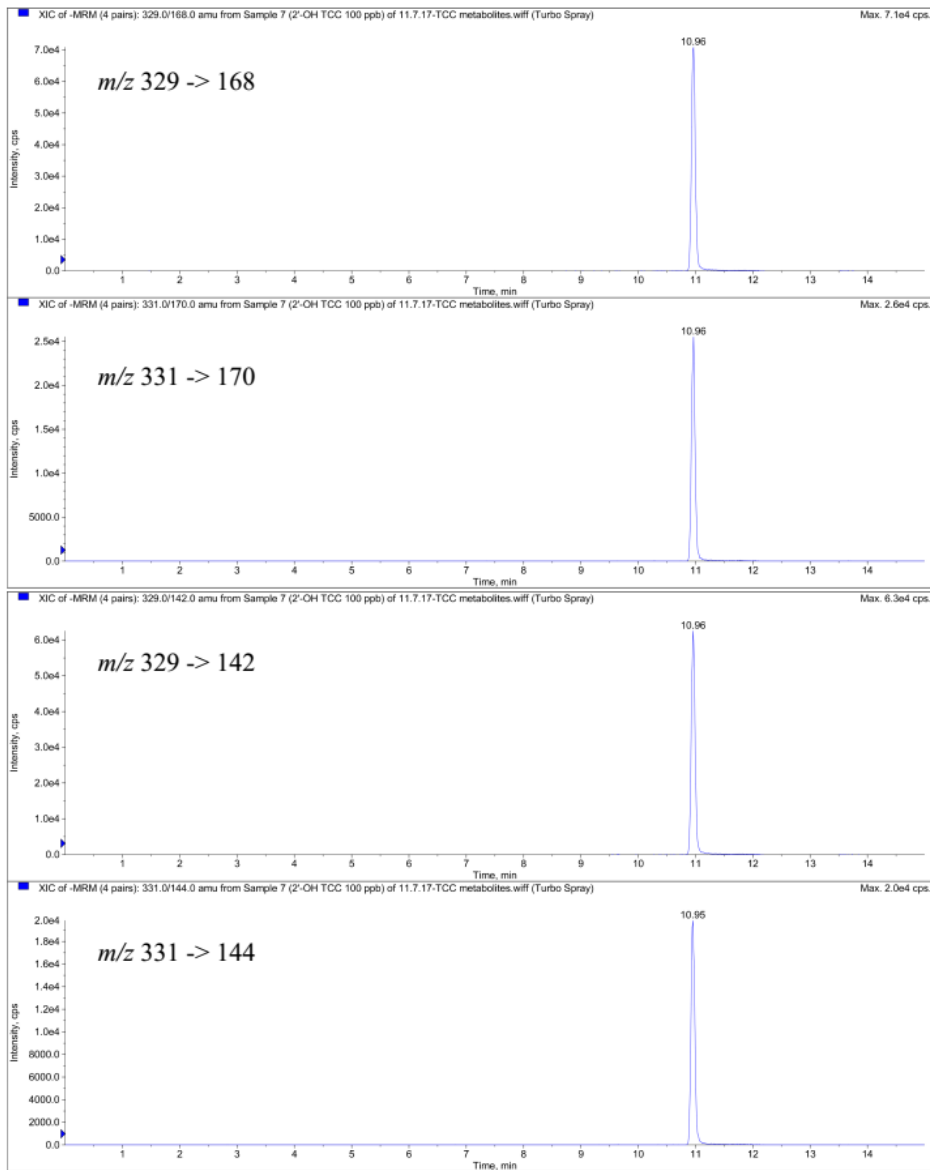
Supplementary Figure 3.6. Extractable and bound residues of ^{14}C (presented as $\mu\text{g } ^{14}\text{C-TCC}$ equivalent/g dw) in plant tissues [(A): roots, (B): stems, (C): leaves and (D) fruits] during long-term exposure. Extractable residues are defined as the ^{14}C fractions detected in NaClO extracts. Meanwhile, ^{14}C bound residues equal the total of ^{14}C concentrations in the acid digestants minus the corresponding extractable residues. Error bars represent means \pm SE ($n = 5$). In each panel, columns marked by different letters are significantly different from each other ($p < 0.05$).



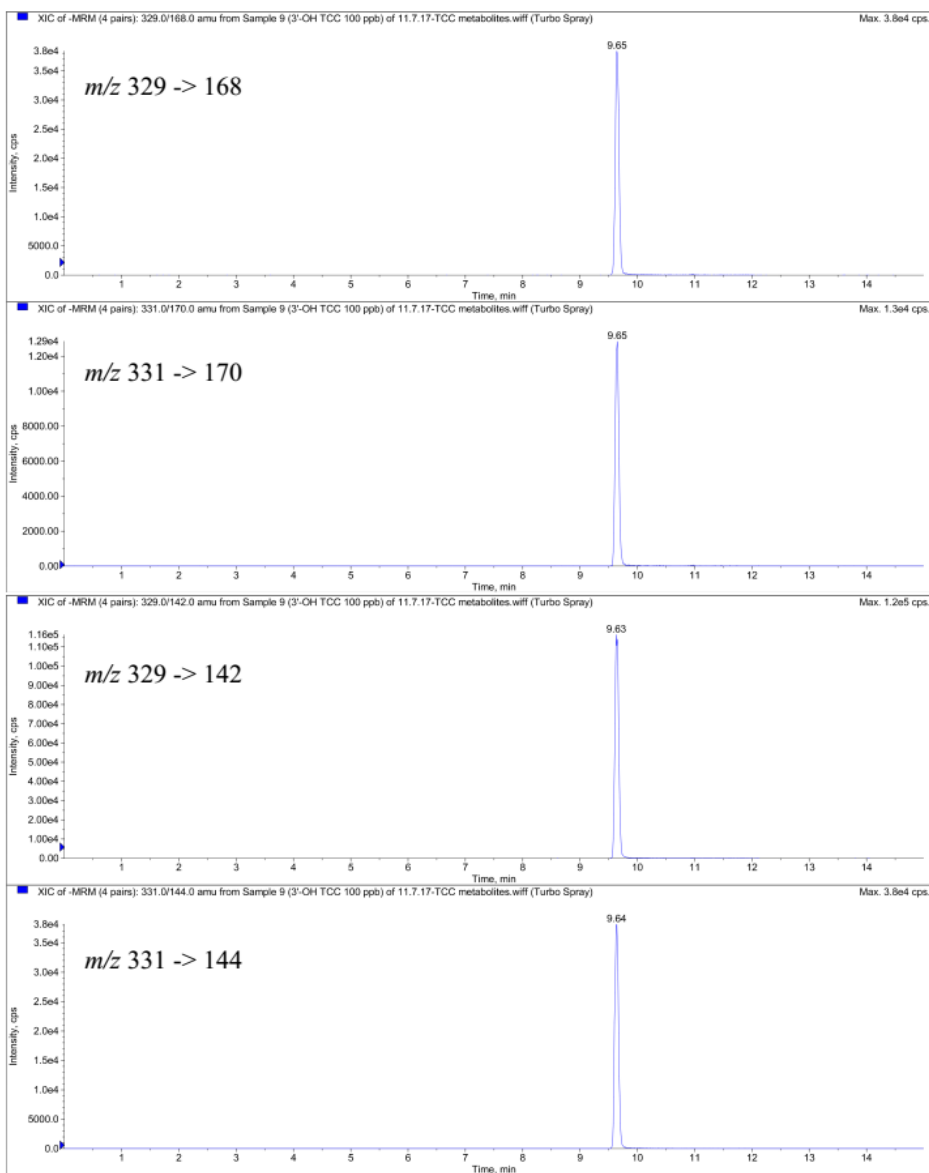
Supplementary Figure 3.7. Based on fragmentations of TCC-*O*-glucuronide metabolites observed by (Schebb et al., 2012) using LC-MS/MS in MRM mode (A and B), a similar approach was employed in this study to confirm the presence of TCC-*O*-glucoside metabolites in pepper plant tissues (C and D). The product ions corresponding to different *O*-glycosyl positions on the monochloroaniline and dichloroaniline rings are also indicated (E and F).



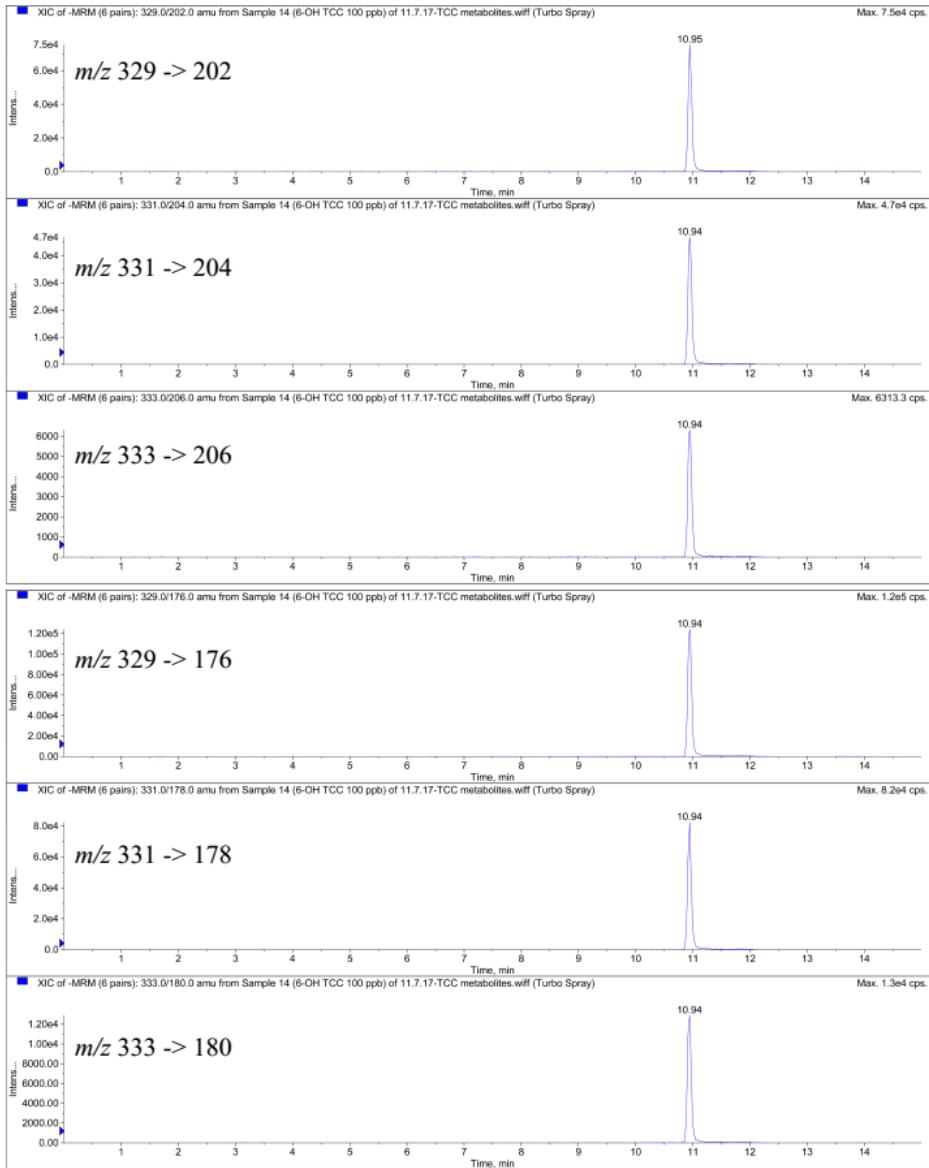
Supplementary Figure 3.8. Selected ion chromatograms of TCC (333 $\mu\text{g/L}$, $R_t = 11.33$ min). Characteristic mass transitions in MRM mode are presented on the chromatograms.



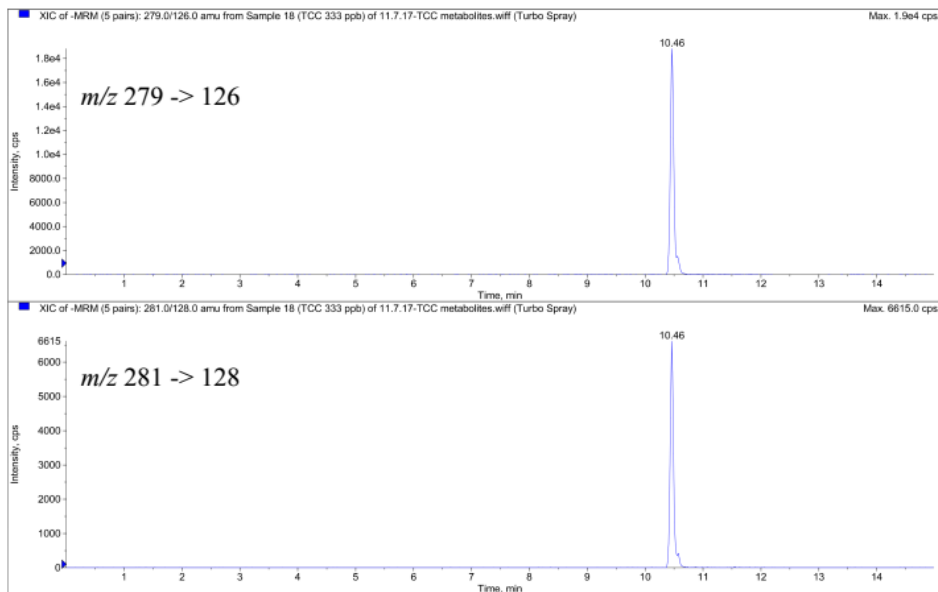
Supplementary Figure 3.9. Selected ion chromatograms of 2'-OH TCC (100 $\mu\text{g/L}$, R_t = 10.96 min). Characteristic mass transitions in MRM mode are presented on the chromatograms.



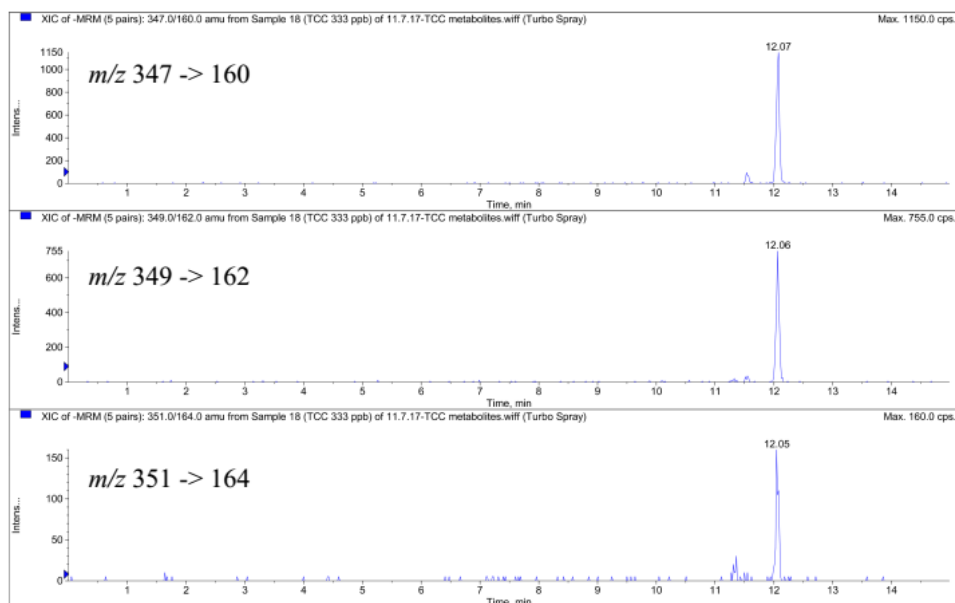
Supplementary Figure 3.10. Selected ion chromatograms of 3'-OH TCC (100 μ g/L, R_t = 9.63 min). Characteristic mass transitions in MRM mode are presented on the chromatograms.



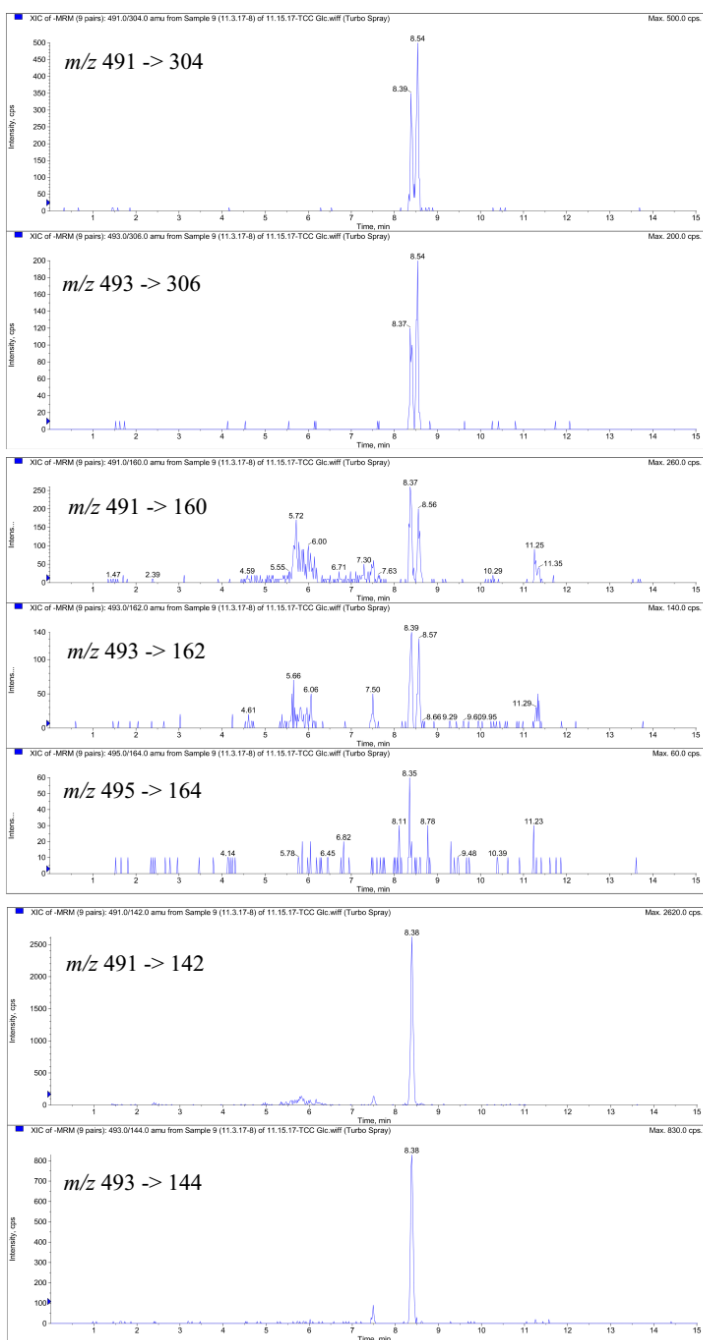
Supplementary Figure 3.11. Selected ion chromatograms of 6-OH TCC (100 $\mu\text{g/L}$, $R_t = 10.94$ min). Characteristic mass transitions in MRM mode are presented on the chromatograms.



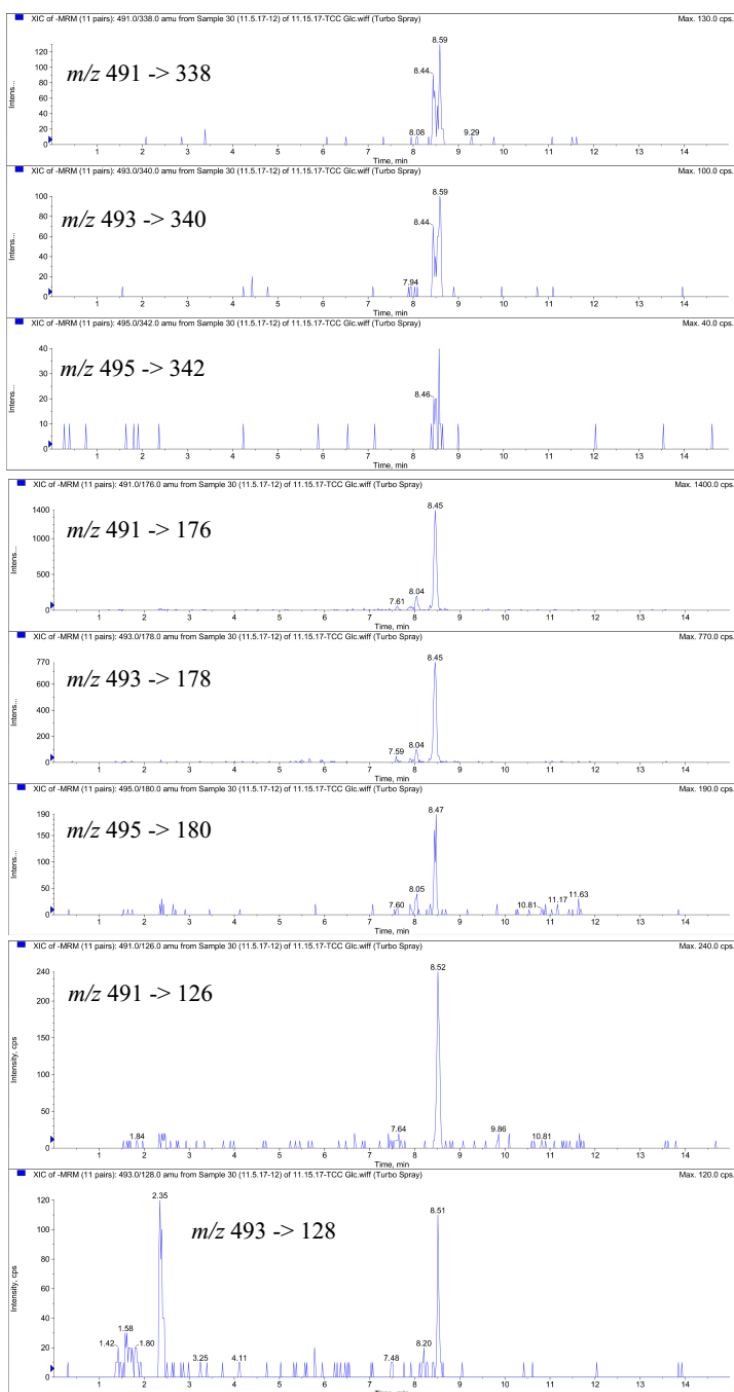
Supplementary Figure 3.12. Selected ion chromatograms of DCC (Rt = 10.46 min as impurity in 333 μg TCC/L standard). Characteristic mass transitions in MRM mode are presented on the chromatograms.



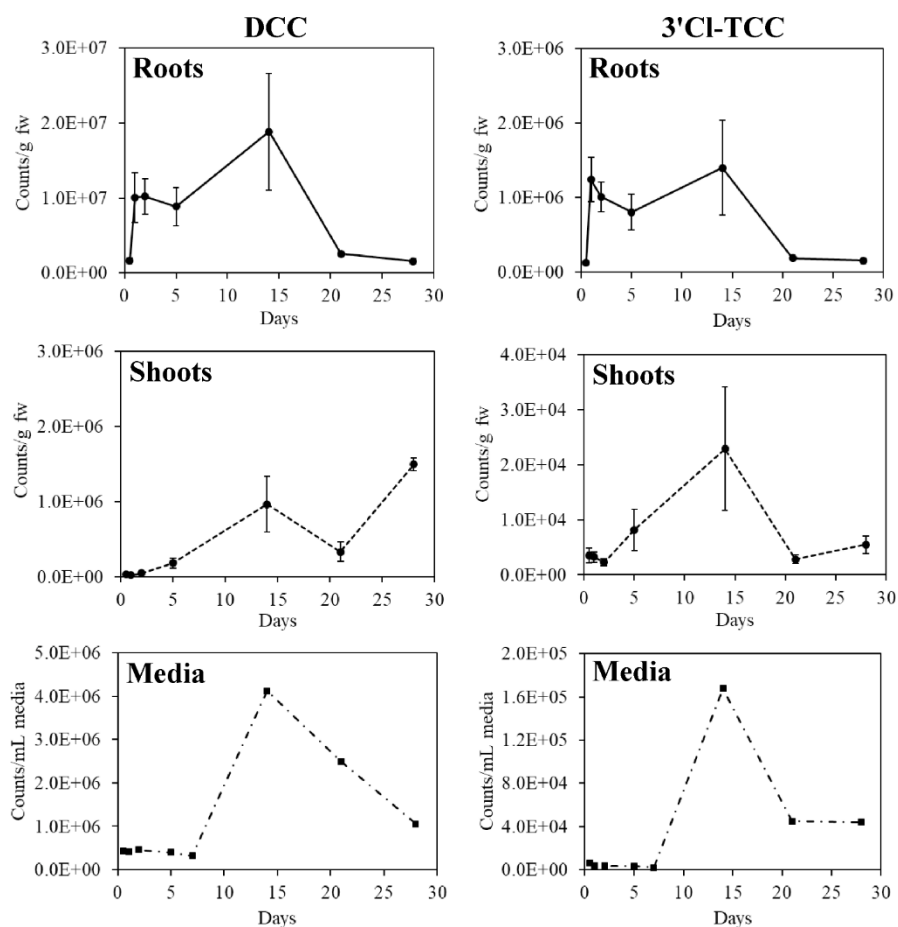
Supplementary Figure 3.13. Selected ion chromatograms of 3'Cl-TCC (Rt = 12.07 min as impurity in 333 μg TCC/L standard). Characteristic mass transitions in MRM mode are presented on the chromatograms.



Supplementary Figure 3.14. Selected ion chromatograms of M491a. Characteristic mass transitions in MRM mode suggested two potential TCC-*O*-glucoside metabolites ($R_t = 8.39$ and 8.54 min, respectively), with the glucose moiety located on the chloroaniline ring. Due to low abundance of the precursor ions, MRM transition of the $M+4$ isotope $m/z 495 \rightarrow 164$ was not observed. The $m/z 491 \rightarrow 142$ and $m/z 493 \rightarrow 144$ were only observed for the peak eluted at 8.39 min, likely attributed to different hydroxyl (-OH) positions on the monochloroaniline ring. Intensity of common product ions of 2'-OH TCC-glucuronide and 3'-OH TCC-glucuronide in MRM mode, including $m/z 142$, was found to be influenced by the positions of the -OH group on TCC molecules (Schebb et al., 2012).



Supplementary Figure 3.15. Selected ion chromatograms of M491b. Characteristic mass transitions in MRM mode suggested two potential TCC-*O*-glucoside metabolites (Rt = 8.44 and 8.59 min, respectively), with the glucose moiety located on the dichloroaniline ring. Due to low abundance of the precursor ions, MRM transition of the M+4 isotope m/z 495 \rightarrow 342 was not observed. The presence of the metabolite at 8.59 min could not be unequivocally confirmed due to lack of some predicted fragment ions.



Supplementary Figure 3.16. Temporal variation of 4,4'-dichlorocarbanilide (DCC) and 3,3',4,4'-tetrachlorocarbanilide (3'Cl-TCC) in pepper roots, shoots and hydroponic media during short-term metabolite screening trial. Initial exposure (0-7 days) and second exposure (7-28 days) were performed at TCC concentrations of 174.8 and 487.4 $\mu\text{g/L}$, respectively. Error bars represent means \pm SE ($n = 3$). Triplicates of media sample at each sampling time were pooled, concentrated on SPE cartridges and analyzed.

REFERENCES

REFERENCES

- Aryal, N. and Reinhold, D., 2013. Phytoaccumulation of antimicrobials by hydroponic *Cucurbita pepo*. *Int. J. Phytoremediation* 15, 330-342.
- Aryal, N. and Reinhold, D.M., 2011. Phytoaccumulation of antimicrobials from biosolids: Impacts on environmental fate and relevance to human exposure. *Water Res.* 45, 5545-5552.
- Audu, A.A. and Heyn, A.H.A., 1988. Comparative hydrolysis of substituted ureas in a mixed alcoholic-water solution. *Water Res.* 22, 1155-1162.
- Baumann, A., Lohmann, W., Rose, T., Ahn, K.C., Hammock, B.D., Karst, U. and Schebb, N.H., 2010. Electrochemistry-Mass Spectrometry Unveils the Formation of Reactive Triclocarban Metabolites. *Drug Metab. Dispos.* 38, 2130-2138.
- Birch, C.G., Hiles, R.A., Eichhold, T.H., Jeffcoat, A.R., Handy, R.W., Hill, J.M., Willis, S.L., Hess, T.R. and Wall, M.E., 1978. Biotransformation products of 3,4,4'-trichlorocarbanilide in rat, monkey, and man. *Drug Metab. Dispos.* 6, 169-176.
- Briggs, G.G., Bromilow, R.H. and Evans, A.A., 1982. Relationships between lipophilicity and root uptake and translocation of non-ionised chemicals by barley. *Pestic. Sci.* 13, 495-504.
- Briggs, G.G., Bromilow, R.H., Evans, A.A. and Williams, M., 1983. Relationships between lipophilicity and the distribution of non-ionized chemicals in barley shoots following uptake by the roots. *Pestic. Sci.* 14, 492-500.
- Burken, J., 2003. *Phytoremediation: Transformation and control of contaminants*. McCutcheon, S. and Schnoor, J. (eds), pp. 59-84, John Wiley & Sons, Inc., New Jersey.
- Collins, C., Fryer, M. and Grosso, A., 2006. Plant uptake of non-ionic organic chemicals. *Environ. Sci. Technol.* 40, 45-52.
- Collins, C., Martin, I. and Doucette, W., 2011. *Organic xenobiotics and plants*. Schroder, P. and Collins, C. (eds), pp. 3-16, Springer.
- Cummings, J.H., 1984. Cellulose and the human gut. *Gut* 25, 805-810.
- Day, J.A. and Saunders, F.M., 2004. Glycosidation of chlorophenols by *Lemna minor*. *Environmental Toxicology and Chemistry* 23, 613-620.
- Ding, S.L., Wang, X.K., Jiang, W.Q., Zhao, R.S., Shen, T.T., Wang, C. and Wang, X., 2015. Influence of pH, inorganic anions, and dissolved organic matter on the photolysis of antimicrobial triclocarban in aqueous systems under simulated sunlight irradiation. *Environ. Sci. Pollut. Res.* 22, 5204-5211.

Dodgen, L.K., Li, J., Parker, D. and Gan, J.J., 2013. Uptake and accumulation of four PPCP/EDCs in two leafy vegetables. *Environ. Pollut.* 182, 150-156.

Dordio, A.V., Belo, M., Martins Teixeira, D., Palace Carvalho, A.J., Dias, C.M.B., Picó, Y. and Pinto, A.P., 2011. Evaluation of carbamazepine uptake and metabolization by *Typha* spp., a plant with potential use in phytotreatment. *Bioresour. Technol.* 102, 7827-7834.

Fu, Q., Zhang, J., Borchardt, D., Schlenk, D. and Gan, J., 2017. Direct Conjugation of Emerging Contaminants in *Arabidopsis* : Indication for an Overlooked Risk in Plants? *Environ. Sci. Technol.* 51, 6071-6081.

Goldstein, M., Shenker, M. and Chefetz, B., 2014. Insights into the Uptake Processes of Wastewater-Borne Pharmaceuticals by Vegetables. *Environ. Sci. Technol.*

Halden, R.U. and Paull, D.H., 2005. Co-occurrence of triclocarban and triclosan in US water resources. *Environ. Sci. Technol.* 39, 1420-1426.

Heidler, J., Sapkota, A. and Halden, R.U., 2006. Partitioning, Persistence, and Accumulation in Digested Sludge of the Topical Antiseptic Triclocarban during Wastewater Treatment. *Environ. Sci. Technol.* 40, 3634–3639.

Herklotz, P.A., Gurung, P., Heuvel, B.V. and Kinney, C.A., 2010. Uptake of human pharmaceuticals by plants grown under hydroponic conditions. *Chemosphere* 78, 1416-1421.

Hoagland, D.R. and Arnon, D.I. (1950) *The Water-Culture Method for Growing Plants without Soil*, California Agricultural Experiment Station.

Hyland, K.C., Blaine, A.C. and Higgins, C.P., 2015. Accumulation of contaminants of emerging concern in food crops part 2: Plant distribution. *Environ. Toxicol. Chem.* 34, 2222-2230.

Kvesitadze, G., Khatisashvili, G., Sadunishvili, T. and Ramsden, J.J., 2006. Biochemical mechanisms of detoxification in higher plants: Basis of phytoremediation, pp. 103-133, Springer.

Kwon, J.-W. and Xia, K., 2012. Fate of triclosan and triclocarban in soil columns with and without biosolids surface application. *Environ. Toxicol. Chem.* 31, 262-269.

Levsen, K., Schiebel, H.M., Behnke, B., Dotzer, R., Dreher, W., Elend, M. and Thiele, H., 2005. Structure elucidation of phase II metabolites by tandem mass spectrometry: an overview. *J. Chromatogr. A* 1067, 55-72.

Li, Y., Hou, X., Yu, M., Zhou, Q., Liu, J., Schnoor, J.L. and Jiang, G., 2017. Dechlorination and chlorine rearrangement of 1,2,5,5,6,9,10-heptachlorodecane mediated by the whole pumpkin seedlings. *Environ. Pollut.* 224, 524-531.

Lozano, N., Rice, C.P., Ramirez, M. and Torrents, A., 2013. Fate of Triclocarban, Triclosan and Methyltriclosan during wastewater and biosolids treatment processes. *Water Res.* 47, 4519–4527.

Macherius, A., Eggen, T., Lorenz, W., Moeder, M., Ondruschka, J. and Reemtsma, T., 2012. Metabolization of the Bacteriostatic Agent Triclosan in Edible Plants and its Consequences for Plant Uptake Assessment. *Environ. Sci. Technol.* 46, 10797-10804.

Macherius, A., Seiwert, B., Schroder, P., Huber, C., Lorenz, W. and Reemtsma, T., 2014. Identification of Plant Metabolites of Environmental Contaminants by UPLC-QToF-MS: The in Vitro Metabolism of Triclosan in Horseradish. *J. Agric. Food Chem.* 62, 1001-1009.

Majewsky, M., Glauner, T. and Horn, H., 2015. Systematic suspect screening and identification of sulfonamide antibiotic transformation products in the aquatic environment. *Anal. Bioanal. Chem.* 407, 5707-5717.

Malchi, T., Maor, Y., Tadmor, G., Shenker, M. and Chefetz, B., 2014. Irrigation of Root Vegetables with Treated Wastewater: Evaluating Uptake of Pharmaceuticals and the Associated Human Health Risks. *Environ. Sci. Technol.* 48, 9325–9333.

Marsik, P., Sisa, M., Lacina, O., Motkova, K., Langhansova, L., Rezek, J. and Vanek, T., 2017. Metabolism of ibuprofen in higher plants: A model *Arabidopsis thaliana* cell suspension culture system. *Environ. Pollut.* 220, 383-392.

Mathews, S., Henderson, S. and Reinhold, D., 2014. Uptake and accumulation of antimicrobials, triclocarban and triclosan, by food crops in a hydroponic system. *Environ. Sci. Pollut. Res.* 21, 6025-6033.

Meggio, R.E., Schnoor, J.L. and Hu, D., 2013. Dechlorination of PCBs in the rhizosphere of switchgrass and poplar. *Environ. Pollut.* 178, 312-321.

Mulla, S.I., Hu, A., Wang, Y., Sun, Q., Huang, S.-L., Wang, H. and Yu, C.-P., 2016. Degradation of triclocarban by a triclosan-degrading *Sphingomonas* sp strain YL-JM2C. *Chemosphere* 144, 292-296.

Paltiel, O., Fedorova, G., Tadmor, G., Kleinstern, G., Maor, Y. and Chefetz, B., 2016. Human Exposure to Wastewater-Derived Pharmaceuticals in Fresh Produce: A Randomized Controlled Trial Focusing on Carbamazepine. *Environ. Sci. Technol.* 50, 4476-4482.

Pascal-Lorber, S., Alsayeda, H., Jouanin, I., Debrauwer, L., Canlet, C. and Laurent, F., 2010. Metabolic Fate of [14C]Diuron and [14C]Linuron in Wheat (*Triticum aestivum*) and Radish (*Raphanus sativus*). *J. Agric. Food Chem.* 58, 10935–10944.

Pascal-Lorber, S., Despoux, S., Rathahao, E., Canlet, C., Debrauwer, L. and Laurent, F., 2008. Metabolic Fate of [14C] Chlorophenols in Radish (*Raphanus sativus*), Lettuce (*Lactuca sativa*), and Spinach (*Spinacia oleracea*). *J. Agric. Food Chem.* 56, 8461–8469.

Reinhold, D., Handell, L. and Saunders, F.M., 2011. Callus Cultures for Phytometabolism Studies: Phytometabolites of 3-Trifluoromethylphenol in Lemnaceae Plants and Callus Cultures. *Int. J. Phytoremediation* 13, 642-656.

Sandermann, H., 1992. Plant metabolism of xenobiotics. *Trends Biochem. Sci.* 17, 82-84.

Schebb, N.H., Buchholz, B.A., Hammock, B.D. and Rice, R.H., 2012a. Metabolism of the Antibacterial Triclocarban by Human Epidermal Keratinocytes to Yield Protein Adducts. *J. Biochem. Mol. Toxicol.* 26, 230-234.

Schebb, N.H., Flores, I., Kurobe, T., Franze, B., Ranganathan, A., Hammock, B.D. and Teh, S.J., 2011a. Bioconcentration, metabolism and excretion of triclocarban in larval Qurt medaka (*Oryzias latipes*). *Aquat. Toxicol.* 105, 448-454.

Schebb, N.H., Franze, B., Maul, R., Ranganathan, A. and Hammock, B.D., 2012b. In vitro glucuronidation of the antibacterial triclocarban and its oxidative metabolites. *Drug Metab. Dispos.* 40, 25-31.

Schebb, N.H., Inceoglu, B., Ahn, K.C., Morisseau, C., Gee, S.J. and Hammock, B.D., 2011b. Investigation of Human Exposure to Triclocarban after Showering and Preliminary Evaluation of Its Biological Effects. *Environ. Sci. Technol.* 45, 3109-3115.

Schebb, N.H., Muvvala, J.B., Morin, D., Buckpitt, A.R., Hammock, B.D. and Rice, R.H., 2014. Metabolic Activation of the Antibacterial Agent Triclocarban by Cytochrome P450 1A1 Yielding Glutathione Adducts. *Drug Metab. Dispos.* 42, 1098-1102.

Schymanski, E.L., Jeon, J., Gulde, R., Fenner, K., Ruff, M., Singer, H.P. and Hollender, J., 2014. Identifying Small Molecules via High Resolution Mass Spectrometry: Communicating Confidence. *Environ. Sci. Technol.* 48, 2097-2098.

Shenker, M., Harush, D., Ben-Ari, J. and Chefetz, B., 2011. Uptake of carbamazepine by cucumber plants - A case study related to irrigation with reclaimed wastewater. *Chemosphere* 82, 905-910.

Souchier, M., Benali-Raclot, D., Benanou, D., Boireau, V., Gomez, E., Casellas, C. and Chiron, S., 2015. Screening triclocarban and its transformation products in river sediment using liquid chromatography and high resolution mass spectrometry. *Sci. Total Environ.* 502, 199-205.

Sun, J., Wu, X. and Gan, J., 2015. Uptake and Metabolism of Phthalate Esters by Edible Plants. *Environ. Sci. Technol.*

Thomson, J., 2012. Handbook of Radioactivity Analysis. L'Annunziata, M. (ed), pp. 589-590, Academic Press, San Diego, CA.

Trapp, S., 2000. Modelling uptake into roots and subsequent translocation of neutral and ionisable organic compounds. *Pest Manage. Sci.* 56, 767-778.

Wang, S., Zhang, S., Huang, H., Zhao, M. and Lv, J., 2011. Uptake, translocation and metabolism of polybrominated diphenyl ethers (PBDEs) and polychlorinated biphenyls (PCBs) in maize (*Zea mays* L.). *Chemosphere* 85, 379-385.

Warren, J.T., Allen, R. and Carter, D.E., 1978. Identification of the metabolites of trichlorocarbanilide in the rat. *Drug Metab. Dispos.* 6, 38-44.

Wild, S.R. and Jones, K.C., 1992. Organic chemicals entering agricultural soils in sewage sludges: screening for their potential to transfer to crop plants and livestock. *Sci. Total Environ.* 119, 85-119.

Wu, C., Spongberg, A.L., Witter, J.D. and Sridhar, B.B.M., 2012a. Transfer of wastewater associated pharmaceuticals and personal care products to crop plants from biosolids treated soil. *Ecotoxicol. Environ. Saf.* 85, 104-109.

Wu, C.X., Spongberg, A.L., Witter, J.D., Fang, M. and Czajkowski, K.P., 2010. Uptake of Pharmaceutical and Personal Care Products by Soybean Plants from Soils Applied with Biosolids and Irrigated with Contaminated Water. *Environ. Sci. Technol.* 44, 6157-6161.

Wu, X., Ernst, F., Conkle, J.L. and Gan, J., 2013. Comparative uptake and translocation of pharmaceutical and personal care products (PPCPs) by common vegetables. *Environ. Int.* 60, 15-22.

Wu, X., Fu, Q. and Gan, J., 2016. Metabolism of pharmaceutical and personal care products by carrot cell cultures. *Environ. Pollut.* 211, 141-147.

Wu, X.Q., Conkle, J.L. and Gan, J., 2012b. Multi-residue determination of pharmaceutical and personal care products in vegetables. *J. Chromatogr.* 1254, 78-86.

Yang, Z., Hou, J.-J., Qi, P., Yang, M., Yan, B.-P., Bi, Q.-R., Feng, R.-H., Yang, W.-Z., Wu, W.-Y. and Guo, D.-A., 2016. Colon-derived uremic biomarkers induced by the acute toxicity of *Kansui radix*: A metabolomics study of rat plasma and intestinal contents by UPLC-QTOF-MSE. *J. Chromatogr. B* 1026, 193-203.

Zhang, H., Wang, Y., Zhu, H., Fei, Z. and Cao, J., 2017. Binding mechanism of triclocarban with human serum albumin: Effect on the conformation and activity of the model transport protein. *J. Mol. Liq.* 247, 281-288.

CHAPTER 4.

UPTAKE AND METABOLISM OF SULFONAMIDES BY *ARABIDOPSIS THALIANA*

4.1. Introduction

Accumulation of antimicrobials in agricultural soils poses a potential risk to agroecosystems and human health (Stein, 2011). Compared to other antimicrobials, sulfonamides are highly mobile in soils (Pan and Chu, 2017, Spielmeier et al., 2017, Wei et al., 2016). For example, residual concentrations of sulfamethoxazole at 40–60 cm beneath the surface of manure-amended soils was 1692 $\mu\text{g}/\text{kg}$, which exceeds the minimum inhibitory concentrations of sulfonamides for *Escherichia coli* (Wei et al., 2016). Sulfonamides were also detected in groundwater below livestock fields (Spielmeier et al., 2017). Microbial degradation of sulfonamides has been observed, with reported half-lives of 18 to 57 days in soils (Accinelli et al., 2007, Pan and Chu, 2016). Despite their mobility and degradability, sulfonamides persist in agricultural soils for months; for example, sulfamethazine was detected at 10.4 $\mu\text{g}/\text{kg}$ in soils one year after manure application (Aust et al., 2008, Stoob et al., 2007).

Many crops, including carrots, lettuce, cucumbers, tomatoes, and corn, uptake and accumulate sulfonamides within edible tissues (Ahmed et al., 2015, Boxall et al., 2006, Dolliver et al., 2007, Franklin et al., 2016, Hu et al., 2010, Li et al., 2013, Tanoue et al., 2012). In general, plant uptake of organic xenobiotics depends on their physiochemical properties, especially hydrophobicity (as measured by octanol-water partitioning coefficient or K_{ow}) and ionization (as determined by pK_a). Sulfonamides are more readily taken up, translocated, and accumulated by crops than other antimicrobials. Because of their relatively low hydrophobicity ($\log K_{ow} < 2$) and weak sorption to soil particles, sulfonamides readily diffuse into root cells and, because of their neutral charge in the xylem, sulfonamides translocate into aboveground tissues during transpiration (Briggs et al., 1982, Briggs et al., 1987, Burken and Schnoor, 1998). Ion trapping of the sulfonamides inside the cells ($\text{pH } 7\text{--}7.5$) is also expected, leading to their accumulation in plant

tissues (Miller et al., 2016). Once inside plant cells, organic xenobiotics are detoxified through sequential transformation, conjugation, and sequestration reactions (Sandermann, 1992), in which conjugation with amino acids and glycosides represents the most common pathways (Fu et al., 2017a, Macherius et al., 2012, Riemenschneider et al., 2017). As a result, studies that only measure the unaltered parent compounds in plant tissues may substantially underestimate total exposure to antimicrobials through crops. For example, following exposure of pepper plants to ^{14}C -triclocarban, unaltered triclocarban accounted for <4.4% of all triclocarban species in pepper fruits after 12 weeks (Huynh et al., 2018). Likewise, plant accumulation of benzotriazole and 2-mercaptobenzothiazole by *A. thaliana* was transitory, with less than 1% of the unaltered parent present in the plant tissues (LeFevre et al., 2015, LeFevre et al., 2016). Importantly, benzotriazole metabolism has been found to depend on plant species and parts (LeFevre et al., 2017).

Due to negligible concentrations of parent antimicrobials in plant tissues, it is commonly concluded that antimicrobials represent a *de minimis* risk to human health through consumption of the contaminated food crops (Prosser and Sibley, 2015). However, the potential role of phytometabolites of antimicrobials is often overlooked. During gastric and intestinal digestion, plant tissues encounter low-pH fluids and enzymes that can convert conjugated forms of xenobiotics back into the parent xenobiotic. For example, complete degradation of octyl- β -D-glucopyranoside and polydatin (glycosylated resveratrol) occurred within 30 min to 1 h, in an *in vitro* Rumen Stimulation System (Birk et al., 2018). Consequently, understanding phytometabolism is essential to comprehensive assessments of human exposure to antimicrobials through food.

In this context, the present study investigated phytometabolism of two sulfonamides that are commonly used in human and veterinary medicine, sulfamethoxazole (SMX) and

sulfamethazine (SMT), in the model plant *Arabidopsis thaliana*. Untargeted metabolomics using high resolution mass-spectral information, coupled with ^{14}C -labeled chemicals studies, was used to identify novel metabolites of SMX and SMT, and quantify the fate of SMX and SMT in plant tissues.

4.2. Materials and Methods

4.2.1. Chemicals

^{14}C -SMX (77 mCi/mmol, 98% purity) and ^{14}C -SMT (80 mCi/mmol, 98% purity) were obtained from American Radiolabeled Chemicals (St. Louis, MO). Unlabeled SMX (>98% purity) was purchased from Tokyo Chemical Industry (Portland, OR). Unlabeled SMT (>99% purity), 2-amino-4,6-dimethylpyrimidine (95% purity), formic acid, and MS grade acetonitrile were purchased from Sigma-Aldrich (St. Louis, MO). N^4 -acetyl SMT and desamino SMT were purchased from AKos GmbH (Baden-Wurttemberg, Germany). Other chemicals (ACS grade) were purchased from VWR, Inc. (Chicago, IL). Formic acid and MS grade acetonitrile were purchased from Sigma-Aldrich (St. Louis, MO).

4.2.2. Preparation of *Arabidopsis thaliana* seeds and culture media

A. thaliana seeds (wild-type quick plantTM) were purchased from VWR, Inc. (Chicago, IL). Seed surface sterilization followed (LeFevre et al., 2016). Sterilization solution was freshly prepared each use by adding 2.0 mL of bleach (8.25% sodium hypochlorite, Clorox) and 100 μl of Tween 20 surfactant (BioRad Laboratories Inc.) into 8.0 mL of autoclaved water and mixed well. Aliquot of 1.0 mL of the sterilization solution was added to a 1.5 mL microcentrifuge tube containing approximately 150 seeds. The tube was slowly pipetted for 5 minutes. The supernatant was removed and 1 mL of autoclaved water was added and then removed to wash the seeds from the sterilization solution. The washing step was repeated for five times. The seeds were then

distributed into the Magenta boxes (GA-7, Magenta Corp., Lockport, IL) containing 25 mL of sterilized culture media and stratified at 4°C for 3 days before transferred to a growth chamber.

Half-strength Murashige and Skoog (0.5X MS) solution was used as the culture media. Per 1 L of Milli-Q water, 2.22 g of MS basal medium (Sigma-Aldrich, St. Louis, MO), 0.5 g of MES buffer (Sigma-Aldrich), and 5 g of sucrose (J. T. Baker, Center Valley, PA) were added. The media pH was adjusted to 5.7 using 1M KOH solution. Finally, the culture media was filter sterilized using a 0.22 µm PES membrane (Sigma-Aldrich).

All procedures for seed sterilization and culture media preparation were conducted in a laminar flow biological safety hood, and 70% ethanol spray solution was used to sterilize the working area.

4.2.3. Plant exposure to ¹⁴C-SMX and unlabeled SMX

All experiments were conducted under sterile conditions. Two-week old, sterile *A. thaliana* plants were exposed to ¹⁴C-SMX and unlabeled-SMX in separate trials. For ¹⁴C-SMX trials, plants were maintained in 75 mL of 0.5X MS media (pH 5.7) containing 0.05 µCi/mL (1.1×10^5 dpm/mL) ¹⁴C-SMX in Magenta boxes. For unlabeled-SMX trials, plants were grown in 75 mL of 0.5X MS media (pH 5.7) containing 3 µg/mL SMX. Controls included: (1) plant controls without SMX, (2) media controls with SMX (3 µg/mL), exposed to light, and (3) media controls with SMX (3 µg/mL), not exposed to light. Dark controls were wrapped in aluminum foil. Control treatments were performed in triplicate. At each sampling interval (1, 2, 4, 7, and 10 days), triplicate boxes of unlabeled-SMX and duplicate boxes of ¹⁴C-SMX exposure, including plants and culture media, were harvested. Plant tissues were ground to fine powder in liquid nitrogen. Media samples were preserved from bacterial degradation by adding 0.75 mL of 0.1 g/mL sodium azide. All samples were stored at -20°C until analysis.

4.2.4. Plant exposure to ¹⁴C-SMT and unlabeled SMT

In this study, whole-plant exposure of *A. thaliana* to ¹⁴C-SMT was carried out to facilitate the detection and quantification of SMT metabolites and their sequestration in plant tissues that would be difficult to measure otherwise (Fu et al., 2017a). Two-week old, sterile *A. thaliana* plants were exposed to 0.05 µCi/mL (1.1×10^5 dpm/mL or 0.17 µg/mL) of ¹⁴C-SMT in half-strength Murashige and Skoog (0.5X MS) media in Magenta boxes for 2, 4, 6, 8 and 10 days. Separately, plants were also exposed to SMT at a nominal concentration of 3 µg/mL in 0.5X MS media for 1, 2 and 4 days. The use of relatively high concentrations of unlabeled SMT was to facilitate detection of metabolite candidates. Boxes containing plants not exposed to SMT and media with only SMT served as controls. At each sampling point, two boxes were randomly sacrificed.

Assessments of root uptake and translocation of SMT by *A. thaliana* were conducted in glass vials (20 mL) with unlabeled SMT. A hole, drilled in the cap of each vial, was filled with 2 mL of autoclaved 0.5X MS media containing 0.8% agar. Three surface sterilized seeds were placed on this agar. The cap was placed onto a vial filled with 0.5X aqueous MS media. Vials were then placed in a sterilized secondary container to prevent environmental contamination. After storage at 4°C for 3 days (for stratification), the vials were transferred to the growth chamber. The seeds germinated on the agar in the first 3 or 4 days; subsequently, the roots penetrated the agar and grew into the media reservoir below.

Two weeks after germination, the caps and whole plants were transferred to new vials containing a nominal concentration of 0.3 µg/mL of unlabeled SMT in 0.5X MS media for 2, 4, 6, 8, 10, 14, and 21 days in the growth chamber. Nine vials were sacrificed at each time interval ($n = 3$ as materials from three randomly-selected vials were composited for each sample). Several controls were conducted in triplicate in parallel with experimental vials: (1) plants grown in media

without SMT, (2) “light controls” of media with SMT (and no plants) that were exposed to light and (3) “dark controls” of media with SMT (and no plants) that were wrapped in aluminum foil to prevent light exposure.

4.2.5. Sample preparation

4.2.5.1. Hydroponic media

For analysis of ^{14}C , aliquots of 0.2 mL of media were mixed with 10 mL of Hionic Fluor cocktail (PerkinElmer, MA) in 20 mL glass scintillation vials. For unlabeled-SMX, aliquots of 50–100 μL of media samples were mixed with 1:1 methanol:water with 0.1% formic acid to make the volume up to 1.0 mL, filtered through 0.2 μm PTFE membrane (13 mm, VWR) into 2 mL amber autosampler vials, and subjected to quantification by LC-MS/MS.

Additionally, media samples were concentrated by solid phase extraction (SPE) to facilitate detection of metabolites in the media following (Yang et al., 2005) with minor modifications. Briefly, 1.0 mL of 5% Na_2EDTA was added to a flask containing 50 mL media, 70 mL of Milli-Q water, and 30 mL of 0.1 M citric acid. The Magenta box was rinsed with 4 mL of methanol, which was added to the mixture. The pH of the mixture was approximately 2.3. SPE cartridges (Oasis HLB 6 cc, 150 mg sorbent, Waters) were preconditioned with 5 mL of methanol, 5 mL of 0.5 N HCl, and 5 mL of Milli-Q water. Samples were then passed through the cartridges under vacuum. The cartridges were then rinsed with 5 mL of Milli-Q water and dried under vacuum. Analytes were eluted using 5 mL of methanol, which was evaporated to dryness using nitrogen gas, reconstituted in 1 mL of methanol:water (1:1, 0.1% formic acid), and filtered through 0.2 μm PTFE membranes into 2 mL amber vials. Approximately 97% of the ^{14}C -radioactivity in media samples was recovered using these procedures.

4.2.5.2. Plant tissues

Plant tissues (approximately 0.5 g) were extracted with 10 mL of methanol with sonication for 15 min at room temperature and then centrifuged at 4,000 rpm for 15 min. The supernatant was then decanted and the extraction was repeated two more times. Extracts were pooled, dried under nitrogen gas, reconstituted in 1 mL of methanol:water (1:1, 0.1% formic acid), and filtered through 0.2 μm PTFE membranes into 2 mL amber vials. Recoveries of ^{14}C -SMX and unlabeled-SMX, as determined by spiking ^{14}C -SMX and unlabeled-SMX standards into blank controls of plant tissues, were $88.9 \pm 4.0\%$ and $80.5 \pm 6.0\%$, respectively. Matrix-matched standard curves with seven concentrations of SMX (1.8–200 ng/mL) were freshly prepared prior to each run in order to minimize the potential matrix effects on quantification of SMX on the LC-MS system. Details of the recovery validation can be found in Supplementary Table Similarly, the recoveries of SMT in plant materials were $86.5 \pm 12.7\%$.

For quantification of the extractable ^{14}C -residues, aliquots of 50 μL of the reconstituted plant extracts from the ^{14}C -SMX/ ^{14}C -SMT samples were mixed with 10 mL of Hionic Fluor cocktail in 20 mL glass scintillation vials and measured for ^{14}C -radioactivity by a Beckman Liquid Scintillation Counter (LSC). Plant residues, after methanol extraction, were oven-dried at 50°C for 48 h and digested using a mixture of perchloric acid:nitric acid (1:1) (Thomson, 2012). The digestate was diluted to 2.0 mL with Milli-Q water. Aliquots of 50 μL were added to 10 mL of Hionic Fluor cocktail and measured for ^{14}C -radioactivity associated with non-extractable or bound residues.

4.2.6. Quantification of SMX and SMT by LC-MS/MS

Analysis was performed on a Shimadzu Prominence high performance liquid chromatography (Columbia, MD) coupled with an Applied Biosystems Sciex 3200 triple

quadrupole mass spectrometer (Foster City, CA), applying electrospray ionization (ESI) positive in multiple reaction monitoring (MRM) mode. Chromatographic separation was performed at room temperature on an Ultra biphenyl column (5 μ m, 50 x 2.1 mm, Restek). Water and acetonitrile, both containing 0.1% formic acid, were used as the mobile phase A and B, respectively. The gradient program was: 0–5.5 min: 98% B; 6.5 min: 98% B; 7.0 min: 5% B; and 10.0 min: 5% B. The flow rate was 0.3 mL/min and the injection volume was 10 μ L. Additional settings were: IonSpray voltage 5500 V at 600°C, curtain gas pressure 25 psi, collision gas pressure 6 psi, and ion source gas pressure 60 psi. For SMX, the MRM transitions m/z 254 \rightarrow m/z 156 was used for quantification and m/z 254 \rightarrow m/z 92 were used for confirmation, respectively. For SMT, the MRM transitions m/z 279 \rightarrow m/z 186 was used for quantification and m/z 279 \rightarrow m/z 156 were used for confirmation, respectively.

4.2.7. Metabolite candidates screening by UPLC-QTOF-MS^E and data processing

Media and plant extracts were analyzed on an Acquity Ultra Performance Liquid Chromatography (UPLC) system coupled with a Xevo G2-XS QTOF mass spectrometer (Waters, Milford, MA) using a data-independent method acquiring data under both non-fragmenting and fragmenting conditions in a single run. Chromatographic separation was achieved using an Acquity BEH C18 column (100 \times 2.1 mm, 1.7 μ m) at a flow rate of 0.3 mL/min and temperature of 40°C. The mobile phases consisted of (A) Milli-Q water and (B) acetonitrile, both containing 0.1% formic acid. The elution gradient was: 0 – 1 min, 5% B; 11 - 13 min, 98% B; and 13.1 - 15 min, 5% B. Analyses were carried out with an ESI source operated in positive mode within a mass range of 50–1500 m/z . Capillary voltage was 3.0 kV and sample cone voltage was 35 V. The MS source and desolvation temperatures were set at 100°C and 350°C, respectively. Desolvation gas flow was 600 L/h and cone gas flow was 25 L/h. The lock mass spray for accurate m/z

measurement used a solution containing 0.1 ng/ μ L of leucine enkephalin (m/z 556.2771 in positive ion mode). Data was collected in centroid mode with two scan functions using MS^E acquisition: function 1 with no collision energy and function 2 with a collision energy ramp of 20–80 eV over the 0.2 s scan.

Centroided MS raw data obtained under low collision energy were processed using Waters Progenesis QI 2.1 for alignment, normalization and peak picking. Multivariate statistical analysis was performed using EZinfo 3.0 software (Umetrics, Malmo, Sweden) for principal component analysis (PCA) and orthogonal projection to latent structures-discriminant analysis (OPLS-DA). The S-plots obtained from the OPLS-DA models were used to determine m/z variables (i.e., unique combinations of retention time and m/z ratios) that significantly contributed to the differences between the controls and SMX/SMT-exposed systems. Metabolite candidates were primarily selected from the m/z variables scattered on the top right corner of the S-plots with $p(\text{corr}) \geq 0.5$ (indicating an increase in intensity of these m/z variables in SMX/SMT-exposed groups compared to control groups). The resulting dataset included both metabolites of SMX and SMT, and plant metabolites or defense chemicals that increased in concentration due to antimicrobial exposure. As plant metabolites were also presumably present in plant tissues in the controls (albeit at lower intensity), the m/z variables that were present in the controls were eliminated as metabolite candidates. An output table was generated to include paired retention times- m/z , isotope distribution, and raw and normalized peak intensities for individual samples. MassLynx 4.1 software (Waters) was used to generate chemical formulas for metabolite candidates with the mass accuracy error ≤ 5 ppm. Proposed structures were confirmed by characteristic fragment ions in high collision energy mass spectra.

4.2.8. Radioactivity analysis

¹⁴C-radioactivity was measured on a Beckman LS 6500 Liquid Scintillation Counter (LSC) (Fullerton, CA) with a background of approximately 30 dpm. The LSC data were corrected for the background by subtracting the dpm value of a blank from those of the samples.

In addition, the ¹⁴C-labeled samples were also analyzed on a Shimadzu LC-MS 2010 EV coupled with an on-line radioactivity detector β -RAM (model 5, LabLogic, Brandon, FL), which facilitates simultaneous identification of the ¹⁴C-metabolite candidates and their molecular ions (m/z). Separation was carried out on an Ultra Biphenyl (5 μ m, 250 x 4.6 mm, Restek) at a flow rate of 1.0 mL/min and temperature of 40°C with water and acetonitrile, both containing 0.1% formic acid, as mobile phases. The gradient program was: 0–1 min, 5% B; 3 min, 20% B; 15 min, 60% B; 17 min, 95% B; 20 min, 95% B; and 26 min, 5% B. The flow was diverted to both the β -RAM (0.8 mL/min) and MS operated in positive ESI (0.2 mL/min) using an adjustable splitter (LabLogic).

4.2.9. Statistical analysis

Data are presented as mean \pm standard error (SE). One-way ANOVA was performed using SPSS 25 (IBM Corp., Armonk, NY) to determine significant differences ($p < 0.05$). Concentrations of SMX and its metabolites in plant tissues were calculated based on fresh weight (fw). In this study, the water/moisture content in *A. thaliana* plants were approximately 97.5%.

4.3. Results and Discussion

4.3.1. Sulfamethoxazole (SMX)

4.3.1.1. Uptake of SMX by *A. thaliana*

The presence of *A. thaliana* plants significantly accelerated dissipation of both SMX and ¹⁴C-SMX from the media ($p < 0.001$, Supplementary Figure 4.1). SMX concentrations in the media

decreased from initially $2.88 \pm 0.01 \mu\text{g/mL}$ to $0.27 \pm 0.03 \mu\text{g/mL}$ after 10 days. In contrast, losses of SMX and ^{14}C -SMX in unplanted light and dark controls were insignificant. The estimated half-lives ($t_{1/2}$) for SMX and ^{14}C -SMX in the culture media with plants were 3.0 and 3.9 days, respectively, as calculated from fitting models (Supplementary Figure 4.2). Since dissipation of SMX and ^{14}C -SMX was negligible in the control media (Supplementary Figure 4.1), SMX losses in *Arabidopsis*-planted treatments were attributed to plant-mediated processes. However, accumulation of SMX and ^{14}C -SMX in *A. thaliana* tissues appeared to be transitory and did not account for the mass and ^{14}C -radioactivity dissipated from the culture media. Only 1.1% of the mass of SMX lost from the media was recovered as SMX in *A. thaliana* plant tissues. Therefore, the majority of the SMX lost from the media was expected to exist as metabolites.

4.3.1.2. Distribution of the ^{14}C -radioactivity in the *Arabidopsis*-planted treatments

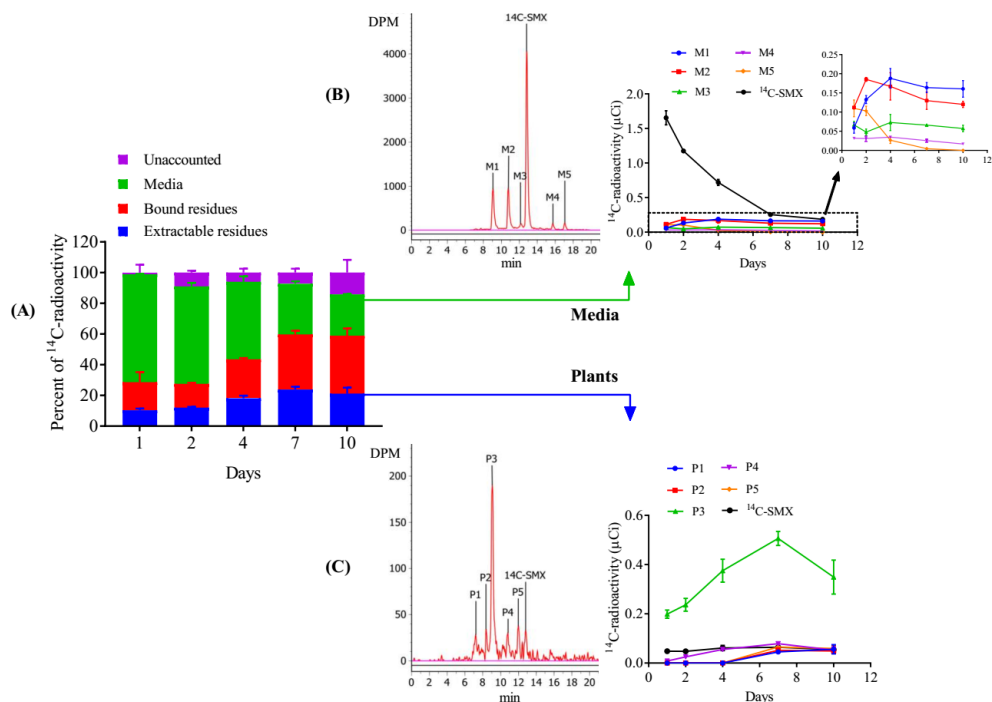


Figure 4. 1. Distribution of the applied ^{14}C -radioactivity in *Arabidopsis* treatments (A), and temporal variation in concentrations of ^{14}C -SMX and its major metabolites detected in media and plant extracts using a radioactivity detector β -RAM (B and C). “M” represents media and “P” represents plant samples, respectively. Error bars represent standard error of duplicates.

Figure 4.1A depicts the distribution of ^{14}C -radioactivity in the *Arabidopsis* systems. In plant tissues, ^{14}C -radioactivity was present as both extractable and bound residues throughout the exposure. Extractable residues, which included ^{14}C -SMX and its extractable metabolites, accounted for $10.4 \pm 1.1 - 23.9 \pm 1.8\%$ of the initially spiked ^{14}C , while bound residues accounted for $15.5 \pm 0.7 - 37.8 \pm 4.8\%$. Additionally, $27.0 \pm 0.3\%$ of the initially spiked ^{14}C still remained in the media, while $14.2 \pm 8.4\%$ of the initially spiked ^{14}C was lost (unaccounted fractions) from the systems after 10 days. The acid digestion method used in this study to quantify the ^{14}C -bound residues potentially resulted in loss of the ^{14}C -label as ^{14}C - CO_2 (Thomson, 2012). Acid digestion using ^{14}C -spiked-blank controls revealed that the ^{14}C lost during digestion were 11.2 ± 3.4 and $10.4 \pm 1.2\%$ of the initially spiked ^{14}C -radioactivity for plant root and shoot residues, respectively. Consequently, the unaccounted fractions in this study most likely consisted of the ^{14}C that had been converted to ^{14}C - CO_2 during solubilization.

4.3.1.3. Multivariate statistical analysis of the SMX dataset

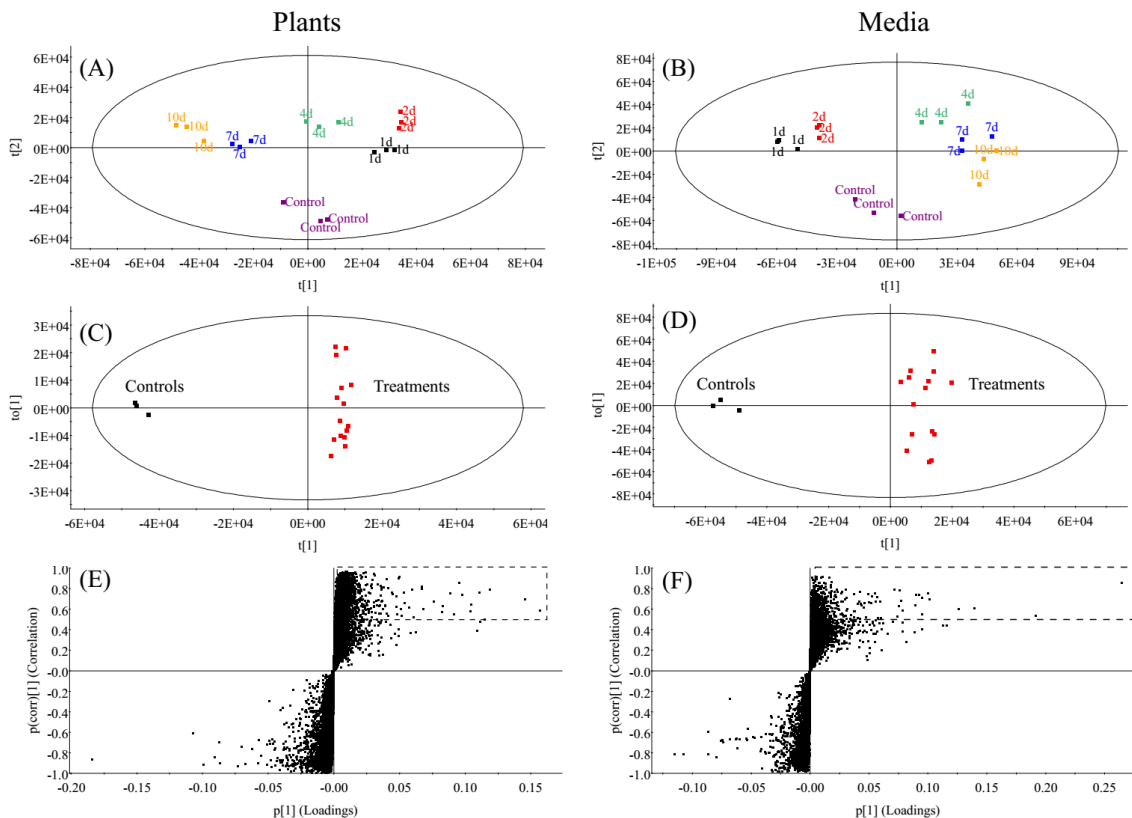


Figure 4. 2. PCA score plots (A and B), OPLS-DA score plots (C and D) and S-plots (E and F) derived from the UPLC-QTOF-MS^E datasets of the control and SMX-exposed plants and media samples (1, 2, 4, 7, and 10 days). The ellipses represent Hotelling's T^2 with 95% confidence. The dashed rectangles on the S-plots include m/z variables that significantly contribute to the difference between the control and SMX-exposed extracts ($p(\text{corr}) \geq 0.5$).

In order to study the metabolic fate of SMX in *A. thaliana* plant, metabolic profiling of SMX-exposed plants was performed and compared to that of control plants through UPLC-QTOF-MS^E platform and multivariate statistical analysis of the acquired dataset. Additionally, plant excretion of the metabolites into the culture media has also been observed in recent studies (LeFevre et al., 2015, LeFevre et al., 2016, Taguchi et al., 2010). Therefore, the planted-media at different time intervals were also subjected to the same analyses to investigate the correlation between intracellular metabolites profiles and those excreted into the media. PCA, an unsupervised model, was initially applied to reduce the dimensionality of the data and visualize clustering

between control and SMX-exposed groups, as well as temporal distribution within the SMX-exposed groups. The PCA models were built with four principal components (PCs), which had explanation ($R^2X(cum)$) and predictability ($Q^2(cum)$) values of 0.82 and 0.68 for plant samples and 0.78 and 0.57 for media samples, respectively, indicating the robust mathematical models with a reliable predictive accuracy (Finnegan et al., 2016). The score plots of the first two PCs are presented in Figure 4.2A and Figure 4.2B, with each point in the score plots represents an individual sample. The distribution of samples indicates the differences or similarities of their metabolic profiles: samples near each other in the plot are similar while samples far away from each other are dissimilar. Figure 4.2A suggests that SMX induced metabolic perturbations in *A. thaliana*, as evident by an obvious separation between the control and treated plants. Additionally, variation in metabolic profiles of the SMX-exposed plants were also found to be time-dependent. For instance, the samples collected after 1 and 2 days were distinctively separated from those of 7 and 10 days (Figure 4.2A), suggesting that they had significantly different metabolic profiles. PCA analysis of media samples revealed a similar clustering trend as observed for plant samples; however, the SMX-exposed samples collected at different time intervals were interestingly separated in a reverse order on the PC1 (Figure 4.2B). Subsequently, supervised OPLS-DA analysis was performed to identify potential biomarkers responsible for differentiating the control and SMX-exposed samples. All the acquired datasets were scaled to Pareto variation prior to model fitting. The OPLS-DA score plots are presented in Figure 4.2C and Figure 4.2D, with the explanation ($R^2Y(cum)$) and predictability ($Q^2(cum)$) were 0.99 and 0.92 for plant samples, and were 0.96 and 0.88 for media samples, respectively. The values of $R^2Y(cum)$ and $Q^2(cum)$ suggested that the models were well established and had high predictability, resulted in clear separation between control and SMX-exposed groups (1, 2, 4, 7, and 10 days) in the score plots.

The S-plot, which is a covariance-correlation-based analysis, was then used to explore the m/z variables which significantly contribute to the observed differences. In the S-plot, the points represent all of the variables in the dataset with the x-axis (p_1) represents the magnitude of the first component while the y-axis ($p(\text{corr})_1$) represents the reliability of the first component for classification (Yang et al., 2016). The intensity of variables plotted in the lower quadrant of the S-plot decreased in the SMX-exposed groups compared to the controls, while those plotted in the upper right quadrant indicate an increase in ion intensity of these variables in the SMX-exposed groups. Differentiation within the S-plot is due to concentration differences and variables with a higher intensity yield a better separation from the background ions (Macherius et al., 2014). Accordingly, in this study, the metabolite candidates were primarily selected from the variables scattered in the upper right quadrant of the S-plot with $p(\text{corr}) > 0.5$ (Figure 4.2E and Figure 4.2F), imported back into Progenesis QI platform for identification of the potential metabolites. Xenobiotic exposure resulted in metabolic perturbations in *A. thaliana* plant. Accordingly, the extracted dataset likely included m/z variables that represent both SMX metabolites and *Arabidopsis* secondary metabolites enhanced by SMX exposure. Nevertheless, the secondary metabolites were presumably to be produced in plant tissues at different levels in both control and SMX-exposed groups. In this study, SMX metabolite candidates were; therefore, identified based on their unique presence in SMX-exposed samples and absence in the controls.

4.3.1.4. Identification of the unlabeled metabolites using high-resolution MS

The MS^E mass spectra of the parent SMX are showed in Supplementary Figure 4.4. Under the analytical conditions applied to the UPLC-QTOF- MS^E , SMX eluted at 4.62 min with the molecular ion $[\text{M}+\text{H}]^+$ of m/z 254.0598, and exhibited fragmentation patterns characteristic of sulfonamide antimicrobials (Majewsky et al., 2015). Three common characteristic product ions

originating from the 4-aminobenzenesulfonamide moiety (m/z 92.0492, 108.0441, and 156.0108) and additional product ion characteristic for SMX (m/z 99.0558) were observed in high collision energy mode. Based on accurate mass (m/z variables) obtained from the multivariate statistical analysis platform, we proposed several potential SMX metabolites and subsequently confirmed their chemical structures using characteristic fragment ions (Table 4.1).

The variable m/z 416.1113 (TP416), which significantly contributed to the differentiation between the extracts of SMX-exposed and control plants, eluted at a retention time of 3.64 min. The proposed elemental composition for this mass is $C_{16}H_{21}N_3O_8S$ with an error of 2.2 ppm. Fragmentation in high collision energy mode revealed a SMX fragment (m/z 254.0591), indicating the loss of the anhydroglucose moiety (162.05 Da), and SMX-characteristic fragments (Supplementary Figure 4.5). Additionally, the m/z 318.0638 acquired during fragmentation suggested the formation of N^4 -glycosyl-SMX, instead of N^1 -glycosyl-SMX (Majewsky et al., 2015). A second metabolite eluted at a retention time of 2.79 min with the accurate mass of m/z 578.1651 (TP578), corresponding to $C_{22}H_{31}N_3O_{13}S$ with an error of 0.2 ppm. Loss of two anhydroglucose moieties during high collision energy fragmentation, revealing SMX (m/z 254.0594) and its three signature fragments, was observed for TP578 (Supplementary Figure 4.6). Consequently, TP578 was determined to be a N^4 -glycosyl glycoside conjugate of SMX, which likely formed from O-glycosidation of N^4 -glycosyl SMX (TP416). Neutral loss of the anhydroglucose moieties was also observed for both TP416 and TP578 in the low collision energy mode, which could be attributed to in-source fragmentation occurring at the intermediate pressure region between the atmospheric pressure ion source and the vacuum chamber of a mass spectrometer (Holder et al., 1999, Justesen, 2000, LeFevre et al., 2016, Xu et al., 2015).

The proposed formula for metabolite TP429 (m/z 429.1087, RT = 4.27 min) was $C_{17}H_{16}N_8O_4S$ with an error of 0.2 ppm. In high collision energy mode, TP429 produced fragments at m/z 176.0574, 267.0994, 283.0932, 331.0592, and 349.0716, which have been previously identified as characteristic fragments of a pterin SMX conjugate (Achermann et al., 2018) (Supplementary Figure 4.7). Similarly, the accurate mass of TP404 (m/z 404.0906, RT = 5.86 min) allowed the prediction of the chemical formula $C_{18}H_{17}N_3O_6S$ with an error of 0.7 ppm. This metabolite was less polar than the parent SMX, as indicated by its longer retention time. Based on the fragments acquired in the high collision energy mode (Supplementary Figure 4.8), we proposed an addition of a methylsalicylate (MeSA) moiety to the parent SMX molecule. The signal at m/z 406.1053 had the same retention time and a mass 2.01 Da heavier than TP404, indicating addition of two hydrogen atoms to TP404, most likely at the carbonyl group of the MeSA moiety (Supplementary Figure 4.8). The metabolites TP566/568 (m/z 566.1443 and m/z 568.1590) differed from TP404/406 by 162.05 Da were observed at RT = 4.79 min, suggesting that TP404/406 were subsequently conjugated with a glucose moiety. Fragmentations of TP566/568 in the high collision energy mode released the intact MeSA-SMX (m/z 404.0906 and m/z 406.1065, respectively) and the characteristic fragments described above for TP404/406 (Supplementary Figure 4.9).

A signal at m/z 288.0202 and its ($m + 2$) chlorine isotopic ion m/z 290.0178 ($\Delta m/z = 1.9976$ u, relative intensities of ($m + 2$)/ $m \sim 30\%$) was detected at RT = 5.68 min, suggesting a monochlorinated metabolite of SMX (TP288). The proposed chemical formula for TP288 is $C_{10}H_{10}N_3O_3SCl$ with an error of 0.7 ppm. Fragmentation of TP288 revealed the fragment of the parent SMX m/z 254.0598 and its characteristic fragments m/z 92.0524, m/z 108.0459, and m/z 156.0125 (Supplementary Figure 4.10). This chlorinated product was also detected in the abiotic

controls, indicating that it was most likely an abiotic product of SMX. Electrophilic substitution of free chlorine in the MS media (approximately 106 mg/L, supplemented as macronutrient CaCl₂) to the SMX molecule likely led to the formation of monochlorinated SMX. Although the exact chlorinated positions could not be unambiguously assigned using the acquired fragmentation patterns, TP288 most likely represented N⁴-chlorinated SMX, which is the most abundant chlorinated product of SMX in the presence of free available chlorine (FAC) (Dodd and Huang, 2004, Gao et al., 2014). Ring chlorinated SMX molecules have only previously appeared to be present at very low yields (Dodd and Huang, 2004).

Other potential minor metabolites of SMX were also proposed based on their observed accurate mass, with an error of ≤ 5 ppm compared to the corresponding calculated accurate mass, including formyl-, hydroxyl-, acetyl-, and desamino-SMX (Table 4.1). However, no characteristic fragments were observed in the high collision energy mode, likely due to low abundance of precursor ions. These minor metabolites were therefore confirmed to level 4 according to the framework proposed by (Schymanski et al., 2014). Finally, TP280 (m/z 280.0509, RT = 6.47 min) corresponded to a predicted formula C₁₀H₁₀N₅O₃S with a mass error of 0.4 ppm. The metabolite TP280 was exclusively detected in the media and absent in plant extracts, indicating limited uptake or quick metabolism of this metabolite by *A. thaliana* plant. Since its fragments obtained in the high collision energy mode were not adequately explained, TP280 was assigned to a level 5, or “unknown structure”, in this study (Schymanski et al., 2014).

4.3.1.5. Identification of the ¹⁴C-labeled metabolites on the LC- β -RAM-MS

Five major ¹⁴C-SMX-metabolites were detected in the plant extracts by LC- β -RAM-MS (Figure 4.1C), with retention times (RTs) of 7.22 min (P1), 8.35 min (P2), 9.05 min (P3), 10.85 min (P4), and 11.97 min (P5). These five ¹⁴C-metabolites were more polar than the parent

compound, as indicated by earlier retention times. P3 was the most abundant metabolite in the plant tissues, accounting for 39.2–50.7% of the extractable ^{14}C -radioactivity during the exposure period. Five major ^{14}C -metabolites were also detected in the culture media (Figure 1B), with RTs of 9.05 min (M1), 10.77 min (M2), 12.13 min (M3), 15.75 min (M4), and 17.07 min (M5). Based on the retention times, metabolites M1, M2, and M3 were more polar, while M4 and M5 were less polar than the parent ^{14}C -SMX. M1 and M2 were the most abundant ^{14}C -metabolites in the media, accounting for 14.2 ± 1.8 and $10.7 \pm 0.8\%$ of the total radioactivity after 10 days of exposure. The radioactivity of ^{14}C -SMX and its five ^{14}C -metabolites in plant extracts and media; however, accounted for only 59.2 ± 3.8 to $81.2 \pm 0.8\%$ and 46.6 ± 1.4 to $69.0 \pm 2.6\%$ of the total ^{14}C -radioactivity measured by LSC during the course of exposure, respectively, indicating the presence of other metabolized forms that were not detectable on the LC- β -RAM. In this study, the presence of ^{14}C -SMX metabolites in the media were potentially attributed to reactions with exudates and/or excretion of the conjugated metabolites by *A. thaliana* following plant uptake and metabolism. For example, P3 and M1 eluted at the same retention time (RT = 9.05 min), suggesting that they were the same metabolite. Excretion of conjugated metabolites by *A. thaliana*, as a defense against phytotoxicity of xenobiotics (Khan et al., 2016), has been reported in several studies on uptake and metabolism of xenobiotics (LeFevre et al., 2015, LeFevre et al., 2016).

A targeted search of the LC- β -RAM-MS data was conducted for the molecular ions associated with the metabolites previously identified using high resolution MS. The suspected signals were then aligned with those of the control samples, and subsequently selected for matching with the β -RAM peaks if they uniquely appeared in the SMX-exposed samples (Supplementary Figure 4.11). In the plant extracts (Figure 4.1B), P3 (RT = 9.05 min) dominated the metabolite pool size during the exposure time, with a molecular ion $[\text{M} + \text{H}]^+$ corresponding

to m/z 416, suggesting that P3 was N⁴-glycosyl-SMX. N⁴-glycosyl-SMX underwent intensive in-source fragmentation during MS analysis, as presented in the Supplementary Figure S11 and Supplementary Figure S12. For example, the extracted ion chromatograms of both plant extracts and media at m/z 254 (parent SMX) on the LC- β -RAM-MS revealed two peaks at RT = 9.05 min and 12.83 min, respectively (Supplementary Figure S11). While the second peak corresponded to the parent SMX, the first peak was the SMX aglycone released from the N⁴-glycosyl-SMX due to loss of an anhydroglucose moiety. Similar fragmentation was observed for N⁴-glycosyl-SMX in the UPLC-QTOF-MS^E data (Supplementary Figures 12A-B) and LC-MS/MS (in MRM mode, Supplementary Figures 12C-D). The metabolite P4 (RT = 10.85 min) was found to have a similar retention time and signal (m/z 429) as the pterin-SMX. For other metabolites (i.e., P1, P2, and P5), the targeted search did not allow for an explicit confirmation of their chemical structures, most likely due to low abundance. In the media (Supplementary Figure 4.11B), M1 (RT = 9.05 min) and M2 (RT = 10.77 min) were the most abundant metabolites. Their molecular ions [M + H]⁺ corresponded to the signals at m/z 416 and m/z 429, respectively, suggesting that M1 was the N⁴-glycosyl-SMX and M2 was the pterin-SMX. The metabolites M4 (RT = 15.75 min) and M5 (RT = 17.07 min) corresponded to the signals at m/z 404/406 and m/z 280, respectively. While M4 was tentatively identified as the methylsalicylate-SMX, the m/z of M5 was consistent with TP280, the “unknown” metabolite with the predicted formula C₁₀H₁₀N₅O₃S. The chemical structure of M3 could not be assigned using the targeted m/z . N⁴-glycosyl glycoside SMX (m/z 578) was not consistent with any of the ¹⁴C-peaks in either plant extracts and media.

4.3.1.6. Major transformation pathways of SMX in *A. thaliana* and implications to human health

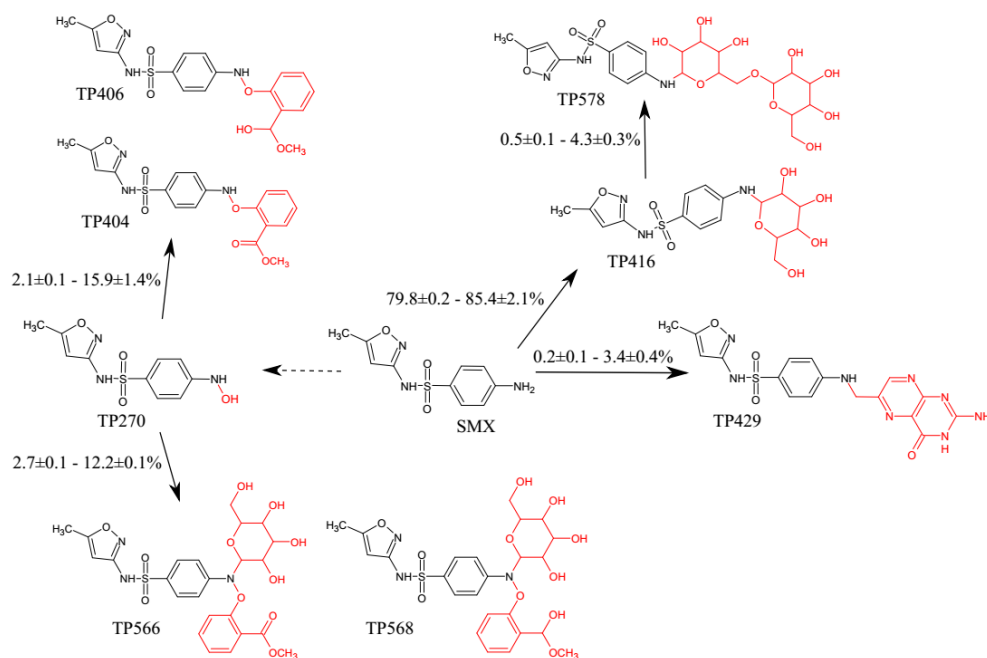


Figure 4. 3. Proposed transformation pathways of SMX in *A. thaliana* plant. The occurrence of N⁴-OH SMX (TP270) was not unequivocally confirmed due to lack of adequate mass-spectral information (dashed arrow). The percentage represents the fractions of each metabolite observed over 10 days of exposure.

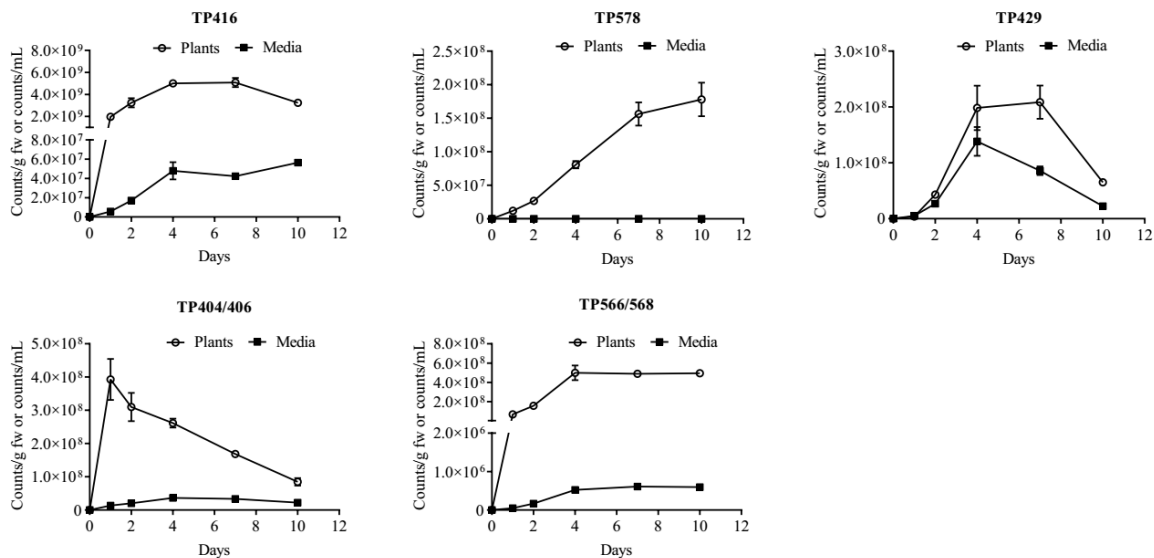


Figure 4. 4. Temporal variation of the major metabolites of SMX in plant tissues and culture media over 10 days of exposure. Error bars represent standard error of triplicates. For some points, the error bars were shorter than the height of the symbol and were not displayed on graphs.

Based on the metabolites identified in this study, the metabolic pathway of SMX in *A. thaliana* is proposed in Figure 4.3. Since reference standards for these metabolites are not available, peak areas obtained from the UPLC-QTOF-MS^E were used for relative quantification of their concentrations. Figure 4.4 presents the temporal variation of the major metabolites of SMX in *A. thaliana* plant and culture media over 10 days of exposure. Upon exposure, *A. thaliana* plant largely transformed SMX through N-glycosylation, in which N⁴-glycosyl SMX (TP416) accounted for up to 79.8–85.4% of the identified metabolites during exposure time. Conjugation with glucose is commonly observed in plant metabolism of organic xenobiotics (LeFevre et al., 2015, LeFevre et al., 2016). The NH₂- group, which is part of the SMX molecule, is known to trigger detoxification *via* glycosyltransferases, resulting in direct conjugation of xenobiotics with sugar molecule(s) in phase-II reactions without addition of other functional groups (Schröder, 2007). Direct N-glycosylation, as observed in this study, has previously been observed in *A. thaliana* and strawberries exposed to 2-mercaptobenzothiazole and benzotriazole (LeFevre et al., 2017, LeFevre et al., 2015, LeFevre et al., 2016). Both N⁴-glycosyl SMX (TP416) and N⁴-glycosyl-glycoside-SMX (TP578) were detected in plant tissues after only 1 day of exposure and their concentrations increased with the exposure time. However, N⁴-glycosyl SMX concentrations in plant tissues decreased after 7 days, suggesting further detoxification, likely through metabolism to N⁴-glycosyl-glycoside-SMX prior to cell wall sequestration (Sandermann, 1992) and/or excretion into the culture media. Plant concentrations of N⁴-glycosyl-glycoside-SMX increased for the duration of the experiment but were always 1-2 orders of magnitude lower than those of N⁴-glycosyl SMX. Following uptake and intracellular glycosylation of SMX, *A. thaliana* subsequently excreted a fraction of the glycosylated conjugate across the plasmatic membrane and cell wall, as evident by detection of N⁴-glycosyl SMX in the media. During the 10-day exposure,

approximately 0.3 – 0.7 μCi of ^{14}C -glycosyl-SMX was measured in the experimental systems; of this, approximately 22.8 – 36.1% was found in the media, indicating that exudation of N^4 -glycosyl-SMX was also a detoxification mechanism in plants, in addition to cellular sequestration. Conversely, N^4 -glycosyl-glycoside-SMX was exclusively detected in plant tissues. Excretion of glycosylated metabolites has been commonly observed in *A. thaliana* (Khan et al., 2016, LeFevre et al., 2015, LeFevre et al., 2016, Taguchi et al., 2010), likely representing a detoxifying mechanism for xenobiotic-exposed plants. Malonylation and vacuole storage following glycosylation has been widely reported as a major detoxification pathway for several organic xenobiotics in higher plants (Khan et al., 2016). However, in this study, no malonylated glycosides were detected.

The metabolites TP404/406, tentatively proposed as the methylsalicylate-SMX conjugates, accounted for up to $15.9 \pm 1.4\%$ of all identified metabolites only after 1 day of exposure and subsequently decreased to $2.1 \pm 0.1\%$ after 10 days of exposure (Figure 4.4). Conversely, the corresponding percentage of glycosylated methylsalicylate-SMX conjugates (TP566/568) increased from $2.7 \pm 0.1\%$ to $12.2 \pm 0.1\%$, respectively. N^4 -OH SMX potentially served as an intermediate for the conjugation reactions; however, the presence of N^4 -OH SMX could not be unequivocally confirmed in this study due to lack of adequate mass-spectral information. Salicylate is a phytohormone regulating plant responses to both biotic and abiotic stresses, as well as controlling plant growth and development (Thompson et al., 2017). In *A. thaliana*, total salicylate levels range from 0.25–1 $\mu\text{g/g}$ fw, mostly present as glycosylated and/or methylated forms (Rivas-San Vicente and Plasencia, 2011). The involvement of salicylate in *A. thaliana* responses to safeners (e.g. isoxadifen-ethyl and mefenpyr-diethyl) (Behringer et al., 2011) and alamethicin (Chen et al., 2003) has been documented in literature. Concentrations of

methylsalicylate-SMX peaked at 1 day and then decreased, while concentrations of the glycoside conjugate of methylsalicylate-SMX increased from days 1 – 4 and then plateaued, supporting the hypothesis that conjugation with methylsalicylate occurred rapidly upon exposure to SMX and was followed by glycosylation.

The pterin-SMX conjugate (TP429) accounted for approximately 0.2–3.4% of the metabolites identified in this study. Pterin-related metabolism, which is relevant to the mode of action of sulfonamides, have recently been reported to occur in microorganisms (Achermann et al., 2018) and freshwater phytoplankton (Stravs et al., 2017). As structural analogs of *p*-aminobenzoic acid (*p*ABA), sulfonamides act as competitive inhibitors of dihydropteroate synthase and consequently interfere with the folate biosynthesis (Stravs et al., 2017). Additionally, sulfonamides can also act as alternative substrates for dihydropteroate synthase, resulting in formation of sulfonamide-pterin conjugates that retain their antibacterial activity (Zhao et al., 2016). Although no visual effects of SMX on plant growth were observed in this study, formation of the pterin-SMX conjugate in *A. thaliana* plant tissues potentially impaired plant folate biosynthesis, leading to a reduction in the plant folate pool size (Zhang et al., 2012).

Uptake and metabolism of SMX by *A. thaliana* cells and higher plants have been reported in recent studies (Chen et al., 2017, Dudley et al., 2018). Although accumulation of the parent SMX was universal, conclusions as to its metabolic fate in plant tissues drastically differ. For instance, no metabolites of SMX were detected in Chinese cabbage and water spinach exposed to 100 µg/mL SMX after 5 days (Chen et al., 2017). Conversely, several phase I and phase II metabolites of SMX were observed in *A. thaliana* cells during a 4-day exposure, of which N⁴-acetyl-SMX was the major metabolite (Dudley et al., 2018). Similar metabolites were also detected in the intact cucumber seedlings, although at lower concentrations compared to those in the cell

culture trials (Dudley et al., 2018). In our current study with *A. thaliana* plants, N⁴-glycosyl-SMX accounted for more than 80% of the extractable metabolites, while the presence of N⁴-acetyl-SMX could not be unequivocally confirmed. A targeted search using accurate masses of the SMX metabolites reported previously (Dudley et al., 2018) was conducted; however, none of these metabolites were present in our plant extracts. One potential explanation is that the previous study had mass errors of the metabolite candidates ranging from 9.4-87.3 ppm, which exceeded our criteria of 5 ppm. Differences in plant species, exposure conditions, and sample preparation might also contribute to the discrepancies observed across studies. For example, phase III metabolism, which is time- and species-dependent, could have decreased the level of phase I and phase II metabolites below the limit of detection (Dudley et al., 2018), potentially explaining the non-detection of previously identified metabolites in this study.

The majority of SMX metabolites identified in this study still carry the intact structure of the parent SMX, with more than 80% of extractable metabolites being glycosylated SMX. Meanwhile, the parent SMX accounted for only 1.1% of all SMX species accumulated in the plant tissues. Consequently, these results raise a concern about the fate of these metabolites during human digestion of the contaminated food crops. In human, after ingestion, materials go through gastric and intestinal digestion, through which the metabolites, especially the glycosylated conjugates, are likely to be hydrolyzed (Sandermann, 1992) or are further transformed by the gut bacteria (Koppel et al., 2017). As a result, human exposure to antimicrobials through consumption of contaminated food crops may have been underestimated. To the best of our knowledge, the pterin-SMX conjugate, which accounted for approximately 3.4% of the extractable metabolites of SMX in *A. thaliana*, has been reported for the first time in this study. Despite of its relatively small proportions in the metabolite pool size, the role of pterin-SMX conjugate in plant folate

biosynthesis merit further studies. While folate is critical for several biological functions of the body, humans cannot synthesize folate and rely on foods (e.g. vegetables) for its supply (Ntaios, 2015). Depletion of folate in plants due to exposure to sulfonamide residuals in the environment may ultimately affect human intake of this vitamin through food chains. In addition to its vital roles for human health, folate is also indispensable for plant growth (e.g. nitrogen and carbon metabolism) and plant response to stress (Gorelova et al., 2017). An impaired folate metabolism in plants caused by sulfonamide antibiotics exposure will ultimately exert potential adverse impacts on plant productivity and stress tolerance.

In this study, the exclusive presence of the SMX-conjugated metabolites in the *A. thaliana*-planted media was attributed to plant excretion. Our findings contribute to a growing body of evidence suggesting that plant excretion of phase II conjugates may be an additional defense mechanism against the phytotoxicity of xenobiotics (Khan et al., 2016), along with phase III sequestration in the “green liver model” (Sandermann, 1992). For example, Taguchi et al. observed that *A. thaliana* excreted glucoside-conjugated 2-naphthol into the culture media (Taguchi et al., 2010). Similarly, glycosylated benzotriazoles were also detected in the hydroponic media when exposing *A. thaliana* to benzotriazoles (LeFevre et al., 2015). The fact that SMX metabolites (e.g. N⁴-acetyl-SMX) can be readily back-transformed to parent SMX in different environments (Achermann et al., 2018, Radke et al., 2009) raises the question of the environmental fate of the excreted metabolites, which also merits further research.

Table 4. 1. Mass-Spectral Information and Proposed Structures of the SMX-Transformation Products Identified by Waters Progenesis QI 2.1 and MassLynx 4.1 Software.

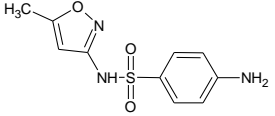
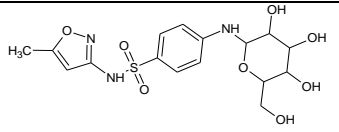
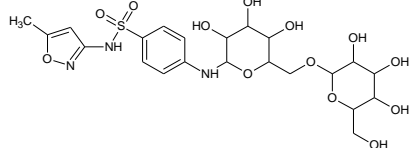
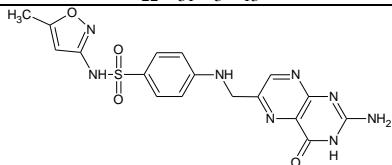
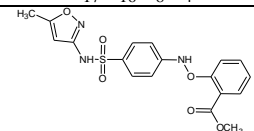
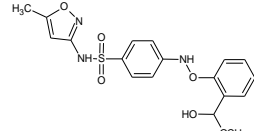
denotation	RT (min) ^a	calcd m/z^b	obsd m/z^c	error (ppm)	predicted formula and structure	fragments (m/z) ^d	level ^e
sulfamethoxazole (SMX)	4.62	254.0594	254.0598	1.6	 <chem>Cc1nc(O1)NS(=O)(=O)c2ccc(N)cc2</chem> $C_{10}H_{11}N_3O_3S$	92 108 156 99 161	1
N ⁴ -glycosyl-SMX (TP416)	3.64	416.1122	416.1113	2.2	 <chem>Cc1nc(O1)NS(=O)(=O)c2ccc(NC3OC(O)C(O)C(O)CO3)cc2</chem> $C_{16}H_{21}N_3O_8S$	92 108 156 254 318	2b
N ⁴ -glycosyl-glycoside-SMX (TP578)	2.79	578.1650	578.1651	0.2	 <chem>Cc1nc(O1)NS(=O)(=O)c2ccc(NC3OC(O)C(O)C(O)CO3)cc2OC4OC(O)C(O)C(O)CO4</chem> $C_{22}H_{31}N_3O_{13}S$	92 108 156 254 416	2b
pterin-SMX (TP429)	4.27	429.1088	429.1087	0.2	 <chem>Cc1nc(O1)NS(=O)(=O)c2ccc(NC3=NC4=NC(=O)N=C4N3)cc2</chem> $C_{17}H_{16}N_8O_4S$	176 267 283 331 349	2b
methylsalicylate-SMX (TP404, TP406)	5.86	404.0911 406.1067	404.0914 406.1053	0.7 3.4	 <chem>Cc1nc(O1)NS(=O)(=O)c2ccc(NC(=O)c3cc(O)ccc3OC)cc2</chem> $C_{18}H_{17}N_3O_6S$  <chem>Cc1nc(O1)NS(=O)(=O)c2ccc(NC(=O)c3cc(O)ccc3OC)cc2</chem> $C_{18}H_{19}N_3O_6S$	215 230 243 245 376	3

Table 4.1 (cont'd). Mass-Spectral Information and Proposed Structures of the SMX-Transformation Products Identified by Waters Progenesis QI 2.1 and MassLynx 4.1 Software.

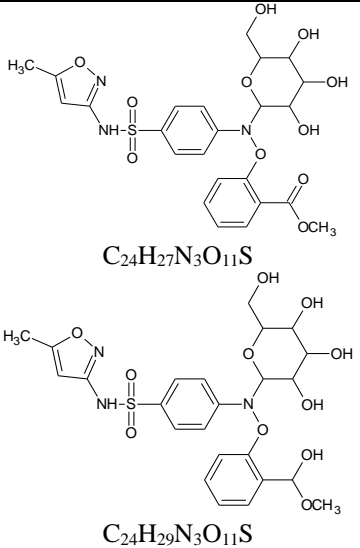
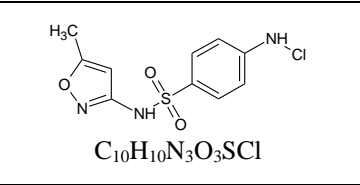
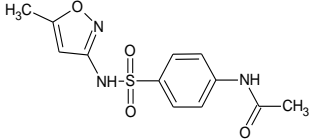
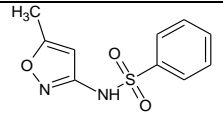
methylsalicylate-glycosyl-SMX (TP566, TP568)	4.79	566.1439 568.1596	566.1443 568.1590	0.7 1.1	 <p> $C_{24}H_{27}N_3O_{11}S$ $C_{24}H_{29}N_3O_{11}S$ </p>	215 230 243 245 404	3
N^4 -Cl-SMX (TP288)	5.68	288.0204	288.0202	0.7	 <p> $C_{10}H_{10}N_3O_3SCL$ </p>	92 108 156 254	3
N^4 -formyl-SMX (TP282)	3.74	282.0543	282.0547	1.4	 <p> $C_{11}H_{11}N_3O_4S$ </p>		4
N^4 -hydroxyl-SMX (TP270)	4.36	270.0543	270.0549	2.2	 <p> $C_{10}H_{11}N_3O_4S$ </p>		4

Table 4.1 (cont'd). Mass-Spectral Information and Proposed Structures of the SMX-Transformation Products Identified by Waters Progenesis QI 2.1 and MassLynx 4.1 Software.

N ⁴ -acetyl-SMX (TP296)	4.85	296.0700	296.0707	2.4	 <chem>CC(=O)Nc1ccc(S(=O)(=O)Nc2oc(C)n2)cc1</chem> $C_{12}H_{13}N_3O_4S$	4
desamino-SMX (TP239)	5.73	239.0485	239.0489	1.7	 <chem>CC1=CN(O)C=C1NS(=O)(=O)c2ccccc2</chem> $C_{10}H_{10}N_2O_3S$	4
TP280	6.47	280.0510	280.0509	0.4	Unknown structure $C_{10}H_{10}N_5O_3S$	5

^aRetention time of SMX and its metabolites when they were analyzed on the UPLC-QTOF-MS^E system. ^bThe accurate calculated masses (calcd m/z) were obtained with Chemsketch software, version 2016.2.2 (ACD/Laboratories, Toronto, ON). ^cThe observed masses (obsd m/z) were obtained from a high-resolution mass analyzer (QTOF-MS^E, Waters Xevo G2-XS). ^dThe fragments ions acquired in the high collision energy mode of UPLC-QTOF-MS^E. ^eAccording to (Schymanski et al., 2014) Level 1: reference standard, HR-MS, MS/MS, RT confirmed; Level 2b: HR-MS, characteristic fragmentation patterns observed; Level 3: HR-MS, characteristic fragmentation patterns observed, alternative structures (e.g. ring chlorinated positions) might be possible; Level 4: HR-MS, chemical formulas unequivocally assigned; Level 5: exact mass of interest.

4.3.2. Sulfamethazine (SMT)

4.3.2.1. Root uptake and translocation of SMT

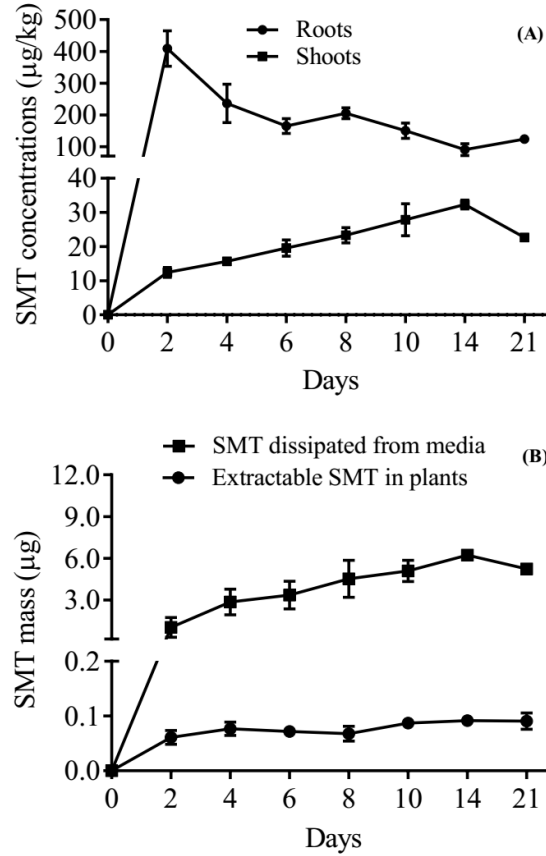


Figure 4. 5. Extractable SMT concentrations in *A. thaliana* plant tissues (A), and mass balance of SMT in the culture media and plant tissues (B) over 21 days of exposure. Error bars represent standard error of triplicates; some error bars are obscured by data symbols.

In roots, the highest SMT concentrations were found after 2 days of exposure ($409.1 \pm 56.1 \mu\text{g}/\text{kg}$) and significantly decreased as exposure time increased ($p < 0.001$), with the lowest concentrations observed after 14 days ($90.9 \pm 19.0 \mu\text{g}/\text{kg}$). On the contrary, SMT concentrations in shoots were $12.5 \pm 1.5 \mu\text{g}/\text{kg}$ after 2 days and significantly increased to $32.3 \pm 1.3 \mu\text{g}/\text{kg}$ after 14 days ($p = 0.001$) (Figure 4.5A). The mass of SMT in shoots accounted for approximately 17.1 and 48.1% of total SMT accumulated in plant tissues after 2 and 14 days, respectively

(Supplementary Figure 4.15). These results indicated that SMT was translocated into the above ground biomass following root uptake. The pH of the nutrient solution was maintained at approximately 5.7; therefore, SMT existed predominantly in its neutral form (>98%) (Zhang et al., 2016) and is thus expected to easily cross the biomembranes of plant roots (Trapp, 2000). However, dissociation of SMT ($pK_{a2} = 7.4$) (Zhang et al., 2016) is expected to occur in cytoplasm (pH = 7.3) (Shen et al., 2013), resulting in accumulation of SMT in root tissues due to the “ion trap effect” (Trapp, 2004). Undissociated SMT can be translocated into plant shoots via xylem vessels during transpiration (Mathews and Reinhold, 2013). In addition, root-to-shoot translocation of SMT can also be facilitated by its hydrophilicity ($\log K_{ow} = 0.27$) (Zhang et al., 2016), as neutral compounds with low hydrophobicity are readily translocated in plants (Briggs et al., 1982, Trapp, 2004).

The presence of *A. thaliana* substantially accelerated depletion of SMT in the media ($p < 0.001$). However, dissipation of SMT in no-plant control media due to abiotic processes was also observed (Supplementary Figure 4.13); therefore, the mass of SMT lost in the *Arabidopsis*-planted media was corrected for the corresponding abiotic loss prior to mass balance calculations. The mass balance of SMT in the systems is shown in Figure 4.5B, in which the total mass of parent SMT in plant tissues (roots and shoots) accounted for $1.5 \pm 0.2 - 5.2 \pm 2.1\%$ of the SMT mass dissipated from the media at the end of this trial. As care was taken to eliminate microorganisms in the systems, this large discrepancy can be explained by an extensive metabolism of SMT by *A. thaliana* following uptake. Our results were consistent with many recent studies on *A. thaliana* assimilation of organic contaminants, in which accumulation of the parent compounds appears to be negligible, with only trace concentrations observed in plant tissues (Fu et al., 2017a, Fu et al., 2017b, LeFevre et al., 2015, LeFevre et al., 2016, Marsik et al., 2017). For example, Fu et al.

observed that naproxen, in the parent form, accounted for only $1.0 \pm 0.1\%$ of the total mass input when exposing *A. thaliana* cells to naproxen (Fu et al., 2017b). Similarly, LeFevre et al. treated *A. thaliana* plants with benzotriazole and 2-mercaptobenzothiazole and reported that plant accumulation of these compounds was transitory and less than 1% of the unaltered form was present as extractable residues in the plant tissues (LeFevre et al., 2015, LeFevre et al., 2016). However, the assimilation rate in our root exposure was substantially lower than those in previous studies, likely attributed to less available absorption sites on *Arabidopsis* root surface compared with cell tissue culture and/or whole-plant treatments.

4.3.2.2. Formation, distribution, and release of SMT metabolites

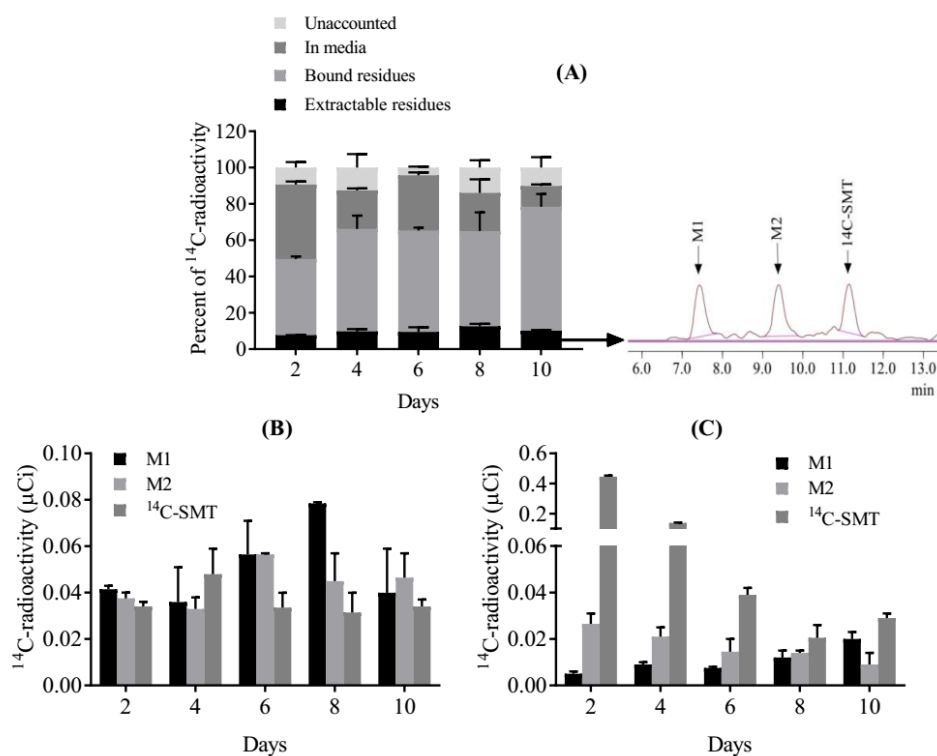


Figure 4. 6. Formation and release of ^{14}C -SMT metabolites by *A. thaliana* in whole-plant exposure. (A): distribution of ^{14}C -SMT and its phytometabolites in various compartments, with radiolabel detection revealed two major extractable metabolites (M1 and M2) upon exposure of *A. thaliana* to ^{14}C -SMT; (B) and (C): temporal variation in ^{14}C -radioactivity of M1, M2 and ^{14}C -SMT in plant tissues (B) and media (C) over 10 days of exposure. Error bars represent standard error of duplicates.

Partitioning of ^{14}C -radioactivity in plant tissues and culture media over 10 days of exposure is shown in Figure 4.6A. The overall mass balance for ^{14}C -radioactivity ranged from 86.2–95.8% throughout the incubation, indicating good recoveries. During the exposure time, plant accumulation accounted for 49.6 – 78.4% of the total ^{14}C initially added to the systems. In plant tissues, bound residues represented 42.0–68.2% of the spiked ^{14}C -radioactivity, while extractable residues, representing ^{14}C -SMT and its metabolites, accounted for only 7.7 – 12.6% of the total ^{14}C -radioactivity. Mass balance calculations also revealed that approximately 4.2 – 13.8% of the initially spiked radioactivity was lost from the systems during incubation; herein, denoted as unaccounted fractions (Figure 4.6A). In this study, ^{14}C bound residues in plant tissues were quantified through acid digestion (Thomson, 2012), which potentially results in loss of the label as ^{14}C - CO_2 during solubilization (Thomson, 2012). Accordingly, the unaccounted fractions most likely consisted of bound residues that had been converted to ^{14}C - CO_2 during digestion.

Two major metabolites (M1 and M2) were identified in plant tissues through detection of the ^{14}C -radioactivity (Figure 4.6A) with the LC-MS/ β -RAM. Both metabolites were more polar than the parent compound, as indicated by shorter retention times. Peaks M1 and M2 were also detected in all hydroponic media containing ^{14}C -SMT-treated plants over 10 days of exposure. Therefore, M1 and M2 were produced either *in planta* and subsequently released by *A. thaliana* into the media or *ex planta* through transformation. Temporal variation of M1, M2, and ^{14}C -SMT in plant tissues and hydroponic media is showed in Figure 4.6B and Figure 4.6C, respectively. ^{14}C -SMT accumulation, metabolism and excretion of its metabolites by *A. thaliana* occurred rapidly. After 2 days, radioactivity of M1, M2 and ^{14}C -SMT in plant tissues were approximately equal (0.041 ± 0.001 , 0.038 ± 0.002 , and 0.034 ± 0.002 μCi , respectively). Concurrently, M1 and M2 was also detected in the hydroponic media at 0.005 ± 0.001 and 0.027 ± 0.005 μCi , respectively.

As incubation time increased, radioactivity associated with M1 and M2 in plant tissues increased, providing direct evidence for the conversion of ^{14}C -SMT to M1 and M2. However, M1 in plant tissues decreased after 8 days, likely due to cell wall sequestration and plant excretion, as corresponding increases in ^{14}C -bound residues and M1 radioactivity in nutrient media were also observed (Figure 4.6).

Supplementary Figure 4.16B shows the representative selected ion chromatograms of the *A. thaliana* extracts on the LC-MS and the equivalent radioactivity peaks on the β -RAM (M1, M2, and ^{14}C -SMT). When plant tissues were subjected to SMT quantification using MS/MS, two peaks exhibiting identical MRM transitions as the parent SMT with earlier retention times were observed (Supplementary Figure 4.16A). Both were absent in the control plants, suggesting that they are the SMT metabolites. In-source fragmentation of plant metabolites on the mass spectrometer may result in cleavage of the conjugated bonds, releasing the parent aglycones prior to MS/MS fragmentation (Holder et al., 1999, Justesen, 2000, LeFevre et al., 2016). As a result, the presence of the metabolites can be detected at different chromatographic retention times, with the identical MS/MS signature as the parent compounds. For example, LeFevre et al. observed that the glucoside and amino acid moieties were lost from the *Arabidopsis*-derived conjugates during MS/MS fragmentation (LeFevre et al., 2016). Accordingly, the two signals observed in the SMT-exposed plants by MS/MS were supposed to be the metabolites of SMT, with the parent SMT structure remained intact through transformation and/or conjugation reactions. MS/MS fragmentations subsequently indicated that the first peak corresponded to the N^4 -glycosyl SMT (m/z 441) (Supplementary Figure 4.24), while the second peak likely corresponded to N^4 -formyl SMT (m/z 307, Supplementary Figure 4.25) or a hydroxylated metabolite of SMT (m/z 295, Supplementary Figure 4.28). On the LC-MS/ β -RAM, the precursor ion of m/z 441 was confirmed

for metabolite M1, corresponding to the N⁴-glycosyl SMT. However, the suspected precursor ions for M2 of m/z 295 or m/z 307 were not clearly observed on the LC-MS/ β -RAM (Supplementary Figure 4.16B). As a result, the chemical structure of the metabolite M2 could not be explicitly confirmed in this study.

4.3.2.3. Screening for SMT transformation products

Multivariate statistical analysis of the QTOF-MS^E high resolution mass-spectral data of plants and culture media provided a clear separation of control and SMT-exposed samples (Supplementary Figure 4.17). The S-plots obtained from the OPLS-DA models were subsequently used to explore the mass-to-charge (m/z) variables with $p(\text{corr}) \geq 0.5$ that were exclusively detected in the SMT-exposed groups. Chemical formulas of the potential metabolite candidates were proposed based on the corresponding m/z variables, followed by confirmation of the structures using characteristic fragmentation patterns under high collision energy. For example, the m/z 441.1434 ($p(\text{corr}) = 0.81$), which significantly contributed to the differentiation between SMT-exposed and controls groups, was detected at a retention time of 2.06 min. The elemental composition for this mass is C₁₈H₂₅N₄O₇S, and corresponds to glycosyl-SMT, which is formed by direct conjugation of a glucose to the SMT molecule. High collision energy mass spectra of this compound revealed the original molecule of SMT as a fragment (m/z 279.0904), and fragments at m/z 254.1041 and m/z 318.0655—characteristic for N⁴-glycosyl-SMT, and m/z 186.0336 and m/z 124.0877—characteristic for the parent SMT (García-Galán et al., 2011b) (Supplementary Figure 4.18). Similarly, multiple potential metabolites of SMT were identified using the same approach, including pterin-SMT, methyl-salicylate-SMT, hydroxyl-SMT, N⁴-formyl-SMT, desulfo-SMT, and N⁴-Cl-SMT (Table 4.2). Details on their characteristic fragmentations can be found in the Supporting Information (Supplementary Figure 4.18 – 4.23). Additionally, the formation of N⁴-

acetyl-SMT, desamino-SMT, and 2-amino-4,6-dimethylpyrimidine was confirmed to Level 1 confidence using reference standards (Schymanski et al., 2014) (Table 4.2). In this study, fragmentation of SMT metabolites using LC-MS/MS were also in agreement with studies by Majewsky et al., in which five different characteristic fragment ions for each of the 15 transformation products of sulfonamide antimicrobials were proposed (Majewsky et al., 2015). Their selected ion chromatograms in MRM mode can be found in the Supplementary Figure 4.24 – 4.31. The transitions in MRM mode were subsequently used for semi-quantification of the metabolites with no reference standards, except for pterin-SMT, methyl-salicylate-SMT, and N⁴-Cl-SMT.

4.3.2.4. Abiotic transformations of SMT

Interestingly, N⁴-glycosyl-SMT, N⁴-formyl-SMT, hydroxyl-SMT, desulfo-SMT, 2-amino-4,6-dimethylpyrimidine, N⁴-acetyl-SMT, desamino-SMT, and N⁴-Cl-SMT also formed in the abiotic controls, most likely *via* direct chemical, photolytic, and/or photosensitized reactions (García-Galán et al., 2012, Nassar et al., 2017, Yi et al., 2018) (Supplementary Figure 4.33 and Supplementary Figure 4.34). Formation of 2-amino-4,6-dimethylpyrimidine, desulfo-, desamino-, and hydroxyl-SMT has previously been observed in aqueous media containing SMT under simulated solar irradiation (García-Galán et al., 2012) or UV irradiation (Nassar et al., 2017, Yi et al., 2018). To the best of our knowledge, N⁴-formyl- and N⁴-acetyl-SMT formed in aqueous media *via* abiotic processes have been observed for the first time in this study; however, elucidation of their reaction mechanisms in the abiotic media is out of the scope of this study. None of these transformation products was detected in the SMT standard using LC-MS/MS, indicating that they were formed chemically in the media, rather than the impurities in the reference standard. Electrophilic substitution of free chlorine in the MS media (approximately 106 mg/L,

supplemented as macronutrient CaCl_2) to the N^4 -amino group potentially led to the formation of N^4 -Cl-SMT. Similar substitution of free chlorine to SMT was also observed by Fu et al., which subsequently resulted in desulfonation of SMT through Smiles-type rearrangement (Fu et al., 2018). The occurrence of N^4 -glucosyl-SMT in the abiotic controls was most likely attributed to chemical affinity of SMT and glucose that was supplemented into the culture media as sucrose (5 g/L), which has also been reported by Garcia-Galan et al (García-Galán et al., 2011b). However, the concentrations of N^4 -glucosyl-SMT in the *A. thaliana*-planted media were approximately two to three orders-of-magnitude higher than those in the abiotic controls, indicating that a substantially larger proportion of N^4 -glycosyl-SMT in the planted media were from plant excretion. In this study, bacterial transformation of SMT could be eliminated, as sterile conditions were thoroughly implemented for all treatments.

4.3.2.5. Transformation and conjugation pathways of SMT

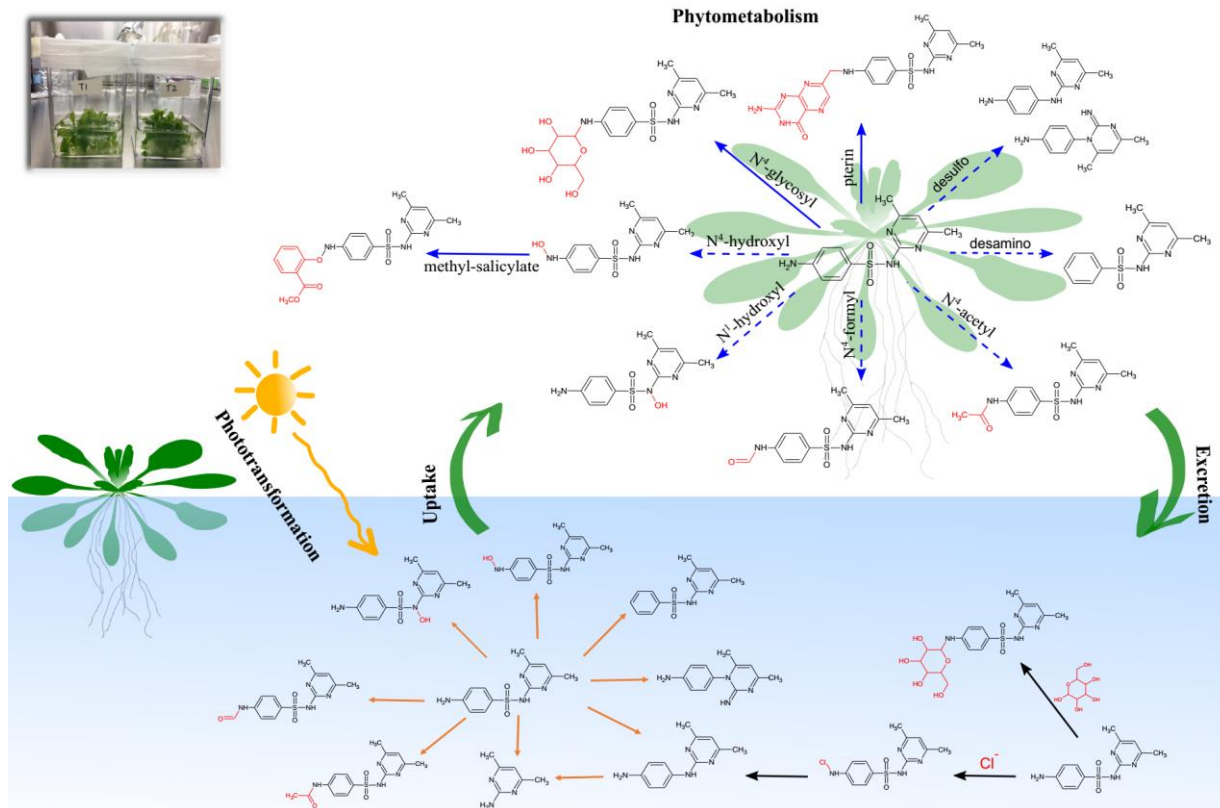


Figure 4. 7. Proposed transformation pathways of SMT in model plant *A. thaliana* and hydroponic media based on the metabolites identified in this study, and other transformation pathways of SMT in aqueous media previously described by (García-Galán et al., 2012), (Nassar et al., 2017), and (Fu et al., 2018). All of the metabolites detected in plant tissues were concurrently present in the culture media, suggesting that *A. thaliana* plants likely excreted a fraction of the metabolites following uptake and metabolism. The dashed arrows indicate that the corresponding metabolites were also detected in the abiotic control media; consequently, their presence in plant tissues may also due to uptake of the abiotic transformation products from the media.

Based on the metabolites identified in *A. thaliana* plants and hydroponic media, and the observed transformation products in the abiotic controls, the metabolic pathways of SMT are proposed in Figure 4.7. Upon exposure to SMT, most of the products were concurrently present in both plant tissues and culture media, except for 2-amino-4,6-dimethylpyrimidine, which was exclusively detected in the media. Metabolism of SMT by *A. thaliana* mainly occurred at the primary N⁴-amino group, in which N⁴-glycosyl-SMT was the most abundant metabolite in plant

tissues. Glycosylation, which is catalyzed by glycosyltransferases, is among the most common conjugation reactions in plants and has been reported for multiple organic xenobiotics (e.g., benzotriazole (LeFevre et al., 2015), diclofenac (Fu et al., 2017a), 2-mercaptobenzothiazole (LeFevre et al., 2016), carbamazepine (Riemenschneider et al., 2017), acetaminophen (Huber et al., 2009), and triclosan (Macherius et al., 2014)). The NH₂- group, which is part of the SMT molecule, is known to trigger detoxification mechanism *via* glycosyltransferases, leading to direct conjugation of xenobiotics with sugar molecule(s) in phase-II reactions without addition of other functional groups (Schröder, 2007). Direct N-glycosylation has also been observed for *A. thaliana* plant exposed to 2-mercaptobenzothiazole and benzotriazole, allowing bypass of the often rate limiting phase-I reactions (e.g. hydroxylation) (LeFevre et al., 2015, LeFevre et al., 2016).

As structural analogs to *p*-aminobenzoic acid, sulfonamides are known as inhibitors of dihydropteroate synthase, exclusively impairing folate synthesis in microorganisms and plants (e.g. *A. thaliana* plants (Zhang et al., 2012)). Sulfonamides can also act as alternative substrates leading to the formation of pterin-sulfonamide conjugates (Achermann et al., 2018). The pterin-related transformation pathways have recently been reported to occur in microorganisms (Achermann et al., 2018) and freshwater phytoplankton (Stravs et al., 2017) upon exposure to sulfonamides. Although no visual adverse effects of SMT on plant growth was observed in this study, formation of the pterin SMT conjugate in *A. thaliana* plant tissues potentially resulted in a reduction in the plant folate pool size as previously reported by (Zhang et al., 2012).

Salicylate is a phytohormone regulating plant responses to both biotic and abiotic stresses, as well as controlling plant growth and development (Thompson et al., 2017). In *A. thaliana*, total salicylate levels range from 0.25–1 µg/g fw, mostly present as glycosylated and/or methylated forms (Rivas-San Vicente and Plasencia, 2011). The involvement of the salicylate pathway in *A.*

thaliana responses to safeners (e.g. isoxadifen-ethyl and mefenpyr-diethyl) (Behringer et al., 2011) and alamethicin (Chen et al., 2003) has been documented in literature. However, its induction following exposure to sulfonamide antimicrobials are still largely unclear. In this study, upon exposure of *A. thaliana* to SMT, we observed the formation of methyl-salicylate-SMT conjugate, suggesting that *A. thaliana* might also recruit the salicylate pathway for detoxification of SMT.

Garcia-Galan et al. observed the formation of desulfo-SMT and N⁴-formyl-SMT following *in vivo* exposure of the white-rot fungus (*Trametes versicolor*) to SMT, while enzymatic degradation experiments, using *T. versicolor*-purified laccase, led to the formation of N⁴-hydroxy-SMT and desamino-SMT (García-Galán et al., 2011b). Additionally, N⁴-acetylation and hydroxylation have been reported as the major metabolic pathways of SMT in human (Gulde et al., 2016) and mammals (Mitchell and Paulson, 1986, Zulalian et al., 1984), while N⁴-glycosyl-SMT and desamino-SMT have been detected in tissues of rats and swine administered SMT (Mitchell and Paulson, 1986, Zulalian et al., 1984). In the current study, N⁴-glucosyl-SMT, N⁴-formyl-SMT, desulfo-SMT, hydroxyl-SMT, N⁴-acetyl-SMT, and desamino-SMT were also detected in the *A. thaliana* plant tissues following exposure to SMT, suggesting that some common metabolic pathways for detoxification of SMT were potentially shared among plants, fungi, and animals. N⁴-acetyl SMT, which is less polar than the parent compound, is excreted more quickly from the body than the parent molecule (García-Galán et al., 2008). Acetylation of the α -amino group of the N-terminal amino acid residues is catalyzed by N ^{α} -acetyltransferases occurring in a wide range of genomes (e.g. animals, humans, *Arabidopsis*), indicating that this mechanism may be common in all eukaryotic organisms (Hwang et al., 2009). Hence, the N⁴-acetyl SMT detected in this study was likely catalyzed by the same N ^{α} -acetyltransferases enzymes in *A. thaliana*.

The presence of pterin-SMT and methyl-salicylate-SMT conjugates in the planted media was attributed to plant excretion and/or potential leakage of the cell membranes due to oxidative stress caused by SMT exposure. Although phase III sequestration plays an important role in detoxification of xenobiotics in plants (Sandermann, 1992), excretion of phase II conjugates by *A. thaliana* has previously been reported, which potentially facilitates plant defenses against the phytotoxicity exerted by xenobiotic exposure (Khan et al., 2016). For examples, Taguchi et al. observed that *A. thaliana* excreted conjugated 2-naphthol as glucosides into the culture media, while reuptake of the glycosylated conjugates into the plant cells was minimal (Taguchi et al., 2010). Similarly, glycosylated benzotriazoles were also detected in the hydroponic media when exposing *A. thaliana* to benzotriazoles (LeFevre et al., 2015). LeFevre et al. hypothesized that direct biotransformation of the xenobiotics on the root surfaces also results in the presence of the metabolites in nutrient solution (LeFevre et al., 2016). In addition, decay of plant materials may also release part of the accumulated parent compounds and metabolites. However, in this study, negligible necrosis or senescence of *A. thaliana* plants was observed across all treatments.

Complementary Figure 4.34 compares the total abundance of SMT products in each container of the *Arabidopsis*-planted treatments and the corresponding abiotic controls. Except for pterin-SMT and methyl-salicylate-SMT, other transformation products that were detected in plant tissues were also present in the abiotic media, suggesting that direct uptake of these abiotic transformation products might also contribute to their abundance in plant tissues. For example, the occurrence of N⁴-Cl-SMT in plant tissues was most likely due to uptake of this product in the media; subsequently, further metabolism in plants possibly led to a substantial reduction of its abundance in the planted-treatments. On the other hand, the total abundance of N⁴-glycosyl-SMT, desulfo-SMT, and hydroxyl-SMT (except hydroxyl-SMT-1b) were found to be substantially

greater than those in the abiotic controls throughout the exposure, suggesting that they were also generated *in planta*. Over 4 days of exposure, we observed no considerable discrepancy in the total amount of N⁴-acetyl-SMT and desamino-SMT between the planted-treatments and abiotic controls, while N⁴-formyl-SMT was more abundant in the abiotic controls. Accordingly, plant direct uptake of N⁴-formyl-SMT, N⁴-acetyl-SMT, and desamino-SMT possibly dominated the corresponding intracellular conversion of the parent SMT. In general, our data indicated that plant uptake and accumulation of the parent compounds and their abiotic transformation products might simultaneously occur, which ultimately contributes to the environmental fate of sulfonamide antimicrobials in the planted systems.

4.3.2.6. Implications to human and environmental health

Uptake and accumulation of antimicrobial residues by food crops grown in contaminated soils have been well documented in literature. Therefore, unintentional human exposure to antimicrobials through consuming contaminated food crops is a realistic possibility. While in the past, studies and risk assessment related to plant uptake and accumulation of these xenobiotics only addressed unaltered parent compounds, this research emphasizes that the fate and toxicity of transformation products and conjugates should also be considered. We identified N⁴-glycosyl SMT as the most abundant metabolite in *A. thaliana*, although other metabolites were also detected. In humans, after ingestion, materials encounter salivary, gastric, and intestinal digestion, through which the glycosylated metabolites of xenobiotics are released and likely to be hydrolyzed (Sandermann, 1992). Release of phytometabolites sequestered into cell walls are expected to be minimal since dietary cellulose is thought not to be digested in the stomach and small intestine, and ultimately excreted from human body (Cummings, 1984).

Sulfonamides have been found to promote antimicrobial resistance, almost twice as much as tetracyclines and many times more than other antimicrobials (Lanz et al., 2003). While degradation products of sulfonamide antimicrobials have been reported to lose their antibacterial activity and their potential to cause antimicrobial resistance, these properties are likely retained for the transformation products (Majewsky et al., 2015, Majewsky et al., 2014). Moreover, conversion of transformation products back to the parent molecules has also been observed (García-Galán et al., 2011a, Göbel et al., 2007, Gros et al., 2010). Release of conjugated metabolites of SMT by *A. thaliana* into the culture media observed in this study has raised concerns regarding total loadings of antimicrobials and potential antimicrobial resistance into the environment, especially in the rhizosphere. Plants exude several antimicrobial compounds (e.g. phytoalexins, salicylic acid and flavonoids) that create a strongly selective environment in the rhizosphere (Yergeau et al., 2014), resulting in increased expression of antimicrobial resistance genes even in the absence of synthetic antimicrobials. The presence of synthetic antimicrobials and metabolites in soils imposes further selection pressure on microorganisms. The double-selection pressure will potentially exaggerate the development of antimicrobial resistant bacteria and resistance genes (Bais et al., 2006, Yergeau et al., 2014). Even though environmental concentrations of those transformation products have been found in the nanogram-per-liter levels (Majewsky et al., 2015), a further step towards comprehensive risk assessments of both sulfonamide residues and their transformation products is necessary.

Table 4. 2. Mass-Spectral Information and Proposed Structures of the SMT-Transformation Products Identified by Waters Progenesis QI 2.1 and MassLynx 4.1 Software.

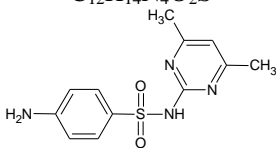
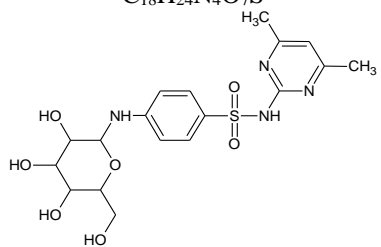
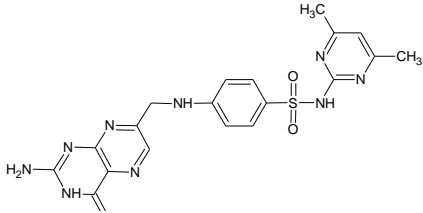
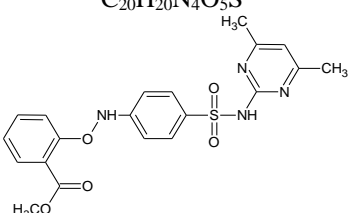
denotation	RT (min) ^a	calcd m/z^b	obsd m/z^c	error (ppm)	predicted formula and structure	fragments (m/z) ^d	level ^e
sulfamethazine (SMT)	3.11	279.0910	279.0915	1.8	$C_{12}H_{14}N_4O_2S$ 	92 108 156 124 186	1
N ⁴ -glycosyl-SMT	2.06	441.1438	441.1434	0.9	$C_{18}H_{24}N_4O_7S$ 	254 270 318 124 186	2b
pterin-SMT	3.01	454.1404	454.1391	2.9	$C_{19}H_{19}N_9O_3S$ 	176 267 283 331 349	2b
methylsalicylate-SMT	4.35	429.1227	429.1231	0.9	$C_{20}H_{20}N_4O_5S$ 	215 243 258 321 365	3

Table 4.2 (cont'd). Mass-Spectral Information and Proposed Structures of the SMT-Transformation Products Identified by Waters Progenesis QI 2.1 and MassLynx 4.1 Software.

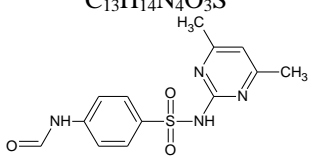
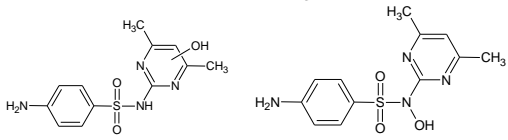
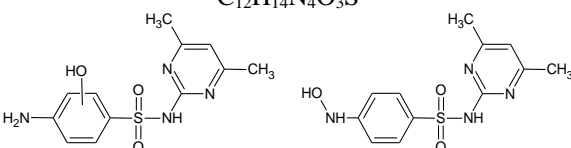
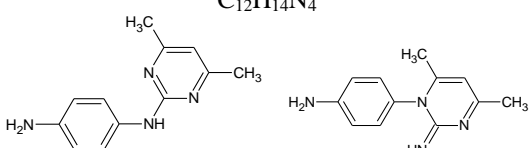
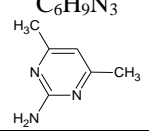
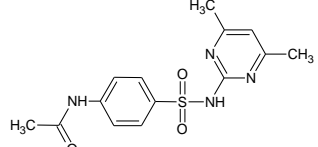
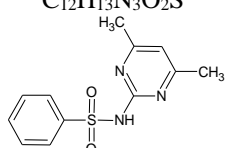
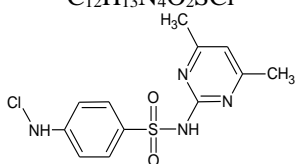
N ⁴ -formyl-SMT	2.84	307.0859	307.0863	1.3	$C_{13}H_{14}N_4O_3S$ 	120 136 184 124 186	3
hydroxyl-SMT-1	2.84	295.0859	295.0863	1.4	$C_{12}H_{14}N_4O_3S$ 	92 108 156 140 202	3
hydroxyl-SMT-2	2.91	295.0859	295.0863	1.4	$C_{12}H_{14}N_4O_3S$ 	108 124 172 186	3
desulfo-SMT	1.20 1.63	215.1291	215.1296 215.1297	2.3 2.8	$C_{12}H_{14}N_4$ 	92 108 133 158 173	3
2-amino-4,6-dimethylpyrimidine	2.50	124.0869	124.0872	2.4	$C_6H_9N_3$ 	67 82 107	1
N ⁴ -acetyl-SMT	3.13	321.1016	321.1018	0.6	$C_{14}H_{16}N_4O_3S$ 	134 150 198 124 186	1

Table 4.2 (cont'd). Mass-Spectral Information and Proposed Structures of the SMT-Transformation Products Identified by Waters Progenesis QI 2.1 and MassLynx 4.1 Software

desamino-SMT	4.02	264.0801	264.0806	1.9	$C_{12}H_{13}N_3O_2S$ 	77 141 124 186	1
N ⁴ -Cl-SMT	4.12	313.0521	313.0523	0.6	$C_{12}H_{13}N_4O_2SCl$ 	124 142 186 211 279	2b

^aRetention time of SMT and its products when analyzed on the UPLC-QTOF-MS^E system. ^bThe accurate calculated masses (calcd m/z) were obtained with Chemsketch software, version 2016.2.2 (ACD/Laboratories, Toronto, ON). ^cThe observed masses (obsd m/z) were obtained from a high-resolution mass analyzer (QTOF-MS^E, Waters Xevo G2-XS). ^dAccording to the current study, (Achermann et al., 2018), (García-Galán et al., 2011b), and (Majewsky et al., 2015), or the reference standards, if available. The fragments ions were acquired with a tandem mass analyzer (MS/MS, Applied Biosystems Sciex 3200). The full MS/MS fragmentations of the SMT metabolites are presented in the Supporting Information (Figure S12–S19). ^eAccording to (Schymanski et al., 2014): Level 1: reference standard, HR-MS, MS/MS, RT confirmed; Level 2b: fragmentation pattern reported, HR-MS, MS/MS; Level 3: fragmentation pattern reported, HR-MS, MS/MS, insufficient information for one exact structure only.

APPENDIX

Supplementary Table 4.1. Recoveries of ¹⁴C-SMX standards in plant materials.

Extractions without plant materials							
¹⁴ C-SMX standard used for spiking		V injected to β-RAM (mL)	β-RAM signal (DPM)	Total DPM in 1 mL	Mean (DPM)	SD	
Run-1		0.05	6858	137160	140080	3788	
Run-2		0.05	6936	138720			
Run-3		0.05	7218	144360			
Spiked samples	V spiked (mL)	V injected to β-RAM (mL)	β-RAM signal (DPM)	DPM recovered	Recoveries (%)	Mean	SD
Replicate-1	1.0	0.05	6470	129400	92.4	95.2	2.4
Replicate-2	1.0	0.05	6780	135600	96.8		
Replicate-3	1.0	0.05	6750	135000	96.4		
Extractions with plant materials							
Day 1							
¹⁴ C-SMX standard used for spiking		V injected to β-RAM (mL)	β-RAM signal (DPM)	Total DPM in 1 mL	Mean	SD	
Run-1		0.05	6996	139920	139200	3182	
Run-2		0.05	7098	141960			
Run-3		0.05	6786	135720			
Spiked samples	V spiked (mL)	V injected to β-RAM (mL)	β-RAM signal (DPM)	DPM recovered	Recoveries (%)	Mean	SD
Replicate-1	1.0	0.05	6390	127800	91.8	90.8	4.8
Replicate-2	1.0	0.05	6612	132240	95.0		
Replicate-3(*)	1.0	0.05	5412	119064	85.5		
*Final reconstituted volumn for this replicate was 1.1 mL							
Day 2							
¹⁴ C-SMX standard used for spiking		V injected to β-RAM (mL)	β-RAM signal (DPM)	Total DPM in 1 mL	Mean	SD	
Run-1		0.05	6756	135120	135320	2227	
Run-2		0.05	6882	137640			
Run-3		0.05	6660	133200			

Supplementary Table 4.1 (cont'd). Recoveries of ¹⁴C-SMX standards in plant materials.

Spiked samples	V spiked (mL)	V injected to β-RAM (mL)	β-RAM signal (DPM)	DPM recovered	Recoveries (%)	Mean	SD
Replicate-1	1.0	0.05	5916	118320	87.4	87.9	2.4
Replicate-2	1.0	0.05	6126	122520	90.5		
Replicate-3	1.0	0.05	5802	116040	85.5		
Day 3							
¹⁴ C-SMX standard used for spiking		V injected to β-RAM (mL)	β-RAM signal (DPM)	Total DPM in 1 mL	Mean	SD	
Run-1		0.05	7128	142560	137240	4925	
Run-2		0.05	6816	136320			
Run-3		0.05	6642	132840			
Spiked samples	V spiked (mL)	V injected to β-RAM (mL)	β-RAM signal (DPM)	DPM recovered	Recoveries (%)	Mean	SD
Replicate-1	1.0	0.05	6066	121320	88.4	88.1	5.2
Replicate-2	1.0	0.05	5676	113520	82.7		
Replicate-3	1.0	0.05	6384	127680	93.0		
Average recoveries for ¹⁴C-SMX in plant materials (average of day 1, day 2, and day 3)							
Mean (%)		88.9					
SD		4.0					

Supplementary Table 4.2. Responses of the MS detector to SMX standards dissolved in different solvents.

SMX standards	Day 1		Day 2		Day 3	
	Peak area		Peak area		Peak area	
	MeOH:H ₂ O (1:1), 0.1% FA	Plant extracts, 0.1% FA	MeOH:H ₂ O (1:1), 0.1% FA	Plant extracts, 0.1% FA	MeOH:H ₂ O (1:1), 0.1% FA	Plant extracts, 0.1% FA
1.8 ng/mL	8915	993	7014	695	6304	578
5.6 ng/mL	21931	14339	19636	7968	14898	9394
9.9 ng/mL	38034	28984	37706	19602	24943	19248
19.6 ng/mL	71127	59545	62596	39306	46814	38667
47.6 ng/mL	163926	144417	151388	99552	110056	89802
90.9 ng/mL	300547	258622	285556	206285	205071	169180
200 ng/mL	650849	558307	604407	475267	450086	413181
FA: formic acid						

Supplementary Table 4.3. Recoveries of 100 ng/mL unlabeled-SMX standards in plant materials.

Spiked samples	Day 1				
	Peak area	Conc-1 (ng/mL)	Conc-2 (ng/mL)	Recoveries-1 (%)	Recoveries-2 (%)
Replicate-1	196376	58.9	69.4	58.9	69.4
Replicate-2	232773	70.2	82.4	70.2	82.4
Replicate-3	201935	60.6	71.4	60.6	71.4
Replicate-4	224475	67.6	79.5	67.6	79.5
Replicate-5	237127	71.5	84.0	71.5	84.0
Replicate-6	207406	62.3	73.4	62.3	73.4
Spiked samples	Day 2				
	Peak area	Conc-1 (ng/mL)	Conc-2 (ng/mL)	Recoveries-1 (%)	Recoveries-2 (%)
Replicate-1	182588	58.8	79.2	58.8	79.2
Replicate-2	201413	65.1	87.2	65.1	87.2
Replicate-3	192108	62.0	83.2	62.0	83.2
Replicate-4	194746	62.9	84.3	62.9	84.3
Replicate-5	205237	66.4	88.7	66.4	88.7
Replicate-6	205924	66.6	89.0	66.6	89.0
Spiked samples	Day 3				
	Peak area	Conc-1 (ng/mL)	Conc-2 (ng/mL)	Recoveries-1 (%)	Recoveries-2 (%)
Replicate-1	161749	71.1	80.9	71.1	80.9
Replicate-2	170996	75.3	85.4	75.3	85.4
Replicate-3	158540	69.7	79.3	69.7	79.3
Replicate-4	169217	74.5	84.5	74.5	84.5
Replicate-5	142401	62.5	71.5	62.5	71.5
Replicate-6	152365	66.9	76.3	66.9	76.3
Average recoveries for unlabeled-SMX in plant materials (average of day 1, day 2, and day 3)					
	Mean (%)	SD			
Recoveries-1 (%)	66.3	5.0	SMX standards dissolved in MeOH:H ₂ O (1:1), 0.1% FA		
Recoveries-2 (%)	80.5	6.0	SMX standards dissolved in plant extracts, with 0.1% FA		

Recoveries of ^{14}C -SMX and unlabeled-SMX in plant matrix

Recovery rates were evaluated by spiking a known amount of ^{14}C -SMX and unlabeled-SMX (approximately 1.4×10^5 dpm and 100 ng, respectively) into *A. thaliana* plant materials prior to extraction. Quantification of ^{14}C -SMX was performed using the LC- β -RAM system while quantification of unlabeled-SMX utilized LC-MS. The recoveries of ^{14}C -SMX are presented in Supplementary Table 4.1. Only 4.8% of the spiked ^{14}C -radioactivity was lost due to physical sorption (to the centrifuge tubes, pipette tips etc.) throughout the extraction steps without plant materials. Recoveries of ^{14}C -SMX in plant materials were $88.9 \pm 4.0\%$. However, the recoveries of unlabeled-SMX on the LC-MS system were found to be substantially lower than those of ^{14}C -SMX, at $66.3 \pm 5.0\%$. Based on this discrepancy, it was suspected that the plant matrix exerted negative effects on quantification of SMX in plant samples, which has been observed in earlier studies. In this study, ion suppression, as determined by comparing signals for in Milli-Q water/methanol (1:1) containing 0.1% formic acid and standards in extractions of non-exposed plant tissues, was observed over a wide range of SMX concentrations (1.8 – 200 ng/mL, Supplementary Table 4.2). Consequently, the “low” recovery rates of SMX in plant materials using LC-MS were actually a result of plant-matrix effects rather than “low” extraction efficiency. Therefore, in this study, matrix-matched standard curves with seven concentrations of SMX (1.8 – 200 ng/mL) were freshly prepared prior to each run to minimize the potential matrix effects. By using this approach, the average recoveries of SMX in plant samples were $80.5 \pm 6.0\%$ (Supplementary Table 4.3).

Supplementary Table 4.4. MRM parameters for the analysis of SMT and its metabolites by LC-MS/MS.

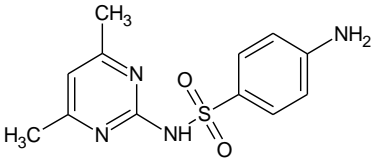
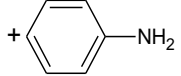
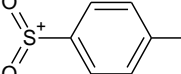
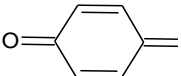
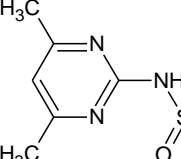
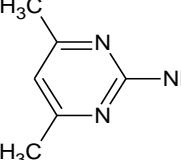
compounds	precursor ion <i>m/z</i>	product ions <i>m/z</i>	DP (eV)	EP (eV)	CEP (eV)	CXP (eV)	CE (eV)
SMT ^a	279	186 (156)	37	5	20	18	23
N ⁴ -acetyl SMT ^a	321	134 (124)	37	5	18	10	40
desamino SMT ^a	264	77 (124)	37	5	15	10	45
2-amino-4,6-dimethylpyrimidine ^a	124	67 (107)	37	5	9	10	35
N ⁴ -Glycosyl SMT ^b	441	186 (124)	40	5	24	10	40
hydroxyl SMT-1 ^b	295	124 (108)	40	5	17	10	40
hydroxyl SMT-2 ^b	295	140 (202)	40	5	17	10	30
formyl SMT ^b	307	124 (184)	40	5	17	10	30
desulfo SMT ^b	215	92 (173)	40	5	13	10	40

DP: Declustering Potential; EP: Entrance Potential; CEP: Collision Cell Entrance Potential; CXP: Collision Cell Exit Potential; CE: Collision Energy.

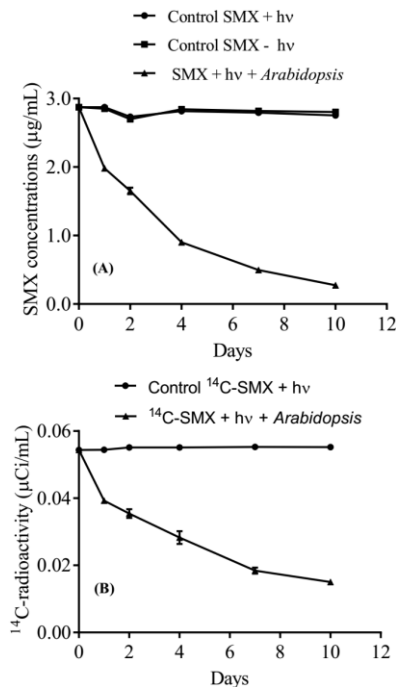
The product ions *m/z* in bold and in parentheses were used as quantifying and qualifying ions, respectively.

^aReference standards available; ^breference standards not available.

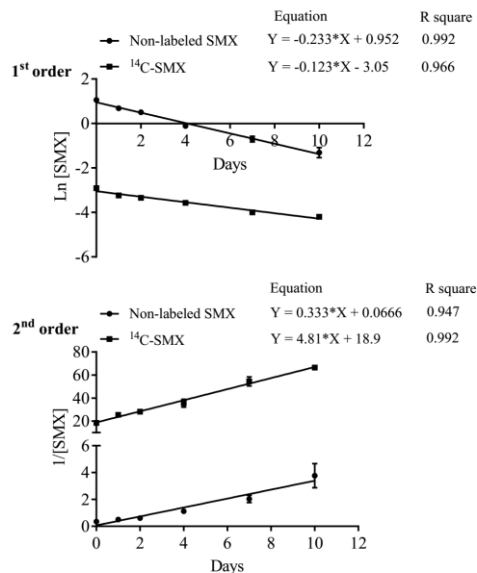
Supplementary Table 4.5. Structures proposed for the fragment ions of SMT under ESI (+)-QTOF-MS^E conditions.

 <p style="text-align: center;">Sulfamethazine (SMT) <i>m/z</i> = 279.0910</p>	Fragment ions	Calculated <i>m/z</i>
		92.0495
		156.0114
		108.0444
		186.0332
		124.0869
	*Loss of H ₂ SO ₂	213.1140

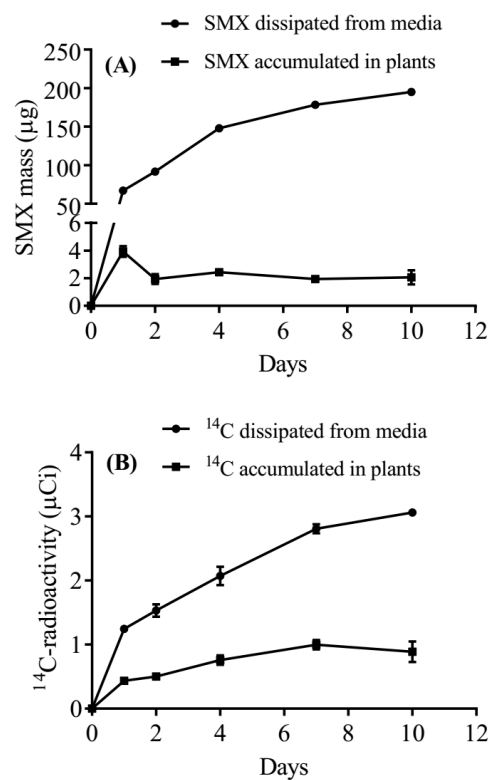
*Klagkou et al. proposed the loss of 66 Da from SMT corresponding to the elimination of H₂SO₂ from the protonated molecule; however, the authors did not suggest a structure for the detected product ion



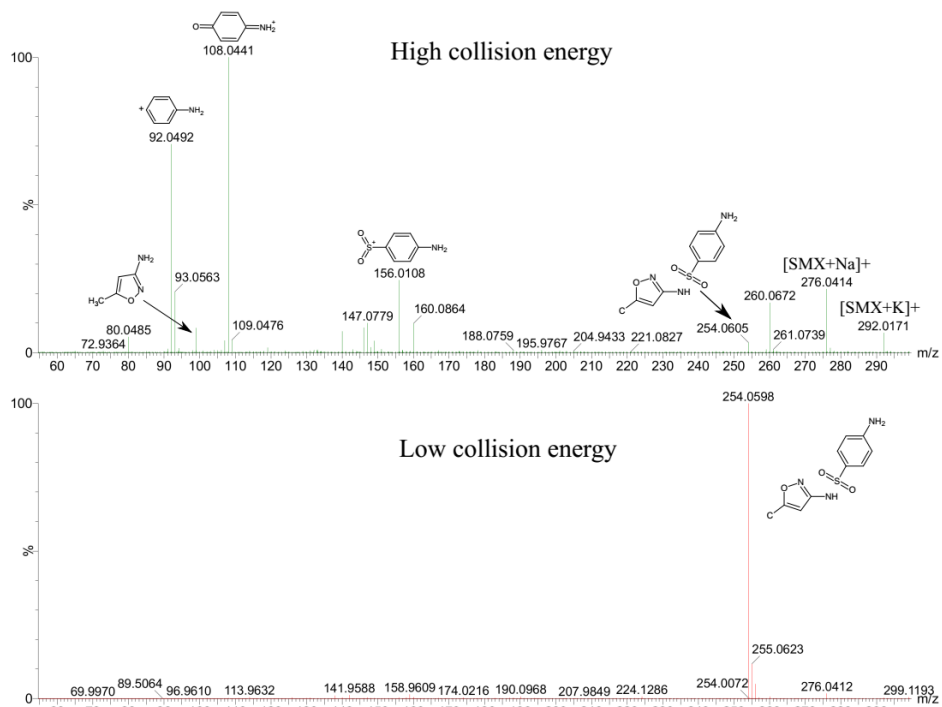
Supplementary Figure 4.1. Temporal variations of unlabelled SMX (A) and ¹⁴C-radioactivity (B) in hydroponic media over 10 d of exposure. “hv” means light exposure. Error bars represent standard error of triplicates for unlabelled SMX exposure, and of duplicates for ¹⁴C-SMX exposure; some error bars are obscured by data symbols.



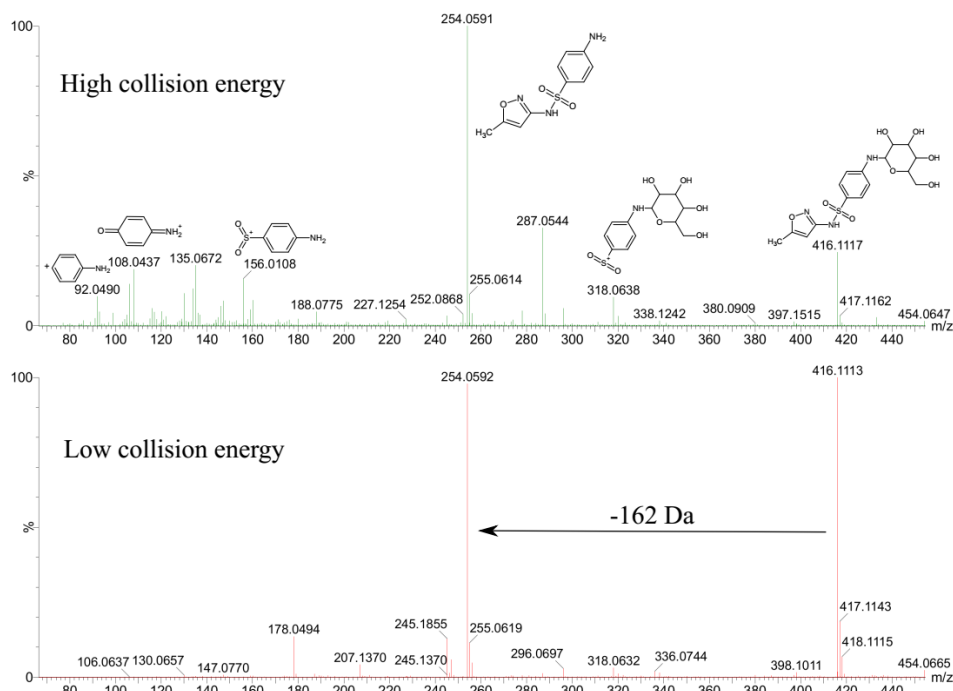
Supplementary Figure 4.2. First-order and second-order models for dissipation of unlabeled SMX and ¹⁴C-SMX in the *Arabidopsis*-planted media, using linear regression. Error bars represent standard error of triplicates for unlabeled SMX exposure and of duplicates for ¹⁴C-SMX exposure, respectively; some error bars are obscured by data symbols.



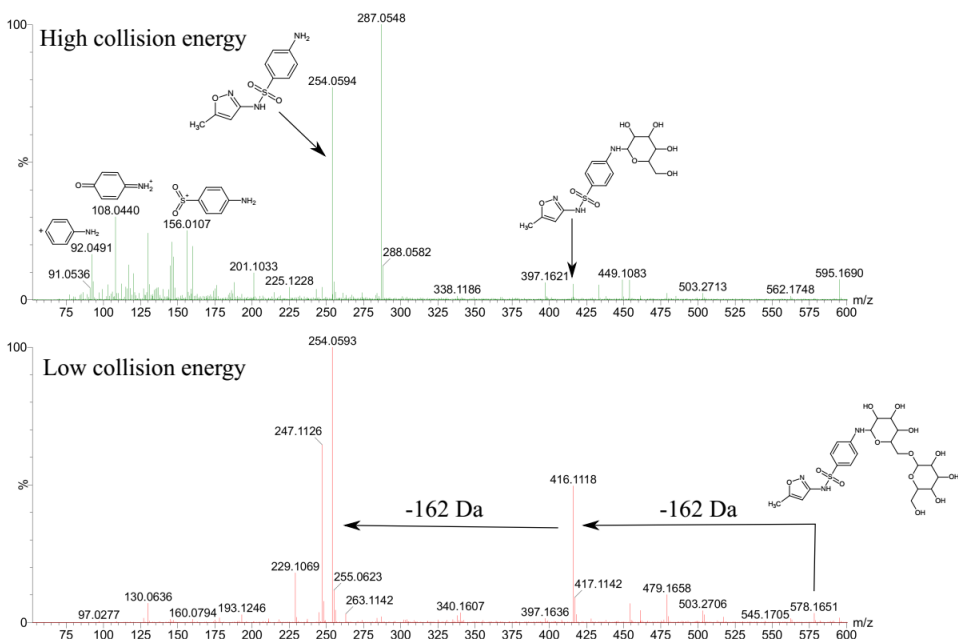
Supplementary Figure 4.3. Mass balance of unlabeled SMX treatments (A) and ^{14}C -SMX treatments (B) in culture media and plant tissues over 10 days of exposure. Error bars represent standard error of triplicates for unlabeled SMX treatments and of duplicates for ^{14}C -SMX treatments; some error bars are obscured by data symbols.



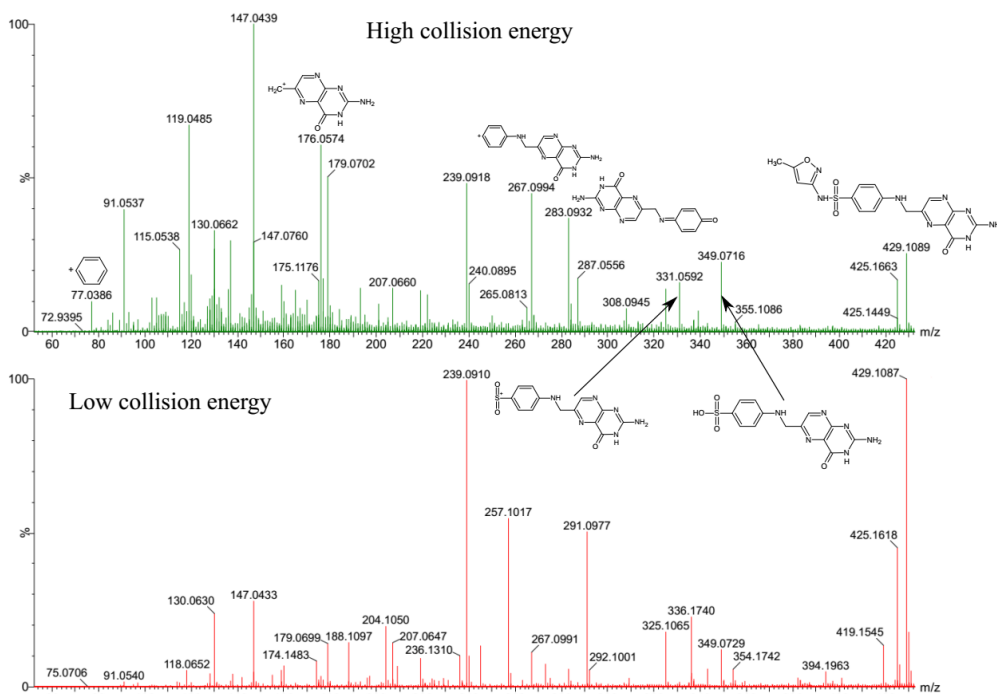
Supplementary Figure 4.4. Low and high collision energy mass spectra of SMX (200 $\mu\text{g/L}$) on the UPLC-QTOF-MS^E. The parent SMX m/z : $[\text{M}+\text{H}]^+=254.0598$. Adducts with Na^+ ($[\text{M}+\text{Na}]^+=276.0414$) and K^+ ($[\text{M}+\text{K}]^+=292.0171$) were also observed.



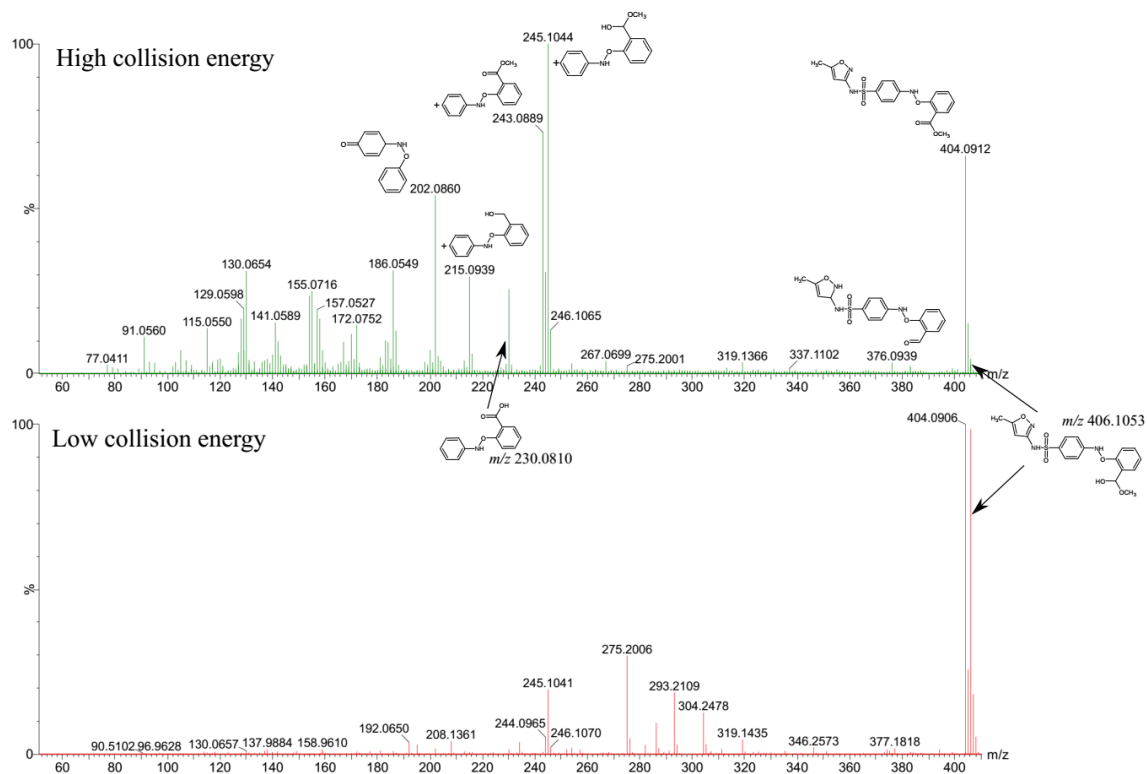
Supplementary Figure 4.5. Low and high collision energy MS^E mass spectra of the most abundant metabolite of SMX in plant tissues, which was identified as N⁴-glycosyl-SMX.



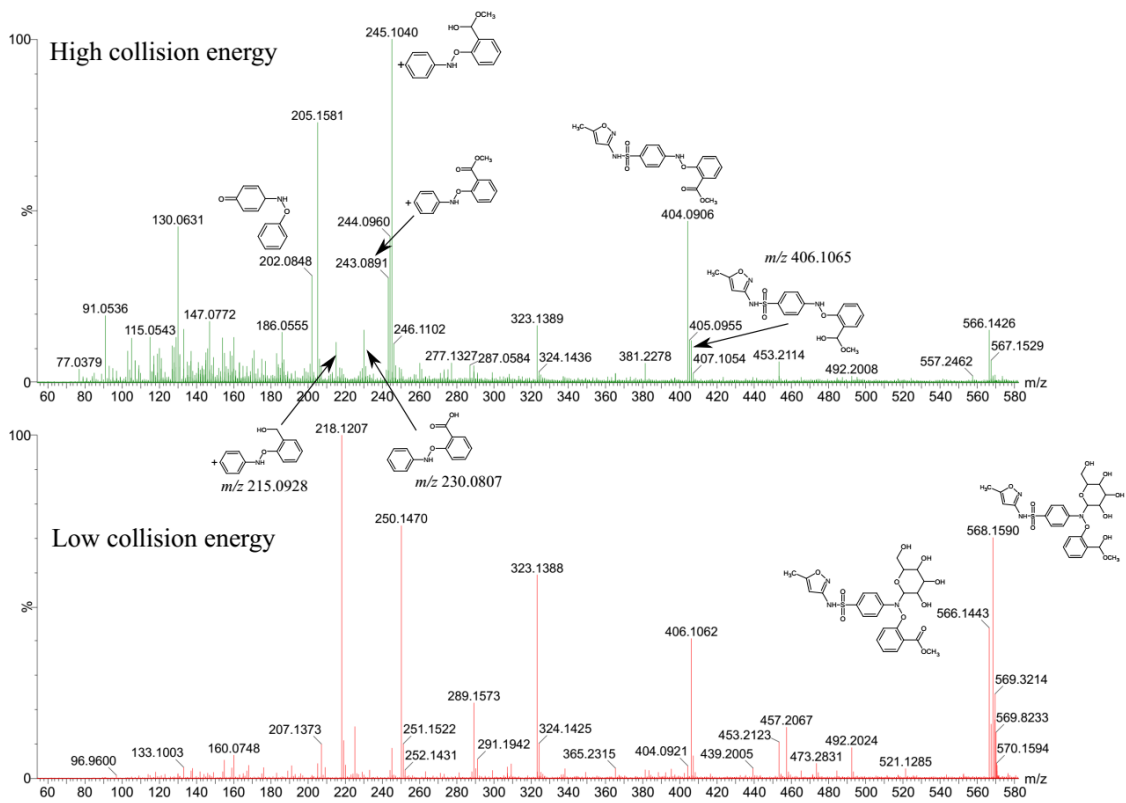
Supplementary Figure 4.6. Low and high collision energy MS^E mass spectra of N⁴-glycosyl glycoside-SMX.



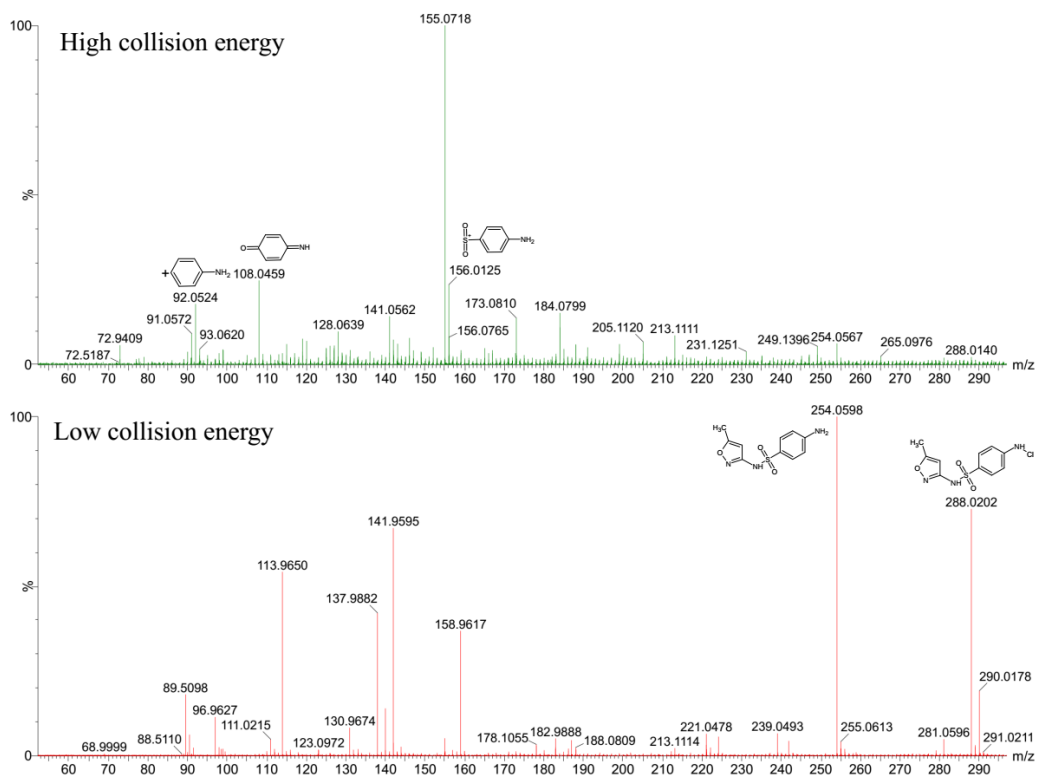
Supplementary Figure 4.7. Low and high collision energy MS^E mass spectra of the pterin-SMX conjugate.



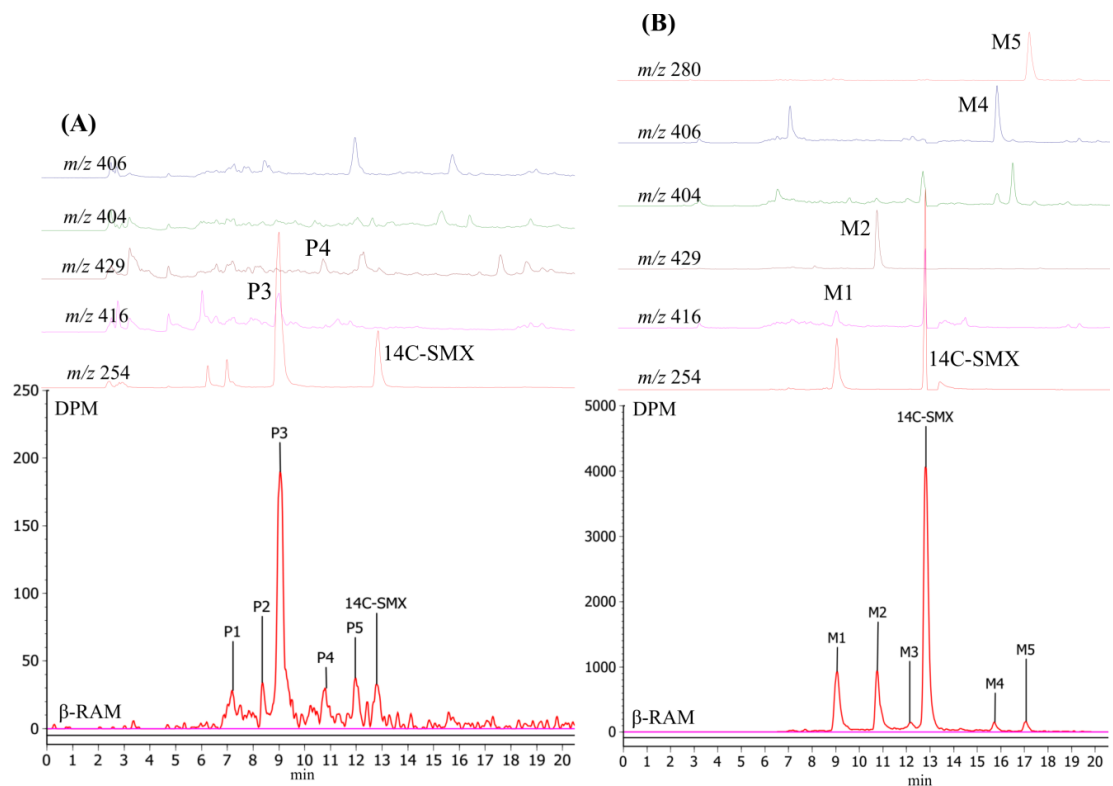
Supplementary Figure 4.8. Low and high collision energy MS^E mass spectra of the MeSA-SMX conjugates.



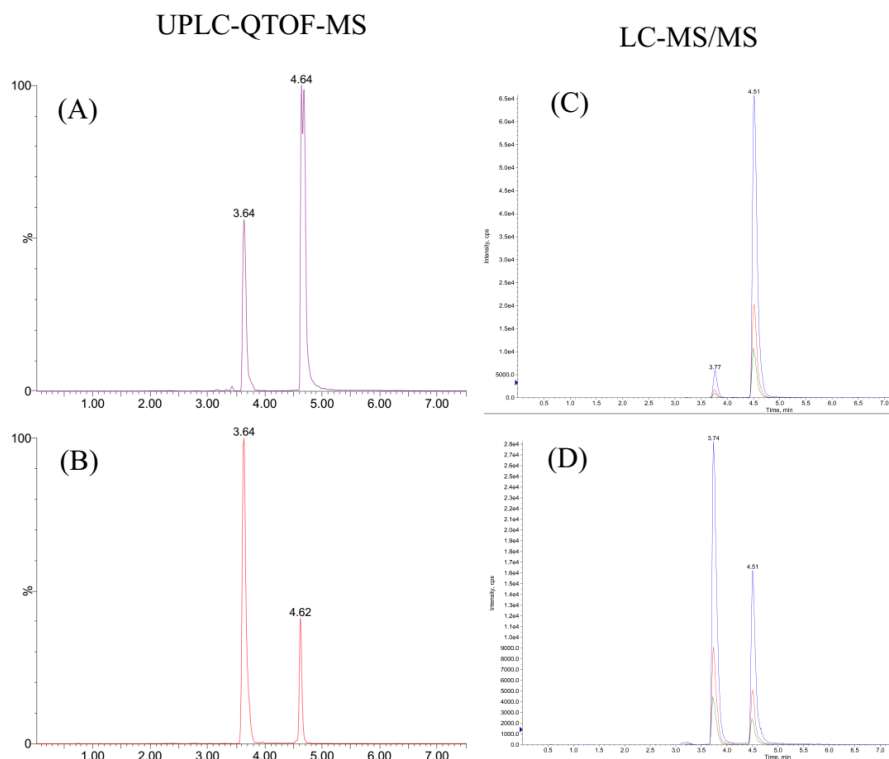
Supplementary Figure 4.9. Low and high collision energy MS^E mass spectra of the glycosylated MeSA-SMX conjugates.



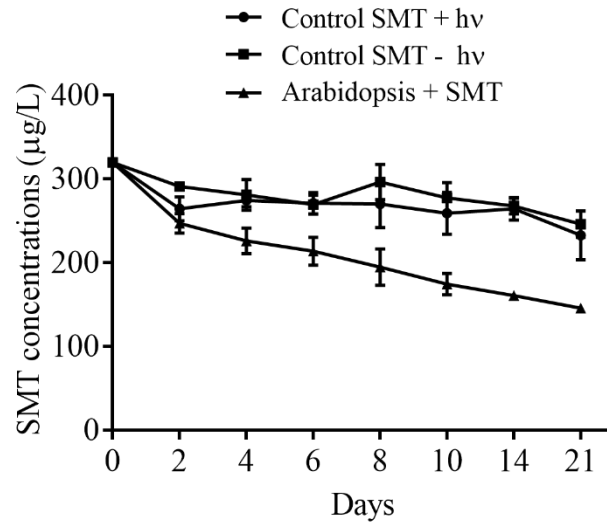
Supplementary Figure 4.10. Low and high collision energy MS^E mass spectra of the chlorinated SMX metabolites.



Supplementary Figure 4.11. Representative selected ion chromatograms of *A. thaliana* extracts (A) and culture media (B) on the LC-MS 2010 EV coupled with the on-line radioactivity detector β -RAM. In-source fragmentation of the metabolite N⁴-glycosyl-SMX (m/z 416) revealed identical mass-spectral signature with the parent SMX (m/z 254).



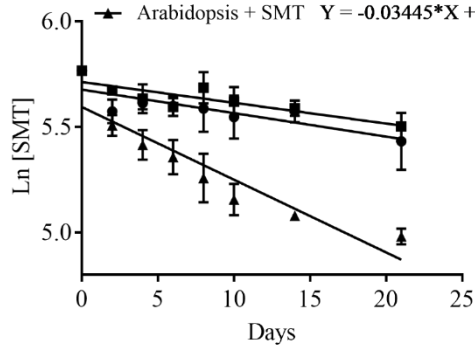
Supplementary Figure 4.12. In-source fragmentation of the metabolite N⁴-glycosyl-SMX (m/z 416) revealed peaks with identical mass-spectral signature with the parent SMX (m/z 254) at earlier retention times. The results were observed for media samples and plant extracts analyzed on UPLC-QTOF-MS^E (A and B, respectively) and LC-MS/MS in MRM mode (C and D, respectively). Accordingly, the weak conjugated bond between SMX and the glycosyl group was cleaved, releasing the parent aglycone, prior to MS analysis.



Supplementary Figure 4.13. Concentrations of SMT in *Arabidopsis*-planted and abiotic controls media (“light” and “dark” controls) during root-shoot exposure. Error bars represent standard error of triplicates; some error bars are obscured by data symbols.

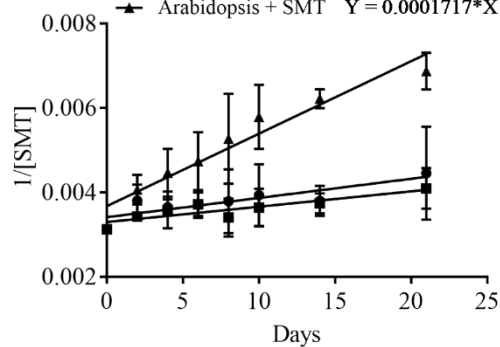
First order

	Equation	R square
● Control SMT + hv	$Y = -0.01113 * X + 5.678$	0.6888
■ Control SMT - hv	$Y = -0.009849 * X + 5.714$	0.7385
▲ Arabidopsis + SMT	$Y = -0.03445 * X + 5.596$	0.8703

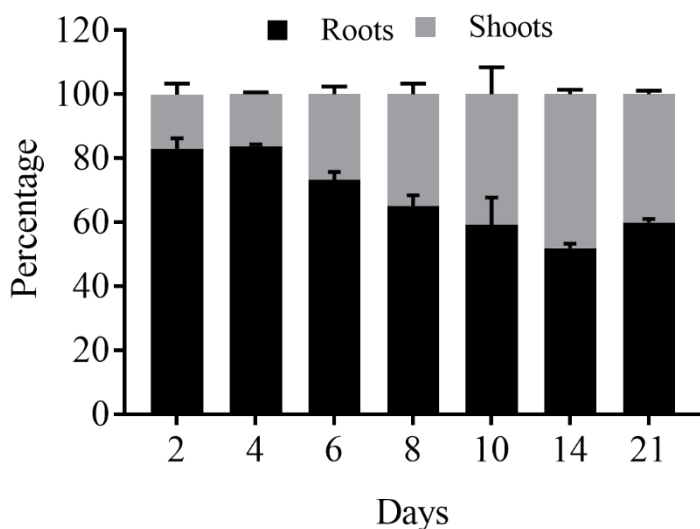


Second order

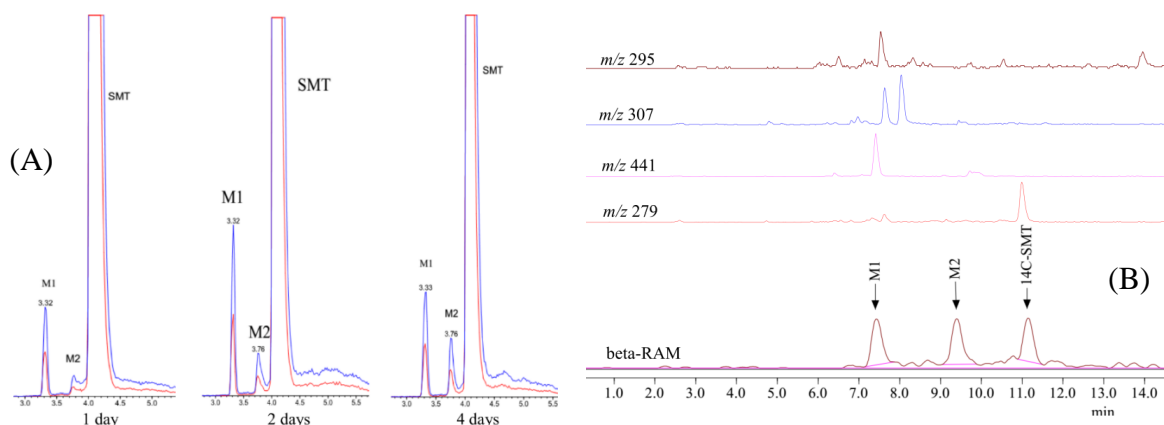
	Equation	R square
● Control SMT + hv	$Y = 4.548e-005 * X + 0.003416$	0.7314
■ Control SMT - hv	$Y = 3.635e-005 * X + 0.0033$	0.7643
▲ Arabidopsis + SMT	$Y = 0.0001717 * X + 0.003676$	0.9319



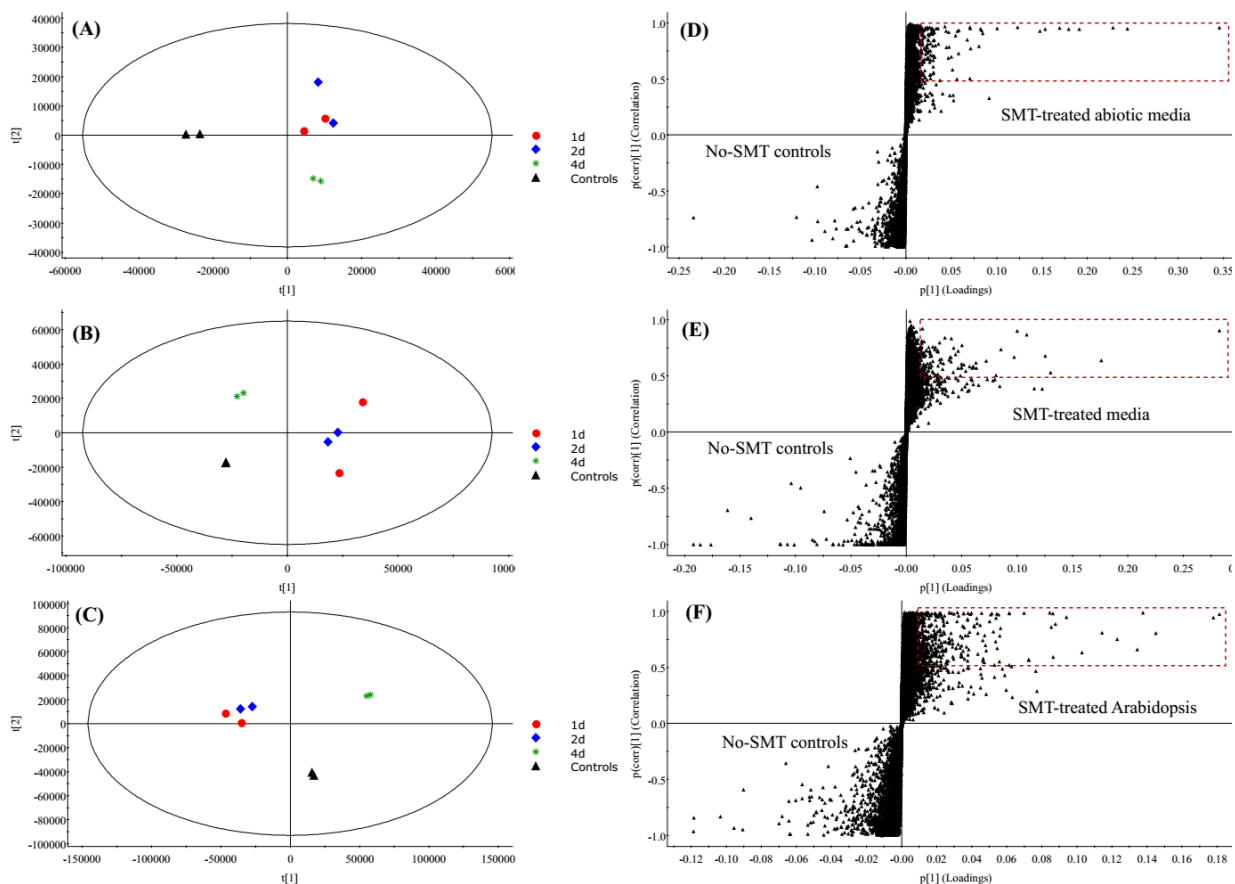
Supplementary Figure 4.14. First-order and second-order models for dissipation of SMT in the hydroponic media during root-shoot exposure (21 days). Error bars represent standard error of triplicates.



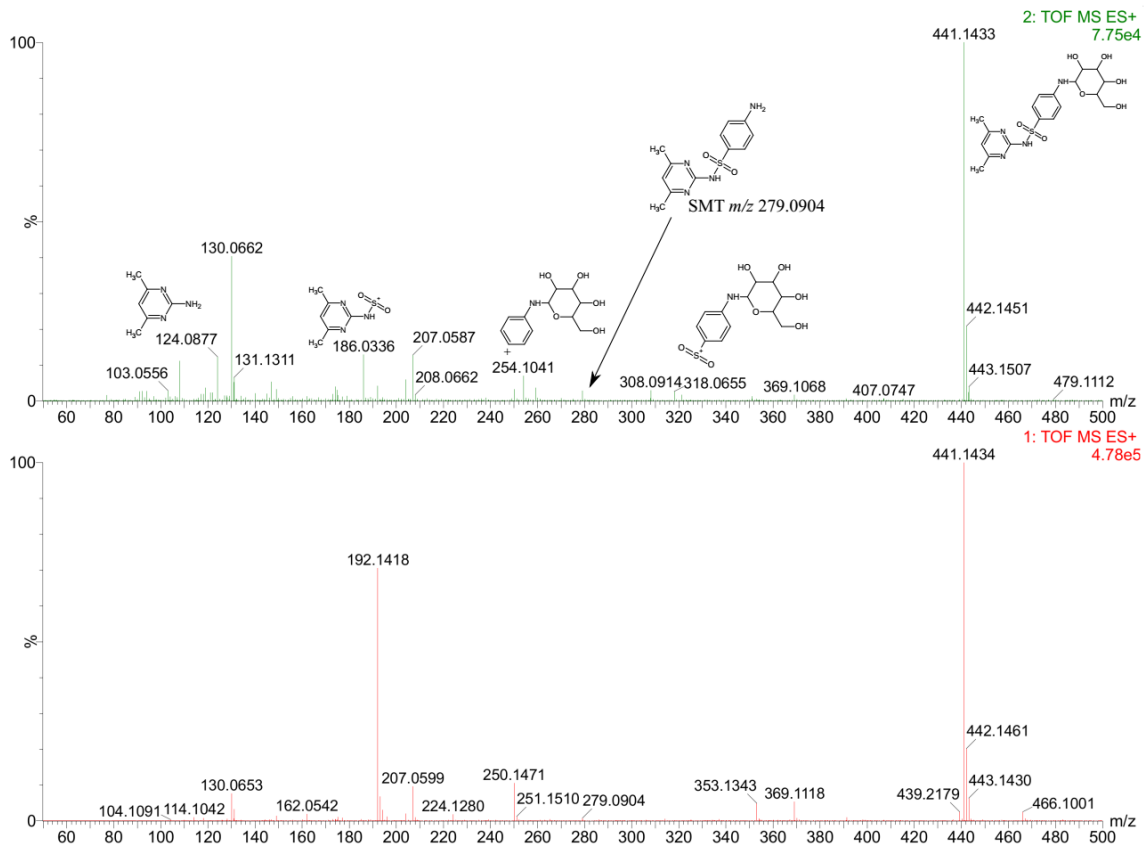
Supplementary Figure 4.15. Temporal variation in percent of SMT mass accumulated in roots and shoots of *A. thaliana* during root-shoot exposure. Error bars represent standard error of triplicates.



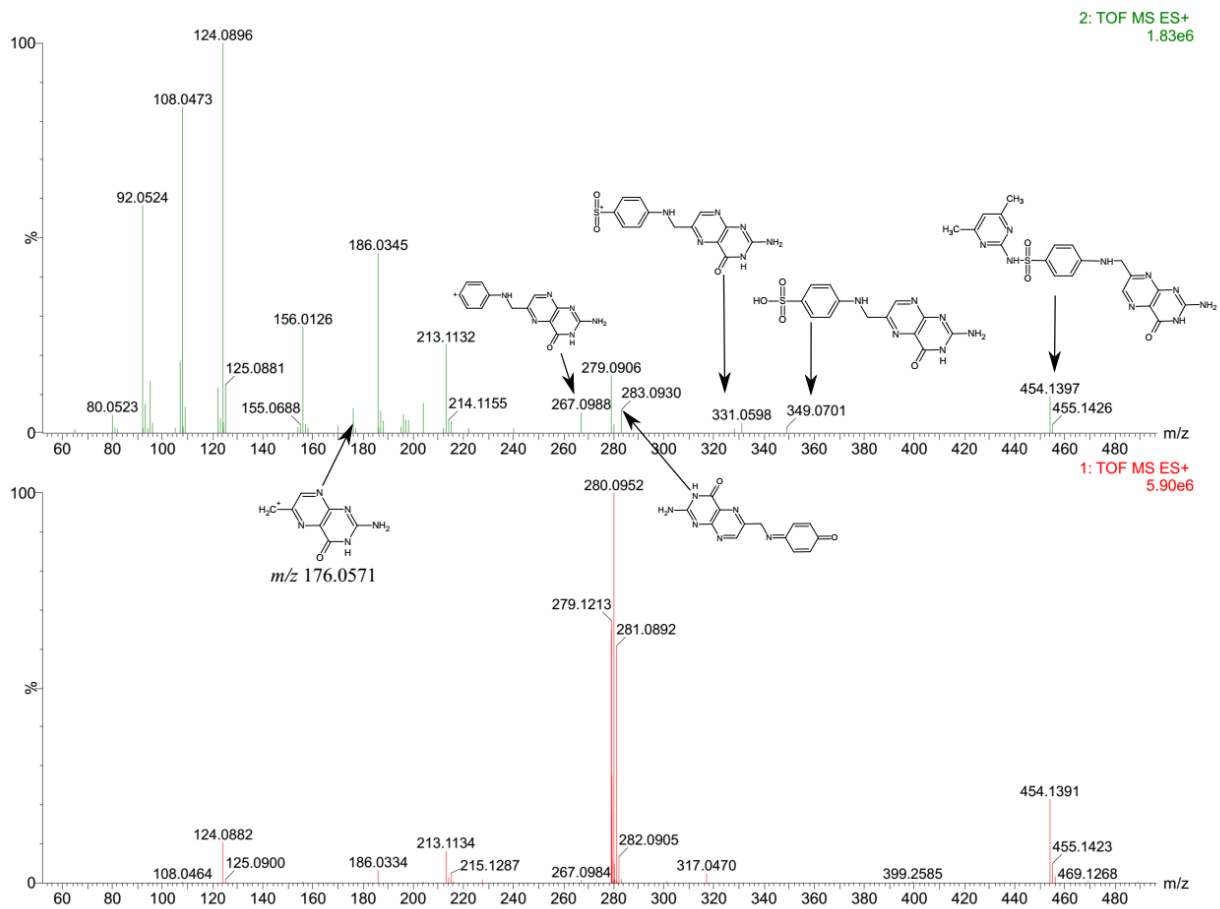
Supplementary Figure 4.16. (A): Representative LC-MS/MS chromatograms of *A. thaliana* extracts. In-source fragmentation on the mass spectrometer revealed two metabolite candidates (M1 and M2), exhibiting identical fragmentation patterns with the parent SMT in MRM mode (blue: m/z 279 \rightarrow m/z 186, red: m/z 279 \rightarrow m/z 156). Accordingly, the weak conjugated bonds between SMT and the functional groups were likely cleaved, releasing the parent molecule, prior to MS/MS analysis. All three chromatograms were magnified using the same scale to visualize M1 and M2 peaks. (B): Selected ion chromatograms of *A. thaliana* extracts on the LC-MS 2010 EV coupled with the on-line radioactivity detector β -RAM.



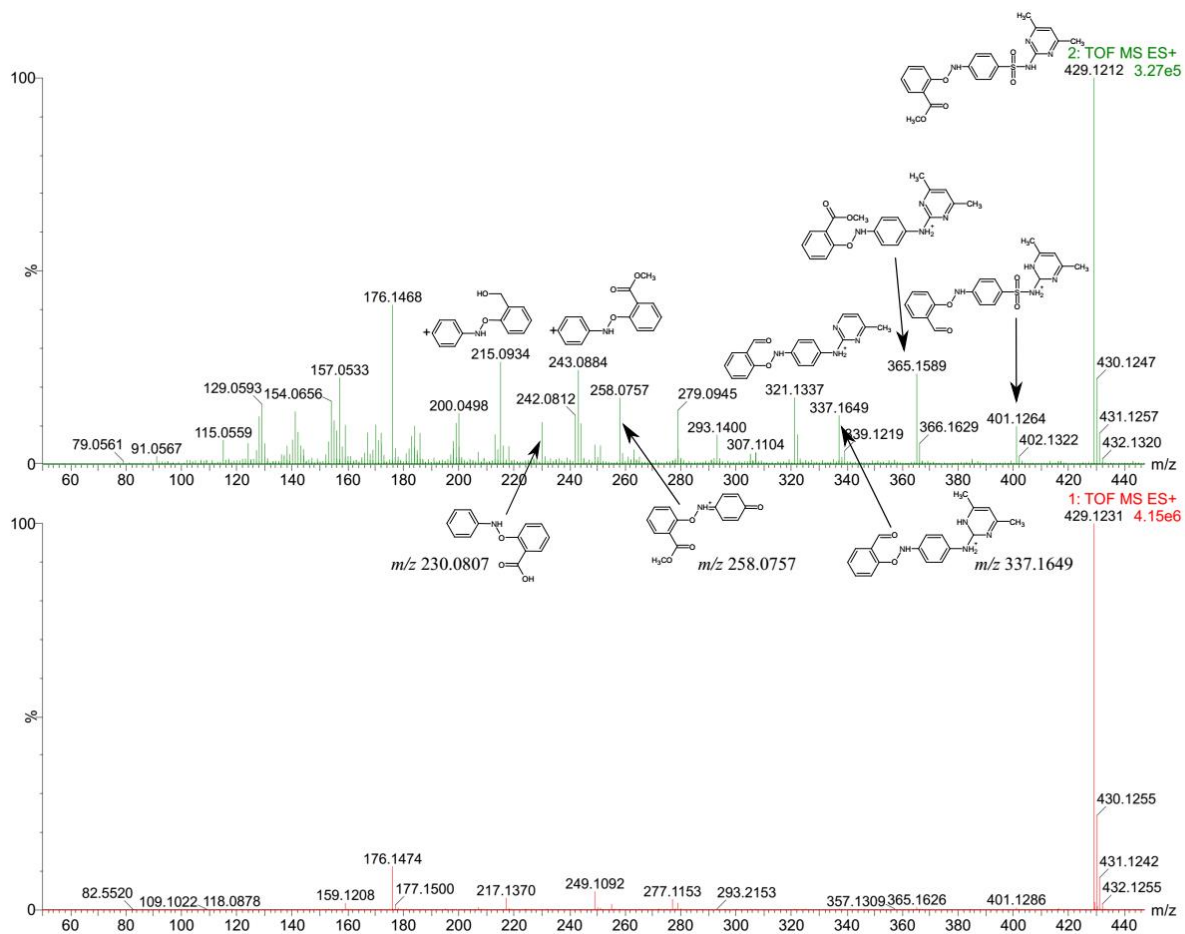
Supplementary Figure 4.17. Principal component analysis (PCA) score plots (A–C) and the S-plots from orthogonal projection to latent structures-discriminant analysis (OPLS-DA) (D–F) of the abiotic media, planted media and *A. thaliana* samples, respectively, obtained by processing QTOF-MS^E high resolution mass spectra using Progenesis QI 2.1 and EZInfo 3.0 platforms. Controls: control plants/media without SMT exposure; 1d, 2d, 4d: plants/media exposed to SMT for 1, 2 and 4 days, respectively. The dashed rectangles on the S-plots include m/z variables that significantly contribute to the differences between control and SMT-exposed samples ($p(\text{corr}) \geq 0.5$). All treatments were performed in duplicates. Some data symbols are overlapped on the PCA score plots.



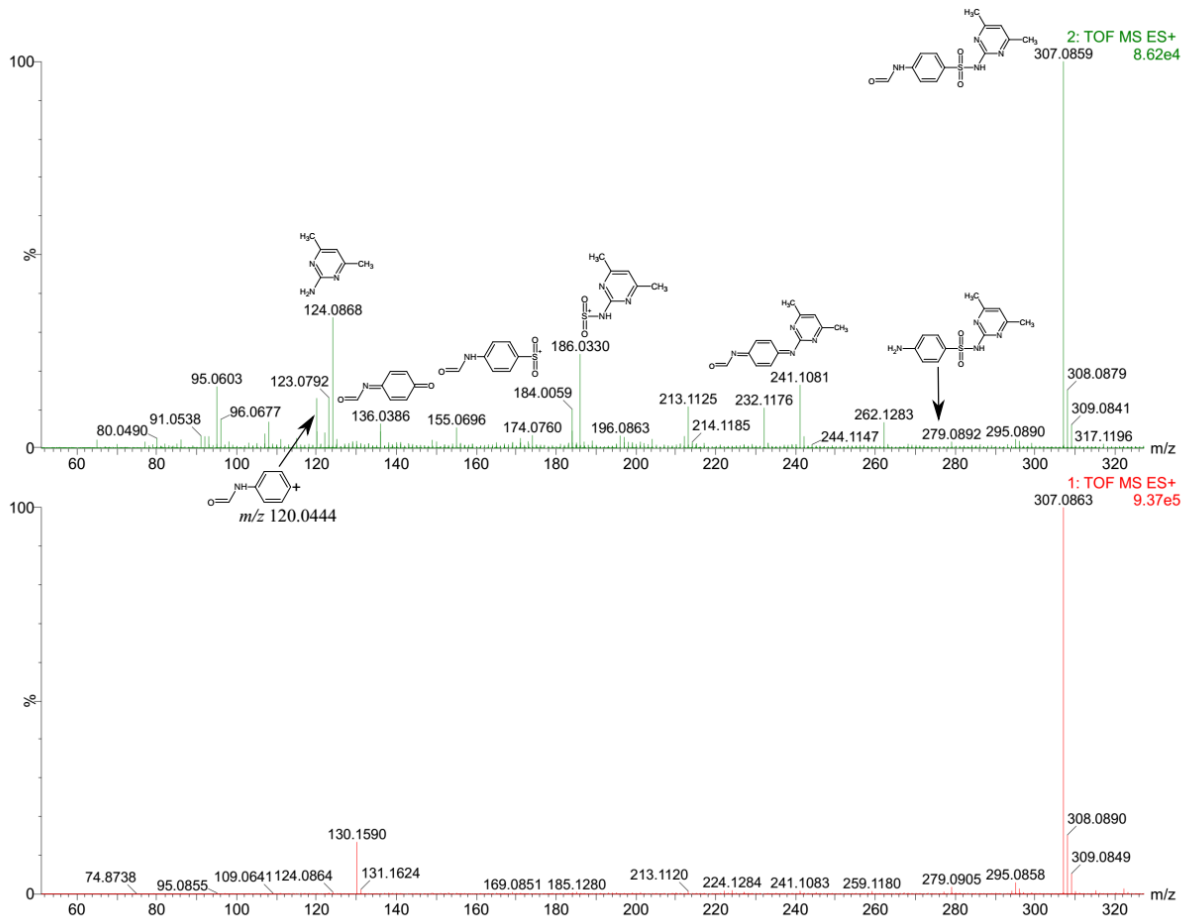
Supplementary Figure 4.18. Low collision energy mass spectra (lower panel) and high collision energy mass spectra (upper panel) obtained using ESI (+)-QTOF-MS^E for N⁴-glycosyl SMT.



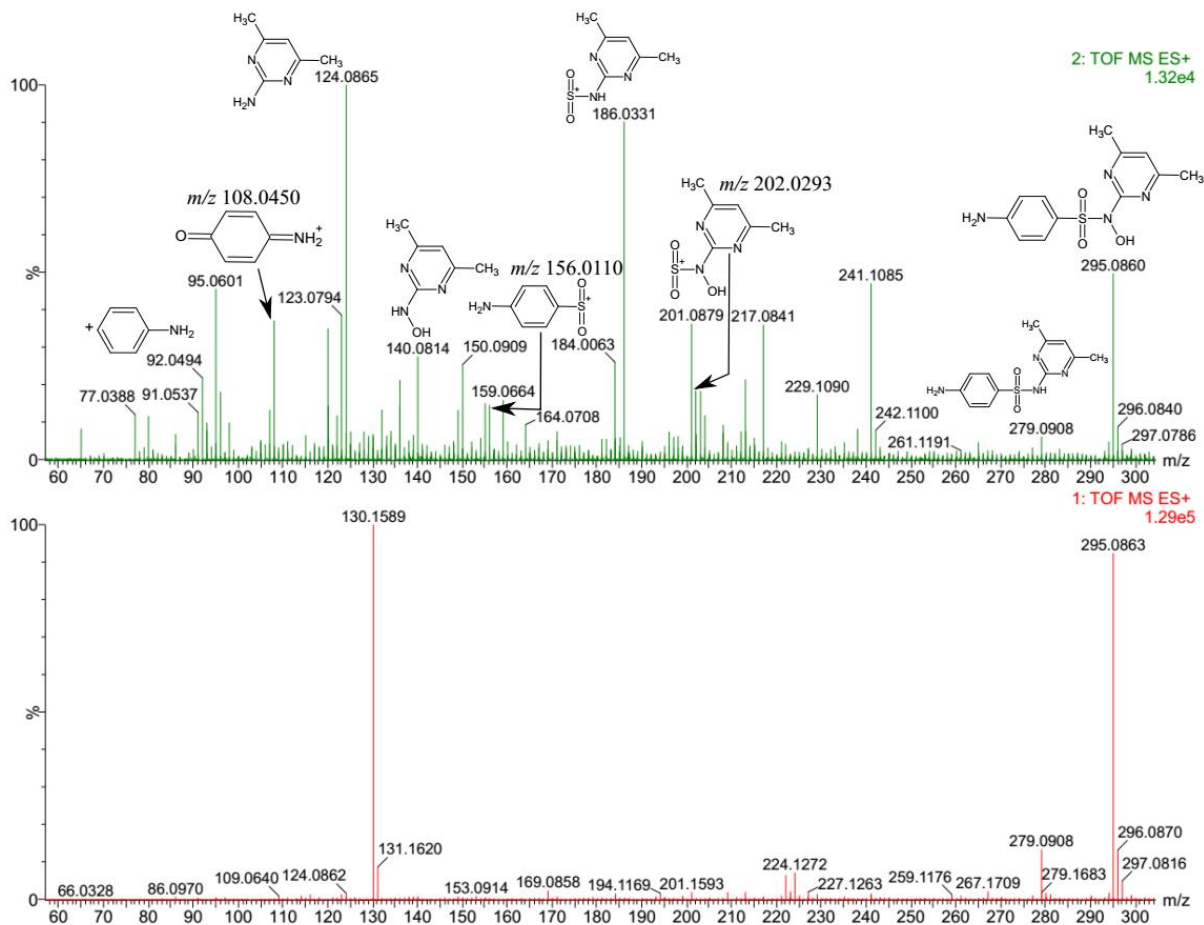
Supplementary Figure 4.19. Low collision energy mass spectra (lower panel) and high collision energy mass spectra (upper panel) obtained using ESI (+)-QTOF-MS^E for pterin SMT.



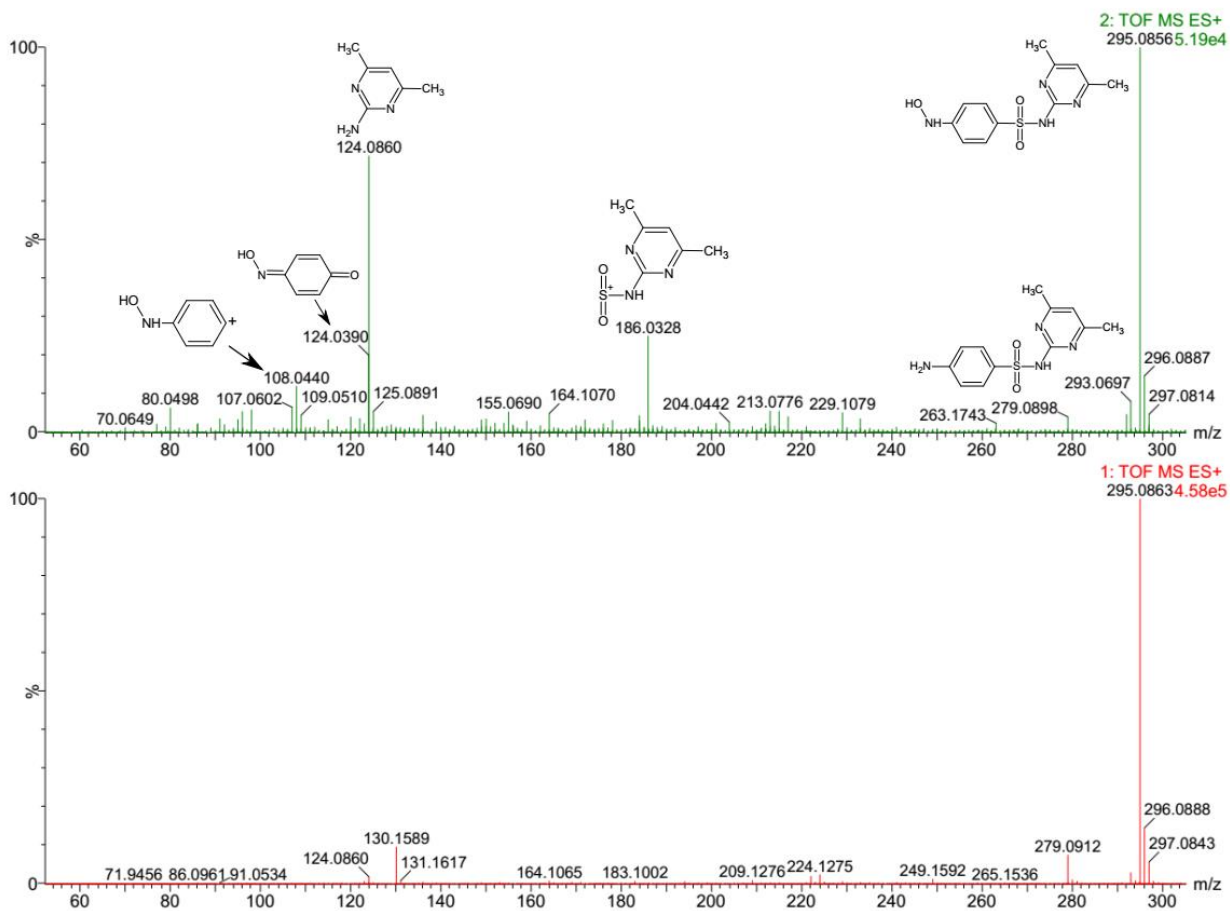
Supplementary Figure 4.20. Low collision energy mass spectra (lower panel) and high collision energy mass spectra (upper panel) obtained using ESI (+)-QTOF-MS^E for methyl-salicylate SMT.



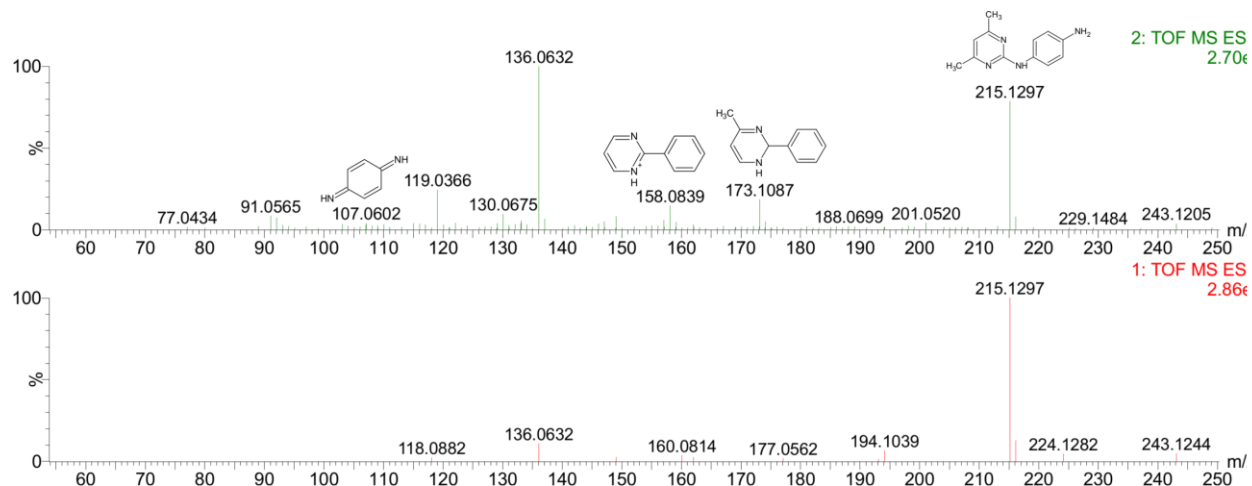
Supplementary Figure 4.21. Low collision energy mass spectra (lower panel) and high collision energy mass spectra (upper panel) obtained using ESI (+)-QTOF-MS^E for N⁴-formyl SMT.



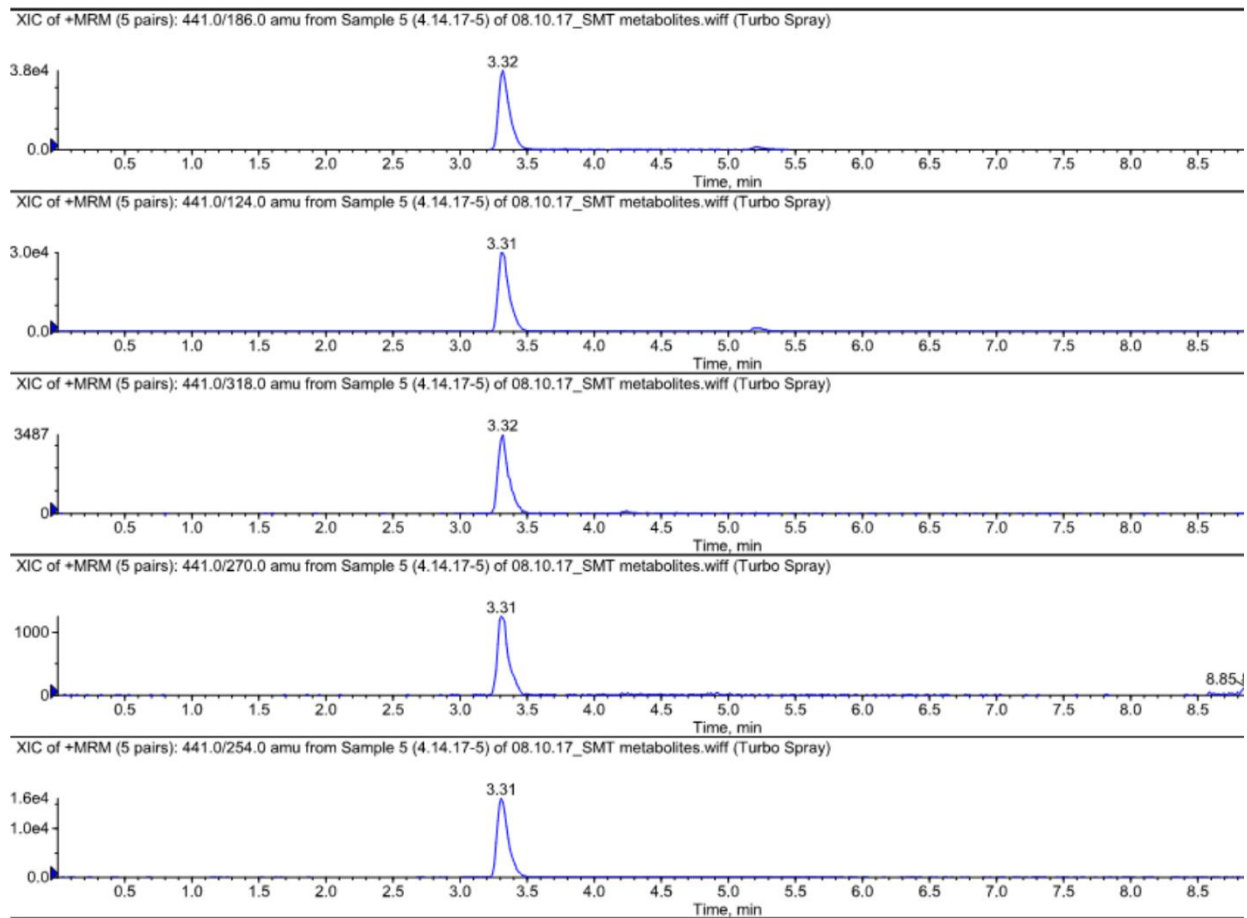
Supplementary Figure 4.22. Low collision energy mass spectra (lower panel) and high collision energy mass spectra (upper panel) obtained using ESI (+)-QTOF-MS^E for hydroxyl SMT-1, with N¹-OH SMT as representative metabolite.



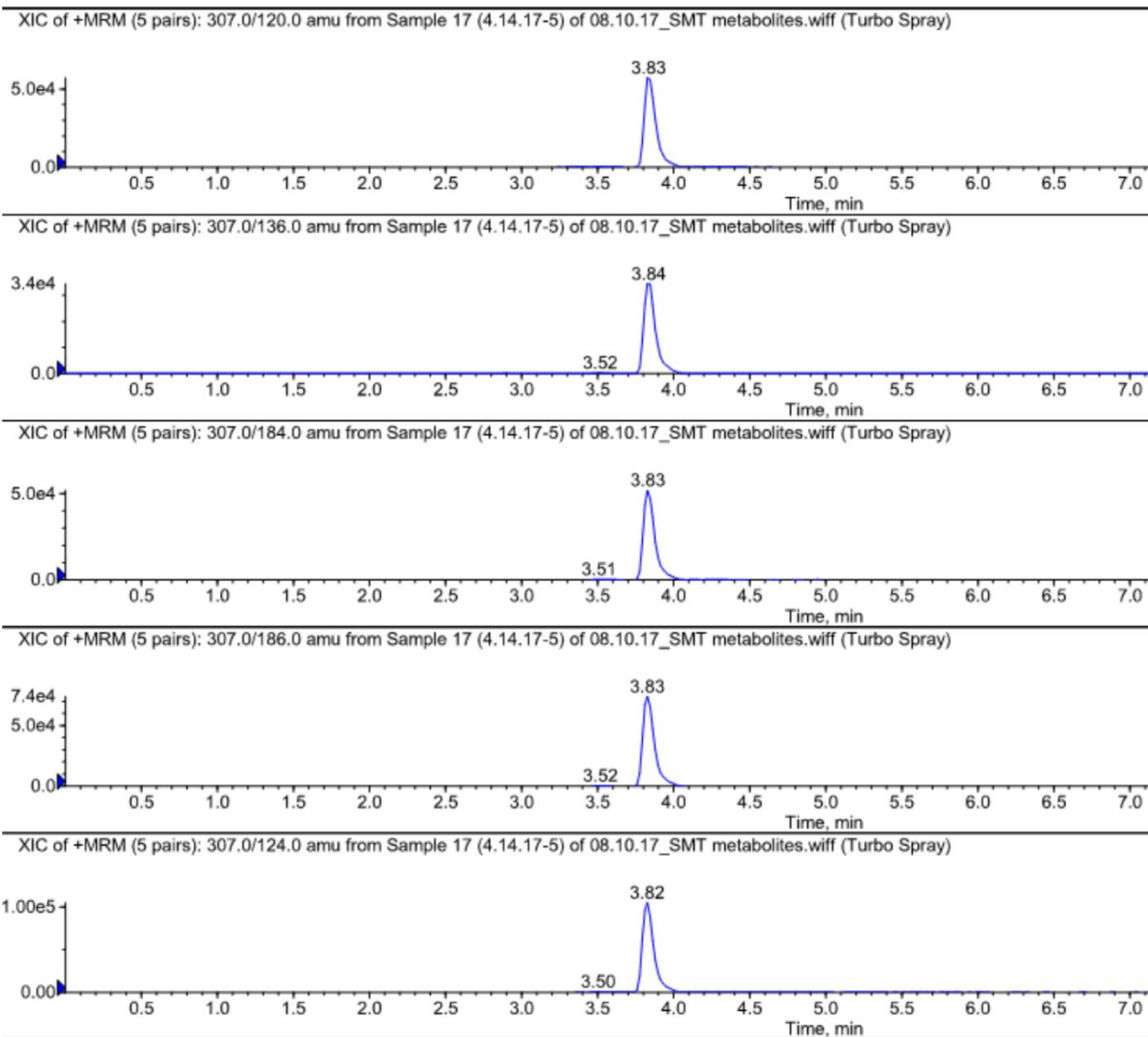
Supplementary Figure 4.23. Low collision energy mass spectra (lower panel) and high collision energy mass spectra (upper panel) obtained using ESI (+)-QTOF-MS^E for hydroxyl SMT-2, with N⁴-OH SMT as representative metabolite.



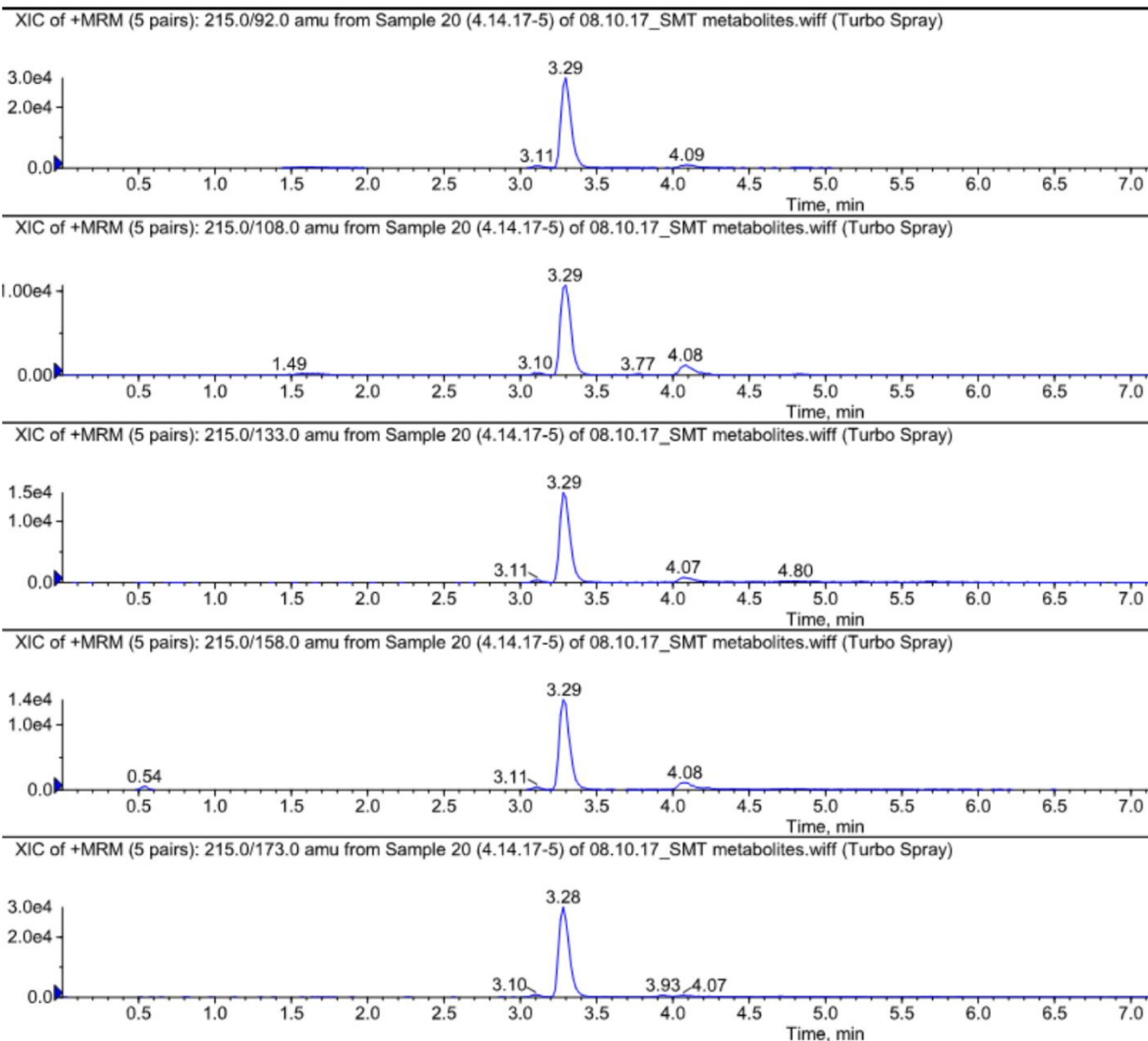
Supplementary Figure 4.24. Low collision energy mass spectra (lower panel) and high collision energy mass spectra (upper panel) obtained using ESI (+)-QTOF-MS^B for desulfo SMT.



Supplementary Figure 4.25. Selected ion chromatograms of N⁴-glycosyl SMT (RT = 3.32 min) on the LC-MS/MS system applying ESI (+) in MRM mode (Majewsky et al., 2015).

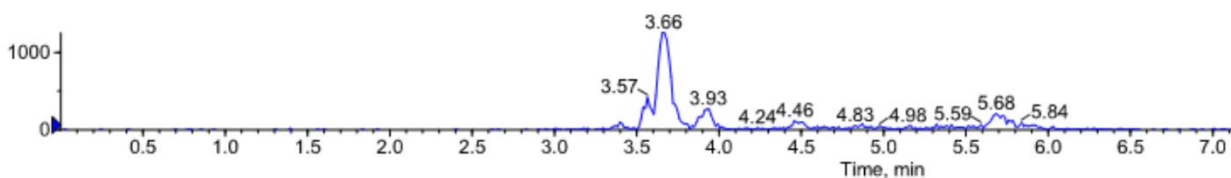


Supplementary Figure 4.26. Selected ion chromatograms of formyl SMT (RT = 3.83 min) on the LC-MS/MS system applying ESI (+) in MRM mode (Majewsky et al., 2015).

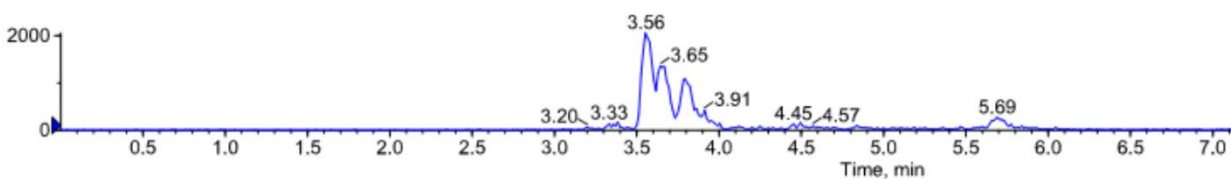


Supplementary Figure 4.27. Selected ion chromatograms of desulfo SMT (RT = 3.11 min and 3.29 min) on the LC-MS/MS system applying ESI (+) in MRM mode (García-Galán et al., 2011). The peak emerged at Rt = 4.09 min potentially represents the artifact from in-source fragmentation of SMT prior to MS analysis (Wang et al., 2003).

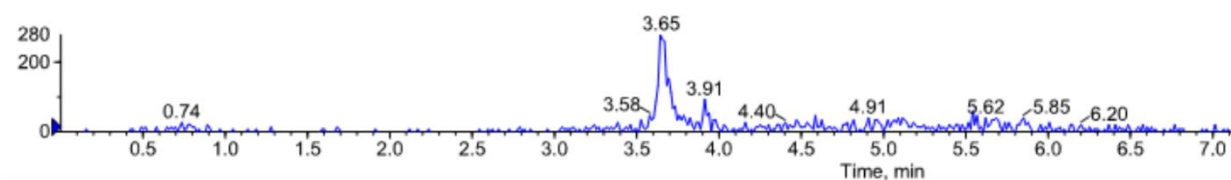
XIC of +MRM (5 pairs): 295.0/92.0 amu from Sample 14 (4.14.17-5) of 08.10.17_SMT metabolites.wiff (Turbo Spray)



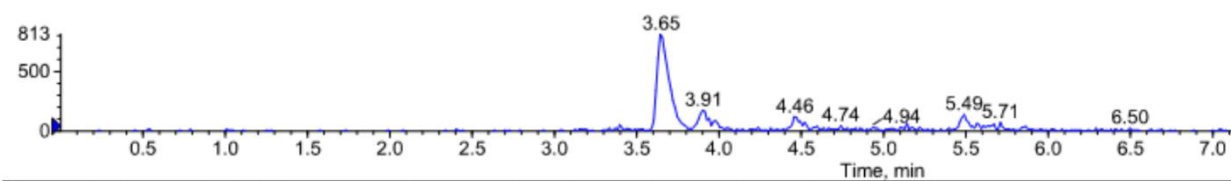
XIC of +MRM (5 pairs): 295.0/108.0 amu from Sample 14 (4.14.17-5) of 08.10.17_SMT metabolites.wiff (Turbo Spray)



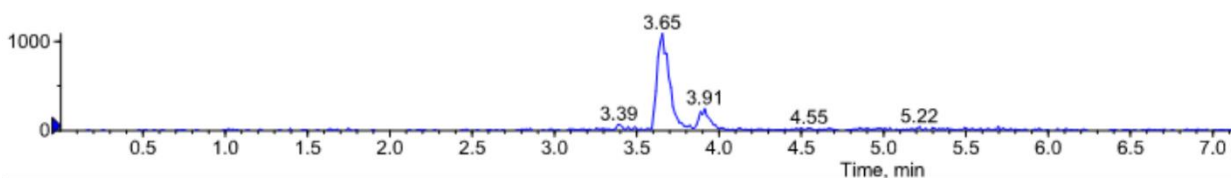
XIC of +MRM (5 pairs): 295.0/156.0 amu from Sample 14 (4.14.17-5) of 08.10.17_SMT metabolites.wiff (Turbo Spray)



XIC of +MRM (5 pairs): 295.0/202.0 amu from Sample 14 (4.14.17-5) of 08.10.17_SMT metabolites.wiff (Turbo Spray)

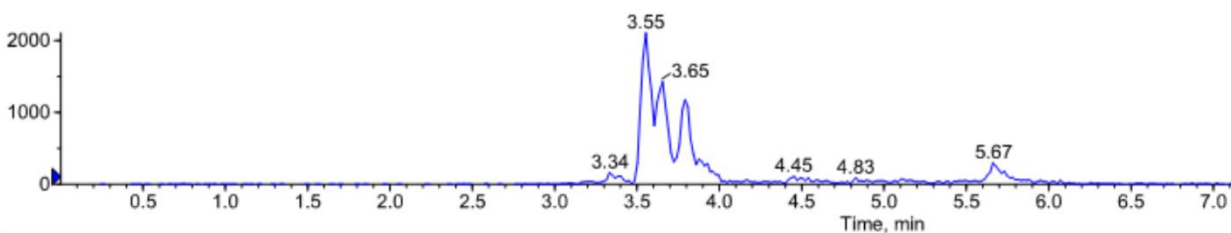


XIC of +MRM (5 pairs): 295.0/140.0 amu from Sample 14 (4.14.17-5) of 08.10.17_SMT metabolites.wiff (Turbo Spray)

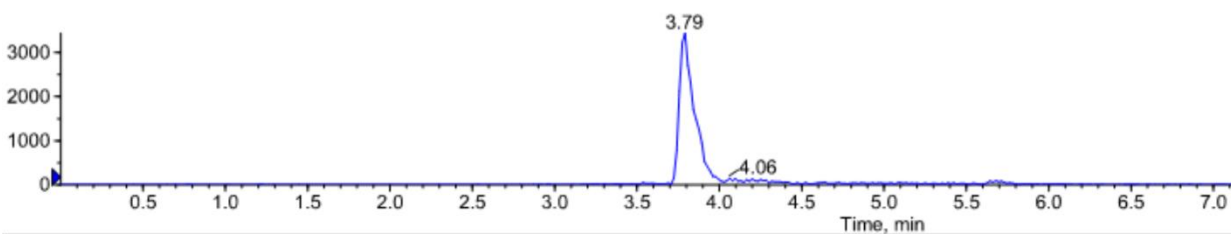


Supplementary Figure 4.28. Selected ion chromatograms of hydroxyl SMT-1 (RT = 3.65 min and 3.91 min) on the LC-MS/MS system applying ESI (+) in MRM mode (Majewsky et al., 2015).

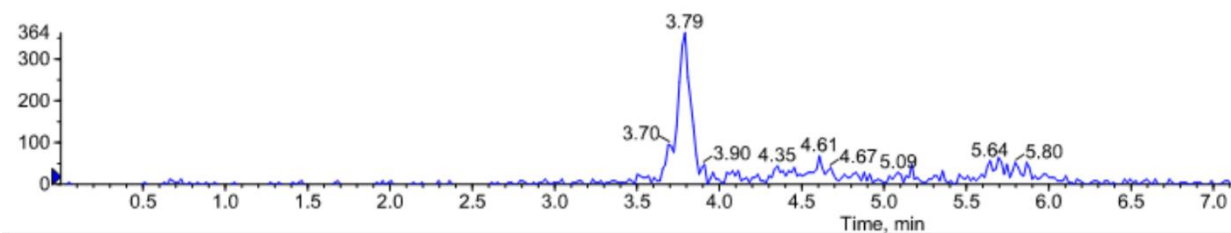
XIC of +MRM (4 pairs): 295.0/108.0 amu from Sample 8 (4.14.17-5) of 08.10.17_SMT metabolites.wiff (Turbo Spray)



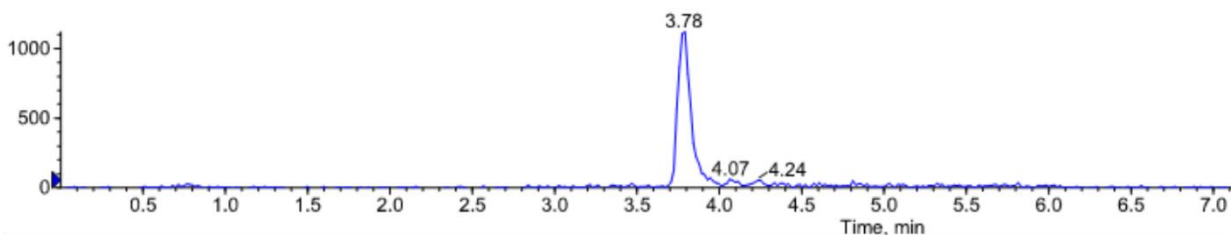
XIC of +MRM (4 pairs): 295.0/124.0 amu from Sample 8 (4.14.17-5) of 08.10.17_SMT metabolites.wiff (Turbo Spray)



XIC of +MRM (4 pairs): 295.0/172.0 amu from Sample 8 (4.14.17-5) of 08.10.17_SMT metabolites.wiff (Turbo Spray)

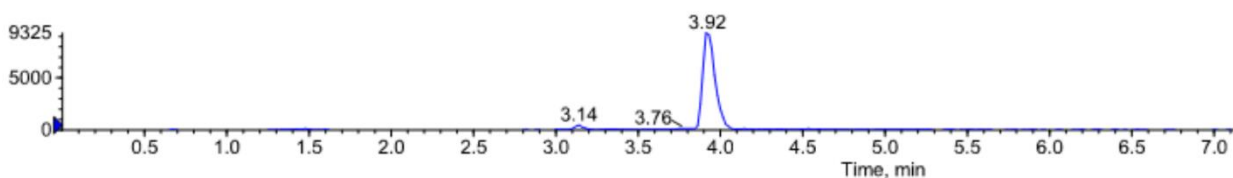


XIC of +MRM (4 pairs): 295.0/186.0 amu from Sample 8 (4.14.17-5) of 08.10.17_SMT metabolites.wiff (Turbo Spray)

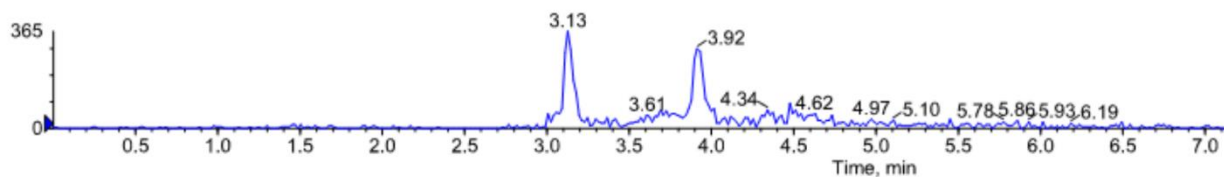


Supplementary Figure 4.29. Selected ion chromatograms of hydroxyl SMT-2 (RT = 3.79 min) on the LC-MS/MS system applying ESI (+) in MRM mode (Majewsky et al., 2015).

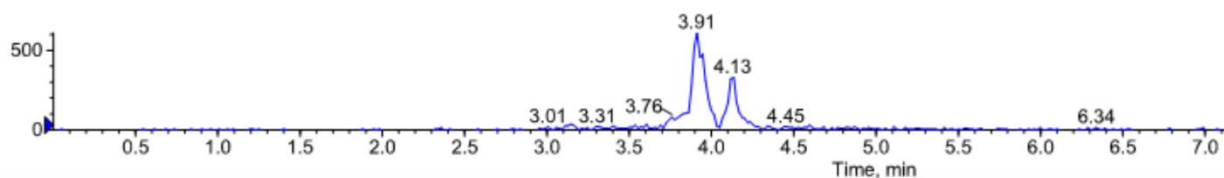
XIC of +MRM (5 pairs): 321.0/134.0 amu from Sample 26 (4.14.17-5) of 08.10.17_SMT metabolites.wiff (Turbo Spray)



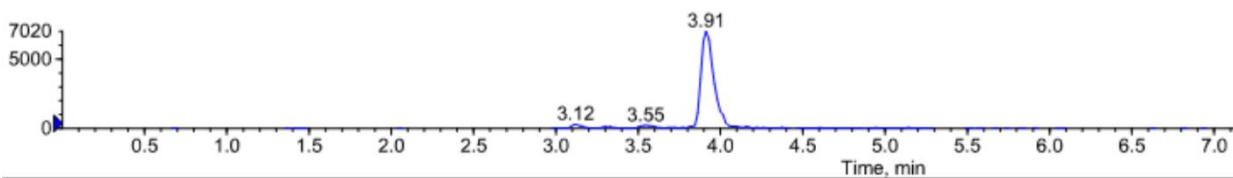
XIC of +MRM (5 pairs): 321.0/150.0 amu from Sample 26 (4.14.17-5) of 08.10.17_SMT metabolites.wiff (Turbo Spray)



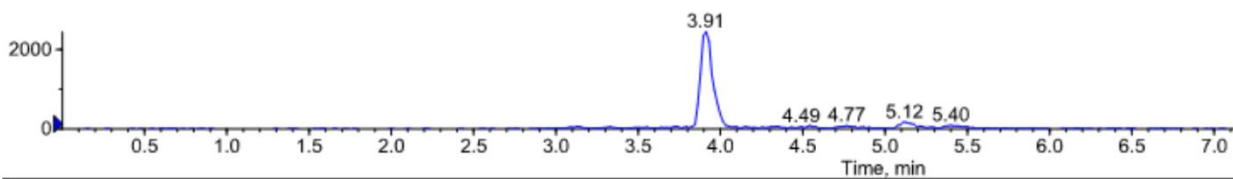
XIC of +MRM (5 pairs): 321.0/198.0 amu from Sample 26 (4.14.17-5) of 08.10.17_SMT metabolites.wiff (Turbo Spray)



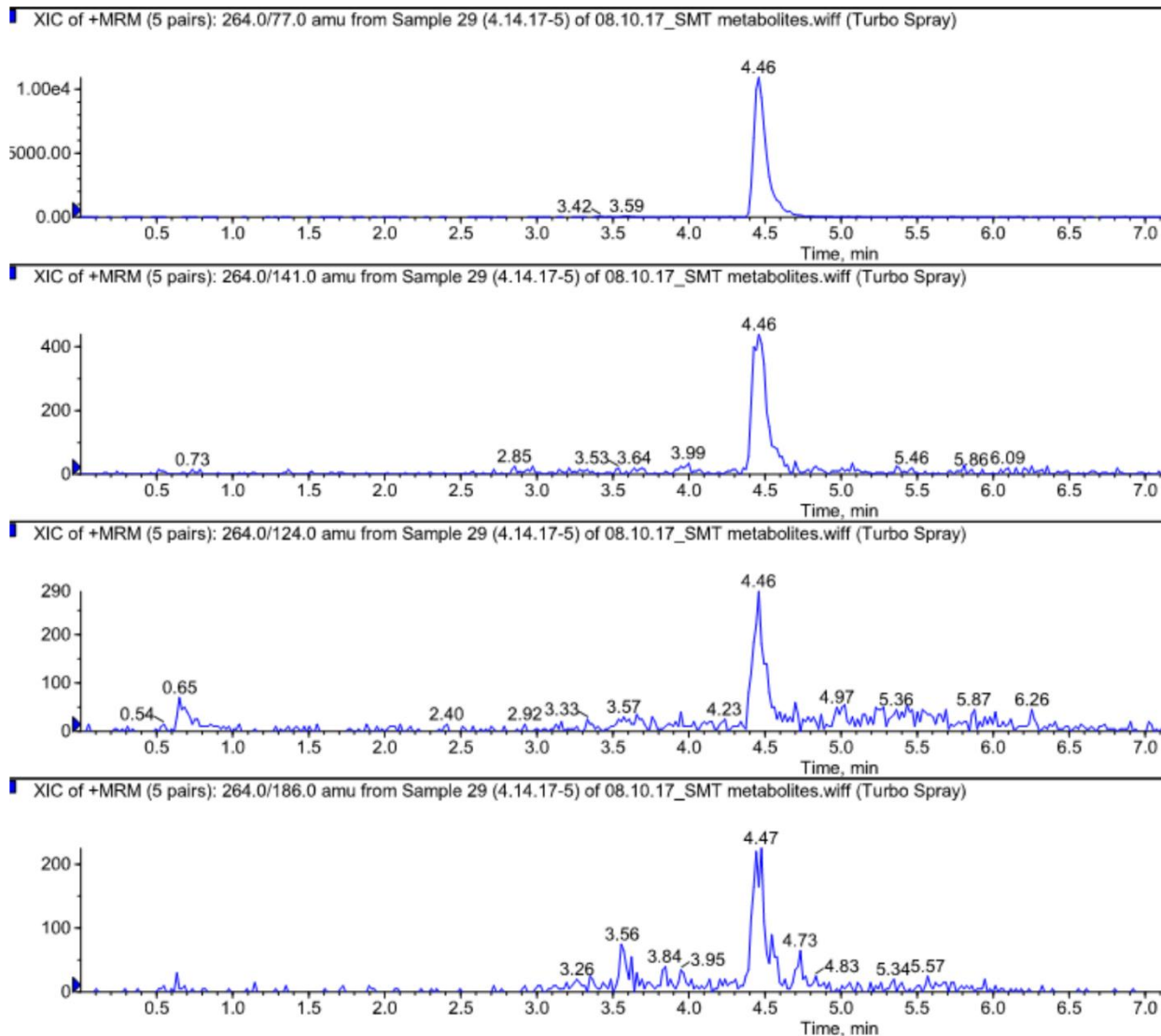
XIC of +MRM (5 pairs): 321.0/124.0 amu from Sample 26 (4.14.17-5) of 08.10.17_SMT metabolites.wiff (Turbo Spray)



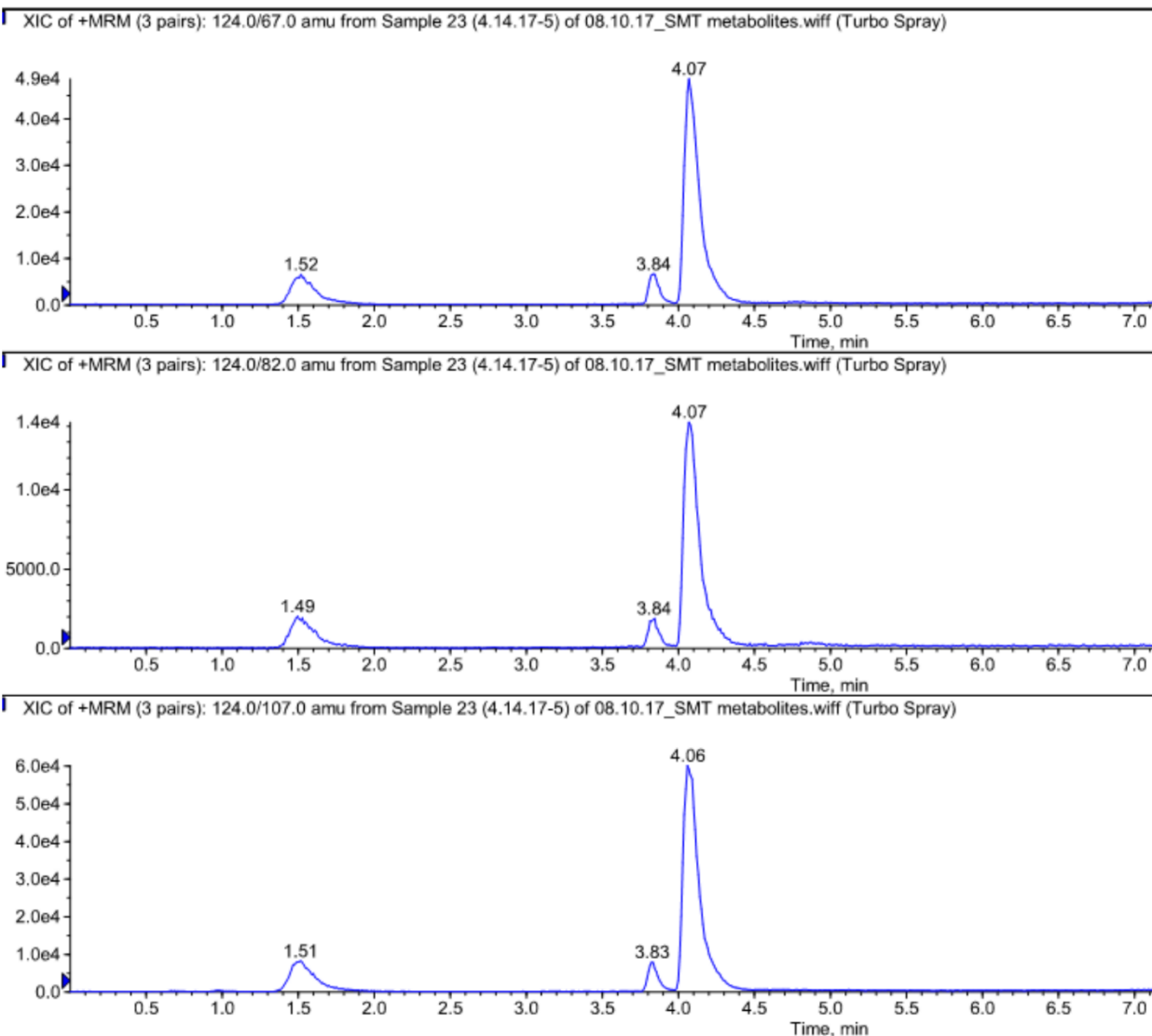
XIC of +MRM (5 pairs): 321.0/186.0 amu from Sample 26 (4.14.17-5) of 08.10.17_SMT metabolites.wiff (Turbo Spray)



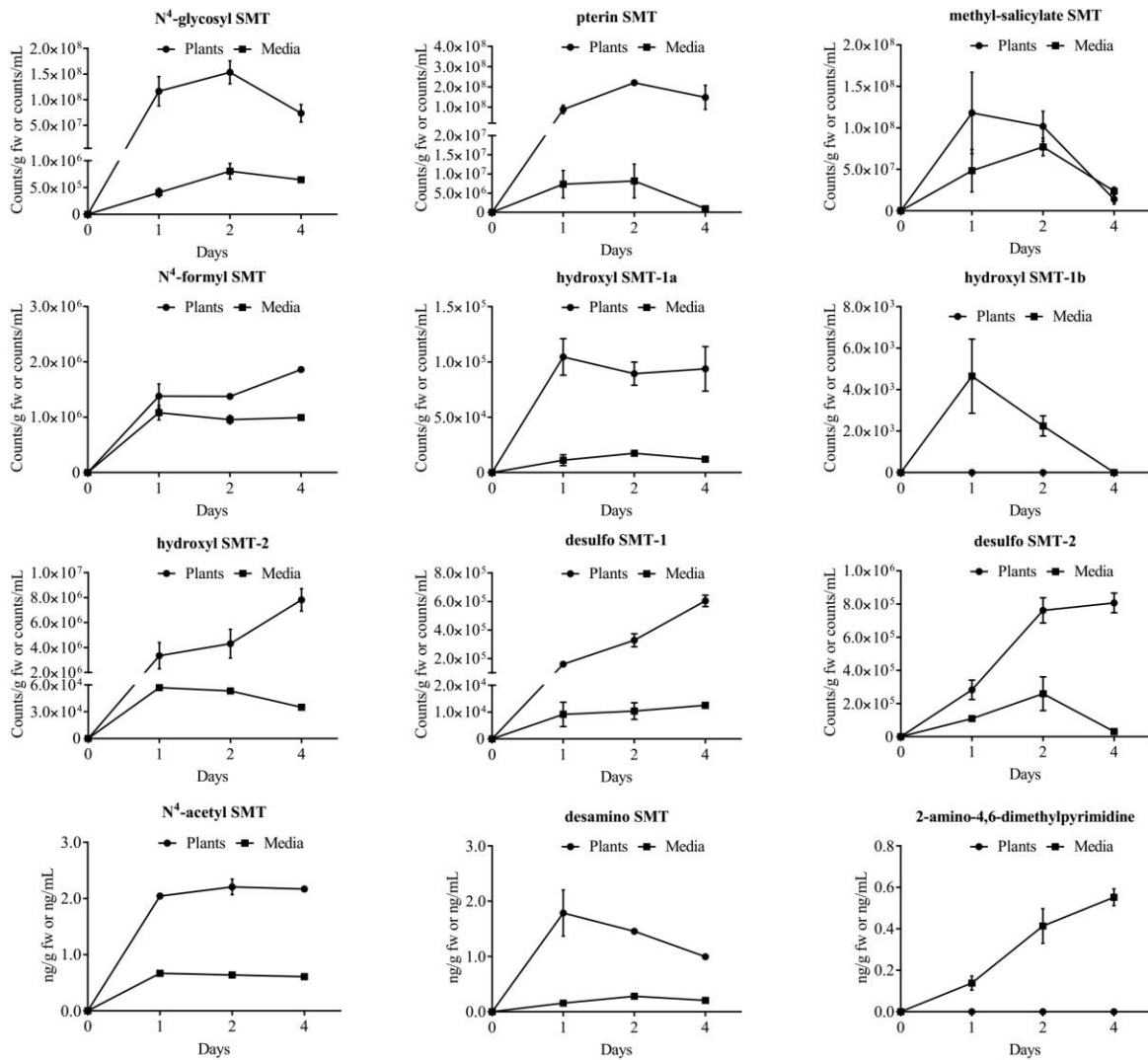
Supplementary Figure 4.30. Selected ion chromatograms of N⁴-acetyl SMT (RT = 3.92 min) on the LC-MS/MS system applying ESI (+) in MRM mode (Majewsky et al., 2015).



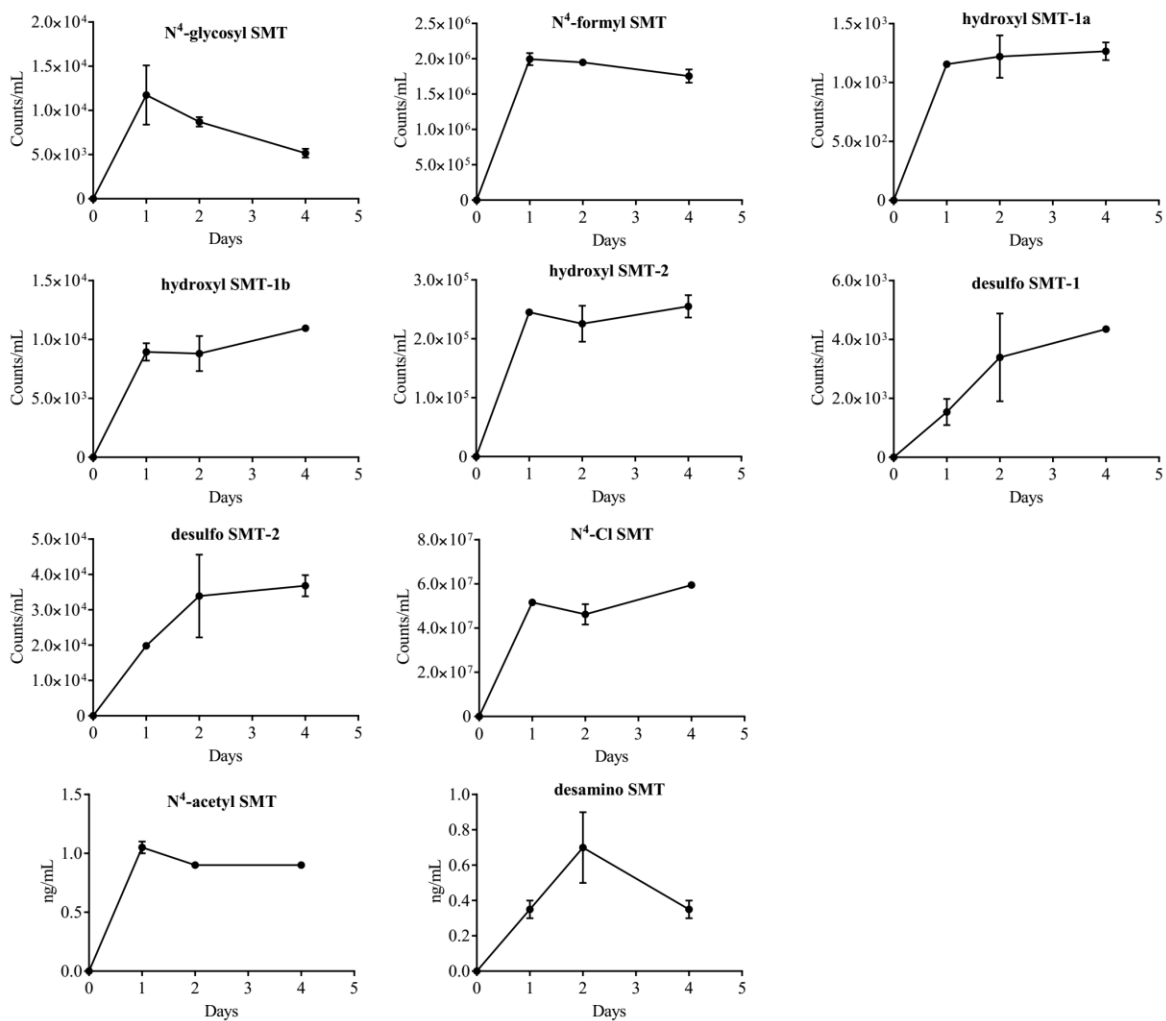
Supplementary Figure 4.31. Selected ion chromatograms of desamino SMT (RT = 4.46 min) on the LC-MS/MS system applying ESI (+) in MRM mode (Majewsky et al., 2015).



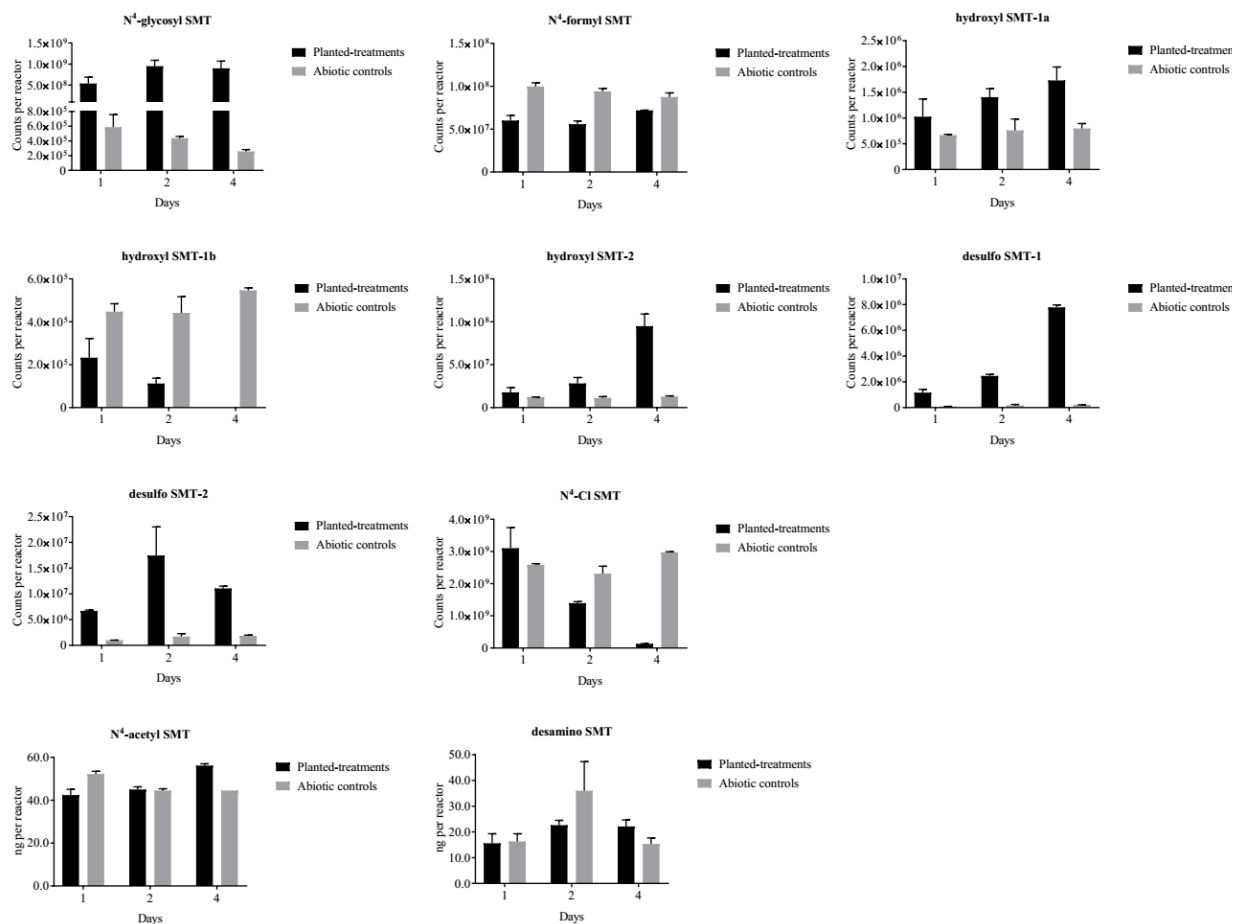
Supplementary Figure 4.32. Selected ion chromatograms of 2-amino-4,6-dimethylpyrimidine on the LC-MS/MS system (RT = 1.52 min) applying ESI (+) in MRM mode. Similar precursor ion (m/z 124) was likely derived from the parent SMT (RT = 4.07 min) and formyl SMT (RT = 3.84 min), leading to similar MRM transitions.



Supplementary Figure 4.33. Temporal variation of SMT metabolites in plant tissues and media during whole-plant exposure of *A. thaliana* to unlabeled SMT at a concentration of 3 µg/mL. The peak areas of pterin SMT and methyl-salicylate SMT were obtained from the UPLC-QTOF-MS^E system, while those of the remaining metabolites were from the LC-MS/MS system in MRM mode.



Supplementary Figure 4.34. Temporal variation of SMT metabolites in the abiotic controls. The peak areas of N⁴-Cl SMT were obtained from the UPLC-QTOF-MS^E system, while those of the remaining metabolites were from the LC-MS/MS system in MRM mode.



Supplementary Figure 4.35. Abundance of the SMT products per each container over 4 days of whole-plant exposure. For the planted-treatments, the amount of each product equals the sum of its abundance in plant tissues and culture media, while that of the corresponding abiotic controls represents the amount in media.

REFERENCES

REFERENCES

- Accinelli, C., Koskinen, W.C., Becker, J.M. and Sadowsky, M.J., 2007. Environmental fate of two sulfonamide antimicrobial agents in soil. *J. Agric. Food Chem.* 55, 2677-2682.
- Achermann, S., Bianco, V., Mansfeldt, C.B., Vogler, B., Kolvenbach, B.A., Corvini, P.F.X. and Fenner, K., 2018. Biotransformation of Sulfonamide Antibiotics in Activated Sludge: The Formation of Pterin-Conjugates Leads to Sustained Risk. *Environ. Sci. Technol.* 52, 6265-6274.
- Ahmed, M.B.M., Rajapaksha, A.U., Lim, J.E., Vu, N.T., Kim, I.S., King, H.M., Lee, S.S. and Ok, Y.S., 2015. Distribution and Accumulative Pattern of Tetracyclines and Sulfonamides in Edible Vegetables of Cucumber, Tomato, and Lettuce. *J. Agric. Food Chem.* 63, 398-405.
- Aust, M.-O., Godlinski, F., Travis, G.R., Hao, X., McAllister, T.A., Leinweber, P. and Thiele-Bruhn, S., 2008. Distribution of sulfamethazine, chlortetracycline and tylosin in manure and soil of Canadian feedlots after subtherapeutic use in cattle. *Environ. Pollut.* 156, 1243-1251.
- Bais, H.P., Weir, T.L., Perry, L.G., Gilroy, S. and Vivanco, J.M., 2006. The role of root exudates in rhizosphere interactions with plants and other organisms. *Annu. Rev. Plant Biol.* 57, 233-266.
- Behringer, C., Bartsch, K. and Schaller, A., 2011. Safeners recruit multiple signalling pathways for the orchestrated induction of the cellular xenobiotic detoxification machinery in Arabidopsis. *Plant Cell Environ.* 34, 1970-1985.
- Birk, B., Stahle, A., Meier, M., Palm, M., Funk-Weyer, D., Breves, G. and Seulberger, H., 2018. Investigation of ruminant xenobiotic metabolism in a modified rumen simulation system (RUSITEC). *Altex* 35, 379-389.
- Boxall, A.B.A., Johnson, P., Smith, E.J., Sinclair, C.J., Stutt, E. and Levy, L.S., 2006. Uptake of Veterinary Medicines from Soils into Plants. *J. Agric. Food Chem.* 54, 2288-2297.
- Briggs, G.G., Bromilow, R.H. and Evans, A.A., 1982. Relationships between lipophilicity and root uptake and translocation of non-ionised chemicals by barley. *Pestic. Sci.* 13, 495-504.
- Briggs, G.G., Rigitano, R.L.O. and Bromilow, R.H., 1987. Physico-chemical factors affecting uptake by roots and translocation to shoots of weak acids in barley. *Pestic. Sci.* 19, 101-112.
- Burken, J.G. and Schnoor, J.L., 1998. Predictive Relationships for Uptake of Organic Contaminants by Hybrid Poplar Trees. *Environ. Sci. Technol.* 32, 3379-3385.
- Chen, F., D'Auria, J.C., Tholl, D., Ross, J.R., Gershenzon, J., Noel, J.P. and Pichersky, E., 2003. An Arabidopsis thaliana gene for methylsalicylate biosynthesis, identified by a biochemical genomics approach, has a role in defense. *Plant J.* 36, 577-588.

Chen, H.R., Rairat, T., Loh, S.H., Wu, Y.C., Vickroy, T.W. and Chou, C.C., 2017. Assessment of veterinary drugs in plants using pharmacokinetic approaches: The absorption, distribution and elimination of tetracycline and sulfamethoxazole in ephemeral vegetables. *PLoS One* 12, e0183087.

Cummings, J.H., 1984. Cellulose and the human gut. *Gut* 25, 805-810.

Dodd, M.C. and Huang, C.H., 2004. Transformation of the antibacterial agent sulfamethoxazole in reactions with chlorine: kinetics, mechanisms, and pathways. *Environ. Sci. Technol.* 38, 5607-5615.

Dolliver, H., Kumar, K. and Gupta, S., 2007. Sulfamethazine Uptake by Plants from Manure-Amended Soil. *J Environ. Qual.* 36, 1224-1224.

Dudley, S., Sun, C., Jiang, J. and Gan, J., 2018. Metabolism of sulfamethoxazole in *Arabidopsis thaliana* cells and cucumber seedlings. *Environ. Pollut.* 242, 1748-1757.

Finnegan, T., Steenkamp, P.A., Piater, L.A. and Dubery, I.A., 2016. The Lipopolysaccharide-Induced Metabolome Signature in *Arabidopsis thaliana* Reveals Dynamic Reprogramming of Phytoalexin and Phytoanticipin Pathways. *PLoS One* 11, e0163572.

Franklin, A.M., Williams, C.F., Andrews, D.M., Woodward, E.E. and Watson, J.E., 2016. Uptake of Three Antibiotics and an Antiepileptic Drug by Wheat Crops Spray Irrigated with Wastewater Treatment Plant Effluent. *J Environ. Qual.* 45, 546-546.

Fu, Q., Ye, Q., Zhang, J., Richards, J., Borchardt, D. and Gan, J., 2017a. Diclofenac in *Arabidopsis* cells: Rapid formation of conjugates. *Environ. Pollut.* 222, 383-392.

Fu, Q., Zhang, J., Borchardt, D., Schlenk, D. and Gan, J., 2017b. Direct Conjugation of Emerging Contaminants in *Arabidopsis*: Indication for an Overlooked Risk in Plants? *Environ. Sci. Technol.* 51, 6071-6081.

Fu, W., Li, B., Yang, J., Yi, H., Chai, L. and Li, X., 2018. New insights into the chlorination of sulfonamide: Smiles-type rearrangement, desulfation, and product toxicity. *Chem. Eng. J.* 331, 785-793.

Gao, S., Zhao, Z., Xu, Y., Tian, J., Qi, H., Lin, W. and Cui, F., 2014. Oxidation of sulfamethoxazole (SMX) by chlorine, ozone and permanganate—A comparative study. *J. Hazard. Mater.* 274, 258-269.

García-Galán, M.J., Díaz-Cruz, M.S. and Barceló, D., 2011a. Occurrence of sulfonamide residues along the Ebro river basin: Removal in wastewater treatment plants and environmental impact assessment. *Environ. Int.* 37, 462-473.

García-Galán, M.J., Díaz-Cruz, M.S., Barceló, D., Garcia-Galan, M.J., Diaz-Cruz, M.S. and Barcelo, D., 2012. Kinetic studies and characterization of photolytic products of sulfamethazine,

sulfapyridine and their acetylated metabolites in water under simulated solar irradiation. *Water Res.* 46, 711-722.

García-Galán, M.J., Rodríguez-Rodríguez, C.E., Vicent, T., Caminal, G., Díaz-Cruz, M.S. and Barceló, D., 2011b. Biodegradation of sulfamethazine by *Trametes versicolor*: Removal from sewage sludge and identification of intermediate products by UPLC–QqTOF-MS. *Sci. Total Environ.* 409, 5505-5512.

García-Galán, M.J., Silvia Díaz-Cruz, M. and Barceló, D., 2008. Identification and determination of metabolites and degradation products of sulfonamide antibiotics. *TrAC, Trends Anal. Chem.* 27, 1008-1022.

Göbel, A., McArdeall, C.S., Joss, A., Siegrist, H. and Giger, W., 2007. Fate of sulfonamides, macrolides, and trimethoprim in different wastewater treatment technologies. *Sci. Total Environ.* 372, 361-371.

Gorelova, V., Ambach, L., Rébeillé, F., Stove, C. and Van Der Straeten, D., 2017. Foliates in Plants: Research Advances and Progress in Crop Biofortification. *Front Chem* 5, 21.

Gros, M., Petrović, M., Ginebreda, A. and Barceló, D., 2010. Removal of pharmaceuticals during wastewater treatment and environmental risk assessment using hazard indexes. *Environ. Int.* 36, 15-26.

Gulde, R., Meier, U., Schymanski, E.L., Kohler, H.-P.E., Helbling, D.E., Derrer, S., Rentsch, D. and Fenner, K., 2016. Systematic Exploration of Biotransformation Reactions of Amine-Containing Micropollutants in Activated Sludge. *Environ. Sci. Technol.* 50, 2908-2920.

Holder, C.L., Mona I. Churchwell, A. and Doerge, D.R., 1999. Quantification of Soy Isoflavones, Genistein and Daidzein, and Conjugates in Rat Blood Using LC/ES-MS. *J. Agric. Food Chem.* 47, 3764-3770.

Hu, X., Zhou, Q. and Luo, Y., 2010. Occurrence and source analysis of typical veterinary antibiotics in manure, soil, vegetables and groundwater from organic vegetable bases, northern China. *Environ. Pollut.* 158, 2992-2998.

Huber, C., Bartha, B., Harpaintner, R. and Schröder, P., 2009. Metabolism of acetaminophen (paracetamol) in plants—two independent pathways result in the formation of a glutathione and a glucose conjugate. *Environmental Science and Pollution Research* 16, 206-213.

Huynh, K., Banach, E. and Reinhold, D., 2018. Transformation, Conjugation, and Sequestration Following the Uptake of Triclocarban by Jalapeno Pepper Plants. *J. Agric. Food Chem.* 66, 4032–4043.

Hwang, S.M., Kim, D.W., Lee, B.H. and Bahk, J.D., 2009. *Arabidopsis* cytoplasmic N-acetyltransferase, as the ortholog of RimL in *E. coli*, controls flowering time via the autonomous pathway. *Plant Sci.* 177, 593-600.

Justesen, U., 2000. Negative atmospheric pressure chemical ionisation low-energy collision activation mass spectrometry for the characterisation of flavonoids in extracts of fresh herbs. *J. Chromatogr.* 902, 369-379.

Khan, B.R., Wherritt, D.J., Huhman, D., Sumner, L.W., Chapman, K.D. and Blancaflor, E.B., 2016. Malonylation of Glucosylated N-Lauroylethanolamine: A new pathway that determines N-Acylethanolamine metabolic fate in plants. *J Biol. Chem.* 291, 27112-27121.

Koppel, N., Maini Rekdal, V. and Balskus, E.P., 2017. Chemical transformation of xenobiotics by the human gut microbiota. *Science* 356, eaag2770-eaag2770.

Lanz, R., Kuhnert, P. and Boerlin, P., 2003. Antimicrobial resistance and resistance gene determinants in clinical *Escherichia coli* from different animal species in Switzerland. *Vet. Microbiol.* 91, 73-84.

LeFevre, G.H., Lipsky, A., Hyland, K.C., Blaine, A.C., Higgins, C.P. and Luthy, R.G., 2017. Benzotriazole (BT) and BT plant metabolites in crops irrigated with recycled water. *Environ. Sci. Water Res. Technol.* 3, 213–223.

LeFevre, G.H., Müller, C.E., Li, R.J., Luthy, R.G. and Sattely, E.S., 2015. Rapid Phytotransformation of Benzotriazole Generates Synthetic Tryptophan and Auxin Analogs in *Arabidopsis*. *Environ. Sci. Technol.* 49, 10959-10968.

LeFevre, G.H., Portmann, A.C., Muller, C.E., Sattely, E.S. and Luthy, R.G., 2016. Plant Assimilation Kinetics and Metabolism of 2-Mercaptobenzothiazole Tire Rubber Vulcanizers by *Arabidopsis*. *Environ. Sci. Technol.* 50, 6762-6771.

Li, X., Yu, H., Xu, S. and Hua, R., 2013. Uptake of three sulfonamides from contaminated soil by pakchoi cabbage. *Ecotoxicol. Environ. Saf.* 92, 297-302.

Macherius, A., Eggen, T., Lorenz, W., Moeder, M., Ondruschka, J. and Reemtsma, T., 2012. Metabolization of the Bacteriostatic Agent Triclosan in Edible Plants and its Consequences for Plant Uptake Assessment. *Environ. Sci. Technol.* 46, 10797-10804.

Macherius, A., Seiwert, B., Schroder, P., Huber, C., Lorenz, W. and Reemtsma, T., 2014. Identification of Plant Metabolites of Environmental Contaminants by UPLC-QToF-MS: The in Vitro Metabolism of Triclosan in Horseradish. *J. Agric. Food Chem.* 62, 1001-1009.

Majewsky, M., Glauner, T. and Horn, H., 2015. Systematic suspect screening and identification of sulfonamide antibiotic transformation products in the aquatic environment. *Anal. Bioanal. Chem.* 407, 5707-5717.

Majewsky, M., Wagner, D., Delay, M., Bräse, S., Yargeau, V. and Horn, H., 2014. Antibacterial Activity of Sulfamethoxazole Transformation Products (TPs): General Relevance for Sulfonamide TPs Modified at the para Position. *Chem. Res. Toxicol.* 27, 1821-1828.

Marsik, P., Sisa, M., Lacina, O., Motkova, K., Langhansova, L., Rezek, J. and Vanek, T., 2017. Metabolism of ibuprofen in higher plants: A model *Arabidopsis thaliana* cell suspension culture system. *Environ. Pollut.* 220, 383-392.

Mathews, S. and Reinhold, D., 2013. Biosolid-borne tetracyclines and sulfonamides in plants. *Environmental Science and Pollution Research* 20, 4327-4338.

Miller, E.L., Nason, S.L., Karthikeyan, K.G. and Pedersen, J.A., 2016. Root Uptake of Pharmaceuticals and Personal Care Product Ingredients. *Environ. Sci. Technol.* 50, 525-541.

Mitchell, A.D. and Paulson, G.D., 1986. Depletion kinetics of ¹⁴C-sulfamethazine [4-amino-N-(4, 6-dimethyl-2-pyrimidinyl)benzene[U-¹⁴C]sulfonamide] metabolism in swine. *Drug Metab. Dispos.* 14, 161-165.

Nassar, R., Trivella, A., Mokh, S., Al-Iskandarani, M., Budzinski, H. and Mazellier, P., 2017. Photodegradation of sulfamethazine, sulfamethoxypyridazine, amitriptyline, and clomipramine drugs in aqueous media. *J. Photochem. Photobiol. A: Chem.* 336, 176-182.

Ntaios, G. (2015) Homocysteine, B vitamins, and cardiovascular risk. Watson, R.R. (ed), p. 309, Academic Press.

Pan, M. and Chu, L.M., 2016. Adsorption and degradation of five selected antibiotics in agricultural soil. *Sci. Total Environ.* 545-546, 48-56.

Pan, M. and Chu, L.M., 2017. Leaching behavior of veterinary antibiotics in animal manure-applied soils. *Sci. Total Environ.* 579, 466-473.

Prosser, R.S. and Sibley, P.K., 2015. Human health risk assessment of pharmaceuticals and personal care products in plant tissue due to biosolids and manure amendments, and wastewater irrigation. *Environ. Int.* 75, 223-233.

Radke, M., Lauwigi, C., Heinkele, G., Murdter, T.E. and Letzel, M., 2009. Fate of the antibiotic sulfamethoxazole and its two major human metabolites in a water sediment test. *Environ. Sci. Technol.* 43, 3135-3141.

Riemenschneider, C., Seiwert, B., Moeder, M., Schwarz, D. and Reemtsma, T., 2017. Extensive Transformation of the Pharmaceutical Carbamazepine Following Uptake into Intact Tomato Plants. *Environ. Sci. Technol.* 51, 6100-6109.

Rivas-San Vicente, M. and Plasencia, J., 2011. Salicylic acid beyond defence: its role in plant growth and development. *J. Exp. Bot.* 62, 3321-3338.

Sandermann, H., 1992. Plant metabolism of xenobiotics. *Trends Biochem. Sci.* 17, 82-84.

Schröder, P., 2007. pp. 251-263, Humana Press.

Schymanski, E.L., Jeon, J., Gulde, R., Fenner, K., Ruff, M., Singer, H.P. and Hollender, J., 2014. Identifying Small Molecules via High Resolution Mass Spectrometry: Communicating Confidence. *Environ. Sci. Technol.* 48, 2097-2098.

Shen, J., Zeng, Y., Zhuang, X., Sun, L., Yao, X., Pimpl, P. and Jiang, L., 2013. Organelle pH in the Arabidopsis Endomembrane System. *Molecular Plant* 6, 1419-1437.

Spielmeier, A., Höper, H. and Hamscher, G., 2017. Long-term monitoring of sulfonamide leaching from manure amended soil into groundwater. *Chemosphere* 177, 232-238.

Stein, R.A., 2011. Antibiotic Resistance: A Global, Interdisciplinary Concern. *American Biology Teacher* 73, 314-321.

Stoob, K., Singer, H.P., Mueller, S.R., Schwarzenbach, R.P. and Stamm, C.H., 2007. Dissipation and transport of veterinary sulfonamide antibiotics after manure application to grassland in a small catchment. *Environ. Sci. Technol.* 41, 7349-7355.

Stravs, M.A., Pomati, F. and Hollender, J., 2017. Exploring micropollutant biotransformation in three freshwater phytoplankton species. *Environ Sci Process Impacts* 19, 822-832.

Taguchi, G., Ubukata, T., Nozue, H., Kobayashi, Y., Takahi, M., Yamamoto, H. and Hayashida, N., 2010. Malonylation is a key reaction in the metabolism of xenobiotic phenolic glucosides in Arabidopsis and tobacco. *The Plant J.* 63, 1031-1041.

Tanoue, R., Sato, Y., Motoyama, M., Nakagawa, S., Shinohara, R. and Nomiyama, K., 2012. Plant Uptake of Pharmaceutical Chemicals Detected in Recycled Organic Manure and Reclaimed Wastewater. *J. Agric. Food Chem.* 60, 10203-10211.

Thompson, A.M.G., Iancu, C.V., Neet, K.E., Dean, J.V. and Choe, J.-y., 2017. Differences in salicylic acid glucose conjugations by UGT74F1 and UGT74F2 from. *Sci. Rep.* 7, 46629.

Thomson, J., 2012. Handbook of Radioactivity Analysis. L'Annunziata, M. (ed), pp. 589-590, Academic Press, San Diego, CA.

Trapp, S., 2000. Modelling uptake into roots and subsequent translocation of neutral and ionisable organic compounds. *Pest Manage. Sci.* 56, 767-778.

Trapp, S., 2004. Plant uptake and transport models for neutral and ionic chemicals. *Environmental Science and Pollution Research* 11, 33-39.

Wei, R., Ge, F., Zhang, L., Hou, X., Cao, Y., Gong, L., Chen, M., Wang, R. and Bao, E., 2016. Occurrence of 13 veterinary drugs in animal manure-amended soils in Eastern China. *Chemosphere* 144, 2377-2383.

Xu, Y.F., Lu, W. and Rabinowitz, J.D., 2015. Avoiding misannotation of in-source fragmentation products as cellular metabolites in liquid chromatography-mass spectrometry-based metabolomics. *Anal. Chem.* 87, 2273-2281.

Yang, S., Cha, J. and Carlson, K., 2005. Simultaneous extraction and analysis of 11 tetracycline and sulfonamide antibiotics in influent and effluent domestic wastewater by solid-phase extraction and liquid chromatography-electrospray ionization tandem mass spectrometry. *J Chromatogr. A.* 1097, 40-53.

Yang, Z., Hou, J.-J., Qi, P., Yang, M., Yan, B.-P., Bi, Q.-R., Feng, R.-H., Yang, W.-Z., Wu, W.-Y. and Guo, D.-A., 2016. Colon-derived uremic biomarkers induced by the acute toxicity of *Kansui radix*: A metabolomics study of rat plasma and intestinal contents by UPLC-QTOF-MSE. *J. Chromatogr. B* 1026, 193–203.

Yergeau, E., Sanschagrin, S., Maynard, C., St-Arnaud, M. and Greer, C.W., 2014. Microbial expression profiles in the rhizosphere of willows depend on soil contamination. *The ISME Journal* 8, 344-358.

Yi, Z., Wang, J., Tang, Q. and Jiang, T., 2018. Photolysis of sulfamethazine using UV irradiation in an aqueous medium. *RSC Adv.* 8, 1427-1435.

Zhang, C., Lai, C., Zeng, G., Huang, D., Yang, C., Wang, Y., Zhou, Y. and Cheng, M., 2016. Efficacy of carbonaceous nanocomposites for sorbing ionizable antibiotic sulfamethazine from aqueous solution. *Water Res.* 95, 103-112.

Zhang, H., Deng, X., Miki, D., Cutler, S., La, H., Hou, Y.J., Oh, J. and Zhu, J.K., 2012. Sulfamethazine suppresses epigenetic silencing in *Arabidopsis* by impairing folate synthesis. *Plant Cell* 24, 1230-1241.

Zhao, Y., Shadrick, W.R., Wallace, M.J., Wu, Y., Griffith, E.C., Qi, J., Yun, M.-K., White, S.W. and Lee, R.E., 2016. Pterin-sulfa conjugates as dihydropteroate synthase inhibitors and antibacterial agents. *Biorg. Med. Chem. Lett.* 26, 3950-3954.

Zulalian, J., Stout, S.J., Babcock, C.N., Lucas, L.M., Miller, P. and Orloski, E.J., 1984. A study of the absorption, excretion, metabolism, and residues in tissues in rats fed carbon-14-labeled sulfamethazine. *J. Agric. Food Chem.* 32, 1434-1440.

CHAPTER 5.

UPTAKE AND METABOLISM OF TETRACYCLINES BY *ARABIDOPSIS THALIANA*

5.1. Introduction

Tetracyclines are broad-spectrum antimicrobials that have been extensively used in humans and food-producing animals. In the U.S., approximately 5.8 tons of tetracyclines were used in animals in 2016, accounted for 70% of the medically important antimicrobials used in food-producing animals (U.S. FDA, 2017). Tetracyclines administered to humans and animals are poorly absorbed in the digestive tracts, with 50–80% of the doses are excreted in urine and feces (Mullen et al., 2019). Residuals of tetracyclines and their metabolites are eventually released into domestic sewage and are discharged to WWTPs. However, conventional biological treatment processes using activated sludge, which are widely adopted by WWTPs around the world (Wang and Wang, 2016), cannot completely eliminate tetracyclines in the influents; consequently, tetracyclines have been widely detected in biosolids and treated wastewater discharged by WWTPs (Ben et al., 2018, Gao et al., 2012, Kim et al., 2014, Tran et al., 2016). Likewise, urine and feces of medicated animals also serve as important reservoirs of tetracycline residues (Conde-Cid et al., 2018, Li et al., 2015, Zhang et al., 2019). Land application of biosolids and animal manure as fertilizers is a common practice in many countries; however, this could lead to accumulation of tetracyclines in agricultural soils and subsequent transfer into crop plants. Several studies have reported the occurrence of tetracyclines in agricultural soils, with the observed concentrations varying from below detection limit to 3,000 $\mu\text{g}/\text{kg}$ (Conde-Cid et al., 2018, Hu et al., 2010, Karci and Balcioğlu, 2009, Li et al., 2015, Li et al., 2011, Xiang et al., 2016). For example, Li et al. reported high levels of tetracyclines (mean concentrations of 102 $\mu\text{g}/\text{kg}$) in soils from vegetable greenhouses in the suburbs of Beijing (China), which were primarily fertilized with animal manures (Li et al., 2015). Likewise, tetracyclines were also detected in different organic vegetable farms in Guangdong Province (China), with the highest concentrations of 120 $\mu\text{g}/\text{kg}$ (Xiang et al.,

2016). Although tetracyclines show a higher affinity to the particulate phase in soil than other classes of antimicrobials (Pan and Chu, 2016), their partition into crop plants grown in contaminated soils has been widely documented in the literature (Azanu et al., 2016, Conde-Cid et al., 2018, Hu et al., 2010, Kang et al., 2013, Kumar et al., 2005, Pan et al., 2014).

Limited information is currently available on the metabolic pathways of the uptaken tetracyclines in plant tissues. Detoxification of CTC in maize (*Zea mays*) through *in vitro* conjugation with glutathione (GSH) was proposed by Farkas et al., although the authors were unable to confirm formation of the CTC–GSH conjugates *in vivo* due to plant matrix interferences (Farkas et al., 2007). Conversely, pinto bean plants (*Phaseolus vulgaris*) were found to be CTC-sensitive and did not induce the formation of the protective glutathione *S*-transferase upon exposure to CTC (Farkas et al., 2009). These findings suggested that plant responses to and subsequent metabolism of CTC are potentially species-specific. In a recent study, Schwake-Anduschus and Langenkamper observed the occurrence of several tetracycline residues (tetracycline, doxycycline, and demeclocycline), as well as isomers of CTC (epi-CTC and iso-CTC) in the wheat and rye grains of plants exposed exclusively to CTC, indicating the conversion of the uptaken CTC into these products *in planta* (Schwake-Anduschus and Langenkamper, 2018). Similarly, tetracycline and epi-tetracycline were also found in pinto beans exclusively treated with tetracycline (Farkas et al., 2009).

This research examined the phytometabolic pathways of tetracycline antimicrobials using the model plant *Arabidopsis thaliana*. CTC and OTC were selected as the compounds of interest based on their ubiquitous occurrence on wastewater and biosolids produced by WWTPs (Ashfaq et al., 2017, Ben et al., 2018, Tran et al., 2016) and animal manures (Conde-Cid et al., 2018, Hou et al., 2015, Li et al., 2015, Zhang et al., 2019), which are commonly applied to agricultural soil.

Both targeted and untargeted metabolomics using high-resolution mass spectrometry coupled with multivariate statistical analysis were used to determine the potential metabolites of CTC and OTC upon hydroponic exposure to axenic *A. thaliana* plants.

5.2. Materials and Methods

5.2.1. Chemicals

Chlortetracycline hydrochloride (CTC, analytical standard grade) and oxytetracycline hydrochloride (OTC, $\geq 95\%$ purity) were purchased from Sigma-Aldrich (St. Louis, MO). 4-epi-chlortetracycline hydrochloride (4-epi-CTC) and 6-iso-chlortetracycline (6-iso-CTC) were purchased from Cayman Chemical Company (Ann Arbor, MI). Formic acid and MS grade acetonitrile were purchased from Sigma-Aldrich (St. Louis, MO). Other chemicals (ACS grade) were purchased from VWR, Inc. (Chicago, IL).

CTC and OTC (1000 $\mu\text{g/mL}$) were separately prepared in methanol, while 4-epi-CTC (46.5 $\mu\text{g/mL}$) and 6-iso-CTC (100 $\mu\text{g/mL}$) were prepared in methanol:water (1:1). All stock solutions were stored in amber high-density polyethylene bottles at -20°C and were stable for one month. Working standard solutions (0–0.5 $\mu\text{g/mL}$) were freshly prepared each use by dilution with methanol:water (1:1) or *A. thaliana* plant extracts.

5.2.2. Preparation of *Arabidopsis thaliana* seeds and culture media

A. thaliana seeds (wild-type quick plantTM) were purchased from VWR, Inc. (Chicago, IL). Seed surface sterilization followed (LeFevre et al., 2016). Sterilization solution was freshly prepared each use by adding 2.0 mL of bleach (8.25% sodium hypochlorite, Clorox) and 100 μl of Tween 20 surfactant (BioRad Laboratories Inc.) into 8.0 mL of autoclaved water and mixed well. Aliquot of 1.0 mL of the sterilization solution was added to a 1.5 mL microcentrifuge tube containing approximately 150 seeds. The tube was slowly pipetted for 5 minutes. The supernatant

was removed and 1 mL of autoclaved water was added and then removed to wash the seeds from the sterilization solution. The washing step was repeated five times. The seeds were then distributed into the Magenta boxes (GA-7, Magenta Corp., Lockport, IL) containing 25 mL of sterilized culture media and stratified at 4°C for 3 days before transferred to a growth chamber.

Half-strength Murashige and Skoog (0.5X MS) solution was used as the culture media. Per 1 L of Milli-Q water, 2.22 g of MS basal medium (Sigma-Aldrich, St. Louis, MO), 0.5 g of MES buffer (Sigma-Aldrich), and 5 g of sucrose (J. T. Baker, Center Valley, PA) were added. The media pH was adjusted to 5.7 using 1M KOH solution. Finally, the culture media was filter sterilized using a 0.22 µm PES membrane (Sigma-Aldrich).

All procedures for seed sterilization and culture media preparation were conducted in a laminar flow biological safety hood, and 70% ethanol spray solution was used to sterilize the working area.

5.2.3. Plant material and exposure to CTC and OTC

All experiments were conducted under sterile conditions to eliminate potential interferences of bacteria and fungi to uptake and metabolism of CTC and OTC by *A. thaliana* plant. Seeds were cultivated in half-strength MS media (0.5X MS) in Magenta boxes (GA-7, Magenta Corp., Lockport, IL). Approximately 15 sterilized seeds were added to each box containing 25 mL of nutrient solution. The boxes were then capped with breathable lids, sealed with permeable tape (Micropore, 3M), and stratified at 4°C in dark for 3 days before transferred to a growth chamber (Conviro A1000, Manitoba, Canada) with the temperature and light intensity set at 22°C and 150 µmol/m²/s for a 16 h photoperiod, respectively.

Two weeks after germination, the media in each box were discarded and replaced with 50 mL of freshly prepared 0.5X MS media (pH 5.7) containing CTC or OTC at a nominal

concentration of 3 $\mu\text{g/mL}$. The discarded media containing plant exudates were subsequently combined and filtered through a 0.22 μm PES membrane (Sigma-Aldrich). After filtration, the sterilized filtrate was used for investigating the effects of plant exudates on abiotic degradation of CTC and OTC in the aqueous solutions. Several controls were included: (1) plant controls without tetracyclines, (2) media control with tetracyclines (3 $\mu\text{g/mL}$), exposed to light-“light controls”, and (3) media control with tetracyclines (3 $\mu\text{g/mL}$), not exposed to light-“dark controls”. The “dark controls” boxes were wrapped in aluminum foil. Each control treatments were performed in triplicates. Sampling was subsequently conducted at 1, 4, 7, and 12-day intervals. Plant tissues were ground to fine powder in liquid nitrogen. Media samples were preserved from bacterial degradation by adding 0.5 mL of 0.1 g/mL sodium azide. All samples were stored at -80°C until analysis.

5.2.4. Sample preparation

At each sampling time, aliquots of 0.1–0.5 mL of media samples were mixed with dilution solvent (methanol:water = 1:1) to make the volume to 1.0 mL, filtered through 0.2 μm PTFE membrane (13 mm, VWR) into 2 mL amber vials and instantly subjected to LC-MS/MS analysis. Additionally, media samples were also concentrated by solid phase extraction (SPE) to facilitate the detection of CTC metabolites in the aqueous phase. The procedure followed (Yang et al., 2005) with some modifications. Briefly, 1.0 mL of 5% Na_2EDTA was added to a flask containing 50 mL of the media, 70 mL of Milli-Q water, and 30 mL of 0.1 M citric acid. The Magenta box was rinsed with 4 mL of methanol which were then combined to the mixture. Accordingly, pH of the mixture was approximately 2.3 prior to clean-up. The SPE cartridges (Oasis HLB 6 cc, 150 mg sorbent, Waters) were preconditioned with 5 mL of methanol, 5 mL of 0.5 N HCl, and 5 mL of Milli-Q water. Samples were then passed through the cartridges using a vacuum manifold. After

sample loading, the cartridges were rinsed with 5 mL of Milli-Q water and dried under vacuum. Analytes were eluted using 5 mL of methanol, which was then evaporated to dryness using nitrogen gas, reconstituted in 1 mL of methanol:water (1:1), and filtered through 0.2 μm PTFE membranes (13 mm, VWR) into 2 mL polypropylene microcentrifuge tubes.

A mixture of methanol/EDTA-McIlvaine buffer (1/1, pH 4) was used as the extraction solvent for plant tissues. Plant tissues (approximately 0.5 g) were extracted three times with aliquots of 5 mL of the extraction solvent in a 50 mL centrifuge tube by sonication for 15 min in a water bath at room temperature, followed by centrifugation at 4,000 rpm for 15 min. Subsequently, the extracts (~15 mL) were pooled and mixed with 135 mL of Milli-Q water (methanol content ~5%) prior to SPE clean-up as described for media samples.

5.2.5. Quantification of CTC, 4-epi-CTC, 6-iso-CTC, and OTC by LC-MS/MS

Analysis was performed on a Shimadzu Prominence high performance liquid chromatography (Columbia, MD) coupled with an Applied Biosystems Sciex 3200 triple quadrupole mass spectrometer (Foster City, CA), applying electrospray ionization (ESI) positive in multiple-reaction-monitoring (MRM) mode. Chromatographic separation was performed at room temperature on an Ultra biphenyl column (5 μm , 50 x 2.1 mm, Restek). Milli-Q water and acetonitrile:methanol (1:1), both contained 0.1% formic acid, were used as the mobile phase A and B, respectively. The gradient program was: 0–5.5 min: 98% B; 6.5 min: 98% B; 7.0 min: 5% B; and 10.0 min: 5% B. The flow rate was 0.3 mL/min and the injection volume was 10 μL . Declustering potential and collision energy were 40V and 27V for CTC, and 28V and 21V for OTC, respectively. Additional settings were IonSpray voltage 5500 V at 600°C, curtain gas pressure 25 psi, collision gas pressure 6 psi, and ion source gas pressure 60 psi. Similar MRM transitions at m/z 479 \rightarrow m/z 444 and m/z 479 \rightarrow m/z 462 were monitored for CTC, 4-epi-CTC,

and 6-iso-CTC. For OTC, MRM transitions m/z 461 \rightarrow m/z 426 and m/z 461 \rightarrow m/z 444 were monitored.

5.2.6. Metabolite candidates screening by UPLC-QTOF-MS^E and data processing

Media and plant extracts were analyzed on an Acquity Ultra Performance Liquid Chromatography (UPLC) system coupled with a Xevo G2-XS QTOF mass spectrometer (Waters, Milford, MA). Chromatographic separation was achieved using an Acquity BEH C18 column (100 \times 2.1 mm, 1.7 μ m) at a flow rate of 0.3 mL/min and temperature of 40°C. Milli-Q water and acetonitrile:methanol (1:1), both contained 0.1% formic acid, were used as the mobile phase A and B, respectively. The elution gradient was: 0–1 min, 5% B; 11 min, 98% B; 13 min, 98% B; 13.1 min, 5% B; and 15 min, 5% B. Analyses were carried out with an ESI source operated in positive mode within a mass range of 50–1500 m/z . The MS source and desolvation temperatures were set at 100°C and 450°C, respectively. Desolvation gas flow was 450 L/h. The lock mass spray for accurate m/z measurement used a solution containing 0.1 ng/ μ L of leucine enkephalin (m/z 556.2771 in positive ion mode). Data was collected in centroid mode with two scan functions using MS^E acquisition: function 1 with low collision energy (0 eV) and function 2 with high collision energy (dynamic ramp of collision energy of 20–80 eV).

The centroided MS raw data obtained under low collision energy were processed using Progenesis QI 2.1 software (for alignment, normalization and peak picking) (Waters). Subsequent multivariate statistical analysis was performed using EZinfo 3.0 software (Umetrics, Malmo, Sweden) for principal component analysis (PCA) and orthogonal projection to latent structures-discriminant analysis (OPLS-DA). The S-plots obtained from the OPLS-DA models were used to determine the m/z variables that significantly contributed to the differences between control and CTC/OTC-exposed groups. Metabolite candidates were primarily selected from the m/z variables

scattered on the top right corner of the S-plots with $p(\text{corr}) \geq 0.5$ (indicating an increase in intensity of these m/z variables in CTC/OTC-exposed groups compared to control groups). Candidates selected from the S-plots were imported back to Progenesis QI as the first tag set. In addition, the ANOVA p -values calculated by Progenesis QI that were ≤ 0.05 (reflecting significant differences between variables of control and CTC/OTC-exposed groups), were used as a second tag set. Data was then filtered using both tag sets. An output table was generated to include paired retention times- m/z , isotope distribution, raw, and normalized peak intensities for individual samples. Next, data from CTC/OTC-exposed groups were compared to controls. The proposed metabolite candidates were based on their presence in the treatments and absence in the controls. MassLynx 4.1 software (Waters) was used to generate possible chemical formulas for the metabolite candidates with the mass accuracy error ≤ 5 ppm. For CTC trials, the metabolite candidates potentially retained the chlorine atom from the parent structure and were further processed via the isotopic patterns of the chlorinated compounds (Macherius et al., 2014b). Following primary identification of the metabolite candidates, the proposed structures were further confirmed by characteristic fragment ions in high collision energy mass spectra.

5.2.7. Statistical analysis

Data are presented as mean \pm standard error (SE). One-way ANOVA was performed using SPSS 25 (IBM Corp., Armonk, NY) to determine significant differences ($p < 0.05$). Concentrations of CTC and its metabolites in plant tissues were calculated based on fresh weight (fw).

5.3. Results and Discussion

5.3.1. Chlortetracycline (CTC)

5.3.1.1. The enol-keto forms of CTC, 4-epi-CTC, and 6-iso-CTC in the standard solutions

The standard solutions of CTC, 4-epi-CTC, and 6-iso-CTC (0.2 $\mu\text{g/mL}$) were analyzed on the UPLC-QTOF-MS^E system, with their protonated precursor ion at m/z 479.121 \pm 0.05 Da was monitored in the low collision energy mode. Their selected ion chromatograms were presented in Supplementary Figure 5.1 – 5.3. For CTC standard, two signals were obtained that exhibited different fragmentation patterns in the high collision energy mode (Supplementary Figure 5.1). While two fragments at m/z 444.0848 and m/z 462.0964 were observed for the greater-intensity peak at retention time of 5.27 min, only one fragment at m/z 462.0946 was observed for the peak at retention time of 4.67 min. It is worth noting that the ($m + 2$) Da fragments in the chromatograms represent the chlorine isotope of CTCs. The peaks at the retention times of 5.27 min and 4.67 min were subsequently identified as CTC-enol and CTC-keto, respectively. The results were in agreement with studies by Gaugain et al., in which both enol and keto forms of CTC simultaneously exist in the standard solutions (Gaugain et al., 2015). According to Gaugain et al., there are two pathways for elimination of H₂O molecule from the fragment m/z 462 ($[\text{M} + \text{H} - \text{NH}_3]^+$), which lead to the formation of fragment m/z 444, for CTC-enol; however, only one pathway was observed for CTC-keto. As a result, the m/z 444 was more abundant for CTC-enol at the same collision energy (Gaugain et al., 2015). In our study, the transition m/z 462 \rightarrow 444 was not observed for the keto form of CTC (Supplementary Figure 5.1B). Fragmentation patterns of 4-epi-CTC revealed similar results (Supplementary Figure 5.2), with the peaks at retention time of 4.45 min and 4.85 min represented the keto and enol forms of 4-epi-CTC, respectively. While the

peak at retention time of 5.27 min was due to the presence of CTC-enol in the standard of 4-epi-CTC (Gaugain et al., 2015), the signal at 4.31 min most likely represented 4-epi-6-iso-CTC. As shown in Supplementary Figure 5.3, for 6-iso-CTC standard, both signals at retention times of 4.30 min and 4.67 min exhibited only one transition m/z 479 \rightarrow 462 and were identified as 4-epi-6-iso-CTC and 6-iso-CTC, respectively (Gaugain et al., 2015). Quantification of the total CTC, 4-epi-CTC, and 6-iso-CTC in this study was carried out by integration of both keto and enol peaks for each standard.

5.3.1.2. CTC and its isomers in media and accumulation in plant tissues

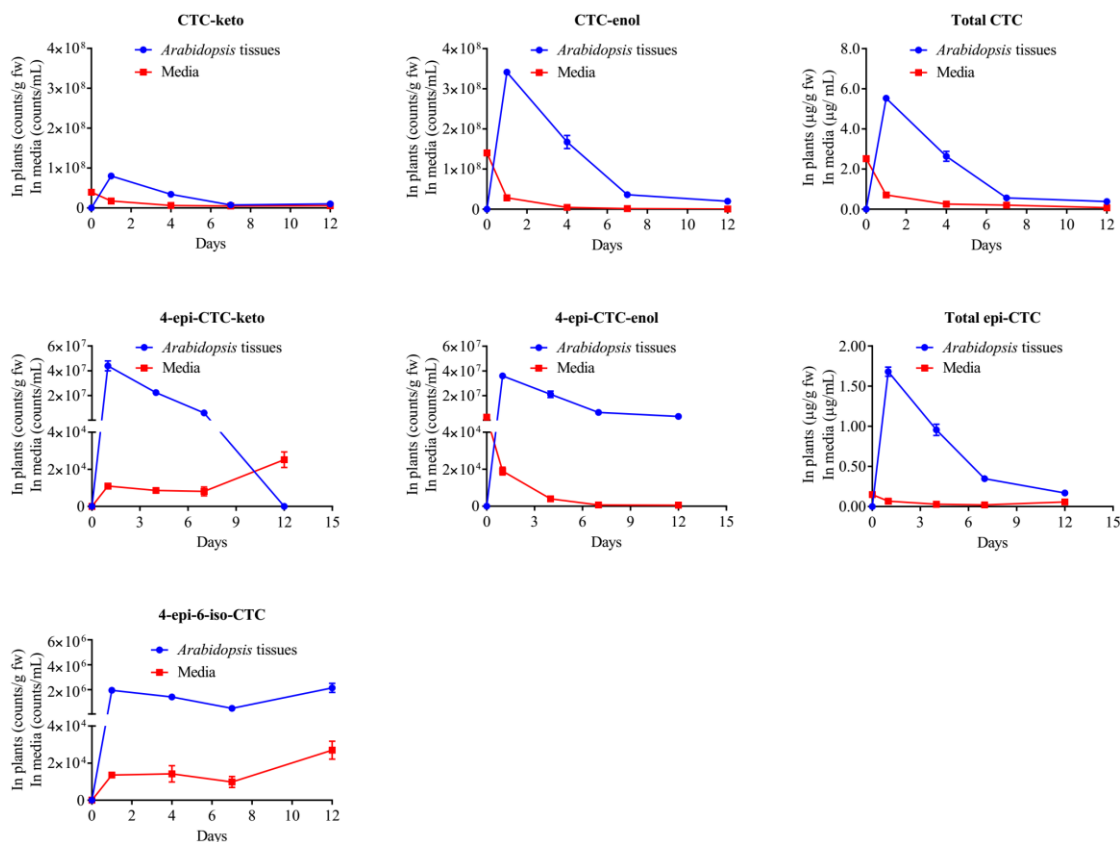


Figure 5. 1. Temporal variations of CTC and its isomers in the *A. thaliana* plant tissues and culture media over 12 days of exposure. Data are presented as mean \pm SE of triplicates, with some error bars are obscured by data symbols.

Figure 5.1 depicts the temporal variations of CTC and its isomers in the culture media and *A. thaliana* plant tissues over 12 days of exposure. In this study, the presence of keto-enol tautomers and epimers of CTC in plant tissues and culture media was confirmed to Level 1 using reference standards (Schymanski et al., 2014). CTC was quickly removed from the media of the *A. thaliana*-planted treatments upon exposure ($p < 0.001$). After 4 days, the concentrations of CTC decreased from initially $2.52 \pm 0.08 \mu\text{g/mL}$ to $0.26 \pm 0.02 \mu\text{g/mL}$, indicating approximately 89.7% removal efficiency, in which both keto- and enol- forms of CTC were found to dissipate from the media (Figure 5.1). Concurrently, both isomers were detected in the plant tissues. The concentrations of CTC in plants were found to be highest after 1 day of exposure at $5.5 \pm 0.3 \mu\text{g/g}$ fw; and then, substantially decreased to $0.2 \pm 0.1 \mu\text{g/g}$ fw after 12 days. At the end of the exposure, CTC residues in the plant tissues and media were negligible. While the loss of CTC in *A. thaliana* plant tissues can be explained by phytometabolism, which is commonly observed in studies on plant exposure to organic xenobiotics (Fu et al., 2017a, Fu et al., 2017b, LeFevre et al., 2015, LeFevre et al., 2016, Marsik et al., 2017), dissipation of CTC in the media can be attributed to plant uptake and accumulation, and other abiotic transformation occurred in the media. In this study, we observed that the concentrations of CTC in the no-plant control media also substantially decreased during the exposure, with approximately 73.0 and 95.7% of the initially added CTC was dissipated after 4 and 12 days, respectively. Photolysis of CTC, facilitating by the presence of Ca^{2+} and NO_3^- in aqueous solution, has previously been reported (Chen et al., 2012). Therefore, an additional trial was conducted to elucidate the role of light exposure in the removal of CTC in the abiotic media. Supplementary Figure 5.4 suggested that photolysis significantly contributed to the dissipation of CTC in the abiotic media at different time intervals ($p < 0.001$), and that the presence of plant exudates likely inhibited phototransformation of CTC in the media. In the “dark control”

media, although the total CTC concentrations were relatively constant over 12 days of exposure, significant keto–enol tautomerism between C-11a and C-12 of CTC was observed. As showed in the Supplementary Figure 5.4, the dissipation of CTC-enol in the “dark control” media was concurrent with an increase in the concentrations of CTC-keto. Similar to the photolysis, the keto–enol tautomerism in the media was also affected by the presence of plant exudates. Additional studies are necessary for elucidating the effects of plant exudates on transformation of CTC, but this was beyond the scope of the present study.

Epimerization of CTC at the carbon C4, which gives rise to 4-epi-CTC (Supplementary Figure 5.6), was also observed in media and plant tissues (Figure 5.1). While the concentrations of 4-epi-CTC in the media were only in range of $0.021 \pm 0.005 - 0.150 \pm 0.004 \mu\text{g/mL}$, its concentrations were substantially higher in the plant tissues, ranging from $0.169 \pm 0.008 - 1.681 \pm 0.057 \mu\text{g/g fw}$ throughout the study. Similar to CTC, the concentrations of 4-epi-CTC in plant tissues were also highest after 1 day of exposure and constantly decreased with increasing exposure time, suggesting that 4-epi-CTC also underwent further transformation/conjugation by *A. thaliana* plants. Additionally, keto-enol tautomerism was also observed for 4-epi-CTC in both media and plant tissues. It has been reported that CTC can reversibly epimerize to form 4-epi-CTC under acidic conditions (pH 2–6) (Gaugain et al., 2015, Kennedy et al., 1998). In this study, methanol/EDTA-McIlvaine buffer (1/1) at pH 4 was used as the extraction solvent for plant tissues; pH of media samples was also ~ 2.3 prior to SPE. Consequently, the epimerization of CTC may also occur during sample preparation.

We observed that the ratio of keto/enol in media samples were substantially greater than those in plant extracts (Supplementary Figure 5.5). For example, the highest ratios in media samples were 14.5 ± 3.2 for CTC and 48.7 ± 8.8 for 4-epi-CTC, respectively, while those found in

plant extracts were only 0.5 ± 0.1 and 1.2 ± 0.2 , respectively. CTC-keto and CTC-enol present in equilibrium in solution, with their ratio depends on the pH of the solution (Gaugain et al., 2015). In this study, the ratios of keto/enol of CTC and 4-epi-CTC in the matrix-matched standards used for their quantification varied in range of 0.2 – 0.3 and 1.5 – 1.7, respectively, suggesting that the keto-forms of both CTC and 4-epi-CTC evolved in the media during the exposure period.

4-epi-6-iso-CTC were also detected in media and plant extracts (Figure 5.1). While the concentrations of CTC and 4-epi-CTC in *A. thaliana* plants decreased with increased exposure time, the concentrations of 4-epi-6-iso-CTC were relatively constant over 12 days of exposure, suggesting that it was poorly metabolized in the plant tissues. As shown in Supplementary Figure 5.6, conversion of CTC to 6-iso-CTC and 4-epi-6-iso-CTC occurs under alkaline conditions (pH 12) or through metabolism (Gaugain et al., 2015). In this study, exposure and sample extraction procedures were conducted under acidic conditions. Therefore, the occurrence of 4-epi-6-iso-CTC in *A. thaliana* was most likely due to plant metabolism.

5.3.1.3. Screening of the CTC metabolites using multivariate statistical analysis

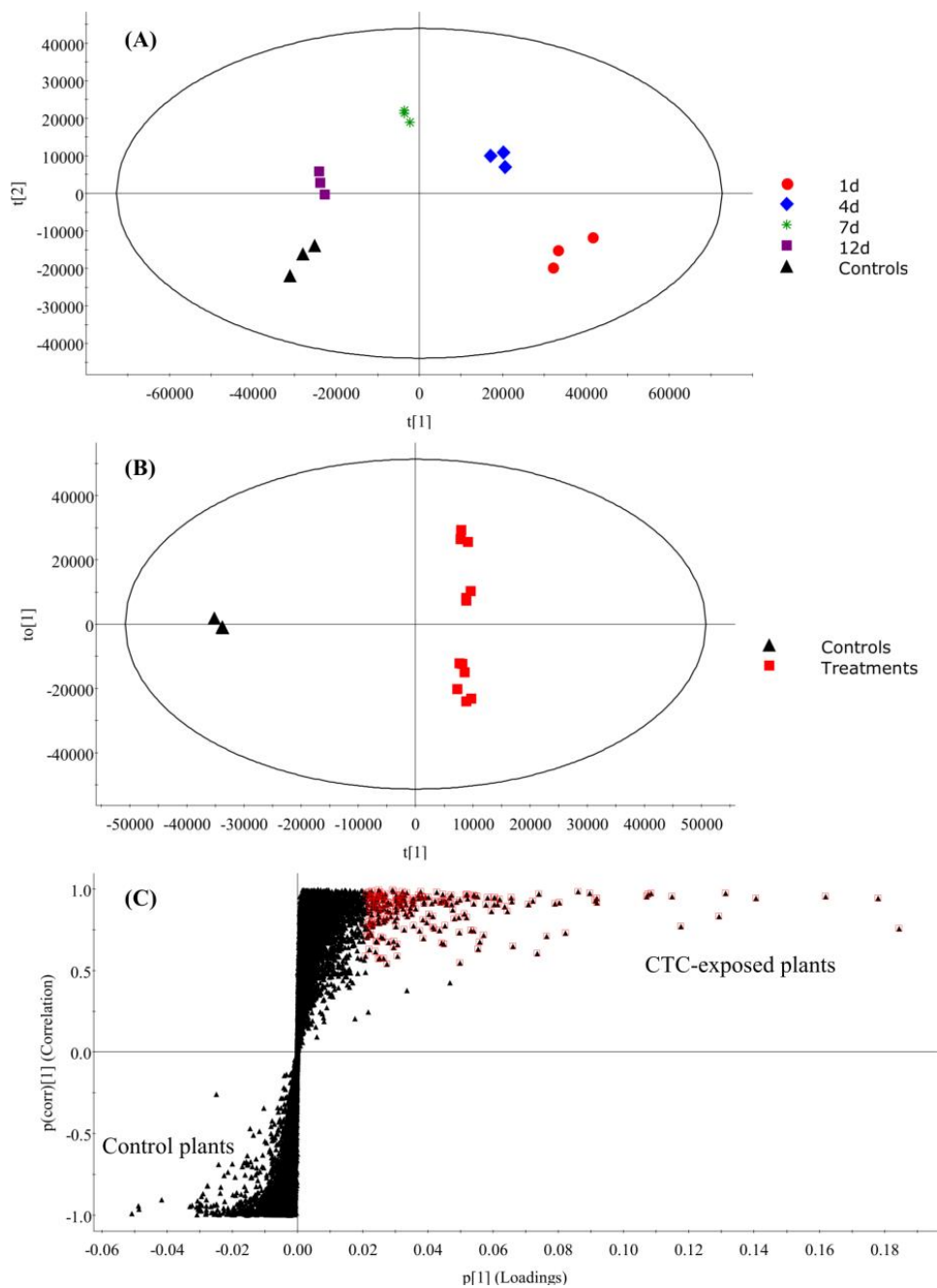


Figure 5. 2. PCA score plots (A), OPLS-DA score plots (B), and S-plots (C) derived from the UPLC-QTOF-MS^E datasets of the control and CTC-exposed plants (1, 4, 7, and 12 days). The ellipses represent Hotelling's T^2 with 95% confidence. The m/z variables on the S-plot that significantly contributed to the differences between control plants and CTC-exposed plants ($p(\text{corr}) \geq 0.5$) were selected for screening of CTC metabolites.

The unsupervised PCA was initially applied to visualize clustering of the control and CTC-exposed *A. thaliana* plant extracts at multiple sampling times. The explanation value ($R^2X(cum)$) and predictability value ($Q^2(cum)$) obtained from the four-component PCA model were 88% and 74%, respectively. The score plot of the first two principal components, which explained 76% of the total variance, is presented in Figure 5.2A, with each point represents an individual plant sample. Generally, samples clustered close to each other have similar metabolic profiles, while those scattered far away from each other are dissimilar. Clear separation of the control and CTC-exposed plants on the score plot of the PCA model clearly indicates that exposure to CTC resulted in significant alteration in *A. thaliana* plant metabolic profiles, in which the largest differences could be observed during the early stage of the exposure (e.i. 1–4 days following CTC exposure). Furthermore, differences in metabolic profiles among the CTC-exposed plants were also time-dependent. Plants sampled at different time intervals (1, 4, 7, and 12 days) were distinctively separated from each other on the score plot. The supervised OPLS-DA model was subsequently used to identify the potential metabolite candidates that significantly contributed to the differentiation between control and CTC-exposed plants. The OPLS-DA score plot is presented in Figure 5.2B, with the explanation value ($R^2Y(cum)$) and predictability value ($Q^2(cum)$) were 99% and 96%, respectively, resulted in a clear separation between the control and CTC-exposed plants (1, 4, 7, and 12 days). The observed differences can be explained by the m/z variables scattering on the upper right and lower left quadrants of the S-plot obtained from the OPLS-DA model (Figure 5.2C). Generally, the intensity of the m/z variables plotted in the lower quadrant of the S-plot decreased in the CTC-exposed plants compared to the control plants, while those plotted in the upper right quadrant indicate an increase in ion intensity of these variables in the CTC-exposed plants. The latter consisted of both the potential metabolites of CTC, as well as other endogenous

secondary metabolites that *A. thaliana* plants produced upon exposure to the stressor, CTC. Differentiation within the S-plot is due to concentration differences and the m/z variables with a higher intensity yield a better separation from the background ions (Macherius et al., 2014a). Accordingly, in this study, the CTC metabolite candidates were primarily screened from the variables scattered in the upper right quadrant of the S-plot with $p(\text{corr}) \geq 0.5$ (Figure 5.2C).

5.3.1.4. Metabolism of CTC by *A. thaliana*

Table 5.1 summarizes the metabolites of CTC upon exposure to axenic *A. thaliana*. As discussed in 5.3.1.2, the presence of keto-enol tautomers and epimers of CTC in plant tissues and culture media was confirmed to Level 1 using reference standards (Schymanski et al., 2014). As shown in Figure 5.1, the concentrations of CTC and 4-epi-CTC in *A. thaliana* plants significantly decreased with increased exposure time, suggesting further metabolism of these compounds in plant tissues. Confirmation of other metabolites followed the framework proposed by (Schymanski et al., 2014). Two signals with m/z 641.1760 eluted at $R_t = 3.35$ min (TP641a) and $R_t = 3.74$ min (TP641b) that differed from the parent CTC by 162.05 Da was observed, suggesting the formation of CTC-*O*-glucosides. Their high-collision-energy mass spectra gave rise to fragment ions at m/z 624.1464 ([TP641a + H - NH₃]⁺) and m/z 624.1503 ([TP641b + H - NH₃]⁺), and the characteristic fragment ions of the parent CTC, m/z 462.0968, respectively (Supplementary Figure 5.7 and Supplementary Figure 5.8). The characteristic fragment ion of CTC m/z 444.0858 was also observed in the high-collision-energy mass spectra of TP641b; however, it was absent in the mass spectra of TP641a. These fragment ions indicated the structure of parent CTC was intact; however, the sites of conjugation could not be unequivocally identified. The potential glycosylation sites were subsequently predicted using the web-based *in silico* tool XenoSite UGT 2.0 (<http://swami.wustl.edu/xenosite/>) (Dang et al., 2016). The results suggested that the glucose

moieties are most likely to be conjugated with the OH- groups at carbon C-10, followed by the OH- groups at carbon C-3 (Figure 5.3). *In vitro* glycosylation of CTC using UDP-glycosyltransferase from *Bacillus licheniformis* has recently been reported by (Pandey et al., 2018). Although the exact glycosylation site was not elucidated in their studies, Pandey et al. suggested that the glucose moieties chemically favor the OH- at carbon C-10 (Pandey et al., 2018).

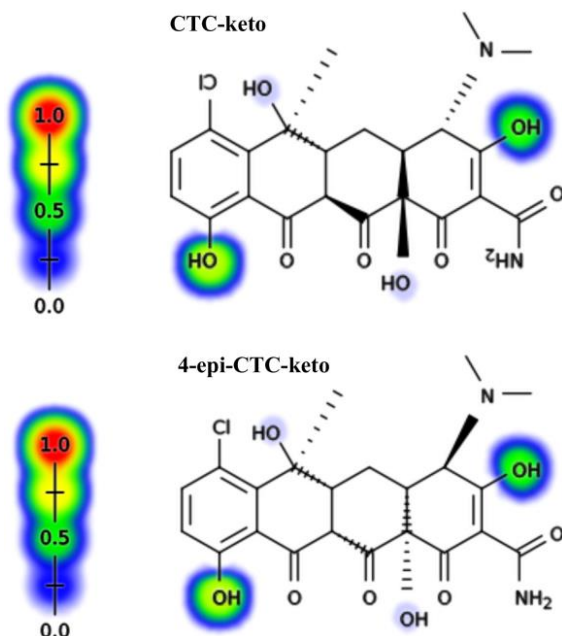


Figure 5. 3. XenoSite prediction of the glycosylation positions on the structures of CTC isomers. The scales from 0.0 to 1.0 indicate higher possibility of conjugation reactions (Dang et al., 2016).

In addition to the glycosylated metabolites, two signals at m/z 445.1606 (R_t = 3.99 min, P445a) and m/z 445.1618 (R_t = 4.38 min, TP445b) were also exclusively detected in the CTC-exposed plants. Their mass-to-charge ratio differed from the parent CTC 33.96 Da. Additionally, no chlorine isotopic pattern ($m + 2$) was observed in their high-resolution mass spectra, suggesting that TP445a and TP445b were dechlorinated products of CTC. Dechlorination of CTC leads to the occurrence of tetracycline (TC) in *A. thaliana* plant tissues, with the corresponding characteristic fragment ions, m/z 410.1235 and m/z 427.1223, were also observed in the high-collision-energy

mass spectra (Supplementary Figure 5.9 and Supplementary Figure 5.10). Two signals at m/z 465.1062 ($R_t = 4.79$ min) and m/z 465.1058 ($R_t = 5.22$ min) exhibited a loss of 14.02 Da, corresponding to a CH_3 - group, from the parent CTC, with the monochlorinated isotopic pattern $[(m + 2)/m \sim 32\%]$. However, their characteristic fragment ions could not be clearly observed in the high-collision-energy mass spectra due to low abundance of the precursor parent ions. Accordingly, these two signals were tentatively identified as the isomers of demeclocycline.

Plant detoxification of CTC is potentially species-specific, in which glutathione *S*-transferase (GST) plays an important role in tolerant plant species (Mathews and Reinhold, 2013). For example, Farkas et al. observed significant increase in GST activity in maize plants grown in CTC-treated soil, while pinto beans showed no difference in the GST activity between control and CTC-treated plants, which may explain the phytotoxicity observed on the pinto beans (Farkas et al., 2007). *In vitro* conjugation reactions subsequently revealed that the induced GST catalyzed the conjugation between CTC and glutathione (GSH) through nucleophilic substitution of the chlorine atom in CTC with sulfur in GSH (Farkas et al., 2007). Bowman et al. also observed no significant increase in GST activity on CTC-exposed *A. thaliana* plants when compared to the control (Bowman et al., 2011). These results suggested that conjugation with glutathione, catalyzed by GST, was likely not the primary detoxification pathway of CTC in pinto bean and *A. thaliana* plants. This assumption was further supported by the fact that no CTC-GSH conjugate was detected in our study over the exposure time, although two dechlorinated products of CTC were detected in *A. thaliana* plant tissues. The removal of the chlorine atom of CTC results in the production of tetracycline (TC), which has been previously observed in aqueous solution under simulated sunlight (Chen et al., 2012). In this study, two isomers of TC were also detected in the culture media, likely as the photodegradation products of CTC. Subsequent uptake of these

transformation products by *A. thaliana* explained their occurrence in the plant tissues. It is possible that the two isomers of TC detected in the culture media and plant tissues could also be the transformation products of CTC. *In vivo* reductive dechlorination has been previously reported for PCBs in maize (Wang et al., 2011) and 1,2,5,5,6,9,10-heptachlorodecan in pumpkin (Li et al., 2017). The occurrence of TC and demeclocycline (DMC) in this study is in accordance with previously reported results, where several tetracycline residues were also detected in wheat and rye grains of plants exclusively treated with CTC (Schwake-Anduschus and Langenkamper, 2018). Glycosylation, catalyzed by glycosyltransferases, is one of the most common conjugation of organic xenobiotics in plants (Schwitzguebel and Vanek, 2003). According to our best knowledge, *O*-glycosylation of CTC in plants is reported for the first time in this study. The concentrations of glycosyl-CTC metabolites in *A. thaliana* plant tissues were highest after 4 days of exposure and were approximately one order-of-magnitude higher than those of TC and DMC over the exposure period (Figure 5.4).

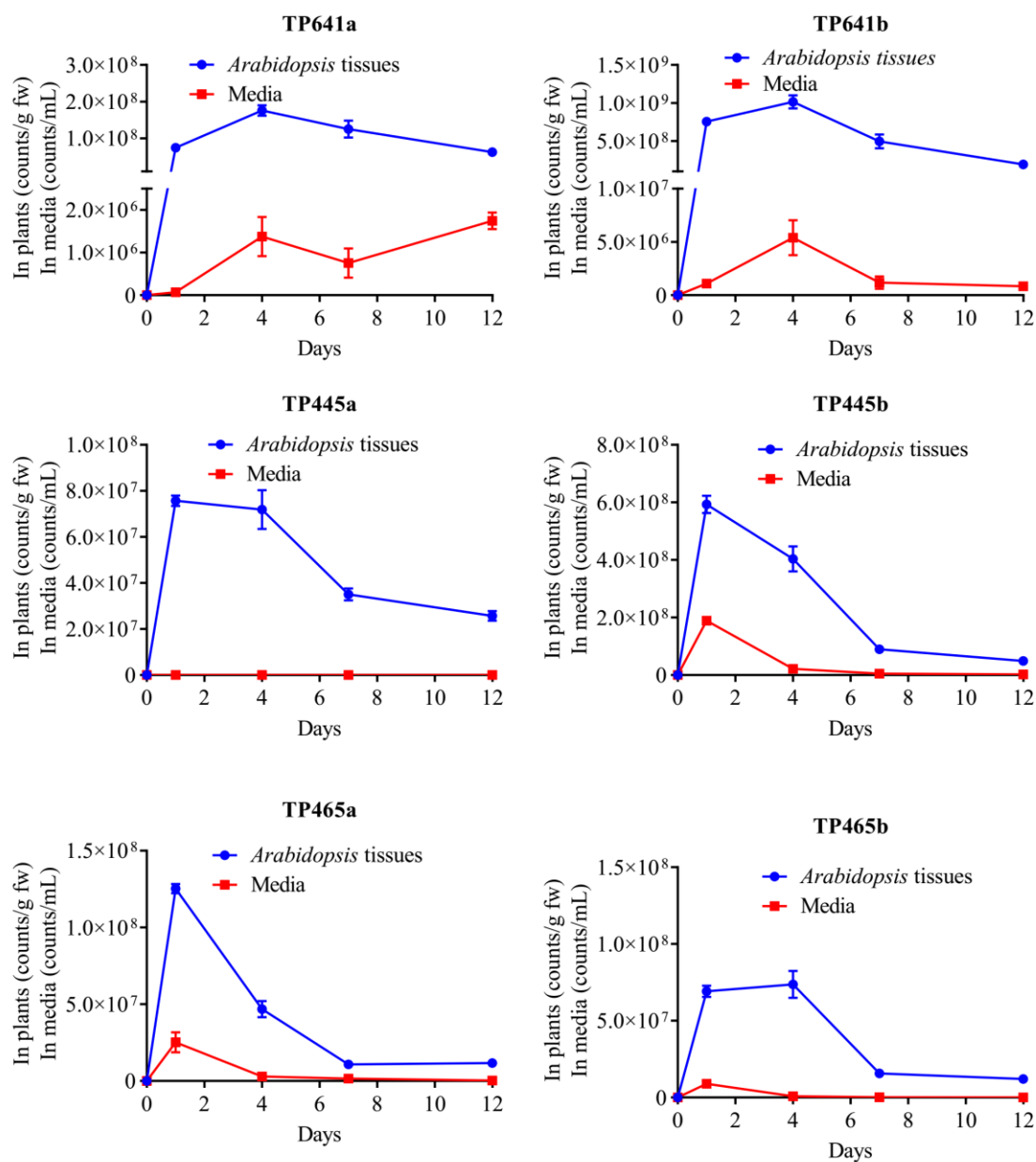


Figure 5. 4. Temporal variations of the metabolites TP641 (glycosyl-CTC), TP445 (TC), and TP465 (DMC) in the *A. thaliana* plant tissues and culture media over 12 days of exposure. Data are presented as mean \pm SE of triplicates, with some error bars are obscured by data symbols.

Table 5. 1. Mass-Spectral Information and Proposed Structures of the CTC-Transformation Products Identified by Waters Progenesis QI 2.1 and MassLynx 4.1 Software.

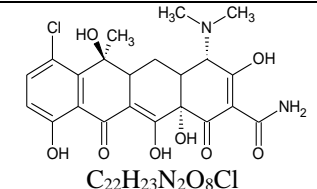
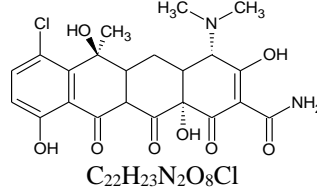
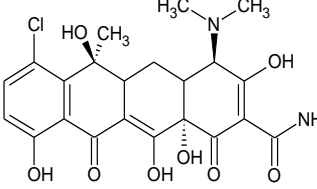
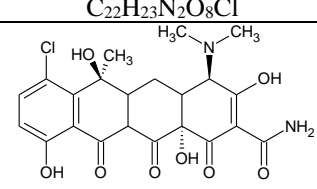
denotation	RT (min) ^a	calcd <i>m/z</i> ^b	obsd <i>m/z</i> ^c	error (ppm)	predicted formula and structure	fragments (<i>m/z</i>) ^d	level ^e
chlortetracycline-enol (CTC-enol)	5.27	479.1216	479.1228	2.5	 <chem>C22H23N2O8Cl</chem>	444.0829 446.0803 462.0927 464.0906	1
chlortetracycline-keto (CTC-keto)	4.67	479.1216	479.1219	0.6	 <chem>C22H23N2O8Cl</chem>	462.0946 464.0907	1
4-epi-chlortetracycline-enol (4-epi-CTC-enol)	4.85	479.1216	479.1226	2.1	 <chem>C22H23N2O8Cl</chem>	444.0858 446.0826 462.0983 464.0942	1
4-epi-chlortetracycline-keto (4-epi-CTC-keto)	4.45	479.1216	479.1231	3.1	 <chem>C22H23N2O8Cl</chem>	462.0962 464.0920	1

Table 5.1 (cont'd). Mass-Spectral Information and Proposed Structures of the CTC-Transformation Products Identified by Waters Progenesis QI 2.1 and MassLynx 4.1 Software.

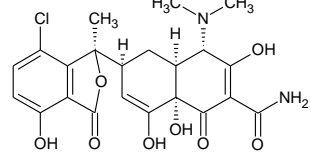
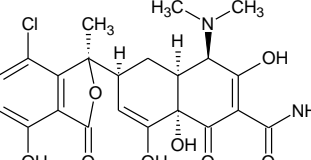
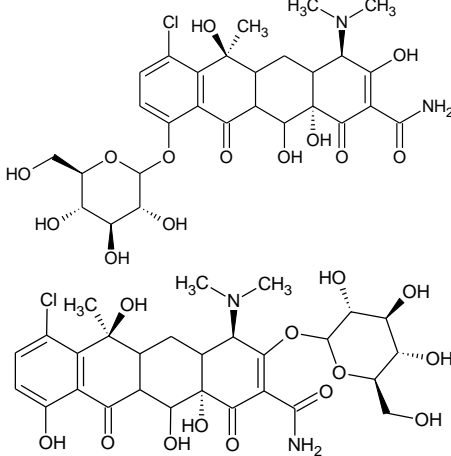
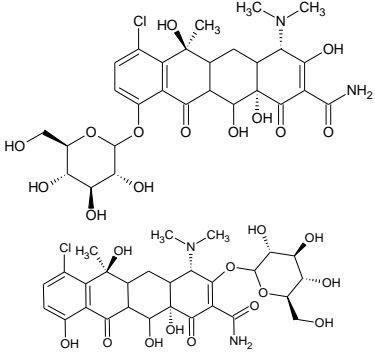
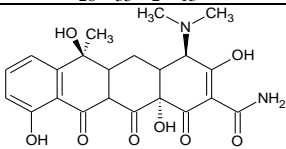
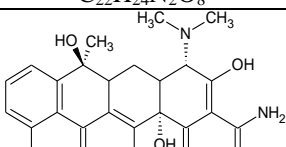
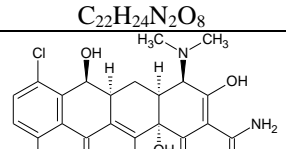
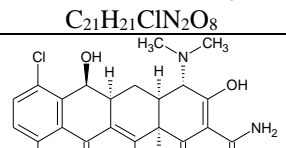
6-iso-chlortetracycline (6-iso-CTC)	4.67	479.1216	479.1234	3.8	 <p style="text-align: center;">$C_{22}H_{23}N_2O_8Cl$</p>	462.0965 464.0948	1
4-epi-6-iso-chlortetracycline (4-epi-6-iso-CTC)	4.30	479.1216	479.1218	0.4	 <p style="text-align: center;">$C_{22}H_{23}N_2O_8Cl$</p>	462.0952 464.0961	1
glycosyl-4-epi-CTC (TP641a)	3.35	641.1744	641.1760	2.5	 <p style="text-align: center;">$C_{28}H_{33}N_2O_{13}Cl$</p>	624.1464 626.1439 462.0968 464.0927	3

Table 5.1 (cont'd). Mass-Spectral Information and Proposed Structures of the CTC-Transformation Products Identified by Waters Progenesis QI 2.1 and MassLynx 4.1 Software.

glycosyl-CTC (TP641b)	3.74	641.1744	641.1760	2.5	 <p>$C_{28}H_{33}N_2O_{13}Cl$</p>	624.1503 626.1487 462.0958 464.0941 444.0858 446.0795	3
4-epi-tetracycline (TP445a)	3.99	445.1605	445.1606	0.2	 <p>$C_{22}H_{24}N_2O_8$</p>	410.1223	3
tetracycline (TP445b)	4.38	445.1605	445.1618	2.9	 <p>$C_{22}H_{24}N_2O_8$</p>	410.1235 427.1223	3
4-epi-demeclocycline (TP465a)	4.79	465.1059	465.1062	0.6	 <p>$C_{21}H_{21}ClN_2O_8$</p>	465.1062 467.1068	4
demeclocycline (TP465b)	5.22	465.1059	465.1058	0.2	 <p>$C_{21}H_{21}ClN_2O_8$</p>	465.1058 467.1033	4

^aRetention time of CTC and its metabolites when they were analyzed on the UPLC-QTOF-MS^E system. ^bThe accurate calculated masses (calcd m/z) were obtained with Chemsketch software, version 2016.2.2 (ACD/Laboratories, Toronto, ON). ^cThe observed masses (obsd m/z) were obtained from a high-resolution mass analyzer (QTOF-MS^E, Waters Xevo G2-XS). ^dThe fragments ions acquired in the high collision energy mode of UPLC-QTOF-MS^E. ^eAccording to Schymanski et al. Level 1: reference standard, HR-MS, MS/MS, RT confirmed; Level 2b: HR-MS, characteristic fragmentation patterns observed; Level 3: HR-MS, characteristic fragmentation patterns observed, alternative structures (e.g. ring glycosylated positions, isomers) might be possible; Level 4: HR-MS, chemical formulas unequivocally assigned; Level 5: exact mass of interest.

5.3.2. Oxytetracycline (OTC)

5.3.2.1. OTC dissipation in media and accumulation in plant tissues

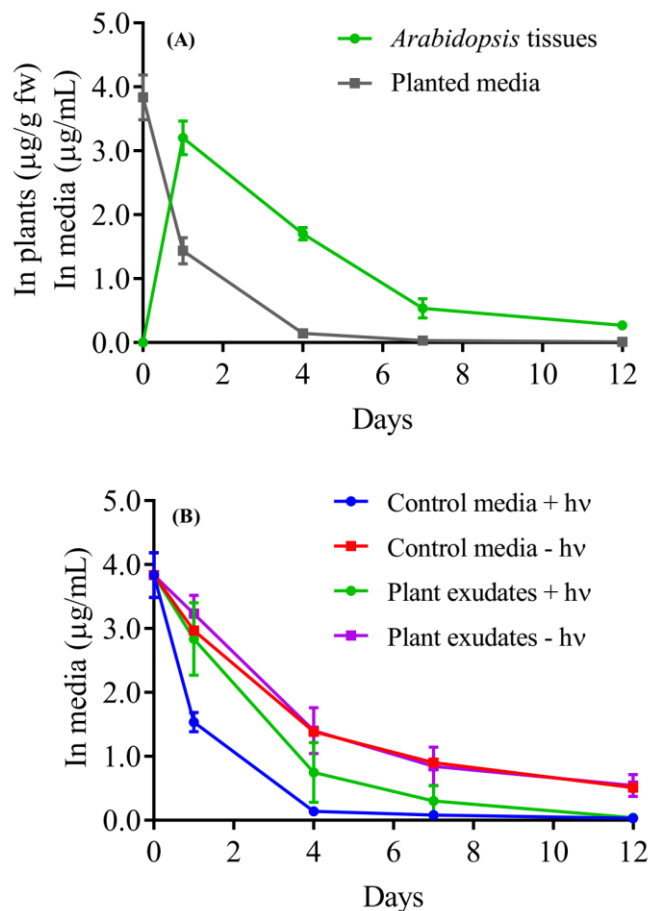


Figure 5. 5. Temporal variations of OTC in the *A. thaliana* plant tissues and planted media (A), and in the control media (B) over 12 days of exposure. Data are presented as mean \pm SE of triplicates, with some error bars are obscured by data symbols.

The concentrations of OTC in the *Arabidopsis*-planted media and control media (with and without plant exudates) were significantly decreased over 12 days of exposure (Figure 5.5). Since all treatments were conducted in sterile conditions, dissipation of OTC in the control media was primarily due to abiotic transformation. As showed in Figure 5.5B, light exposure (+ hv) significantly increased the removal of OTC in the media compared to the dark treatments (- hv) ($p < 0.001$); however, the removal was decelerated by the presence of plant exudates ($p = 0.001$). For

example, OTC concentrations in the control media decreased from initially $3.83 \pm 0.20 \mu\text{g/mL}$ to $1.53 \pm 0.09 \mu\text{g/mL}$ after only 1 day of exposure, while those in the media containing plant exudates were $2.83 \pm 0.33 \mu\text{g/mL}$. After 12 days, only trace amounts of OTC were detected in both light exposure controls (approximately $0.03 \mu\text{g/mL}$ and $0.04 \mu\text{g/L}$, respectively). The concentrations of OTC were also decreased in the dark controls; however, there were no differences between the media containing plant exudates and those without plant exudates ($p = 0.955$) (Figure 5.5B). Photolysis has been reported as an important elimination pathway of OTC in aqueous solutions, in which the solution pH, temperature, complexation with cations (e.g. Fe^{3+} , Ca^{2+} , Mg^{2+}), and co-presence of anions (e.g. NO_3^- , HCO_3^-) imposed significant impacts on OTC photolysis (Chen et al., 2011, Jin et al., 2017, Li et al., 2018, Xuan et al., 2010, Zhao et al., 2013). For direct photolysis, degradation of OTC in acidic condition was negligible due to the poor visible light absorption; however, increasing solution pH enhanced the photolytic degradation of OTC (Li et al., 2018, Zhao et al., 2013). In other words, the photolytic reactions favorably occurred with the negatively charged states of OTC (e.i. OTC^- and OTC^{2-} states) (Li et al., 2018, Zhao et al., 2013). In the current study, pH of the media was maintained at approximately 5.7; therefore, direct photolysis was supposedly minimal according to (Zhao et al., 2013). As a result, in our study, indirect photolysis might have contributed to the dissipation of OTC in the control media and the media containing plant exudates. For example, Li et al. observed that increasing NO_3^- and HCO_3^- concentrations in aqueous solutions promoted indirect photolysis of OTC by generating the hydroxyl radicals $\text{HO}\cdot$ and adjusting the solution pH, respectively (Li et al., 2018). The 0.5X MS media used in the current study contained approximately 10 mM of NO_3^- , which potentially played an important role in the indirect photolysis of OTC. Interestingly, while Fe^{3+} was found to inhibit the photodegradation of OTC under simulated sunlight (Li et al., 2018), the presence of Fe^{3+}

induced degradation of OTC in aqueous solutions without light exposure (Wang et al., 2015), which potentially explained the decrease in OTC concentrations in the dark controls observed in our study. According to Wang et al., Fe^{3+} first complexes with OTC molecule via the A ring's C-4 dimethylamino group and oxidizes OTC to form Fe^{2+} and OTC radical; subsequently, Fe^{2+} can be oxidized back to Fe^{3+} by dissolved oxygen and OTC radicals can be further transformed to other products in the solutions. In our study, the 0.5X MS media contained approximately 50 μM of Fe^{2+} , which was likely to be oxidized by the dissolved oxygen in the solutions and promoted the degradation of OTC in the dark controls over 12 days of exposure.

In addition to abiotic degradation, plant uptake also contributed to the dissipation of OTC in the *A. thaliana*-planted media (Figure 5.5A). The concentrations of OTC in plant tissues were highest after 1 day of exposure ($3.20 \pm 0.15 \mu\text{g/g fw}$) and then decreased with increasing exposure time. After 12 days of exposure, plant OTC concentrations were $0.27 \pm 0.03 \mu\text{g/g fw}$. The dilution effect due to plant growth during exposure on the decrease in plant OTC concentrations was found to be negligible, as evident by a consistent loss of OTC mass in plant tissues. For example, the amounts of OTC accumulated in plant tissues were $12.80 \pm 0.91 \mu\text{g}$ after 1 day and decreased to $2.07 \pm 0.34 \mu\text{g}$ after 12 days of exposure. The results implied that OTC was extensively metabolized by *A. thaliana* following plant uptake.

5.3.2.2. Screening of the OTC metabolites using multivariate statistical analysis

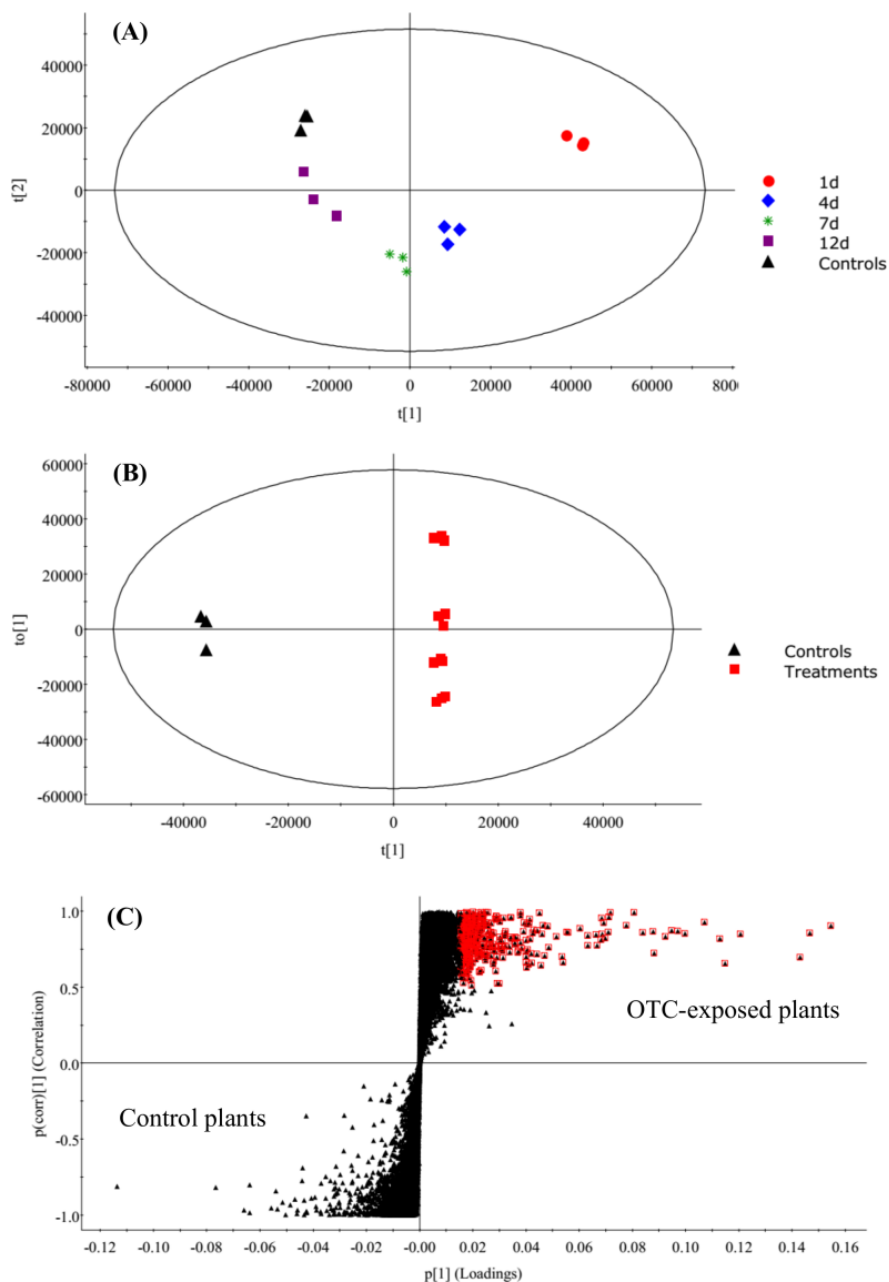


Figure 5. 6. PCA score plots (A), OPLS-DA score plots (B), and S-plots (C) derived from the UPLC-QTOF-MS^E datasets of the control and OTC-exposed plants (1, 4, 7, and 12 days). The ellipses represent Hotelling's T^2 with 95% confidence. The m/z variables on the S-plot that significantly contributed to the differences between control plants and OTC-exposed plants ($p(\text{corr}) \geq 0.5$) were selected for screening of OTC metabolites.

The unsupervised PCA was initially applied to visualize clustering of the control and OTC-exposed *A. thaliana* plant extracts at multiple sampling times. The explanation value ($R^2X(\text{cum})$)

and predictability value ($Q^2(cum)$) obtained from the three-component PCA model were 86% and 76%, respectively. The score plot of the first two principal components, which explained 75% of the total variance, is presented in Figure 5.6A, with each point represents an individual plant sample. Generally, samples clustered close to each other have similar metabolic profiles, while those scattered far away from each other are dissimilar. Clear separation of the control and OTC-exposed plants on the score plot of the PCA model clearly indicates that exposure to OTC resulted in significant alteration in *A. thaliana* plant metabolic profiles, in which the largest differences could be observed during the early stage of the exposure (e.i. 1–4 days following CTC exposure). Furthermore, differences in metabolic profiles among the OTC-exposed plants were also time-dependent: plants sampled at different time intervals (1, 4, 7, and 12 days) were distinctively separated from each other on the score plot. The supervised OPLS-DA model was subsequently used to identify the potential metabolite candidates that significantly contributed to the differentiation between control and OTC-exposed plants. The OPLS-DA score plot is presented in Figure 5.6B, with the explanation value ($R^2Y(cum)$) and predictability value ($Q^2(cum)$) were 99% and 87%, respectively, resulted in a clear separation between the control and OTC-exposed plants (1, 4, 7, and 12 days). The observed differences can be explained by the m/z variables scattering on the upper right and lower left quadrants of the S-plot obtained from the OPLS-DA model (Figure 5.6C). Generally, the intensity of the m/z variables plotted in the lower quadrant of the S-plot decreased in the OTC-exposed plants compared to the control plants, while those plotted in the upper right quadrant indicate an increase in ion intensity of these variables in the OTC-exposed plants. The latter consisted of both the potential metabolites of OTC, as well as other endogenous secondary metabolites that *A. thaliana* plants produced upon exposure to the stressor, OTC. Differentiation within the S-plot is due to concentration differences and the m/z variables with a

higher intensity yield a better separation from the background ions (Macherius et al., 2014a). Accordingly, in this study, the OTC metabolite candidates were primarily screened from the variables scattered in the upper right quadrant of the S-plot with $p(\text{corr}) \geq 0.5$ (Figure 5.6C).

5.3.2.3. Metabolism of OTC by *A. thaliana*

Similar to CTC, plant uptake and metabolism of OTC occurred shortly upon exposure to *A. thaliana* (Figure 5.5-A). On the UPLC-QTOF-MS^E system, the parent OTC eluted at $R_t = 4.24$ min (m/z 461.1572), with two characteristic fragment ions at m/z 426.1108 and m/z 444.1299 (Supplementary Figure 5.11). A signal at m/z 461.1569 eluted at $R_t = 4.06$ min (TP461) that has the same mass with the parent OTC. In high-collision-energy mode, TP461 also produced fragment ions at m/z 426.1189 ($[\text{TP461} + \text{H} - \text{NH}_3 - \text{H}_2\text{O}]^+$) and m/z 444.1289 ($[\text{TP461} + \text{H} - \text{NH}_3]^+$), which are identical to those of the parent OTC, suggesting that TP461 is likely 4-epi-OTC. As revealed in Supplementary Figure 5.11, along with m/z 461.1569, another signal at m/z 447.1423 ($R_t = 4.06$ min) was also acquired in the low collision energy mode, which differed from the parent OTC by 14.01 Da was observed, suggesting the formation of a demethylated products (TP447). Its high-collision-energy mass spectra gave rise to fragment ions at m/z 412.1037 ($[\text{TP447} + \text{H} - \text{NH}_3 - \text{H}_2\text{O}]^+$) and m/z 429.1313 ($[\text{TP447} + \text{H} - \text{NH}_3]^+$) (Supplementary Figure 5.12). However, the current mass-spectral data are insufficient to confirm that TP447 and TP461 are two different metabolites based on the fact that they have exactly the same retention time (Table 5.2).

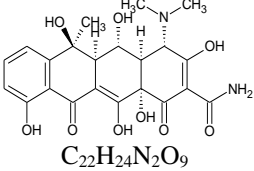
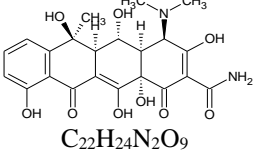
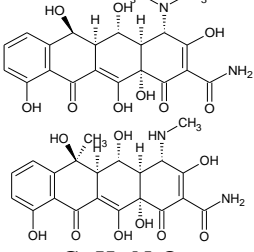
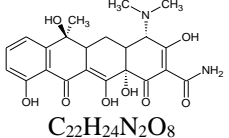
A signal at m/z 445.1613 ($R_t = 4.38$ min, TP445) was exclusively detected in the OTC-exposed plants. Their mass-to-charge ratio differed from the parent OTC 15.99 Da, suggesting loss of an -OH group. However, the position of the -OH group cannot be exactly identified based on the mass-spectral data. Two characteristic fragment ions, m/z 410.1240 and m/z 427.1224, were observed in the high-collision-energy mass spectra (Supplementary Figure 5.13), which was

identical to the fragment ions obtained from the dechlorinated products of CTC in the CTC treatments (Table 5.1), suggesting TP445 in this study was also tetracycline.

Three signals, including m/z 577.1252 (TP577, R_t = 2.65 min), m/z 817.1721 (TP817, R_t = 3.66 min), and m/z 795.2308 (TP795, R_t = 4.09 min), were exclusively detected in the OTC-exposed plants and absent in the control plants; therefore, they are likely the metabolites of OTC in plant tissues; however, their fragment ions obtained in the high collision energy mode were not adequately explained. Consequently, TP577, TP817, and TP795 were assigned to a level 5, or “unknown structure”, in this study (Schymanski et al., 2014).

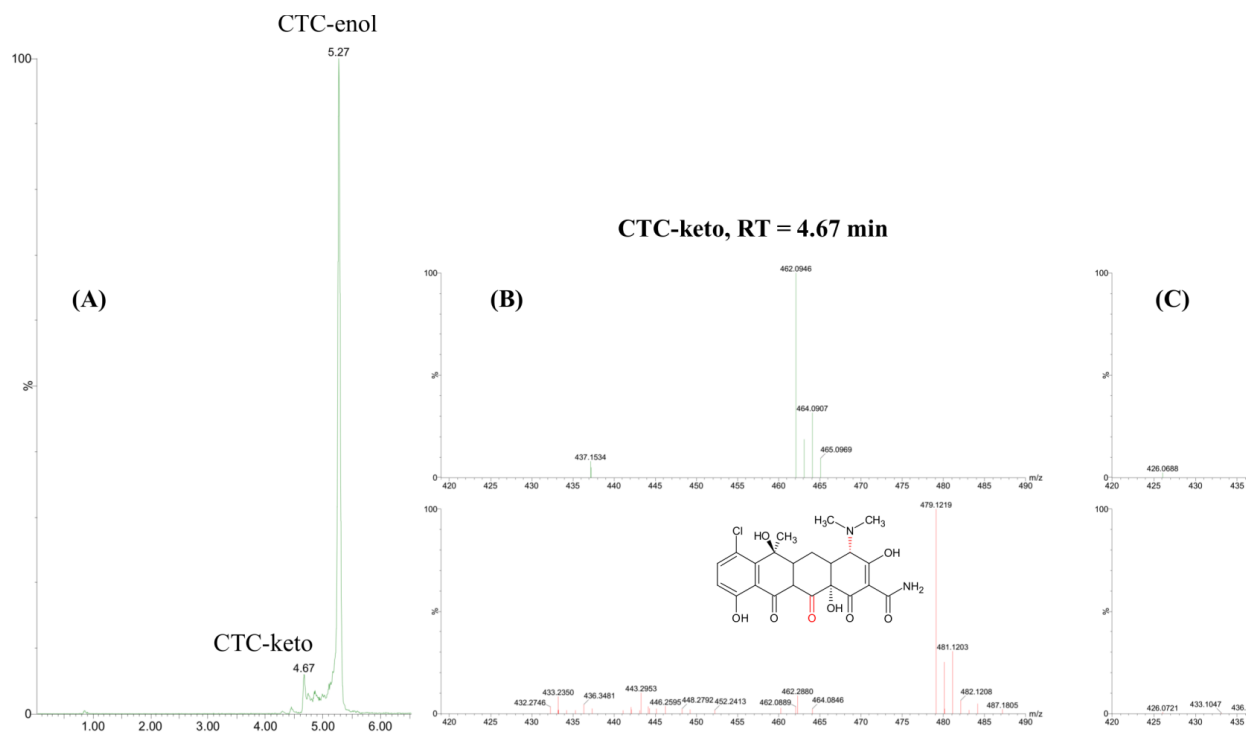
Unexpectedly, glycosylated metabolites were not detected in the *A. thaliana* plant extracts during the exposure time. The results suggested that, while glycosylation is among the most commonly observed detoxification pathways of organic xenobiotics in planted systems, it might not be the major metabolic pathway of OTC in plants. However, further studies on other plant species are necessary because differences in plant species and exposure conditions have been reported to considerably affect the metabolic pathways of antimicrobials in plant tissues (Dudley et al., 2018).

Table 5. 2. Mass-Spectral Information and Proposed Structures of the OTC-Transformation Products Identified by Waters Progenesis QI 2.1 and MassLynx 4.1 Software.

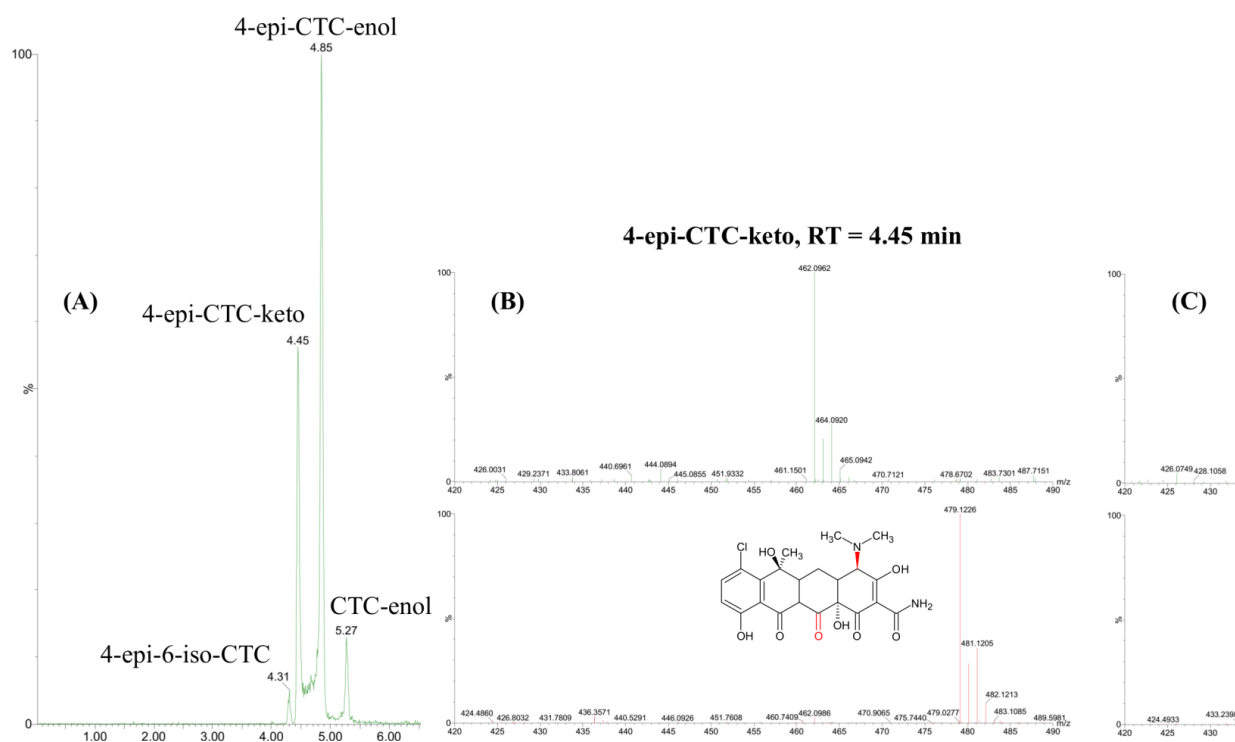
denotation	RT (min) ^a	calcd <i>m/z</i> ^b	obsd <i>m/z</i> ^c	error (ppm)	predicted formula and structure	fragments (<i>m/z</i>) ^d	level ^e
oxytetracycline (OTC)	4.24	461.1555	461.1572	3.7	 C ₂₂ H ₂₄ N ₂ O ₉	426.1180 444.1299	1
4-epi-OTC (TP461)	4.06	461.1555	461.1569	3.0	 C ₂₂ H ₂₄ N ₂ O ₉	426.1189 444.1289	3
demethyl-OTC (TP447)	4.06	447.1398	447.1423	5.6	 C ₂₁ H ₂₂ N ₂ O ₉	412.1037 429.1313	3
tetracycline (TP445)	4.38	445.1605	445.1613	1.8	 C ₂₂ H ₂₄ N ₂ O ₈	410.1235 427.1223	3
TP577	2.64		577.1252		unknow structure		5
TP817	3.66		817.1721		unknow structure		5
TP795	4.09		795.2308		unknow structure		5

^aRetention time of OTC and its metabolites when they were analyzed on the UPLC-QTOF-MS^E system. ^bThe accurate calculated masses (calcd *m/z*) were obtained with Chemsketch software, version 2016.2.2 (ACD/Laboratories, Toronto, ON). ^cThe observed masses (obsd *m/z*) were obtained from a high-resolution mass analyzer (QTOF-MS^E, Waters Xevo G2-XS). ^dThe fragments ions acquired in the high collision energy mode of UPLC-QTOF-MS^E. ^eAccording to Schymanski et al. Level 1: reference standard, HR-MS, MS/MS, RT confirmed; Level 3: HR-MS, characteristic fragmentation patterns observed, alternative structures might be possible; Level 5: exact mass of interest.

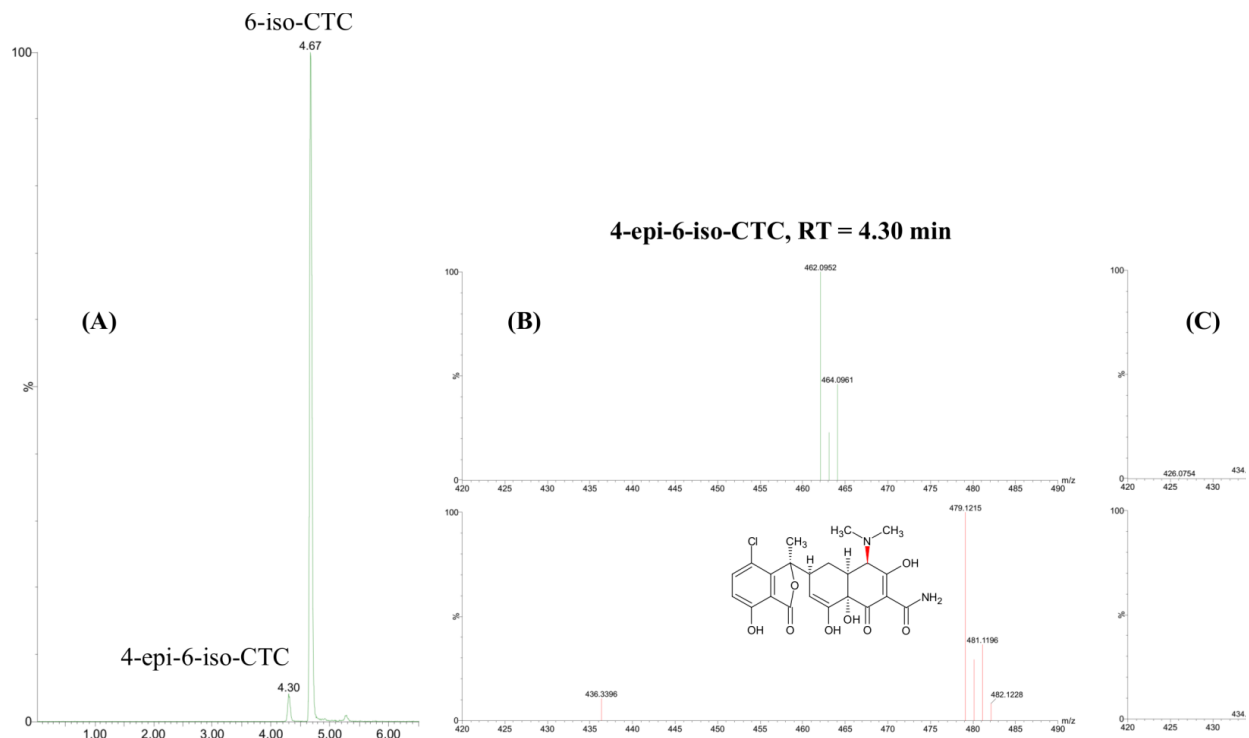
APPENDIX



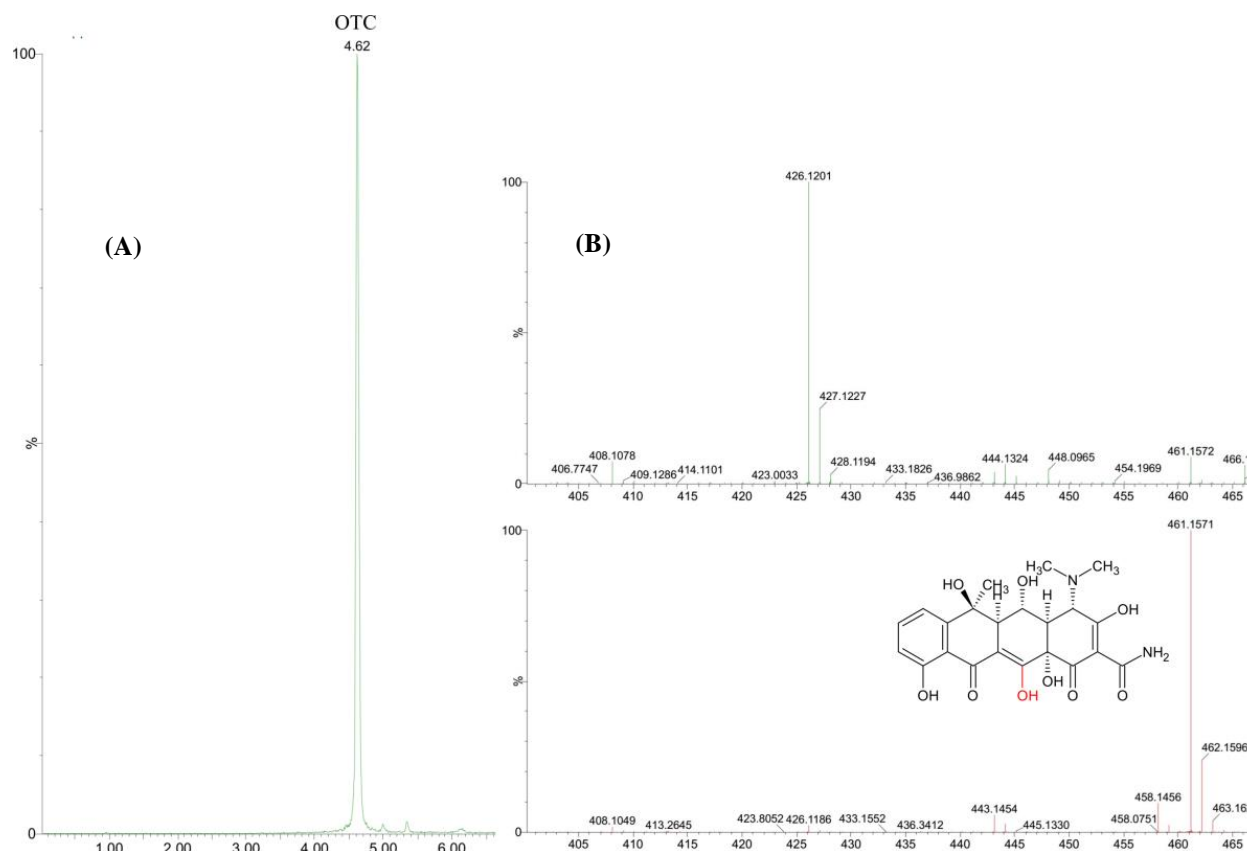
Supplementary Figure 5.1. Selected ion chromatogram of CTC standard (0.2 $\mu\text{g/mL}$) at m/z 479.12 (A), and the characteristic fragmentation patterns of the two main signals at RT = 4.67 min (B) and RT = 5.27 min (C), respectively, on the UPLC-QTOF-MS^E system.



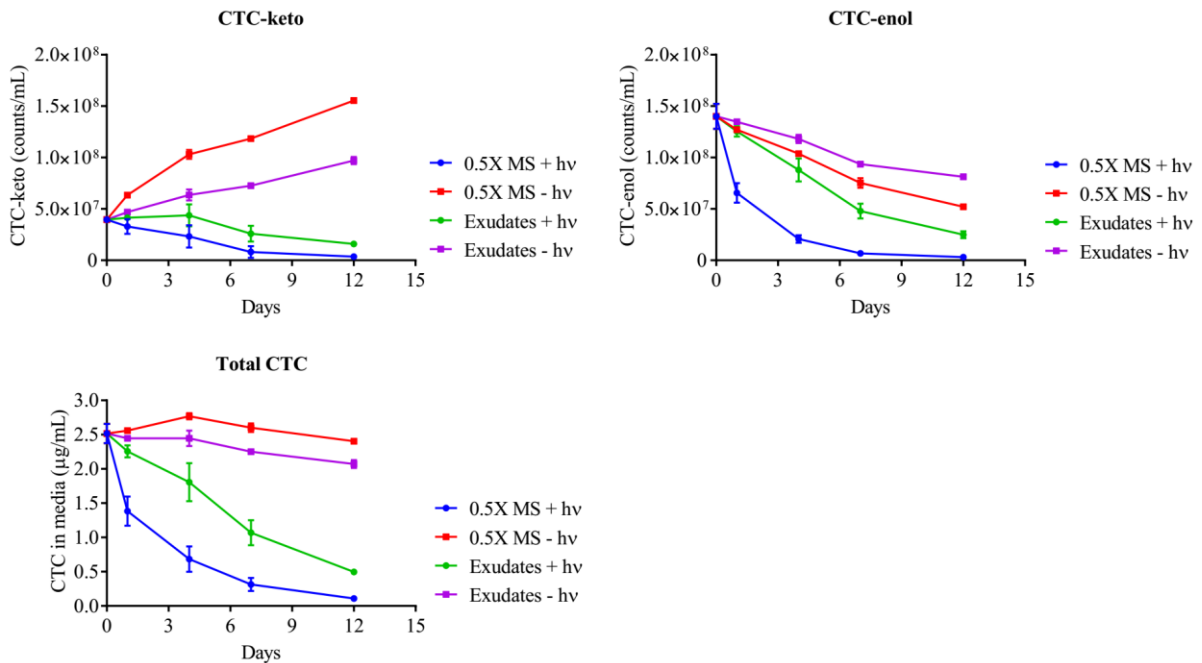
Supplementary Figure 5.2. Selected ion chromatogram of 4-epi-CTC standard (0.2 $\mu\text{g/mL}$) at m/z 479.12 (A), and the characteristic fragmentation patterns of the two main signals at RT = 4.45 min (B) and RT = 4.85 min (C), respectively, on the UPLC-QTOF-MS^E system.



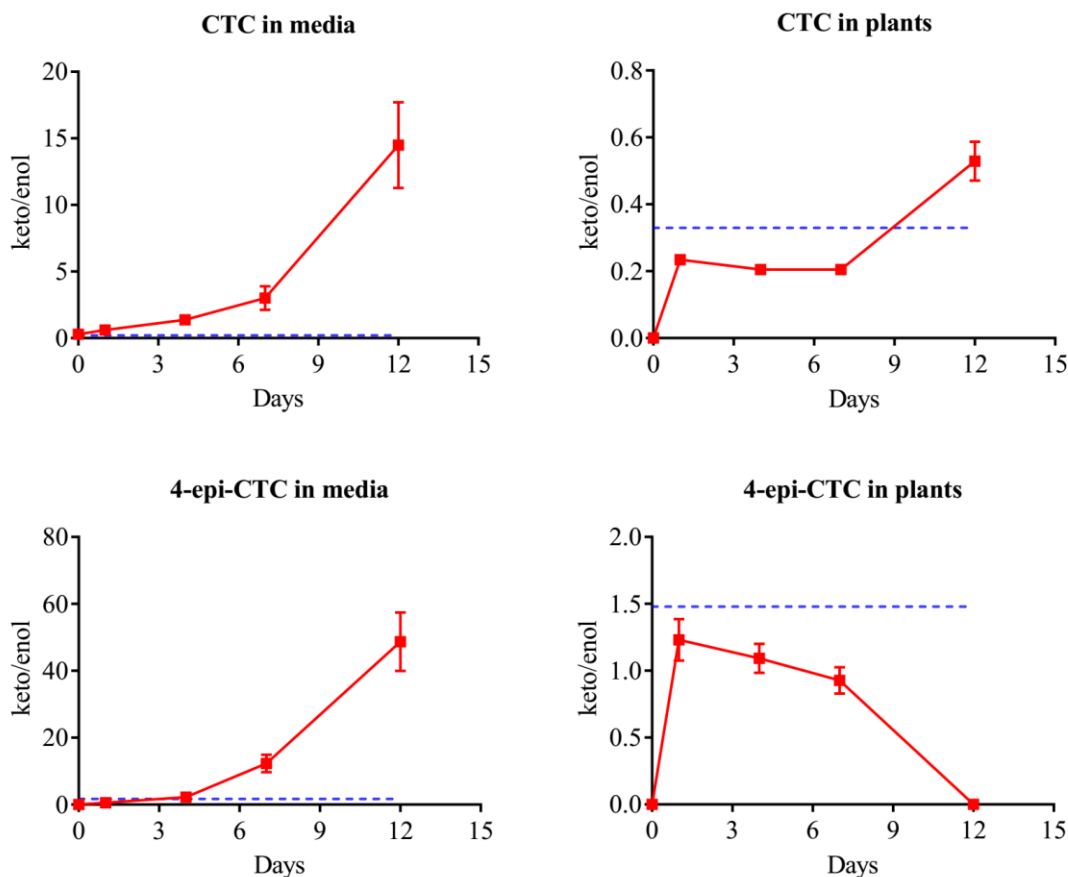
Supplementary Figure 5.3. Selected ion chromatogram of 6-iso-CTC standard (0.2 $\mu\text{g/mL}$) at m/z 479.12 (A), and the characteristic fragmentation patterns of the two main signals at RT = 4.30 min (B) and RT = 4.67 min (C), respectively, on the UPLC-QTOF-MS^E system.



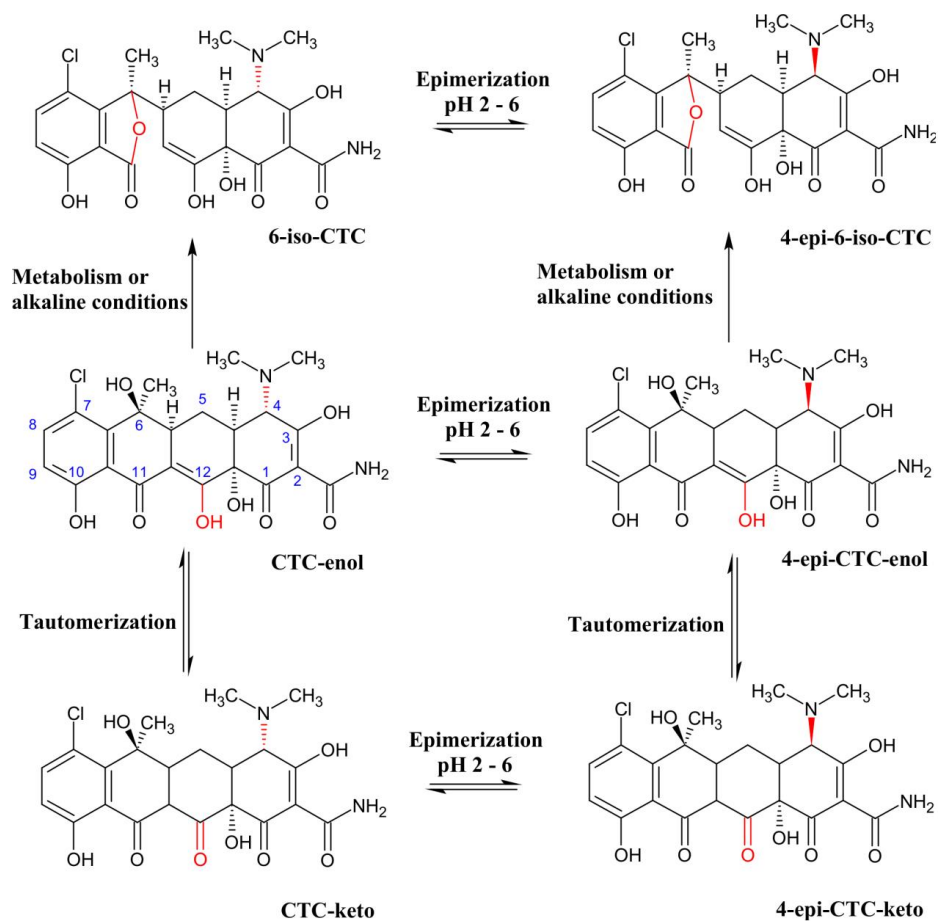
Supplementary Figure 5.4. Selected ion chromatogram of OTC standard (0.2 $\mu\text{g/mL}$) at m/z 461.15 (A), and its characteristic fragmentation patterns (B) on the UPLC-QTOF-MS^E system.



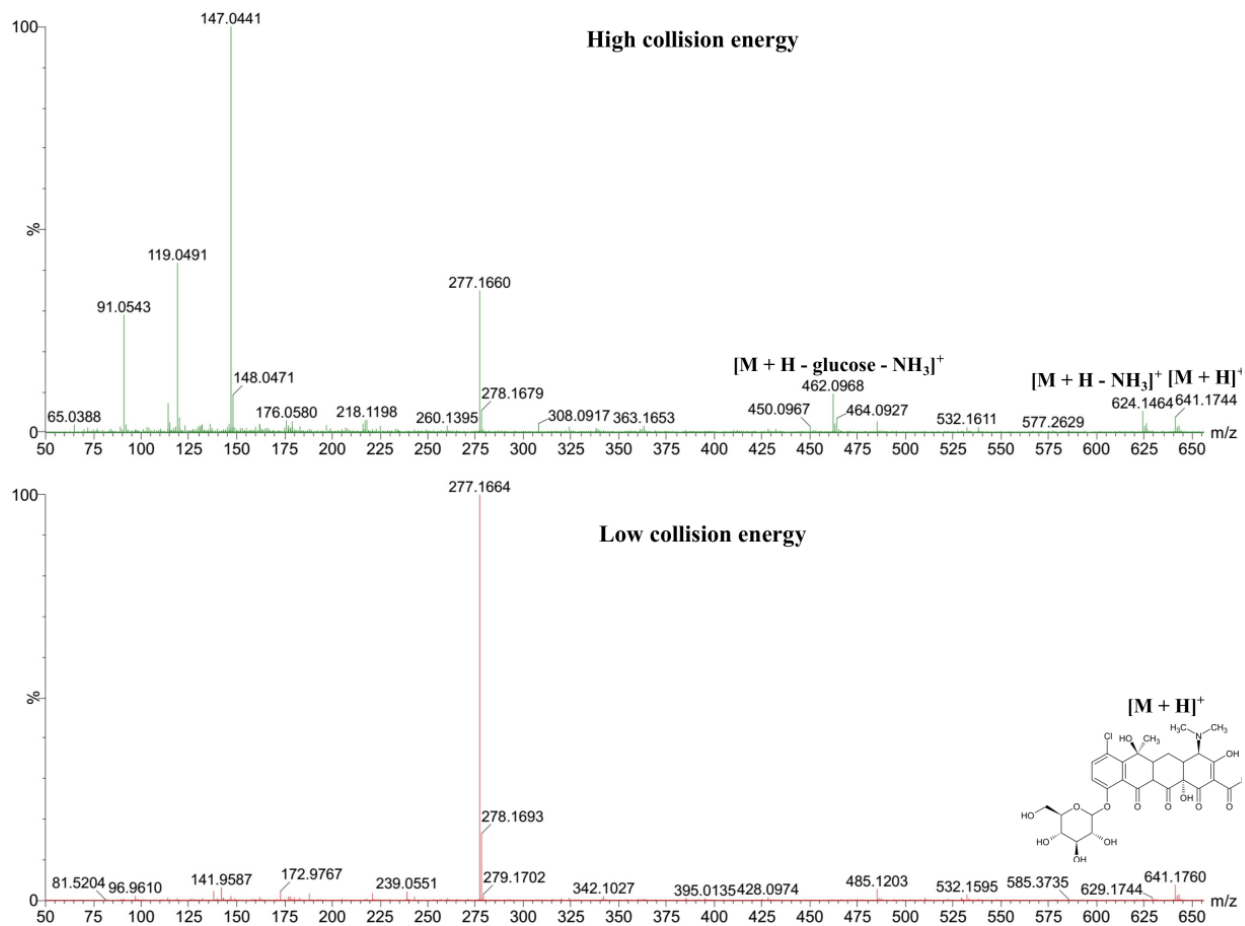
Supplementary Figure 5.5. Effects of light exposure (+/- hv) on removal of CTC in 0.5X MS media with and without plant exudates. The abiotic media containing CTC at a concentration of $2.52 \pm 0.08 \mu\text{g/mL}$ was exposed to fluorescence light in a plant growth chamber under similar conditions with the CTC plant uptake studies. For the no-light exposure, the containers were wrapped in aluminum foil. Data are presented as mean \pm SE of triplicates, with some error bars are obscured by data symbols.



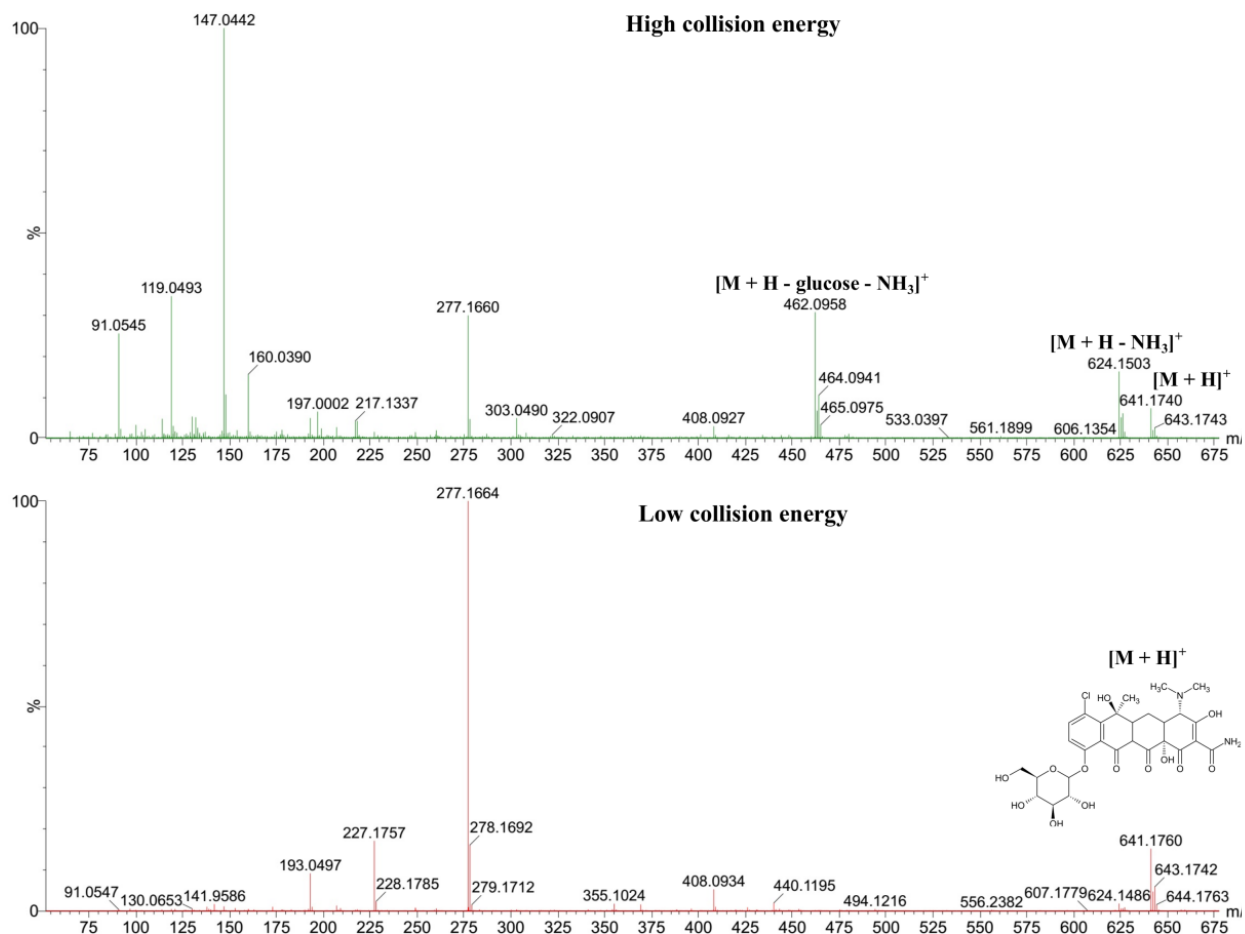
Supplementary Figure 5.6. The ratio of keto/enol tautomers of CTC and 4-epi-CTC in media samples and plant extracts at various sampling intervals (red lines). The dotted blue lines represent the mean values of the keto/enol ratio identified in the matrix-matched standard series used for quantification of CTC and 4-epi-CTC in the corresponding sample matrices. Data are presented as mean \pm SE of triplicates, with some error bars are obscured by data symbols.



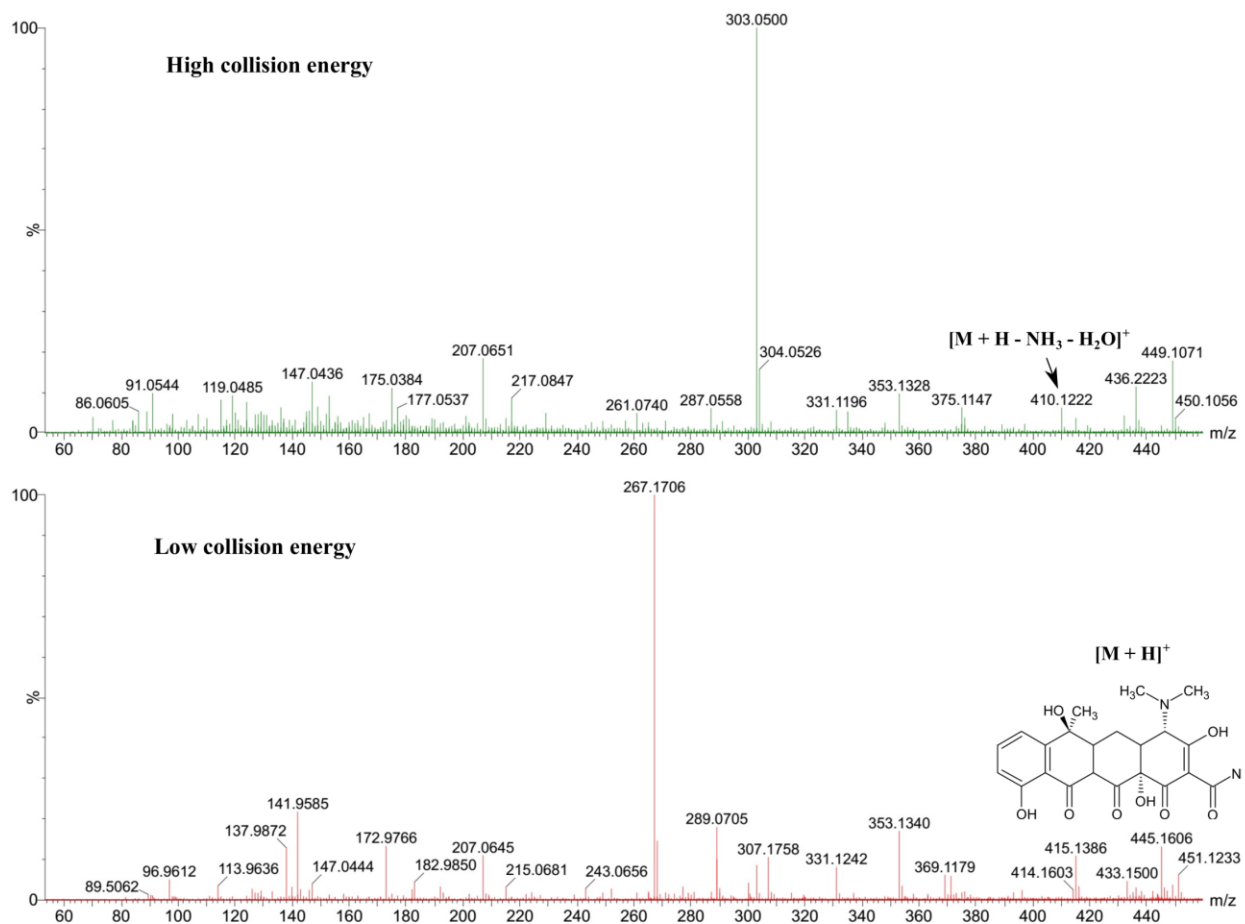
Supplementary Figure 5.7. Structure of CTC and related compounds .



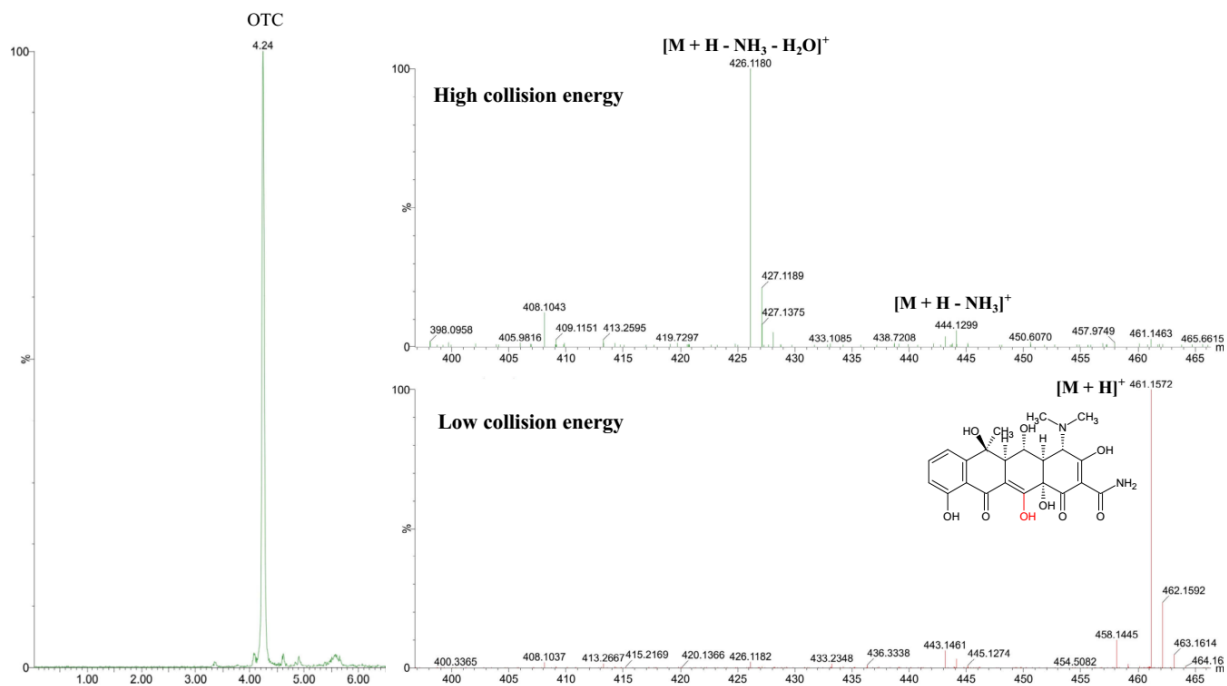
Supplementary Figure 5.8. Low- and high-collision-energy mass spectra of TP641a (m/z 641.1760) on the UPLC-QTOF-MS^E.



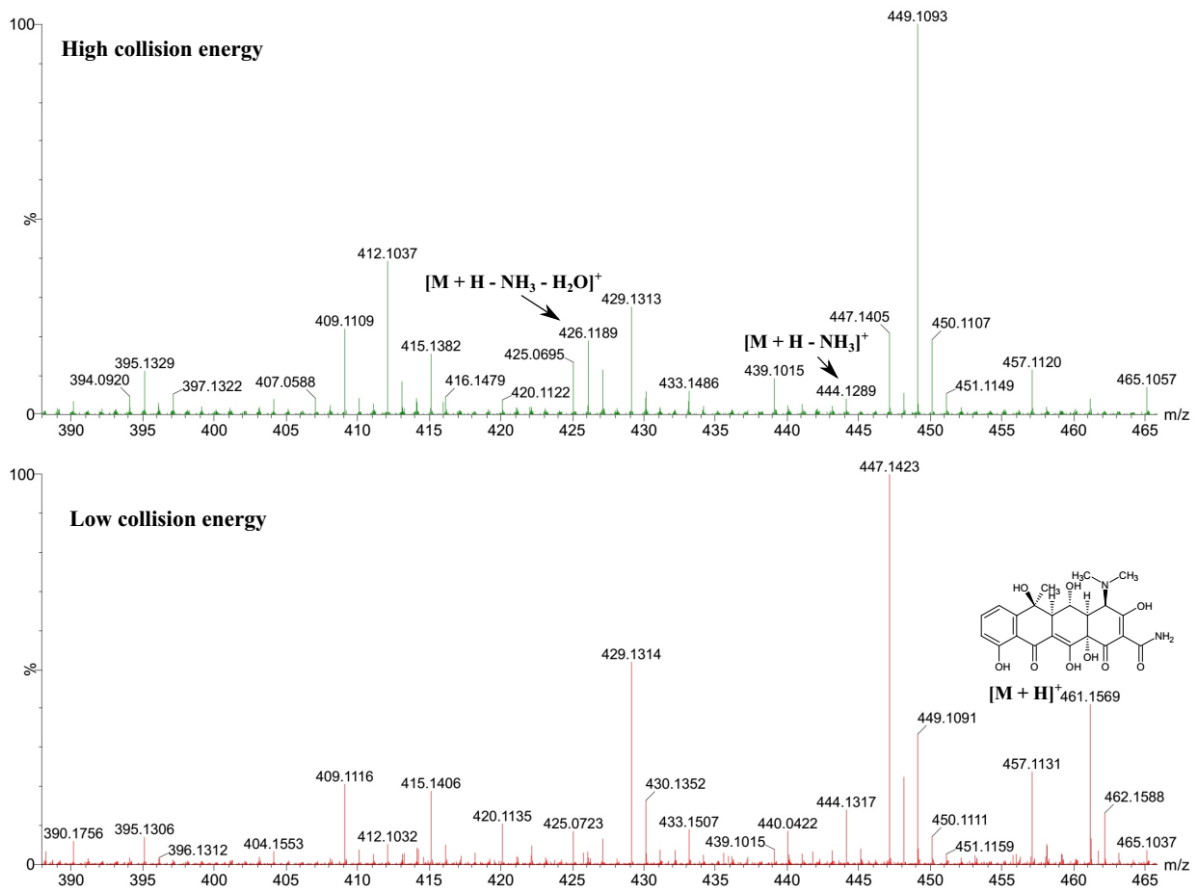
Supplementary Figure 5.9. Low- and high-collision-energy mass spectra of TP641b (m/z 641.1760) on the UPLC-QTOF-MS^E.



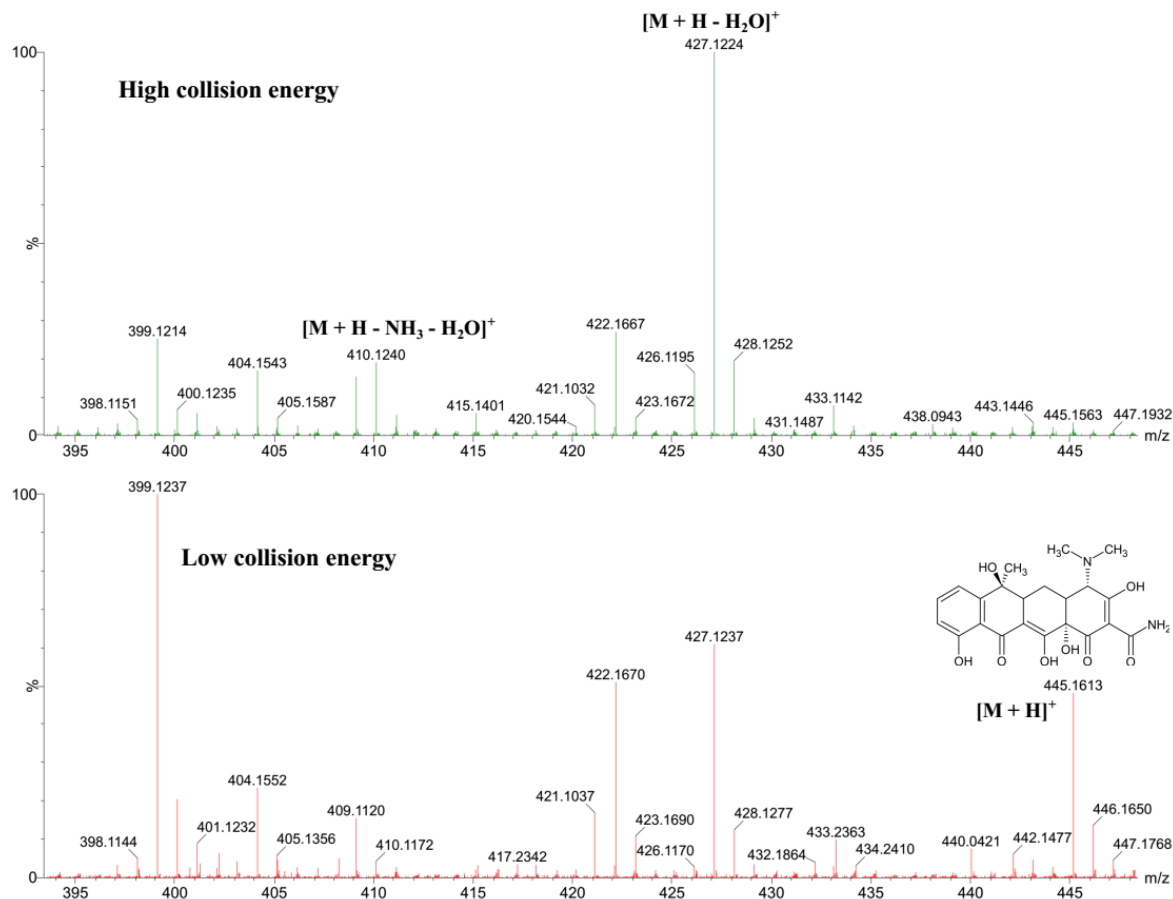
Supplementary Figure 5.10. Low- and high-collision-energy mass spectra of TP445a (m/z 445.1606) on the UPLC-QTOF-MS^E.



Supplementary Figure 5.12. Selected ion chromatogram of OTC standard (0.2 $\mu\text{g/mL}$) at m/z 461.15, and its characteristic fragmentation patterns at RT = 4.24 min on the UPLC-QTOF-MS^E system.



Supplementary Figure 5.13. Low- and high-collision-energy mass spectra of 4-epi-OTC (TP461) on the UPLC-QTOF-MS^E.



Supplementary Figure 5.14. Low- and high-collision-energy mass spectra of tetracycline (TP445) on the UPLC-QTOF-MS^E.

REFERENCES

REFERENCES

- Ashfaq, M., Li, Y., Wang, Y., Chen, W., Wang, H., Chen, X., Wu, W., Huang, Z., Yu, C.P. and Sun, Q., 2017. Occurrence, fate, and mass balance of different classes of pharmaceuticals and personal care products in an anaerobic-anoxic-oxic wastewater treatment plant in Xiamen, China. *Water Res.* 123, 655-667.
- Azanu, D., Mortey, C., Darko, G., Weisser, J.J., Styryshave, B. and Abaidoo, R.C., 2016. Uptake of antibiotics from irrigation water by plants. *Chemosphere* 157, 107-114.
- Ben, W., Zhu, B., Yuan, X., Zhang, Y., Yang, M. and Qiang, Z., 2018. Occurrence, removal and risk of organic micropollutants in wastewater treatment plants across China: Comparison of wastewater treatment processes. *Water Res.* 130, 38-46.
- Bowman, S.M., Drzewiecki, K.E., Mojica, E.R., Zielinski, A.M., Siegel, A., Aga, D.S. and Berry, J.O., 2011. Toxicity and reductions in intracellular calcium levels following uptake of a tetracycline antibiotic in *Arabidopsis*. *Environ. Sci. Technol.* 45, 8958-8964.
- Chen, Y., Li, H., Wang, Z., Tao, T. and Hu, C., 2011. Photoproducts of tetracycline and oxytetracycline involving self-sensitized oxidation in aqueous solutions: effects of Ca²⁺ and Mg²⁺. *J. Environ. Sci. (China)* 23, 1634-1639.
- Chen, Y., Li, H., Wang, Z., Tao, T., Wei, D. and Hu, C., 2012. Photolysis of Chlortetracycline in aqueous solution: Kinetics, toxicity and products. *Journal of Environmental Sciences* 24, 254-260.
- Conde-Cid, M., Álvarez-Esmorís, C., Paradelo-Núñez, R., Nóvoa-Muñoz, J.C., Arias-Estévez, M., Álvarez-Rodríguez, E., Fernández-Sanjurjo, M.J. and Núñez-Delgado, A., 2018. Occurrence of tetracyclines and sulfonamides in manures, agricultural soils and crops from different areas in Galicia (NW Spain). *Journal of Cleaner Production* 197, 491-500.
- Dang, N.L., Hughes, T.B., Krishnamurthy, V. and Swamidass, S.J., 2016. A simple model predicts UGT-mediated metabolism. *Bioinformatics* 32, 3183-3189.
- Dudley, S., Sun, C., Jiang, J. and Gan, J., 2018. Metabolism of sulfamethoxazole in *Arabidopsis thaliana* cells and cucumber seedlings. *Environ. Pollut.* 242, 1748-1757.
- Farkas, M.H., Berry, J.O. and Aga, D.S., 2007. Chlortetracycline detoxification in maize via induction of glutathione S-transferases after antibiotic exposure. *Environ. Sci. Technol.* 41, 1450-1456.
- Farkas, M.H., Mojica, E.R., Patel, M., Aga, D.S. and Berry, J.O., 2009. Development of a rapid biolistic assay to determine changes in relative levels of intracellular calcium in leaves following tetracycline uptake by pinto bean plants. *Analyst* 134, 1594-1600.

Fu, Q., Ye, Q., Zhang, J., Richards, J., Borchardt, D. and Gan, J., 2017a. Diclofenac in Arabidopsis cells: Rapid formation of conjugates. *Environ. Pollut.* 222, 383-392.

Fu, Q., Zhang, J., Borchardt, D., Schlenk, D. and Gan, J., 2017b. Direct Conjugation of Emerging Contaminants in Arabidopsis: Indication for an Overlooked Risk in Plants? *Environ. Sci. Technol.* 51, 6071-6081.

Gao, P., Munir, M. and Xagorarakı, I., 2012. Correlation of tetracycline and sulfonamide antibiotics with corresponding resistance genes and resistant bacteria in a conventional municipal wastewater treatment plant. *Sci. Total Environ.* 421, 173-183.

Gaugain, M., Gautier, S., Bourcier, S., Jacques, A.M., Laurentie, M., Abjean, J.P., Hurtaud-Pessel, D. and Verdon, E., 2015. 6-Iso-chlortetracycline or keto form of chlortetracycline? Need for clarification for relevant monitoring of chlortetracycline residues in food. *Food Addit. Contam. Part A Chem. Anal. Control Expo. Risk Assess.* 32, 1105-1015.

Hou, J., Wan, W., Mao, D., Wang, C., Mu, Q., Qin, S. and Luo, Y., 2015. Occurrence and distribution of sulfonamides, tetracyclines, quinolones, macrolides, and nitrofurans in livestock manure and amended soils of Northern China. *Environ. Sci. Pollut. Res. Int.* 22, 4545-4554.

Hu, X., Zhou, Q. and Luo, Y., 2010. Occurrence and source analysis of typical veterinary antibiotics in manure, soil, vegetables and groundwater from organic vegetable bases, northern China. *Environ. Pollut.* 158, 2992-2998.

Jin, X., Xu, H., Qiu, S., Jia, M., Wang, F., Zhang, A. and Jiang, X., 2017. Direct photolysis of oxytetracycline: Influence of initial concentration, pH and temperature. *J. Photochem. Photobiol. A: Chem.* 332, 224-231.

Kang, D.H., Gupta, S., Rosen, C., Fritz, V., Singh, A., Chander, Y., Murray, H. and Rohwer, C., 2013. Antibiotic uptake by vegetable crops from manure-applied soils. *J. Agric. Food Chem.* 61, 9992-10001.

Karacı, A. and Balçioğlu, I.A., 2009. Investigation of the tetracycline, sulfonamide, and fluoroquinolone antimicrobial compounds in animal manure and agricultural soils in Turkey. *Sci. Total Environ.* 407, 4652-4664.

Kennedy, D.G., McCracken, R.J., Carey, M.P., Blanchflower, W.J. and Hewitt, S.A., 1998. Iso- and epi-iso-chlortetracycline and the principal metabolites of chlortetracycline in the hen's egg. *J. Chromatogr. A* 812, 327-337.

Kim, M., Guerra, P., Shah, A., Parsa, M., Alaei, M. and Smyth, S.A., 2014. Removal of pharmaceuticals and personal care products in a membrane bioreactor wastewater treatment plant. *Water Sci. Technol.* 69, 2221-2229.

Kumar, K., Gupta, S.C., Baidoo, S.K., Chander, Y. and Rosen, C.J., 2005. Antibiotic uptake by plants from soil fertilized with animal manure. *J. Environ. Qual.* 34, 2082-2085.

- LeFevre, G.H., Müller, C.E., Li, R.J., Luthy, R.G. and Sattely, E.S., 2015. Rapid Phytotransformation of Benzotriazole Generates Synthetic Tryptophan and Auxin Analogs in Arabidopsis. *Environ. Sci. Technol.* 49, 10959-10968.
- LeFevre, G.H., Portmann, A.C., Muller, C.E., Sattely, E.S. and Luthy, R.G., 2016. Plant Assimilation Kinetics and Metabolism of 2-Mercaptobenzothiazole Tire Rubber Vulcanizers by Arabidopsis. *Environ. Sci. Technol.* 50, 6762-6771.
- Li, C., Chen, J., Wang, J., Ma, Z., Han, P., Luan, Y. and Lu, A., 2015. Occurrence of antibiotics in soils and manures from greenhouse vegetable production bases of Beijing, China and an associated risk assessment. *Sci. Total Environ.* 521-522, 101-107.
- Li, C., Zhang, D., Peng, J. and Li, X., 2018. The effect of pH, nitrate, iron (III) and bicarbonate on photodegradation of oxytetracycline in aqueous solution. *J. Photochem. Photobiol. A Chem.* 356, 239-247.
- Li, Y., Hou, X., Yu, M., Zhou, Q., Liu, J., Schnoor, J.L. and Jiang, G., 2017. Dechlorination and chlorine rearrangement of 1,2,5,5,6,9,10-heptachlorodecane mediated by the whole pumpkin seedlings. *Environ. Pollut.* 224, 524-531.
- Li, Y.W., Wu, X.L., Mo, C.H., Tai, Y.P., Huang, X.P. and Xiang, L., 2011. Investigation of sulfonamide, tetracycline, and quinolone antibiotics in vegetable farmland soil in the Pearl River Delta area, southern China. *J. Agric. Food Chem.* 59, 7268-7276.
- Macherius, A., Seiwert, B., Schroder, P., Huber, C., Lorenz, W. and Reemtsma, T., 2014a. Identification of Plant Metabolites of Environmental Contaminants by UPLC-QToF-MS: The in Vitro Metabolism of Triclosan in Horseradish. *J. Agric. Food Chem.* 62, 1001-1009.
- Macherius, A., Seiwert, B., Schröder, P., Huber, C., Lorenz, W. and Reemtsma, T., 2014b. Identification of Plant Metabolites of Environmental Contaminants by UPLC-QToF-MS: The in Vitro Metabolism of Triclosan in Horseradish.
- Marsik, P., Sisa, M., Lacina, O., Motkova, K., Langhansova, L., Rezek, J. and Vanek, T., 2017. Metabolism of ibuprofen in higher plants: A model Arabidopsis thaliana cell suspension culture system. *Environ. Pollut.* 220, 383-392.
- Mathews, S. and Reinhold, D., 2013. Biosolid-borne tetracyclines and sulfonamides in plants. *Environmental Science and Pollution Research* 20, 4327-4338.
- Mullen, R.A., Hurst, J.J., Naas, K.M., Sassoubre, L.M. and Aga, D.S., 2019. Assessing uptake of antimicrobials by Zea mays L. and prevalence of antimicrobial resistance genes in manure-fertilized soil. *Sci. Total Environ.* 646, 409-415.
- Pan, M. and Chu, L.M., 2016. Adsorption and degradation of five selected antibiotics in agricultural soil. *Sci. Total Environ.* 545-546, 48-56.

- Pan, M., Wong, C.K. and Chu, L.M., 2014. Distribution of antibiotics in wastewater-irrigated soils and their accumulation in vegetable crops in the Pearl River Delta, southern China. *J. Agric. Food Chem.* 62, 11062-11069.
- Pandey, R.P., Chu, L.L., Kim, T.S. and Sohng, J.K., 2018. Bioconversion of Tetracycline Antibiotics to Novel Glucoside Derivatives by Single-Vessel Multienzymatic Glycosylation. *J. Microbiol. Biotechnol.* 28, 298-304.
- Schwake-Anduschus, C. and Langenkamper, G., 2018. Chlortetracycline and related tetracyclines: detection in wheat and rye grain. *J. Sci. Food Agric.* 98, 4542–4549.
- Schwitzguebel, J.P. and Vanek, T., 2003. Phytoremediation: Transformation and control of contaminants. McCutcheon, S. and Schnoor, J. (eds), pp. 123-157, John Wiley & Sons, Inc., New Jersey.
- Schymanski, E.L., Jeon, J., Gulde, R., Fenner, K., Ruff, M., Singer, H.P. and Hollender, J., 2014. Identifying Small Molecules via High Resolution Mass Spectrometry: Communicating Confidence. *Environ. Sci. Technol.* 48, 2097-2098.
- Tran, N.H., Chen, H., Reinhard, M., Mao, F. and Gin, K.Y., 2016. Occurrence and removal of multiple classes of antibiotics and antimicrobial agents in biological wastewater treatment processes. *Water Res.* 104, 461-472.
- U.S. FDA (2017) 2016 Summary Report on Antimicrobials Sold or Distributed for Use in Food-Producing Animals.
- Wang, H., Yao, H., Sun, P., Pei, J., Li, D. and Huang, C.H., 2015. Oxidation of tetracycline antibiotics induced by Fe(III) ions without light irradiation. *Chemosphere* 119, 1255-1261.
- Wang, J. and Wang, S., 2016. Removal of pharmaceuticals and personal care products (PPCPs) from wastewater: A review. *J. Environ. Manage.* 182, 620-640.
- Wang, S., Zhang, S., Huang, H., Zhao, M. and Lv, J., 2011. Uptake, translocation and metabolism of polybrominated diphenyl ethers (PBDEs) and polychlorinated biphenyls (PCBs) in maize (*Zea mays* L.). *Chemosphere* 85, 379-385.
- Xiang, L., Wu, X.L., Jiang, Y.N., Yan, Q.Y., Li, Y.W., Huang, X.P., Cai, Q.Y. and Mo, C.H., 2016. Occurrence and risk assessment of tetracycline antibiotics in soil from organic vegetable farms in a subtropical city, south China. *Environ. Sci. Pollut. Res. Int.* 23, 13984-13995.
- Xuan, R., Arisi, L., Wang, Q., Yates, S.R. and Biswas, K.C., 2010. Hydrolysis and photolysis of oxytetracycline in aqueous solution. *J. Environ. Sci. Health. B* 45, 73-81.
- Yang, S., Cha, J. and Carlson, K., 2005. Simultaneous extraction and analysis of 11 tetracycline and sulfonamide antibiotics in influent and effluent domestic wastewater by solid-phase extraction

and liquid chromatography-electrospray ionization tandem mass spectrometry. *J Chromatogr. A.* 1097, 40-53.

Zhang, M., He, L.Y., Liu, Y.S., Zhao, J.L., Liu, W.R., Zhang, J.N., Chen, J., He, L.K., Zhang, Q.Q. and Ying, G.G., 2019. Fate of veterinary antibiotics during animal manure composting. *Sci. Total Environ.* 650, 1363-1370.

Zhao, C., Pelaez, M., Duan, X.D., Deng, H.P., O'Shea, K., Fatta-Kassinos, D. and Dionysiou, D.D., 2013. Role of pH on photolytic and photocatalytic degradation of antibiotic oxytetracycline in aqueous solution under visible/solar light: Kinetics and mechanism studies. *Appl Catal B-Environ* 134, 83-92.

CHAPTER 6.

**QUANTIFICATION OF PHYTOMETABOLITES OF SULFONAMIDES IN SOIL
ECOSYSTEMS PLANTED WITH *ARABIDOPSIS THALIANA***

6.1. Introduction

The ubiquitous use of sulfonamide antimicrobials in human and veterinary medicine has prompted growing concerns about antimicrobial contamination and resistance in food production systems. Due to their highly bioactive nature, presence of antimicrobials, even at trace concentrations, has been linked to alteration of the composition of bacterial communities, causing or promoting antimicrobial resistance.

On the other hand, uptake and accumulation of residual antimicrobials by food crops grown in contaminated soils have been well-documented, prompting substantial concern about unintentional exposure to antimicrobials through consumption of contaminated food crops. Past studies and risk assessments related to plant uptake and accumulation of these xenobiotics only addressed the unaltered parent compounds; however, our research indicates that untransformed antimicrobials represent a small proportion of the total antimicrobial species in plant tissues when transformed, conjugated, and sequestered phytometabolites are considered (Huynh et al., 2018). Additionally, although accumulation of the parent compounds is universal, conclusions as to their metabolic fate in plant tissues drastically differ. For example, no metabolites of sulfamethoxazole (SMX) were detected in Chinese cabbage and water spinach exposed to 100 µg SMX/mL after 5 days (Chen et al., 2017). Conversely, several phase I and phase II metabolites of SMX were observed in *A. thaliana* cells during a 4-day exposure, of which N⁴-acetyl-SMX was the major metabolite (Dudley et al., 2018). Similar metabolites were also detected in the intact cucumber seedlings, although at lower concentrations compared to those in the cell culture trials (Dudley et al., 2018). In our study with *A. thaliana* plants, N⁴-glycosyl-SMX accounted for more than 80% of the extractable metabolites, while the presence of N⁴-acetyl-SMX could not be unequivocally confirmed. A targeted search using accurate masses of the SMX metabolites reported previously

(Dudley et al., 2018) was conducted; however, none of these metabolites were present in our plant extracts. One potential explanation is that the previous study had mass errors of the metabolite candidates ranging from 9.4-87.3 ppm, which exceeded our criteria of 5 ppm. Differences in plant species, exposure conditions, and sample preparation might also contribute to the discrepancies observed across studies. For example, phase III metabolism, which is time- and species-dependent, could have decreased the level of phase I and phase II metabolites below the limit of detection (Dudley et al., 2018), potentially explaining the non-detection of previously identified metabolites in our study.

While idealized, hydroponic experiments are essential to elucidating phytometabolic pathways, they likely overestimate the importance of phytometabolism in the environment where competing biological and physicochemical processes will be present. According to our best knowledge, fate of sulfonamides in plant-soil systems has not been well-elucidated. Therefore, the main objective of this study is to characterize the contribution of phytometabolism to fate of sulfonamides, including sulfamethazine (SMT) and SMX, in the soil ecosystems planted with *Arabidopsis thaliana*. Based on the results obtained in Chapter 4, a targeted search using the mass-to-charge (m/z) ratios of the potential phytometabolites was conducted, coupled with ^{14}C -labeled sulfonamides studies to elucidate their distribution in the plant tissues following plant uptake and metabolism.

6.2. Materials and Methods

6.2.1. Chemicals

^{14}C -SMX (77 mCi/mmol, 98% purity) and ^{14}C -SMT (80 mCi/mmol, 98% purity) were obtained from American Radiolabeled Chemicals (St. Louis, MO). Unlabeled SMX (>98% purity) was purchased from Tokyo Chemical Industry (Portland, OR). Unlabeled SMT (>99% purity),

formic acid, and MS grade acetonitrile were purchased from Sigma-Aldrich (St. Louis, MO). Other chemicals (ACS grade) were purchased from VWR, Inc. (Chicago, IL). Formic acid and MS grade acetonitrile were purchased from Sigma-Aldrich (St. Louis, MO).

6.2.2. Soil columns and experimental setups

Experiments were conducted using a sandy loam topsoil obtained from Hammond Farms Landscape Supply (East Lansing, MI). The soil had no history of biosolids, treated wastewater or manure application, and was tested for residues of SMT and SMX prior to use. Once air-dried, the soil was passed through a 2-mm sieve and used for subsequent experiments. Selected properties of the soil are reported in Table 6.1.

Table 6. 1. Basic properties of the sandy loam topsoil used in this study.

pH	7.6
Cation exchange capacity (meq/100g)	10.5
Organic matter %	2.5
Sand %	59.8
Silt %	25.0
Clay %	15.2
Exchangeable bases %	
K	4.5
Mg	15.5
Ca	80.0

A. thaliana seeds were germinated in the Miracle-Gro potting mix and Miracle-Gro Perlite (10:1) for two weeks and the seedlings were subsequently transferred to experimental soil columns, two plants per column. The experimental soil columns (diameter of 6.4 cm and length of 10.8 cm) were filled with approximately 150 g of the sieved soil and was partly covered by aluminum foil to minimize photodegradation of the spiked antimicrobials (Figure 6.1-C). One week after plants were transferred to the soil columns, antimicrobials (SMT and SMX) were separately spiked into the soil through irrigation water. Using a micropipette, the irrigation water

containing unlabeled- and ^{14}C -labeled standards of each antimicrobial was added dropwise to the soil surface to obtain nominal concentrations of approximately $3\ \mu\text{g/g}$ soil (or $450\ \mu\text{g/column}$) and $3\ \text{nCi/g}$ soil (or $0.45\ \mu\text{Ci/column}$), respectively. The columns were then placed in secondary glass containers. The whole reactors were constructed as airtight systems with the flow of influent and effluent air regulated to allow capture of any $^{14}\text{C-CO}_2$ that was produced by microbial degradation of ^{14}C -labeled antimicrobials in a Permafluor® E+ trap. A flow of air was provided to the systems after every two days (5 min each time) to prevent accumulation of CO_2 , which would limit photosynthesis and plant growth (airtight, with frequent air purging treatments). Two additional treatments were also conducted to elucidate the potential effects on airtight conditions on accumulation and metabolism of antimicrobials by *A. thaliana* plants: (1) completely airtight with no air exchange, and (2) no airtight (open-space reactors) with fully air exchange. Soil columns with no plant were also included as controls. All treatments and controls were performed in triplicates and were maintained in a plant growth chamber (Conviron A1000, Manitoba, Canada) with temperature and light intensity of 22°C and $150\ \mu\text{mol/m}^2/\text{s}$ for a 16 h photoperiod.

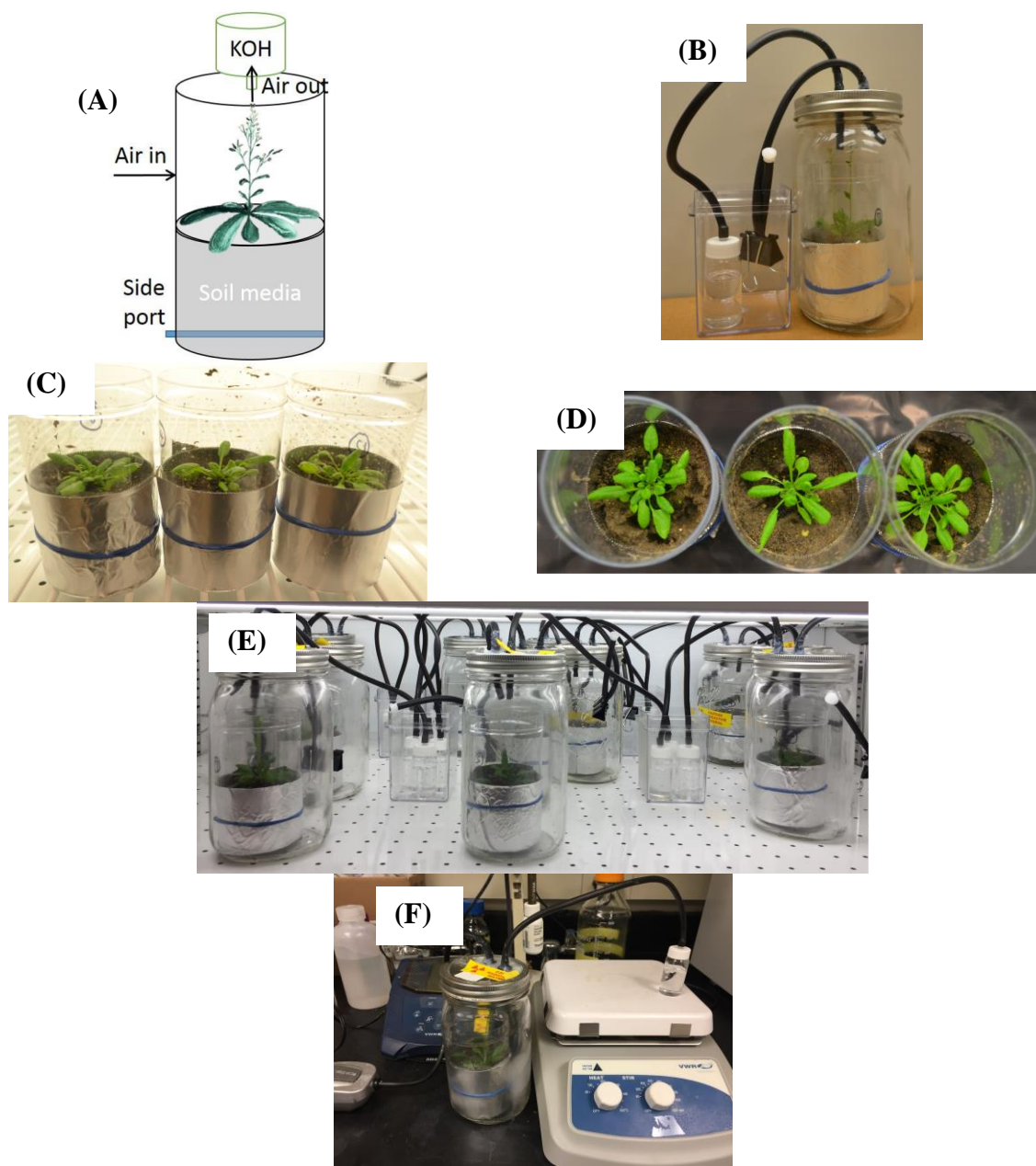


Figure 6. 1. Soil column design for studying the fate of SMT and SMX in soil systems planted with *A. thaliana*.

(A): Proposed column design.

(B): A modified experimental reactor: soil column with plants was placed in an airtight mason jar. $^{14}\text{C-CO}_2$ generated by mineralization, if any, was captured into a glass scintillation vial containing 15 mL of Permafluor® E+ (PerkinElmer) by pumping air through the inlet.

(C) and (D): Soil columns planted with *A. thaliana*.

(E): The reactors were kept in a plant growth chamber during the exposure time.

(F): Air was pumped through the reactor to capture the $^{14}\text{C-CO}_2$ generated in the system.

6.2.3. Sampling

Plants were harvested after 7 days of exposure. Plants were rinsed with tap water and DI water to remove soil particles on root surface, blotted dry with paper towels to remove excess water, separated into roots and shoots (including leaves, stems, and flowers), and the fresh biomass of each plant tissue was weighed. The plant materials were ground to fine powder in liquid nitrogen and stored at -20°C until analysis.

Soil samples from each column were oven-dried at 55°C to constant weights, homogenized by mixing, and stored at 4°C until analysis.

6.2.4. Sample preparation

Plant tissues were extracted with 5 mL of methanol with sonication for 15 min at room temperature and then centrifuged at 4,000 rpm for 15 min. The supernatant was then decanted and the extraction was repeated two more times. Extracts were pooled, dried under nitrogen gas, reconstituted in 1 mL of methanol:water (1:1, 0.1% formic acid), and filtered through 0.2 µm PTFE membranes into 2 mL amber vials.

Soil samples were extracted as described by (Pamreddy et al., 2013) with some minor modifications. Briefly, dried soil samples (approximately 5.0 g) were extracted using a Dionex ASE 200 accelerated solvent extractor (Sunnyvale, CA). Two cycles of extraction with methanol:0.2 M citric acid, pH 3.0 (1:1) was carried out under the following operating conditions: oven temperature, 50°C; extraction pressure, 1500 psi; preheat time, 5 min; heat time, 5 min; static time, 10 min; flush volume, 100% and 120 sec purge time. Following ASE, Milli-Q water was added to the soil extracts to make the final volume of 40 mL; subsequently, aliquots of 20 mL were mixed with 180 mL of Milli-Q water (methanol content ~5%) prior to SPE. The SPE cartridges were sequentially conditioned with 5 mL of methanol and 5 mL of 0.04 M citric acid (pH 3.0). Samples were then

passed through the conditioned cartridges using a vacuum manifold. After samples loading, cartridges were sequentially rinsed with 5 mL of 0.04 M citric acid (pH 3.0) and 5 mL of 0.1 M sodium acetate, and dried under vacuum until fully dry. Analytes were eluted using 5 mL of methanol, dried under nitrogen gas, reconstituted in 1 mL of methanol:water (1:1, 0.1% formic acid), and filtered through 0.2 μm PTFE membranes (13 mm, VWR) into 2 mL amber vials.

For quantification of the extractable ^{14}C -residues, aliquots of 100 μL of the reconstituted plant and soil extracts were mixed with 10 mL of Hionic Fluor cocktail in 20 mL glass scintillation vials and measured for ^{14}C -radioactivity by a Beckman Liquid Scintillation Counter (LSC). Plant residues, after methanol extraction, were oven-dried at 50°C for 48 h and digested using a mixture of perchloric acid:nitric acid (1:1) (Thomson, 2012). The digestate was diluted to 2.0 mL with Milli-Q water. Aliquots of 30 – 100 μL were added to 10 mL of Hionic Fluor cocktail and measured for ^{14}C -radioactivity associated with non-extractable or bound residues.

6.2.5. LC-MS- β -RAM and radioactivity analysis

Analysis of SMT and SMX, and their metabolites was performed on a Shimadzu LC-MS 2010 EV EV coupled with an on-line radioactivity detector β -RAM (model 5, LabLogic, Brandon, FL). Separation was carried out on an Ultra Biphenyl (5 μm , 250 x 4.6 mm, Restek) at a flow rate of 1.0 mL/min and temperature of 40°C with water and acetonitrile, both containing 0.1% formic acid, as mobile phases. The gradient program was: 0–1 min, 5% B; 3 min, 20% B; 15 min, 60% B; 17 min, 95% B; 20 min, 95% B; and 26 min, 5% B. The flow was diverted to both the β -RAM (0.8 mL/min) and MS operated in positive ESI (0.2 mL/min) using an adjustable splitter (LabLogic). SMT and SMX were identified by their retention times and characteristic molecular ions: m/z 279 for SMT and m/z 254 for SMX, respectively. Matrix-matched standard curves of SMT and SMX were developed to minimize the matrix effects. The m/z of the metabolites

previously identified in Chapter 4 were also monitored. A list of these metabolites and the corresponding m/z were showed in Table 6.2.

Table 6. 2. The potential metabolites of SMT and SMX (as identified in Chapter 4), and their corresponding m/z monitored in this study.

Metabolites	Mass-to-charge (m/z) ratios	
	SMT	SMX
N ⁴ -glycosyl-	441	416
N ⁴ -glycosyl-glycoside-	nd	578
Pterin-	454	429
Methylsalicylate-	429	404/406
Methylsalicylate-glycosyl-	nd	566/568
Chlorinated-	313/315	288/230
N ⁴ -formyl-	307	282
Hydroxyl-	295	270
N ⁴ -acetyl-	321	296
Desamino-	264	239

nd: not detected

¹⁴C-radioactivity was measured on a Beckman LS 6500 Liquid Scintillation Counter (LSC) (Fullerton, CA) with a background of approximately 30 dpm. LSC data were corrected for the background by subtracting the dpm value of the blank.

6.2.6. Statistical analysis

Data are presented as mean \pm standard error (SE). Analysis of variance (ANOVA) and post-hoc comparisons of means using the Tukey's HSD test were performed using SPSS 25 (IBM Corp., Armonk, NY) to determine significant differences ($p < 0.05$). Concentrations of the antimicrobials and their metabolites in plant tissues were calculated based on fresh weight (fw), while those in soils were based on dry weight (dw).

6.3. Results and Discussion

6.3.1. Dissipation of SMT and SMX in soils

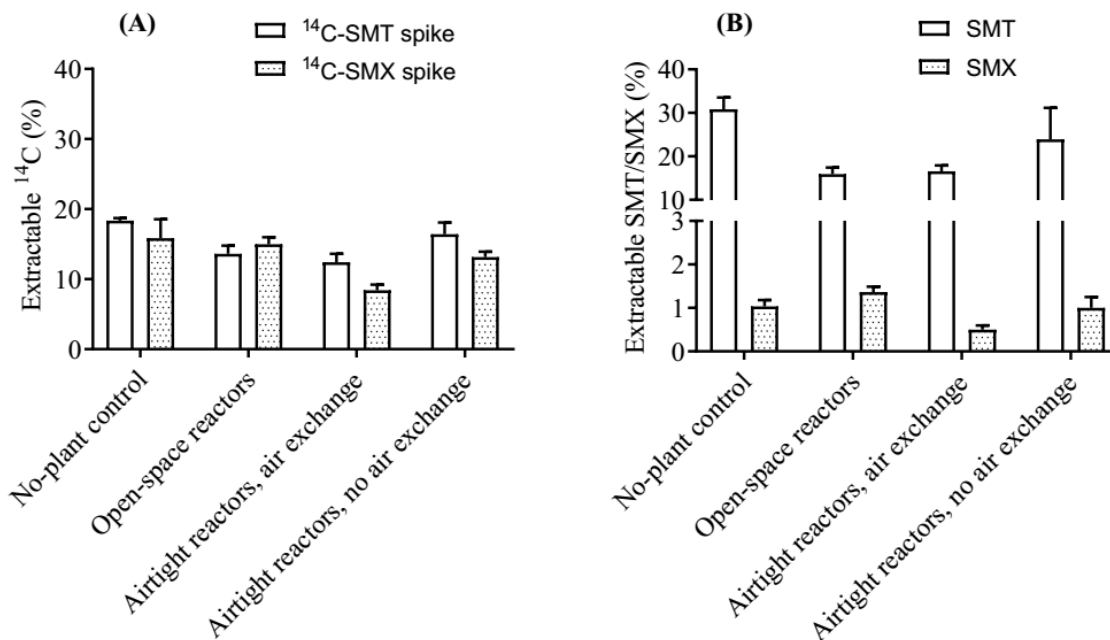


Figure 6. 2. Percentage of the extractable ^{14}C (A) and parent SMT/SMX (B) in soils after 7 days of exposure compared to the initially added concentrations of approximately 3 nCi/g and 3 $\mu\text{g/g}$, respectively. Error bars represent standard error of triplicates.

Extractable residues of ^{14}C - and unlabeled-SMT/SMX in soil samples after 7 days of exposure are shown in Figure 6.1. ^{14}C - and unlabeled-SMT/SMX were initially spiked into the soil columns at the concentrations of approximately 3 nCi/g and 3 $\mu\text{g/g}$, respectively. At these initial concentrations, SMT and SMX were expected not to inhibit growth of soil microorganisms. It has been reported that SMX only inhibits soil microorganisms at a concentration of 20 $\mu\text{g/g}$ (Demoling et al., 2009), while concentrations of SMT up to 100 $\mu\text{g/g}$ had no effect on soil microorganisms (Accinelli et al., 2007). As showed in Figure 6.1, the extractable ^{14}C -radioactivity decreased rapidly within 7 days, in which ^{14}C -SMX was more readily to be removed in soils compared to ^{14}C -SMT ($p = 0.048$) (Figure 6.1-A). Across all treatments and no-plant controls, the

extractable ^{14}C -residues accounted for only $12.5 \pm 1.2 - 18.3 \pm 0.4\%$ and $8.4 \pm 0.8 - 15.9 \pm 2.7\%$ of the initially spiked ^{14}C -SMT and ^{14}C -SMX, respectively. However, the decreases in the extractable ^{14}C was not attributed to mineralization of the parent sulfonamides. The radioactivity of ^{14}C - CO_2 generated over 7 days of exposure was equal to the background values (~ 30 dpm), suggesting that mineralization was negligible in these trials. This is in agreement with previous studies reporting relatively low mineralization rates (0 – 3%) of sulfonamides in soils (Alvarino et al., 2016, Andriamalala et al., 2018, Gulkowska et al., 2014, Höltge and Kreuzig, 2007, Junge et al., 2011), although higher mineralization rates (approximately 10.5% in 156 days) have also been reported (Andriamalala et al., 2018). Although sulfonamides show great potential for leaching due to their relatively low sorption affinity to soils (Pan and Chu, 2017), the ^{14}C -radioactivity leached through application of irrigation water was $<0.5\%$ of the total ^{14}C -radioactivity added to the soil columns. Altogether, the decreases in extractable ^{14}C -radioactivity was likely due to: (i): sorption and subsequent sequestration on soil constituents, and (ii): uptake by plants. Sulfonamides are relatively water soluble and polar compounds; therefore, their soil sorption is pH-dependent (Accinelli et al., 2007). Under environmental pHs, sulfonamides may undergo partial dissociation and be present in both ionized and neutral forms, in which the fraction f_n of the neutral molecule at a given pH can be derived from (Trapp, 2000):

$$f_n = \frac{1}{1 + 10^{i(\text{pH} - \text{pK}_a)}}$$

where i is 1 for acids and -1 for bases, pK_a is the negative log of the dissociation constant, and the fraction of the ionized species is $1 - f_n$.

In this study, the soil pH was approximately 7.6, and the pK_{a2} of SMT and SMX are 7.65 and 5.7, respectively (Peiris et al., 2017); accordingly, 47.1% of SMT and 98.8% of SMX species existed in their anion forms in soil solution, limiting ionic interactions with clay minerals (Gao

and Pedersen, 2005). On the other hand, SMT and SMX may also interact with soil organic matters, forming nonextractable residues (NERs) (Gao and Pedersen, 2005, Gulkowska et al., 2014, Thiele-Bruhn et al., 2004). Previous studies on fate of sulfonamides in soils revealed an initially fast formation of nonextractable residues (NERs) up to 50% of the applied antibiotics within a few days (Andriamalala et al., 2018, Gulkowska et al., 2014, Hölting and Kreuzig, 2007), suggesting NERs formation was due to chemicals reactions (e.i. covalent bonding to reactive quinones) rather than slow sorption processes (Gulkowska et al., 2014). For example, >75% of ^{14}C -SMX became NERs in soils amended with liquid sludge in the first week (Hölting and Kreuzig, 2007). In general, NERs may be formed through chemical bonding between the parent SMT/SMX molecules and their biotransformation products to soil constituents (Gulkowska et al., 2014), but can also from incorporation of these compounds into microbial biomass (Goulas et al., 2019, Kästner et al., 2013). The NERs of sulfonamides in soils became poorly bioavailable for soil microorganisms and plant roots (Goulas et al., 2019). In this study, we observed that the presence of *A. thaliana* plants in soil columns had inconsistent effects on the dissipation of ^{14}C -radioactivity. While the presence of plants significantly increased the dissipation of ^{14}C -radioactivity in the airtight reactors with frequent air purging ($p = 0.001$), no differences were observed for the airtight reactors without air exchange and the open-space reactors when compared to no-plant controls ($p > 0.05$). Dissipation of ^{14}C -radioactivity was also equal for all planted treatments.

The extractable residues of the parent SMT/SMX also substantially decreased after 7 days of exposure (Figure 6.1-B). Extractable residues of SMT accounted for $16.6 \pm 1.3\%$ – $30.8 \pm 2.7\%$ of the initially spiked SMT, while those for SMX were only 0.5 ± 0.1 – $1.4 \pm 0.1\%$. The results demonstrated that SMX was more readily available for biotransformation in experimental soil columns. As discussed in the ^{14}C treatments, dissipation of SMT/SMX could be attributed to quick

formation of NERs. Additionally, the discrepancies between extractable ^{14}C -radioactivity (Figure 6.1-A) and extractable SMX (Figure 6.1-B) suggested the presence of other biotransformation products in addition to the parent compound in the SMX-treated soil columns. On the contrary, the unaltered parent SMT likely accounted for the predominant proportions of the extractable residues in the SMT-treated soil columns.

6.3.2. Accumulation and metabolism of SMT and SMX in plant tissues

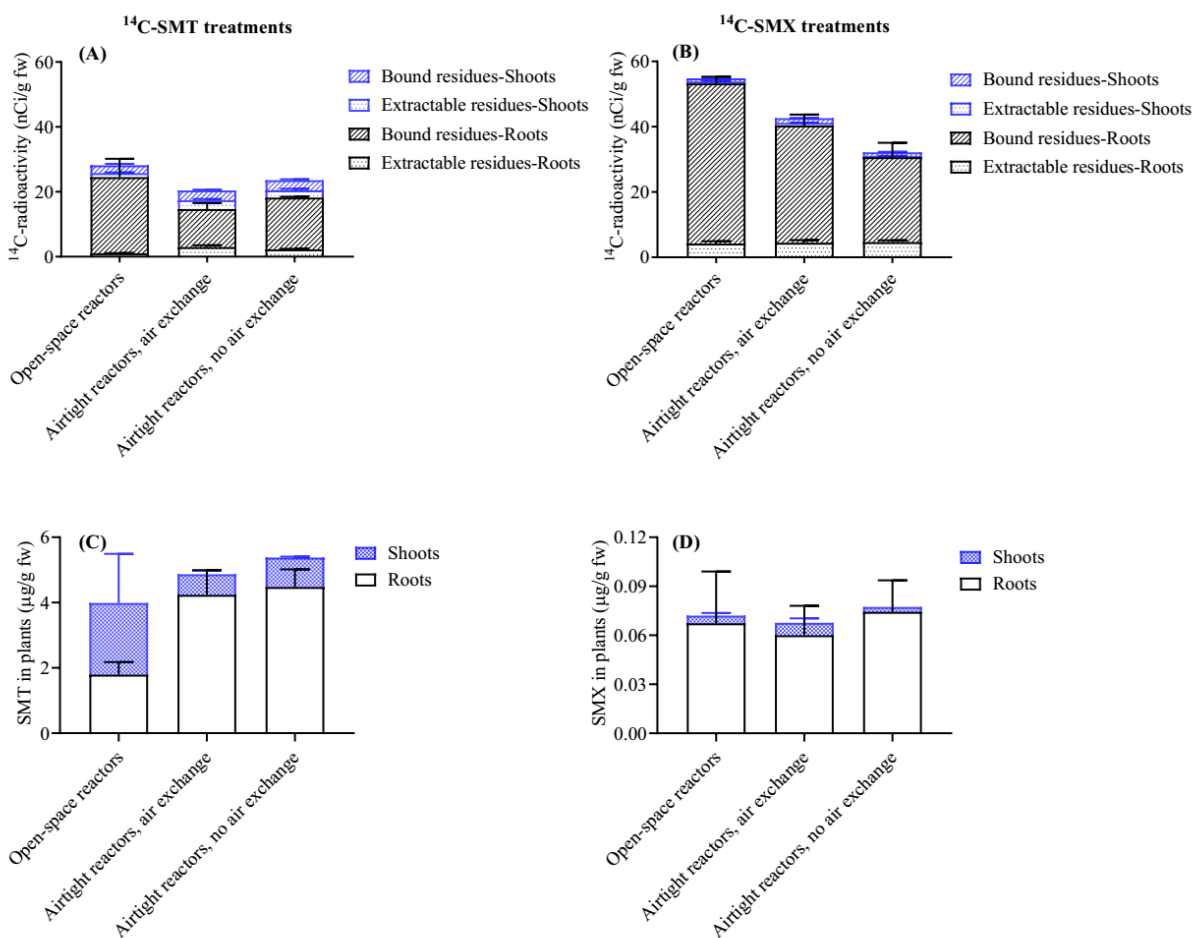


Figure 6. 3. Distribution of ^{14}C -radioactivity into extractable and bound residues in plant tissues (A and B) and concentrations of parent SMT and SMX in *A. thaliana* plant tissues (C and D) after 7 days of exposure in the experimental soil columns. Error bars represent standard error of triplicates.

In the ^{14}C -SMT/SMT treatments, there were no significant differences in the total ^{14}C -radioactivity accumulated in plant tissues across all treatments ($p = 0.330$). The highest ^{14}C -radioactivity was found in plants grown in the open-space reactors (28.2 ± 6.0 nCi/g), followed by those in the airtight reactors without air exchange (23.6 ± 0.5 nCi/g fw) and the airtight reactors with frequent air purging (20.4 ± 2.8 nCi/g fw). In the ^{14}C -SMX/SMX treatments, the highest ^{14}C -radioactivity was found in plants grown in the open-space reactors (54.8 ± 2.0 nCi/g fw), which was higher than those in the airtight reactors without air exchange (32.2 ± 4.8 nCi/g fw) ($p = 0.003$), and those in the airtight reactors with frequent air purging (42.6 ± 3.5 nCi/g fw) ($p = 0.091$). In both treatments, higher ^{14}C -radioactivity was found in plant roots compared to shoots ($p < 0.001$). Interestingly, plants grown in ^{14}C -SMX-spiked soil columns accumulated higher radioactivity than those grown in ^{14}C -SMT-spiked soil columns ($p < 0.001$). Modeling the plant uptake of the organic chemicals suggested that the passive uptake of a neutral molecule into plant roots occurs at a higher rate than that of its corresponding anion species because biological membranes are negatively charged, which leads to the repulsion of anions (Trapp, 2000). As discussed above, approximately 47.1% of SMT ($\text{pK}_{\text{a}2} = 7.65$) and 98.8% of SMX species ($\text{pK}_{\text{a}2} = 5.7$) existed in their anion forms in soil solution (pH 7.6). Consequently, uptake of SMX by plant roots was expected to occur to a lesser extent compared to that of SMT, given that their initial concentrations in soil columns are equal. This hypothesis was supported by that fact that significantly higher concentrations of the parent SMT compared to SMX were observed in plant tissues ($p < 0.001$). Plant concentrations of SMT and SMX were in range of $4.0 \pm 1.2 - 5.4 \pm 0.5$ $\mu\text{g/g}$ fw and $0.068 \pm 0.016 - 0.077 \pm 0.019$ $\mu\text{g/g}$ fw, respectively (Figure 6.2-C and D). Higher ^{14}C -radioactivity accumulated in plants grown in the ^{14}C -SMX/SMX treatments compared to plants grown in the ^{14}C -SMT/SMT treatments can be explained by the biotransformation of the

parent compounds mediated by soil microorganisms. As discussed in section 4.3.1, SMX seemed to be more readily for bacterial degradation than SMT in experimental soil columns. Therefore, while the unaltered parent ^{14}C -SMT likely accounted for the predominant proportions of the extractable ^{14}C -radioactivity in the ^{14}C -SMT-spiked soil columns, the presence of biotransformation products was expected in the ^{14}C -SMX-spiked soil columns. Although their chemical structures could not be elucidated in these trials, these biotransformation products were also likely prone to plant uptake. In other words, the ^{14}C -radioactivity detected in plant tissues in the ^{14}C -SMX/SMX treatments might include the radioactivity of the unaltered ^{14}C -SMX and its biotransformation products that were taken up by plant roots.

Plant accumulation of SMT showed no significant differences among treatments ($p > 0.05$); however, higher SMT concentrations were found in plant roots than shoots ($p = 0.003$). For example, SMT concentrations in plant roots grown in the airtight reactors with and without frequent air purging were $4.2 \pm 0.8 \mu\text{g/g}$ and $4.5 \pm 0.5 \mu\text{g/g}$, respectively, while those in shoots were only $0.6 \pm 0.1 \mu\text{g/g}$ and $0.9 \pm 0.03 \mu\text{g/g}$, respectively (Figure 6.2-C). Interestingly, *A. thaliana* plants grown in open-space reactors had greater SMT concentrations in shoots ($2.2 \pm 1.5 \mu\text{g/g}$) when compared to those in the airtight reactors, indicating that SMT was translocated into the above ground biomass more effectively following root uptake. In the soil solution, 52.9% of SMT existed in its neutral form and is thus expected to easily cross the biomembranes of plant roots (Trapp, 2000). However, dissociation of SMT ($\text{pK}_{\text{a}2} = 7.65$) (Peiris et al., 2017) is expected to occur in cytoplasm ($\text{pH} = 7.3$) (Shen et al., 2013), resulting in accumulation of SMT in root tissues due to “ion trap effect” (Trapp, 2004). In addition, root-to-shoot translocation of SMT can also be facilitated by its hydrophilicity ($\log K_{\text{ow}} = 0.27$) (Zhang et al., 2016), as neutral compounds with low hydrophobicity are readily translocated in plants (Briggs et al., 1982, Burken and Schnoor,

1998, Trapp, 2004). This flux is driven by the transpiration stream which reflects the root-to-shoot movement of water and other solutes in plants (Collins et al., 2006). We conjectured that a higher evapotranspiration rate in plants grown in the open-space reactors potentially resulted in higher translocation of SMT into the above ground biomass when compared to those in the airtight reactors.

Similar to the SMT treatments, there was no significant difference in plant accumulation of SMX among the treatments ($p = 0.960$), with SMX concentrations in plant roots was substantially higher than those in plant shoots ($p = 0.001$). Root SMX concentrations ranged from $0.060 \pm 0.018 - 0.074 \pm 0.019 \mu\text{g/g}$, while shoot SMX concentrations were only $0.003 - 0.008 \pm 0.003 \mu\text{g/g}$ (Figure 6.2-D). In these trials, SMX ($\text{pK}_{\text{a}2} = 5.7$) (Peiris et al., 2017) existed predominantly in its anion forms (approximately 98.8%), limiting its penetration through plant root biomembranes (Trapp, 2000). This explained the substantially lower concentrations of SMX in plant roots compared to those in the SMT treatments, even though their initial concentrations in soils were equal (approximately $3 \mu\text{g/g}$). The low concentrations of SMX in plant tissues was also likely the results of rapid degradation of SMX in the soils (Dalkmann et al., 2012, Malchi et al., 2014) as discussed in the previous section. Dissociation of the uptaken SMX ($\text{pK}_{\text{a}2} = 5.7$) (Peiris et al., 2017) in root cells' cytoplasm also deterred its root-to-shoot translocation, leading to negligible SMX concentrations in plant shoots across all treatments (Figure 6.3-D). It is also possible that a faster metabolism of the uptaken SMX compared to SMT might also result in its smaller concentrations in plant tissues.

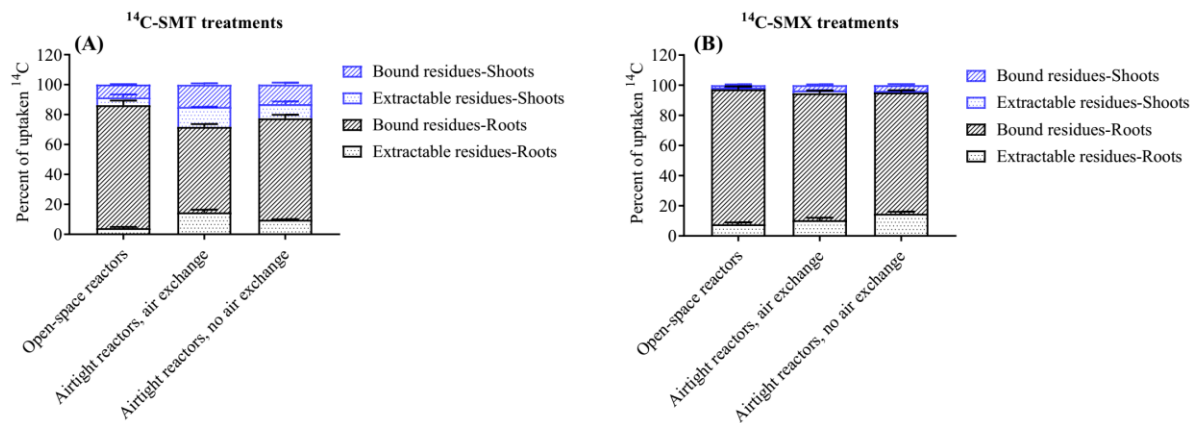


Figure 6. 4. Distribution of ¹⁴C-radioactivity (in percentage) into extractable and bound residues in plant tissues after 7 days of exposure. (A): ¹⁴C-SMT treatments, (B): ¹⁴C-SMX treatments. Error bars represent standard error of triplicates.

As discussed in Chapter 4, both SMT and SMX were readily taken up by *A. thaliana* plants. In the plant-soil systems, accumulation of both sulfonamides also occurred although to a lesser extent than in the hydroponic systems, which can be explained by their reduced bioavailability in the soil settings. Additionally, the soil pH of approximately 7.6 also resulted in higher fractions of the negatively charged SMT/SMX, limiting their root uptake (Trapp, 2000). In this study, by using ¹⁴C-labeled compounds, we were able to further elucidate the distribution of ¹⁴C in plant tissues. The results demonstrated that the uptaken SMT and SMX also underwent extensive metabolism in *A. thaliana* plant tissues following uptake. As showed in Figure 6.3, ¹⁴C-radioactivity taken up by plants were predominantly present in the root tissues, in which bound residues accounted for up to $57.1 \pm 1.9 - 82.1 \pm 3.0\%$ and $80.4 \pm 1.5 - 89.5 \pm 1.9\%$ of the initially spiked ¹⁴C-SMT and ¹⁴C-SMX after 7 days of exposure, respectively. Limited root-to-shoot translocation was observed in both treatments, in which translocation of ¹⁴C-SMX was negligible (Figure 6.3). These results have prompted concerns about root crops grown in sulfonamides-contaminated soils, especially those usually “eaten fresh”. For example, under field conditions, Malchi et al. reported that SMX was detected in the roots of sweet potato and carrot (0.05 – 0.24 ng/g), while the leaves of both

crops were SMX-free (Malchi et al., 2014). Given the results obtained in this study, SMX metabolites might also exist in those experimental food crops in the forms of extractable and bound residues. Therefore, the presence of plant metabolites of organic xenobiotics, with their unknown fate and health risks, merits further research because their concentrations in plant tissues are often substantially greater than those of the unaltered parent compounds.

6.3.3. N⁴-glycosyl-SMT and N⁴-glycosyl-SMX in plant tissues

Based on the assumption that plant metabolites of xenobiotics are identical between hydroponic and soil systems, several metabolites of SMT and SMX identified in the previous studies (Chapter 4) were monitored in the current plant-soil treatments. However, except for the glycosylated conjugates, other metabolites were undetectable on the LC/single-quadrupole MS system, potentially due to their low abundances in the samples. As discussed in Chapter 4, glycosylated conjugates of SMT and SMX were the most abundant metabolites upon exposure to *A. thaliana* plants under hydroponic conditions, representing approximately 80–90% of the metabolites pool size. In human, after ingestion, materials go through gastric and intestinal digestion, through which the metabolites, especially the glycosylated conjugates, are likely to be hydrolyzed (Sandermann, 1992) or further transformed by the gut bacteria (Koppel et al., 2017). Therefore, production of these glycosylated conjugates in plant-soil systems became the main focus of this study. Quantification of the ¹⁴C-conjugates using the radioactivity detector β-RAM was unsuccessful due to low extractable ¹⁴C-radioactivity in both soil and plant samples, leading to a poor separation of the ¹⁴C-metabolite peaks from the background. Authentic standards for these metabolites were also not available. Alternatively, peak areas obtained from the LC-MS system were used for relative quantification of their concentrations in plant tissues.

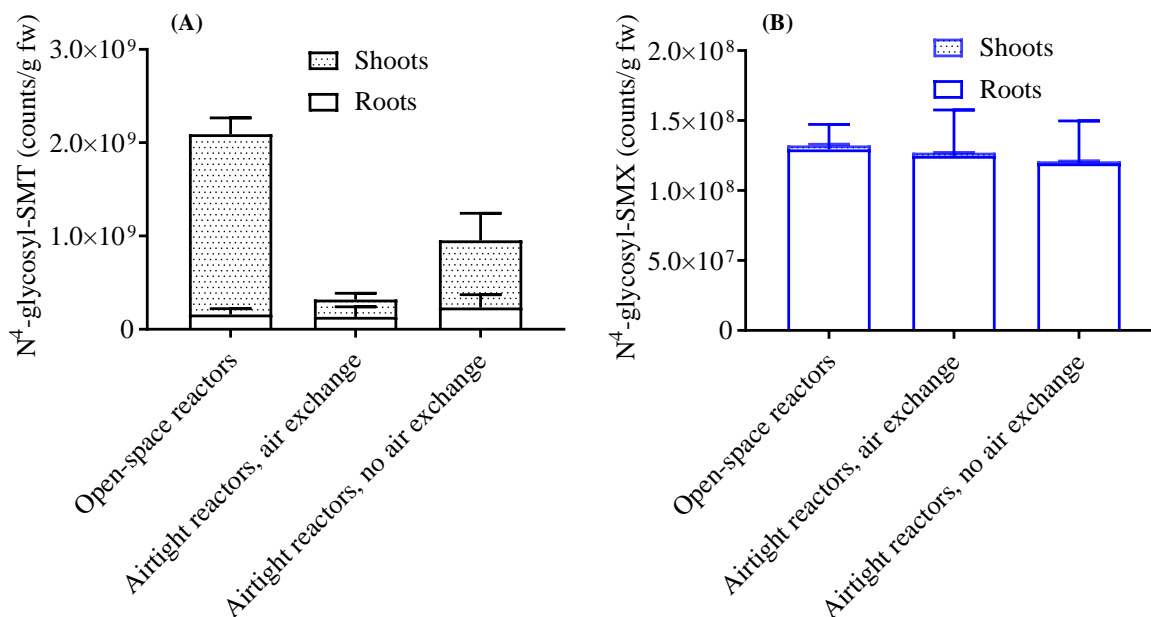


Figure 6. 5. Distribution of N⁴-glycosyl-SMT (A) and N⁴-glycosyl-SMX (B) in *A. thaliana* plant tissues after 7 days of separate exposure to SMT and SMX in the experimental soil columns.

Figure 6.4 shows the production of N⁴-glycosylated conjugates of SMT and SMX in the plant-soil systems. In the SMT-treatments, concentrations of N⁴-glycosyl-SMT in the open-space reactors were significantly greater than those in the airtight reactors with frequent air purging ($p < 0.001$) and the airtight reactors without air exchange ($p = 0.006$). However, there was no difference in the total N⁴-glycosyl-SMT between the two airtight treatments ($p = 0.138$). Across three treatments, N⁴-glycosyl-SMT was detected in both roots and shoots of the *A. thaliana* plants (Figure 6.4-A), in which its concentrations were higher in shoots than in roots. However, only those in the open-space reactions revealed a significant difference ($p < 0.001$).

Conversely, production of the N⁴-glycosyl-SMX was relatively equal in all treatments ($p > 0.05$), with predominant concentrations found in plant roots ($p = 0.002$ – 0.004) (Figure 6.4-B). Relative quantification based on their MS peak areas (counts/g fw) revealed a higher production of total N⁴-glycosyl-SMT compared to N⁴-glycosyl-SMX in the plant tissues. Nevertheless, this

comparison needs to be cautiously interpreted because differences in their ionization during MS analysis might result in the observed discrepancies. In other words, authentic standards are necessary for accurate quantification and comparison of their concentrations in plant tissues.

Although some other minor phytochemicals were not detected in this study, we demonstrated that glycosylated conjugates of SMT and SMX, which presented 80–90% of the metabolites in the hydroponic studies, were also produced in the soil ecosystems planted with *A. thaliana*. Based on the assumption that sulfonamides undergo similar phytochemical pathways in food crops, these results raise a concern about the fate of these metabolites during human digestion of the contaminated food crops. In humans, after ingestion, materials go through gastric and intestinal digestion through which the metabolites, especially the glycosylated conjugates, are likely to be hydrolyzed (Sandermann, 1992) or further transformed by the gut bacteria (Koppel et al., 2017). As a result, human exposure to antimicrobial through consumption of contaminated food crops may have been underestimated. However, plant metabolism of organic xenobiotics is expected to be affected by several factors such as plant species, exposure conditions, and sample preparation (Dudley et al., 2018). Substantially greater concentrations of parent sulfonamides and metabolites were detected in plant tissues under hydroponic exposure (Chapter 4) when compared to plant-soil systems (this chapter). Their bioavailability is also expected to be reduced in soil settings due to sorption to soil constituents and subsequent formation of NERs. Additionally, biotransformation reactions mediated by soil microorganism may also play an important role in fate of sulfonamides in soils, as proven in this study for SMX. Therefore, further studies on common food crops under field conditions using more environmental relevant concentrations of antimicrobials are necessary for an accurate assessment of the proposed risks.

REFERENCES

REFERENCES

- Accinelli, C., Koskinen, W.C., Becker, J.M. and Sadowsky, M.J., 2007. Environmental fate of two sulfonamide antimicrobial agents in soil. *J. Agric. Food Chem.* 55, 2677-2682.
- Alvarino, T., Nastold, P., Suarez, S., Omil, F., Corvini, P.F. and Bouju, H., 2016. Role of biotransformation, sorption and mineralization of (14)C-labelled sulfamethoxazole under different redox conditions. *Sci. Total Environ.* 542, 706-715.
- Andriamalala, A., Vieuble-Gonod, L., Dumeny, V. and Cambier, P., 2018. Fate of sulfamethoxazole, its main metabolite N-ac-sulfamethoxazole and ciprofloxacin in agricultural soils amended or not by organic waste products. *Chemosphere* 191, 607-615.
- Briggs, G.G., Bromilow, R.H. and Evans, A.A., 1982. Relationships between lipophilicity and root uptake and translocation of non-ionised chemicals by barley. *Pestic. Sci.* 13, 495-504.
- Burken, J.G. and Schnoor, J.L., 1998. Predictive Relationships for Uptake of Organic Contaminants by Hybrid Poplar Trees. *Environ. Sci. Technol.* 32, 3379–3385.
- Chen, H.R., Rairat, T., Loh, S.H., Wu, Y.C., Vickroy, T.W. and Chou, C.C., 2017. Assessment of veterinary drugs in plants using pharmacokinetic approaches: The absorption, distribution and elimination of tetracycline and sulfamethoxazole in ephemeral vegetables. *PLoS One* 12, e0183087.
- Collins, C., Fryer, M. and Grosso, A., 2006. Plant uptake of non-ionic organic chemicals. *Environ. Sci. Technol.* 40, 45-52.
- Dalkmann, P., Broszat, M., Siebe, C., Willaschek, E., Sakinc, T., Huebner, J., Amelung, W., Grohmann, E. and Siemens, J., 2012. Accumulation of pharmaceuticals, Enterococcus, and resistance genes in soils irrigated with wastewater for zero to 100 years in central Mexico. *PLoS One* 7, e45397.
- Demoling, L.A., E., B., G., G., M., W. and H., S., 2009. Effects of sulfamethoxazole on soil microbial communities after adding substrate. *Soil Biol. Biochem.* 41, 840–848.
- Dudley, S., Sun, C., Jiang, J. and Gan, J., 2018. Metabolism of sulfamethoxazole in Arabidopsis thaliana cells and cucumber seedlings. *Environ. Pollut.* 242, 1748-1757.
- Gao, J. and Pedersen, J.A., 2005. Adsorption of sulfonamide antimicrobial agents to clay minerals. *Environ. Sci. Technol.* 39, 9509-9516.
- Goulas, A., Sertillanges, N., Brimo, K., Garnier, P., Bergheaud, V., Dumeny, V., Benoit, P. and Haudin, C.S., 2019. Environmental availability of sulfamethoxazole and its acetylated metabolite added to soils via sludge compost or bovine manure. *Sci. Total Environ.* 651, 506-515.

Gulkowska, A., Thalmann, B., Hollender, J. and Krauss, M., 2014. Nonextractable residue formation of sulfonamide antimicrobials: new insights from soil incubation experiments. *Chemosphere* 107, 366-372.

Höltge, S. and Kreuzig, R., 2007. Laboratory Testing of Sulfamethoxazole and its Metabolite Acetyl-Sulfamethoxazole in Soil. *Clean* 35, 104-110.

Huynh, K., Banach, E. and Reinhold, D., 2018. Transformation, Conjugation, and Sequestration Following the Uptake of Triclocarban by Jalapeno Pepper Plants. *J. Agric. Food Chem.* 66, 4032–4043.

Junge, T., Meyer, K.C., Ciecieski, K., Adams, A., Schaffer, A. and Schmidt, B., 2011. Characterization of non-extractable ¹⁴C- and ¹³C-sulfadiazine residues in soil including simultaneous amendment of pig manure. *Journal of Environmental Science and Health, Part B* 46, 137-149.

Kästner, M., Nowak, K.M., Miltner, A., Trapp, S. and Schäffer, A., 2013. Classification and Modelling of Nonextractable Residue (NER) Formation of Xenobiotics in Soil – A Synthesis. *Crit. Rev. Environ. Sci. Technol.* 44, 2107-2171.

Koppel, N., Maini Rekdal, V. and Balskus, E.P., 2017. Chemical transformation of xenobiotics by the human gut microbiota. *Science* 356, eaag2770.

Malchi, T., Maor, Y., Tadmor, G., Shenker, M. and Chefetz, B., 2014. Irrigation of Root Vegetables with Treated Wastewater: Evaluating Uptake of Pharmaceuticals and the Associated Human Health Risks. *Environ. Sci. Technol.* 48, 9325–9333.

Pamreddy, A., Hidalgo, M., Havel, J. and Salvado, V., 2013. Determination of antibiotics (tetracyclines and sulfonamides) in biosolids by pressurized liquid extraction and liquid chromatography-tandem mass spectrometry. *J. Chromatogr.* 1298, 68-75.

Pan, M. and Chu, L.M., 2017. Fate of antibiotics in soil and their uptake by edible crops. *Sci. Total Environ.* 599-600, 500-512.

Peiris, C., Gunatilake, S.R., Mlsna, T.E., Mohan, D. and Vithanage, M., 2017. Biochar based removal of antibiotic sulfonamides and tetracyclines in aquatic environments: A critical review. *Bioresour. Technol.* 246, 150-159.

Sandermann, H., 1992. Plant metabolism of xenobiotics. *Trends Biochem. Sci.* 17, 82-84.

Shen, J., Zeng, Y., Zhuang, X., Sun, L., Yao, X., Pimpl, P. and Jiang, L., 2013. Organelle pH in the Arabidopsis Endomembrane System. *Molecular Plant* 6, 1419-1437.

Thiele-Bruhn, S., Seibicke, T., Schulten, H.R. and Leinweber, P., 2004. Sorption of sulfonamide pharmaceutical antibiotics on whole soils and particle-size fractions. *J. Environ. Qual.* 33, 1331-1342.

Thomson, J., 2012. Handbook of Radioactivity Analysis. L'Annunziata, M. (ed), pp. 589-590, Academic Press, San Diego, CA.

Trapp, S., 2000. Modelling uptake into roots and subsequent translocation of neutral and ionisable organic compounds. *Pest Manage. Sci.* 56, 767-778.

Trapp, S., 2004. Plant uptake and transport models for neutral and ionic chemicals. *Environmental Science and Pollution Research* 11, 33-39.

Zhang, C., Lai, C., Zeng, G., Huang, D., Yang, C., Wang, Y., Zhou, Y. and Cheng, M., 2016. Efficacy of carbonaceous nanocomposites for sorbing ionizable antibiotic sulfamethazine from aqueous solution. *Water Res.* 95, 103-112.

CHAPTER 7.
CONCLUSION REMARKS

7.1. Research contribution to the field

In this research project, targeted and untargeted metabolomics using high resolution mass spectrometry and multivariate statistical analysis coupled with ^{14}C -labeled chemicals studies were used to identify novel phytometabolites and quantify the fate of common antimicrobials in plant tissues.

We demonstrated that pepper plants metabolized the recalcitrant TCC upon long-term exposure. More importantly, a substantial portion of TCC taken up by plants was metabolized, especially in the stems, leaves and fruits. Hydroxylated TCC (e.g. 2'-OH TCC and 6-OH TCC) and glycosylated OH-TCC were found to be the main phase I and phase II metabolites in plant tissues, respectively.

We also observed that the model plant *Arabidopsis thaliana* extensively metabolized two commonly used classes of antimicrobials, including sulfonamides (SMT and SMX) and tetracyclines (CTC and OTC), shortly upon exposure. For sulfonamides, untargeted screening of extractable metabolites revealed that glycosylated conjugates were the most abundant metabolites, which accounted for 80–90% of the total metabolites, in plant tissues. Other conjugates, such as pterin- and methylsalicylate-, were present at lower concentrations. Phase I transformation products, such as hydroxyl-, acetyl-, desulfo, and desamino-, were identified as minor metabolites in plant tissues. For tetracyclines, abiotic transformation and plant metabolism played the key roles in their fate during the exposure. Plant metabolism of CTC also resulted in the formation of glycosylated conjugates and the corresponding 4-epi isomers. More importantly, although CTC was solely added into the experimental reactors, other tetracycline antimicrobials such as tetracycline, 4-epi-tetracycline, demeclocycline, and 4-pei-demeclocycline were also detected in the plant tissues. Enzymatic degradation of CTC in plant tissues following uptake might result in

the formation of these tetracyclines. On the other hand, their presence in plant tissues was also likely due to uptake of abiotic transformation products in the culture media. These are among the first studies that identified phytometabolites and quantified the fate of sulfonamide and tetracycline antimicrobials in planted systems.

Despite of their relatively small proportions in the metabolite pool size, the role of pterin-sulfonamide conjugates in plant folate biosynthesis merit further studies. While folate is critical for several biological functions of the body, humans cannot synthesize folate and rely on foods (e.g. vegetables) for its supply. Depletion of folate in plants due to exposure to sulfonamide residuals in the environment may ultimately affect human intake of this vitamin through food chains. In addition to its vital roles for human health, folate is also indispensable for plant growth (e.g. nitrogen and carbon metabolism) and plant response to biotic and abiotic stress conditions. An impaired folate metabolism in plant caused by sulfonamide antibiotics exposure will ultimately exert potential adverse impacts on plant productivity and stress tolerance.

The exclusive presence of the conjugated metabolites in the *A. thaliana*-planted media was attributed to plant excretion. Our findings contribute to a growing body of evidence suggesting that plant excretion of phase II conjugates may be an additional defense mechanism against the phytotoxicity of xenobiotics, along with phase III sequestration in the “green liver model”.

Preliminary studies using soil columns planted with *A. thaliana* plants showed that phytometabolism of sulfonamides was probably similar with that under hydroponic conditions. Although other minor metabolites were undetectable, the presence of glycosylated conjugates in plant tissues could be confirmed. The majority of the uptaken parent sulfonamides and metabolites were found in the plant roots, with limited root-to-shoot translocation. Translocation of the parent sulfonamides and production of their glycosylated conjugates in different tissues (e.g. roots and

shoots) was compound-specific. For instance, in the SMT treatments, we detected higher concentrations of SMT and N⁴-glycosyl-SMT in the shoots of *A. thaliana* plants compared to those in the SMX treatments.

7.2. Research limitations

Sterile hydroponic culture is ideal for elucidating phytometabolic pathways of organic xenobiotics. However, it may overestimate the importance of phytometabolism under real-world conditions where other competing biological and physicochemical processes will also affect the fate of these contaminants. As proven in our studies (Chapter 6), sulfonamides spiked into soils were mainly prone to microbial transformation and/or quickly became nonextractable residues (NERs). Consequently, plant uptake, accumulation, and metabolism in soil ecosystems may occur to a lesser extent compared to that in sterile hydroponic systems.

While *Arabidopsis thaliana* is a model plant that is widely used in biological research, it is possible that the phytometabolic pathways of antimicrobials in real food crops under field conditions may be different. Previous studies have suggested that differences in plant species and exposure conditions might affect the phytometabolic pathways of the uptaken xenobiotics.

Authentic standards for most of the important metabolites detected in this study were not available. As a result, their concentrations in plant tissues could not be accurately quantified, which would ultimately become an obstacle for future human health risk assessment studies.